POLITECNICO DI TORINO

Collegio di Ingegneria Chimica e dei Materiali

Corso di Laurea Magistrale
in Ingegneria Chimica e dei Processi Sostenibili

Tesi di Laurea Magistrale

PEDOT in dye-sensitized solar cells: an electrode and a hole-transporting material

Relatore

Prof. Federico Bella

Candidato

Erica Varaia

Ottobre 2020

Riassunto in lingua italiana

I. Introduzione

Il lavoro di Tesi qua presentato consiste in una review che raccoglie l'avanzamento della tecnologia delle celle solari sensitizzate al colorante utilizzanti: PEDOT (Poli(3,4-etilendioxitiofene)) come catodo e PEDOT come trasportatore di lacune. Prima di tale review è presente un excursus sullo scenario energetico globale con un successivo focus sulle celle solari sensitizzate al colorante. Per leggere in modo più chiaro la parte di review è stata poi inserita una sezione che raccoglie le principali prove attuate sulle celle solari. Dopo la review, viene presentata l'esperienza presso i laboratori DISAT del Politecnico di Torino.

II. Scenario energetico globale

La pandemia che abbiamo appena affrontato ha creato un enorme shock economico e sanitario destinato a rimodellare l'economia globale. Questa situazione evidenzia l'opportunità di cambiare le tendenze e di accelerare quelle emergenti spostando la situazione energetica verso un percorso più sostenibile. Lo stop forzato portato dal COVID-19 ha messo in evidenza le principali sfide a lungo termine, come il cambiamento climatico.

Lo scenario presentato nel 2019 mostra alcuni aspetti incoraggianti: protagonista principale la continua e forte crescita delle energie rinnovabili, trainata dall'energia eolica e solare. Infatti, le energie rinnovabili hanno visto un aumento record di oltre il 40% di crescita dell'energia primaria nel 2019. Il carbone, invece, è sceso, per la quarta volta negli ultimi sei anni, al livello più basso degli ultimi 16 anni. Ma nonostante questo, il carbone rappresentava ancora il 36% dell'energia globale nel 2018, rispetto al 10% di energia rinnovabile. Queste cifre dimostrano che la decarbonizzazione è ancora molto lontana e che le energie rinnovabili devono crescere sempre più rapidamente.

Nonostante gli aspetti incoraggianti di cui sopra, le emissioni di carbonio sono la preoccupazione maggiore nello scenario energetico globale. L'andamento delle emissioni di carbonio mostra un rallentamento dello 0,5 % nel 2019. Questa decelerazione deve essere però osservata nel contesto del forte aumento delle emissioni nel 2018: +2.1 %. La speranza del settore energetico era che il terribile aumento nel 2018 fosse attenuato da una drastica diminuzione nel 2019. Questo calo delle emissioni non si è verificato, la crescita media annua delle emissioni di carbonio nel 2018 e nel 2019 è stata superiore alla sua media decennale.

Questi dati hanno dimostrato quanto sia necessario un riavvio sostenibile dal punto di vista ambientale dalla stagnazione portata da COVID-19. Lo sconvolgimento della vita quotidiana della società ha portato a una migliore qualità dell'aria e a basse emissioni ponendo davanti agli occhi una realtà pulita, possibili sono con un drastico cambiamento.

L'IAE (International Energy Agency) stima che le emissioni globali di anidride carbonica potrebbero diminuire di 2,6 gigatoni nel 2020. La sfida di raggiungere lo zero netto nel 2050 può essere vinta solo attraverso un cambiamento radicale delle abitudini e dei consumi. Infatti, un uso più responsabile dell'energia aiuterà a raggiungerlo. L'energia in questione dovrà essere a bassa emissione di carbonio: rinnovabili, elettrificazione, CCUS (uso e stoccaggio del carbonio), bioenergia, ecc.

Tabella 1 *Quote e contributi per i combustibili primari nel 2019.*

Fonte di energia	Consumi [exajoules]	Cambiamento annuale [exajoules]	Quota di energia primaria [%]	Variazione percentuale di un'azione a partire dal 2018 [%]
Oil	193.0	1.6	33.1	-0.2
Gas	141.5	2.8	24.2	0.2
Carbone	157.9	-0.9	27.0	-0.5
Rinnovabili*	29.0	3.2	5.0	0.5
Idro	37.6	0.3	6.4	-0.0
Nucleare	24.9	0.8	4.3	0.1
Total	**583.9**	**7.7**		

*** energia rinnovabile (esclusa l'energia idroelettrica) più biocarburanti**

Per concludere, la spinta verso le energie rinnovabili è una questione aperta e necessaria per raggiungere lo zero netto di emissioni nel 2050. Il fotovoltaico e il solare a concentrazione rappresentano una grande opportunità per sfruttare la forte radiazione solare che ogni giorno colpisce il globo terrestre, una radiazione continua che può essere sfruttata al massimo della tecnologia disponibile. Di seguito è riportata una panoramica delle principali tecnologie fotovoltaiche esistenti dalle loro generazioni fino al DSSC.

III. Il fotovoltaico

Il fotovoltaico consiste nella produzione di elettricità o di tensione da parte di fotoni dalla luce del sole. Il metodo sviluppato è un metodo diretto in cui un substrato semiconduttore genera elettroni grazie all'eccitazione da parte di fotoni con energia sufficiente. Lo scenario mondiale della produzione di energia ha messo in chiarezza come il solare (fotovoltaico più solare a concentrazione) rappresenti una buona fetta della produzione globale di energia sostenibile e che il fotovoltaico ne sia principalmente il protagonista.

Nel 1839 A.E. Becquerel scoprì per la prima volta l'effetto fotovoltaico, mostrando il principio di base di una cella solare. Nel corso degli anni la tecnologia ha visto molti miglioramenti grazie alla ricerca scientifica. Ora le celle solari possono essere classificate in tre generazioni:

1) Prima generazione: celle composte da substrati monocristallini o policristallini a base di silicio.
2) Seconda generazione: utilizzo del silicio insieme ad altri semiconduttori come l'arseniuro di gallio (GaAs) e il tellururo di cadmio (CdTe), un miglioramento della prima generazione.
3) Terza generazione: vengono introdotte celle solari sensitizzate con coloranti, le celle organiche, le celle a perovskite e i quantum dots.

IV. Celle solari sensitizzate con colorante

Le celle solari sensitizzate con colorante (DSSC), o anche note come celle di Grätzel, sono unità fotoelettrochimiche utilizzate come alternative a quelle a base di silicio. La prima cella è stata testata nel 1991 da O'Regan e Grätzel e ha raggiunto un'efficienza del 7,1-7,9 %, attraverso un processo a basso costo con una realistica efficienza di conversione energetica in un contesto industriale e civile.

Le DSSC sono composte da:

- Una superficie conduttiva trasparente di ossido (TCO), su entrambi i lati. Questo tipo di substrato deve permettere alla luce di incidere e penetrare facilmente, facilitare il trasporto della carica verso il circuito esterno, avere una buona trasparenza alla luce nella regione visibile e infrarossa ed essere stabile alle alte temperature (nel processo di sinterizzazione fino a 500 °C).
- Materiali semiconduttori, principalmente ossidi metallici come TiO_2, ZnO e SnO_2. Il biossido di titanio è l'anodo semiconduttore più utilizzato nei DSSC; si presenta in varie forme cristalline: anatasio, brookite e rutilo. Il rutilo è termodinamicamente più stabile ma l'anatasio ha un'alta conducibilità, per questo è preferito nelle DSSC.
- Il colorante, necessario per consentire l'assorbimento delle radiazioni, sia nella regione del visibile che in quella dell'infrarosso.
- L'elettrolita gioca un ruolo molto importante. Esso rigenera la molecola di colorante ossidata attraverso il meccanismo di trasferimento: gli elettroni del gruppo di circuito esterno al catodo, passando attraverso l'elettrolita, rigenerano il colorante fino al suo stato fondamentale. Può essere solido, liquido o quasi-solido.
- Il contro elettrodo (CE) è l'ultima parte che chiude il circuito, raccoglie gli elettroni provenienti dal circuito esterno e catalizza la riduzione dell'elettrolita. La necessità di catalizzare il trasferimento di carica è quella di superare le resistenze tra FTO e l'elettrolita. Il materiale più comunemente usato come CE è il platino, ottenuto dalla decomposizione termica dell'acido esacloroplatinico (H_2PtCl_6). Il platino è un metallo raro e molto prezioso; inoltre, il costo di produzione è estremamente elevato grazie alle alte temperature raggiunte; per questi motivi la ricerca scientifica sta esplorando nuovi materiali utilizzabili che siano più ecosostenibili e meno costosi. In alternativa, la ricerca sta indagando l'uso del PEDOT come CE. Il PEDOT è un polimero, ed è il polimero più usato come CE, spesso usato con additivi e drogato con PSS. Ad esempio, il PEDOT è spesso studiato in combinazione con il carbonio unendo le proprietà del polimero con le proprietà conduttive e morfologiche del carbonio. Le sue caratteristiche, la facilità di produzione e il basso costo lo rendono competitivo anche a livello industriale, per produrre DSSC prive di Pt.

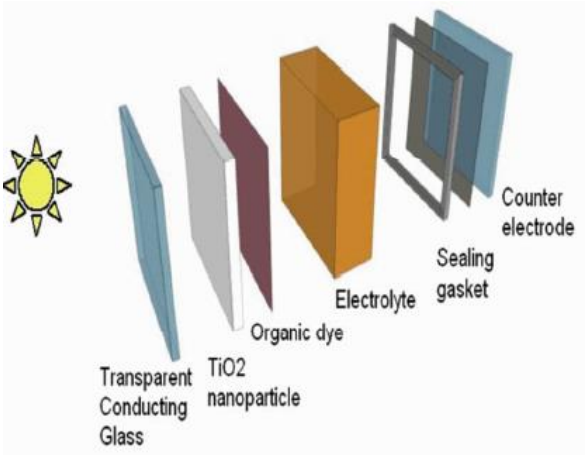

Figura 1 *Componenti principali di una cella solare sensitizzata con colorante.*

A differenza delle classiche celle solari, nelle DSSC la luce del sole viene trasportata per mezzo di molecole di colorante. Queste molecole sono legate al materiale semiconduttore. Dopo l'assorbimento della luce solare, la separazione delle cariche elettriche avviene nell'interfaccia dye-TiO_2.

Il funzionamento di un DSSC è concettualmente simile al processo di fotosintesi naturale nelle piante. Nel caso della tecnologia DSSC il colorante ha il ruolo della clorofilla, cioè assorbe la radiazione solare. Il processo avviene attraverso:

- l'assorbimento della luce solare con conseguente eccitazione degli elettroni nelle molecole del colorante;
- l'iniezione di elettroni nello strato di TiO_2 e la separazione della carica;
- reazione redox tra elettrolita e CE.

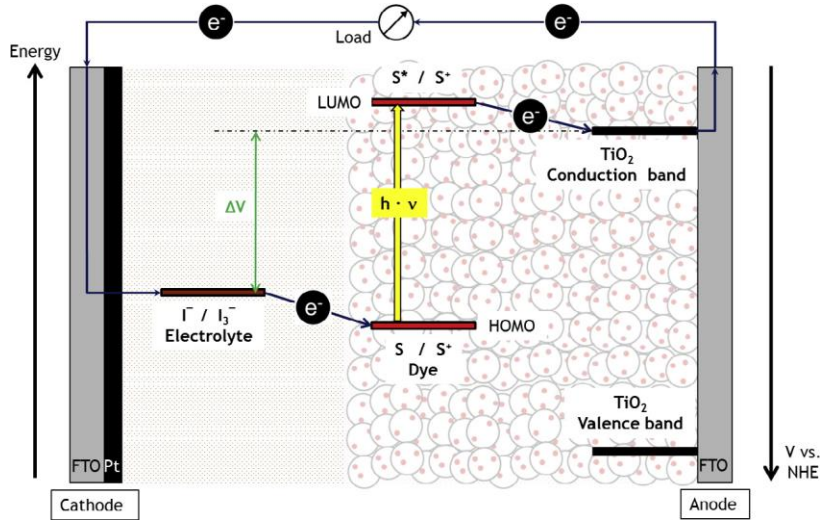

Figura 2 *Esempio schematico del meccanismo di funzionamento che coinvolge i livelli energetici della titania abbinati a quelli del colorante.*

V. Test effettuati sulle DSSC

In modo tale da rendere più agevole la lettura della review sono riportati i principali test eseguiti per la caratterizzazione delle DSSC.

L'analisi morfologica attraverso misure SEM, TEM, FE-SEM e AFM. A seconda del tipo di CE, è utile analizzare la sua morfologia superficiale in quanto: più lo strato è poroso, migliore è la permeazione dell'elettrolita e più sono attivi i siti per catalizzare la sua reazione di riduzione. Infatti, molto spesso il PEDOT viene utilizzato in combinazione con il carbonio con forme diverse, perché è possibile creare particolari conformazioni che aumentano notevolmente la superficie del CE.

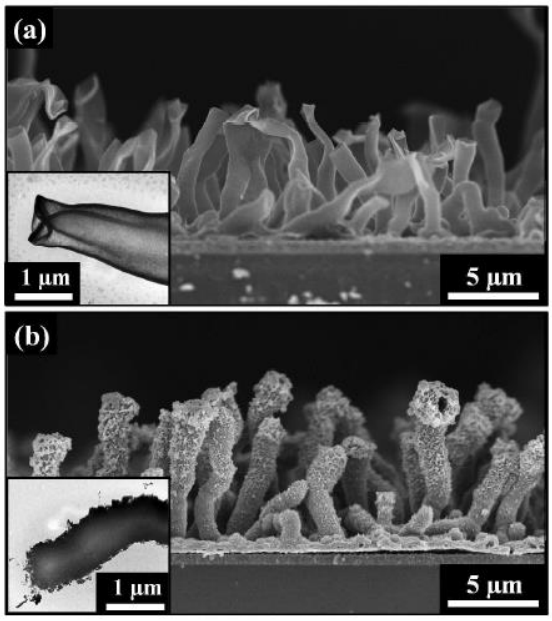

Figura 3 *Esempio di immagini FE-SEM. Il catodo in questione è PEDOT-MeOH: a) matrici di tubi e b) matrici di coralli a tubi.*

Voltammetria ciclica. La voltammetria ciclica (CV) viene eseguita per esplorare la cinetica di reazione della reazione elettrolitica redox e per valutarne l'attività elettrocatalitica. La soluzione elettrolitica più comunemente usata è quella allo iodio, sfruttante la coppia redox I^-/I_3^-, quindi sarà presa come esempio con PEDOT come CE. Le curve possono essere realizzate anche variando la densità di carica.

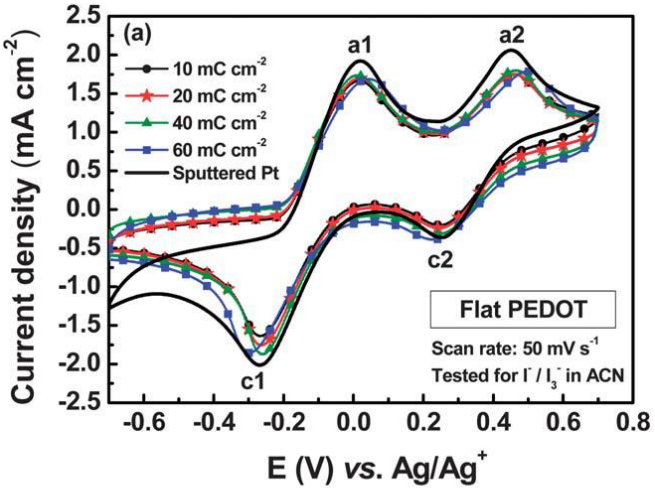

Figura 4 *Esempio di voltammetria ciclica eseguita su un catodo di PEDOT.*

Electrochemical Impedance Spectroscopy. Le misure EIS sono effettuate in modo da indagare le resistenze interne delle celle e cercare di spiegare l'andamento dei parametri fotovoltaici ottenuti. Ad esempio, il fill factor è molto influenzato dalle resistenze interne.

Curve J-V o I-V per valutarne le prestazioni fotovoltaiche. Le celle vengono simulate tramite un simulatore solare ottenendo così uno spettro J.V da cui si possono ricavare i parametri fondamentali per caratterizzare la cella:

- Voc: tensione a circuito aperto, misurata quando la corrente raggiunge 0 A.
- Jsc: densità di corrente di corto circuito, calcolata quando la tensione è di 0 V.
- FF: fattore di riempimento, è un valore compreso tra 0 e 1 che descrive la forma della curva J-V; un valore alto indica una curva rettangolare che è quella preferibile nelle DSSC.
- PCE: efficienza di conversione di potenza, è l'efficienza della cella.

VI. Sezione di review

Il corpo principale di questo elaborato consiste in una Review che indaga: il PEDOT utilizzato come CE al posto del platino e il PEDOT utilizzato come trasportatore di lacune (hole transporting material, HTM), quindi al posto della soluzione elettrolitica. Entrambe le sezioni di review raccolgono gli elaborati disponibili in letteratura a partire dal primo anno (2002) fino al 2020.

Principalmente, il PEDOT utilizzato come CE è stato sempre studiato maggiormente rispetto al PEDOT usato al posto della soluzione elettrolitica. Andando avanti negli anni di studi e ricerca si può osservare come il PEDOT si avvicini sempre di più alle performance ottenute con il platino. È particolare anche osservare che in generale, la tecnologia delle DSSC si sia sviluppata, partendo da delle efficienze di 2.10 % e arrivando a toccare valori anche di 9.2 %.

Di seguito vengono riportati i principali risultati dei test J-V. Le tabelle sono suddivise a seconda del CE, partendo dal PEDOT puro e proseguendo verso le principali molecole utilizzate insieme al PEDOT (per esempio il PSS, Grafene etc).

Tabella 2 *Raccolta delle performance fotovoltaiche di celle basate sul PEDOT, nano-fibre di PEDOT (PEDOT NF), PEDOT nanotubi (PEDOT NT), e cPEDOT.*

CE	V_{OC} [V]	J_{SC} [mA cm^{-2}]	FF	η [%]
PEDOT (Pringle 2010)	0.78	14.1	0.73	8.0
Pt (Pringle 2010)	0.78	14.0	0.72	7.9
PEDOT (Ahmad 2010)	0.68	15.2	0.76	7.93
Pt (Ahmad 2010)	0.74	15.9	0.73	8.71
PEDOT (Zhang 2011)	0.74	10.3	0.63	4.84
Pt (Zhang 2011)	0.76	11.3	0.63	5.43
PEDOT NT (Trevisan 2011)	0.72	16.24	0.70	8.3
Pt (Trevisan 2011)	0.74	16.21	0.71	8.5
PEDOT NF (Lee 2012)	0.72	17.5	0.72	9.2
Pt (Lee 2012)	0.74	15.8	0.73	8.6
PEDOT (Nagarajan 2013)	0.77	10.2	0.72	5.78
Pt (Nagarajan 2013)	0.79	9.01	0.63	4.49
PEDOT NF (Li 2014)	0.72	12.52	0.68	6.19
Pt (Li 2014)	0.72	14.46	0.68	8.08
PEDOT (Chen 2014)	0.79	9.0	0.69	4.9
PEDOT (Gao 2014)	0.68	15.27	0.61	6.33
Pt (Gao 2014)	0.68	16.66	0.57	6.46
PEDOT (Koussi 2014)	0.70	3.6	0.56	1.4
Pt (Koussi 2014)	0.71	3.3	0.59	1.3
PEDOT (Ma 2015)	0.73	14.85	0.57	6.18
Pt (Ma 2015)	0.73	15.81	0.63	7.30
PEDOT (Chen 2015)	0.71	13.96	0.70	6.96
Pt (Chen 2015)	0.78	14.93	0.70	8.17
PEDOT (Han 2015)	0.73	14.18	0.68	7.42
PEDOT (Koussi 2015)	0.92	8.4	0.67	5.1
PEDOT (Mustafa 2017)	0.30	1.87	0.26	0.015
Pt (Mustafa 2017)	0.59	3.71	0.33	0.72
PEDOT (Li 2017)	0.76	17.72	0.67	9.12
PEDOT (Wu 2017)	0.64	8.69	0.66	3.26
PEDOT (Thuy 2017)	0.66	16.8	0.65	6.73
Pt (Thuy 2017)	0.64	15.9	0.65	6.73
PEDOT (Li 2017)	0.76	15.42	0.64	7.51
Pt (Li 2017)	0.76	15.60	0.65	7.71
PEDOT (Ma 2018)	0.78	15.23	0.58	6.88
Pt (Ma 2018)	0.78	17.03	0.63	8.33
PEDOT (Basri 2019)	0.66	4.05	0.52	1.39
Pt (Basri 2019)	0.59	3.68	0.52	1.14
PEDOT (Peri 2020)	0.63	14.30	0.48	4.30
cPEDOT (Bella 2020)	0.69	12.41	0.77	6.64
Pt (Bella 2020)	0.66	11.06	0.68	4.95

Tabella 3 Raccolta delle performance fotovoltaiche di celle basaste sul PEDOT:PSS.

CE	V_{OC} [V]	J_{SC} [mA cm^{-2}]	FF	η [%]
PEDOT.PSS (Saito 2002)	0.68	11.0	0.28	2.10
Pt (Saito 2002)	0.68	11.1	0.62	4.67
PEDOT:PSS (Park 2007)	0.65	10.78	0.36	2.49
Pt (Park 2007)	0.67	9.75	0.54	3.55
PEDOT:PSS (Xia 2007)	0.65	10.78	0.36	2.49
Pt (Xia 2007)	0.67	9.75	0.54	3.55
PEDOT:PSS (Hong 2008)	0.72	10.99	0.28	2.33
Pt (Hong 2008)	0.72	13.05	0.68	6.3
PEDOT:PSS (Yue 2012)	0.73	12.53	0.69	6.31
Pt (Yue 2012)	0.76	14.75	0.69	7.73
PEDOT:PSS (Yue 2013)	0.81	13.6	0.69	7.6
PEDOT:PSS (Guan 2013)	0.72	14.5	0.33	3.4
Pt (Guan 2013)	0.72	16.2	0.64	7.5
PEDOT:PSS (Song 2013)	0.71	15.0	0.39	4.2
PEDOT:PSS (Chang 2014)	0.68	12.96	0.49	4.36
Pt (Chang 2014)	0.70	15.80	0.69	7.63
PEDOT:PSS (Jeong 2015)	0.67	8.8	0.41	2.4
Pt (Jeong 2015)	0.68	10.9	0.63	4.6
PEDOT:PSS (Seo 2016)	0.72	16.39	0.72	8.27
Pt (Seo 2016)	0.73	14.75	0.71	7.59
PEDOT:PSS (Khalit 2019)	0.68	11.0	0.28	2.10

Tabella 4 *Raccolta delle performance fotovoltaiche di celle basate sul PEDOT-MWCNT (nanotubi di carbonio a più pareti), PEDOT-CNT (nanotubi di carbonio).*

CE	V_{OC} [V]	J_{SC} [mA cm^{-2}]	FF	η [%]
PEDOT-MWCNT (Zhang 2011)	0.74	11.5	0.64	5.47
Pt (Zhang 2011)	0.76	11.3	0.63	5.43
PEDOT-CNT (Shin 2002)	0.70	9.0	0.73	4.62
PEDOT:PSS-MWCNT (Yun 2013)	0.71	12.4	0.63	6.0
PEDOT:PSS-CNT (Guan 2013)	0.73	16.1	0.71	8.3
Pt (2002)	0.73	16.2	0.64	7.5
PEDOT-MWCNT (Li 2017)	0.79	17.09	0.67	9.07
Pt (Li 2017)	0.76	15.60	0.65	7.71
PEDOT:PSS-MWCNT (Yun 2018)	0.81	12.9	0.55	5.8

Tabella 5 *Raccolta delle performance fotovoltaiche di celle basate sul PEDOT-TsO.*

CE	V_{OC} [V]	J_{SC} [mA cm^{-2}]	FF	η [%]
PEDOT-TsO (Saito 2002)	0.67	11.2	0.61	4.60
Pt (Saito 2002)	0.68	11.1	0.62	4.67
PEDOT-TsO (Xia 2007)	0.68	9.5	0.63	4.1
Pt (Xia 2007)	0.68	9.8	0.65	4.3
PEDOT-TsO (Li 2017)	0.72	14.25	0.48	4.93
Pt (Li 2017)	0.75	14.44	0.65	7.05

Tabella 6 *Raccolta delle performance fotovoltaiche di celle basate sul PEDOT-ClO_4^-, PEDOT:PSS-ClO_4^-.*

CE	V_{OC} [V]	J_{SC} [$mAcm^{-2}$]	FF	η [%]
PEDOT-ClO_4^- (Xia 2007)	0.68	9.6	0.66	4.2
Pt (Xia 2007)	0.68	9.8	0.65	4.30
PEDOT-ClO_4^- (Jang 2009)	0.76	1.98	0.55	1.23
Pt (Jang 2009)	0.77	11.85	0.55	1.23

Tabella 7 *Raccolta delle performance fotovoltaiche di celle basate su: PEDOT:PSS-Grafene, PEDOT-EFG (grafene esfoliato), PEDOT-NGr (nano grafene), PEDOT-PPT-RGO (grafene ossido ridotto), PEDOT:PSS-GD (punti di grafene).*

CE	V_{OC} [V]	J_{SC} [$mAcm^{-2}$]	FF	η [%]
PEDOT:PSS-Grafene (Hong 2007)	0.72	12.96	0.48	4.5
Pt (Hong 2007)	0.72	13.05	0.68	6.3
PEDOT-EFG (Nagarajan 2013)	0.77	10.2	0.72	5.78
Pt (Nagarajan 2013)	0.79	9.01	0.63	4.49
PEDOT:PSS-Grafene (Yue 2013)	0.77	15.7	0.65	7.86
PEDOT-NGr (Chen 2015)	0.74	15.60	0.72	8.30
Pt (Chen 2015)	0.78	14.93	0.70	8.17
PEDOT-PPY-rGO Sekkarapatti 2015)	0.76	17.0	0.55	7.1
Pt (Sekkarapatti 2015)	0.78	19.2	0.62	9.3
PEDOT:PSS-rGO (Jeong 2015)	0.73	10.4	0.68	5.1
Pt (Jeong 2015)	0.68	10.9	0.63	4.6
PEDOT:PSS-GD (Lee 2013)	0.72	7.36	0.70	7.36
PEDOT-GO (Mustafa 2017)	0.65	2.026	0.51	0.68
Pt (Mustafa 2017)	0.59	3.71	0.33	0.72
PEDOT-rGO (Ma 2018)	0.73	15.82	0.66	7.56
Pt (Ma 2018)	0.78	17.03	0.63	8.33
PEDOT:Al_2O_3-rGO (Khalit 2019)	0.58	7.4	0.50	2.15

Da come si può osservare nei dati riportati nelle tabelle la tecnologia delle DSSC utilizzanti PEDOT ha efficienze comparabili con quelle del Pt. Andando avanti negli anni si nota anche che le efficienze salgono gradualmente. Questa crescita è probabilmente dovuta ad un miglioramento della tecnologia stessa con l'avanzare della ricerca.

In generale si può osservare che il PEDOT:PSS raggiunge valori di efficienza minori di quelli del PEDOT puro. Infatti il PEDOT:PSS presenta fenomeni di repulsione quando si trova in contatto intimo con l'elettrolita I^-/I_3^-, il PEDOT non è affetto da questa complicazione.

Per quanto riguarda il PEDOT utilizzato come HTM nelle DSSC il bacino di articoli e scritti risulta nettamente minore. In generale non si è quasi mai riuscito a raggiungere efficienze elevate come quelle ottenute da un comune elettrolita allo iodio. Di seguito vengono riportati a scopo esplicativo alcuni risultati delle prove J-V effettuate su celle utilizzanti PEDOT come trasportatore di lacune.

Tabella 8 *Esempi di PEDOT utilizzato come trasportatore di lacune nelle DSSC.*

HTM	V_{OC} [V]	J_{SC} [mAcm^{-2}]	FF	η [%]
PEDOT (Saito 2002)	0.34	48E-3	0.33	5.4E-3
PEDOT (Liu 2010)	0.86	9.3	0.75	6.1
PEDOT (Liu 2012)	0.93	10.1	0.76	7.1
DNA-PEDOT:PSS (Jayme 2016)	0.54	0.56	0.25	0.08

VII. Sezione sperimentale

VII.I Procedure effettuate in laboratorio

La parte finale della tesi è costituita dall'esperienza di laboratorio svolta presso il DISAT del Politecnico di Torino. Vengono descritti i processi di sintesi e produzione di DSSC composte da biossido di titanio come anodo, colorante N719, elettrolita a base di I^-/I_3^- e controelettrodi composti da platino o PEDOT. Le prestazioni fotovoltaiche sono state poi abbinate per confrontare e comprendere efficacemente la differenza tra una cella che utilizza il platino e una che utilizza il PEDOT.

I fotoanodi sono stati preparati a partire da una pasta precursore di titania. La pasta è stata stesa con la tecnica Doctor Blade su un'area di 5x5 mm spessa 55 µm. Dopo un trattamento termico a 450 °C per 30 min l'anodo è stato trattato con $TiCl_4$ in modo tale da aumentare l'area superficiale e la capacità di assorbimento dei fotoni. Dopo il trattamento i fotoanodi sono stati inseriti per 15 h nella soluzione di colorante in modo tale da permettere alle molecole del colorante di aderire alla superficie di titania.

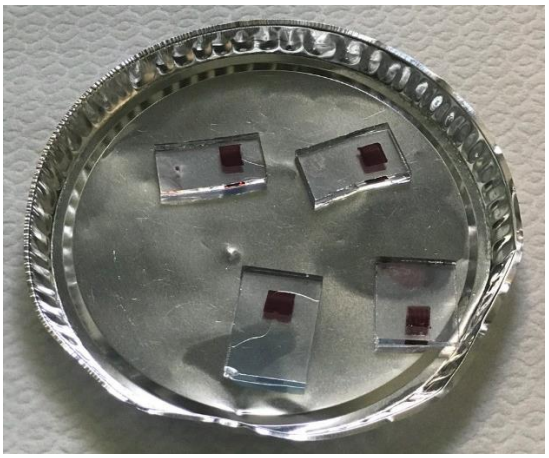

Figura 5 *Fotoanodi dopo 15 ore nel colorante.*

Il colorante utilizzato è stato l'N719 in etanolo. L'N719 è a base di rutenio ed è il colorante maggiormente utilizzato nel campo delle DSSC.

L'elettrolita utilizzato è stato quello a base di iodio sfruttante la coppia redox I^-/I_3^-. In questo caso si è optato per utilizzare un elettrolita gel, quindi chiudere una cella quasi solida. L'elettrolita gel è stato pensato per una questione di facilità a livello di chiusura e sigillatura. Il gelificante utilizzato è stato il PEO (polietilene ossido PM: 400000 g/mol).

I catodi utilizzati sono stati: 4 di PEDOT steso a 40 rps, 4 di PEDOT steso a 20 rps e 4 di platino.

I catodi in PEDOT sono stati stesi con uno spin coater e poi sono stati cotti in forno per 30 min a 70 °C. I catodi in Pt invece sono stati depositati con micropipetta e sono poi stati cotti in forno a 450 °C. Il processo è stato ripetuto due volte. È subito evidente come il platino risulti molto più dispendioso a livello energetico in confronto al PEDOT. Queste due ricotture sono una grande spesa energetica in confronto alla cottura del PEDOT a 70 °C.

VII.II Chiusura delle celle

La chiusura della cella è stata effettuata tramite una pressa termo-riscaldata. L'iter seguito per la chiusura della cella è stato: inserire il catodo con la faccia conduttiva verso l'alto, appoggiare una cornice di materiale termoplastico (dimensioni: diametro interno 6 mm e diametro esterno 10 mm), premurarsi di appoggiare la cornice in un zona in cui il PEDOT risulti ben distribuito e uniforme, depositare sull'area 5x5 di TiO_2 2 µg di elettrolita e chiudere la cella inserendo l'area attiva di TiO_2 in corrispondenza della cornice. Successivamente pressare a circa 1 bar per 20 s con la piastra superiore riscaldata a 105 °C.

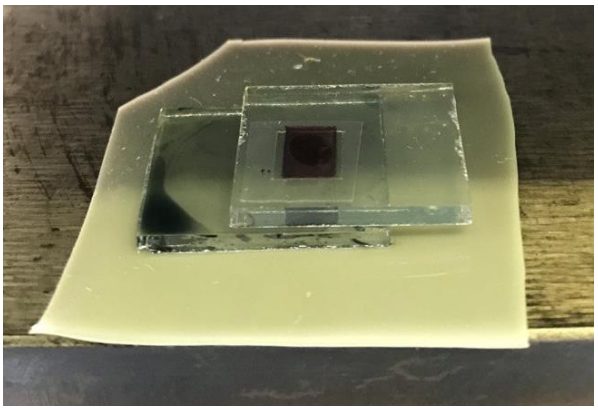

Figura 6 *Chiusura della cella mediante piastra riscaldata. Il vetro in basso è il catodo di PEDOT, in mezzo è possibile osservare il materiale termoplastico e sopra la porzione del fotoanodo inserita nella cornice.*

VII.III Caratterizzazione delle celle

Una volta che le celle sono state chiuse sono state eseguite prove sotto simulatore solare. Le prove sono poi state ripetute ogni giorno possibile in modo tale da investigare l'invecchiamento delle celle prodotte.

VII.IV Conclusioni

In generale le celle utilizzanti PEDOT hanno ottenuto performance fotovoltaiche nettamente minori rispetto a quelle utilizzanti il platino. Soprattutto le prime 4 celle (PEDOT steso a 40 rps) hanno ottenuto valori di efficienza inferiori all'1 %, invece le ultime 4 hanno raggiunto valori di efficienza di 1.45 %. Essendo lo spessore del film di PEDOT inversamente proporzionale rispetto alla velocità di stesura del macchinario (lo spessore del PEDOT steso a 40 rps sarà minore di quello steso a 20 rps) le celle con il film più sottile hanno dimostrato efficienze più scarse di quelle con il film più spesso. Lo spessore del catodo quindi affligge molto le performance.

In Tabella 9 e

Tabella 10 si possono osservare i valori mediati di performance fotovoltaiche con i corrispettivi errori.

Tabella 9 *Performance fotovoltaiche mediate delle 8 celle al PEDOT con i rispettivi errori.*

Day	V_{OC} [V]	J_{SC} [mA cm^{-2}]	FF	η [%]
0	0,530 ± 0,06	6,93 ± 0,06	32,67 ± 0,25	1,2 ± 0,26
1	0,519 ± 0,09	5,77 ± 0,53	32,86 ± 0,44	1,0 ± 0,81
2	0,523 ± 0,12	5,61 ± 0,63	34,61 ± 0,43	1,0 ± 0,85
5	0,515 ± 0,09	3,50 ± 0,10	35,66 ± 0,40	0,6 ± 0,72
7	0,530 ± 0,08	3,68 ± 0,10	36,42 ± 0,35	0,6 ± 0,71
8	0,535 ± 0,08	3,39 ± 0,12	41,83 ± 0,42	0,7 ± 0,71
9	0,541 ± 0,06	3,16 ± 0,13	46,15 ± 0,52	0,7 ± 0,72

Tabella 10 *Performance fotovoltaiche mediate delle 4 celle al Pt con i rispettivi errori.*

Day	Voc [V]	Jsc [mA cm^{-2}]	FF	η [%]
0	0,529 ± 0,03	6,86 ± 0,34	66,34 ± 0,04	2,4 ± 0,32
1	0,521 ± 0,05	6,66 ± 0,33	66,21 ± 0,04	2,3 ± 0,41
4	0,526 ± 0,07	6,09 ± 0,26	67,21 ± 0,05	2,2 ± 0,32
5	0,527 ± 0,06	6,00 ± 0,22	67,47 ± 0,04	2,1 ± 0,27
6	0,528 ± 0,07	5,88 ± 0,20	68,38 ± 0,06	2,1 ± 0,28
8	0,528 ± 0,08	5,49 ± 0,20	68,31 ± 0,05	2,0 ± 0,22

Le proprietà fotovoltaiche di tutti i samples analizzati sono state raccolte in un grafico (Figura 7 e Figura 8) e studiate nel tempo. Si può osservare che:

- All'aumentare dell'invecchiamento il PEDOT presenta una buona stabilità. Infatti il Voc cresce dopo una iniziale oscillazione; il FF rimane pressoché stabile con un leggero aumento; Jsc presenta un andamento decrescente così come l'efficienza. Le celle composte con il PEDOT come catodo sono state testate innumerevoli volte sotto simulatore solare in quanto era difficile stabilizzarle.
- Il platino invece presenta andamenti leggermente diversi: il Voc dopo un iniziale decrescita aumenta in maniera consistente; Jsc invece cala in maniera graduale; FF aumenta costantemente con il passare del tempo, suggerendo una stabilizzazione e rimodifica interna della cella consistente; l'efficienza rimane pressoché costante.

In generale il platino possiede più stabilità nel tempo rispetto al PEDOT ma nonostante questo i gravi e dispendiosi problemi portati dall'utilizzo dello stesso non precludono al PEDOT di essere una valida e sostenibile alternativa.

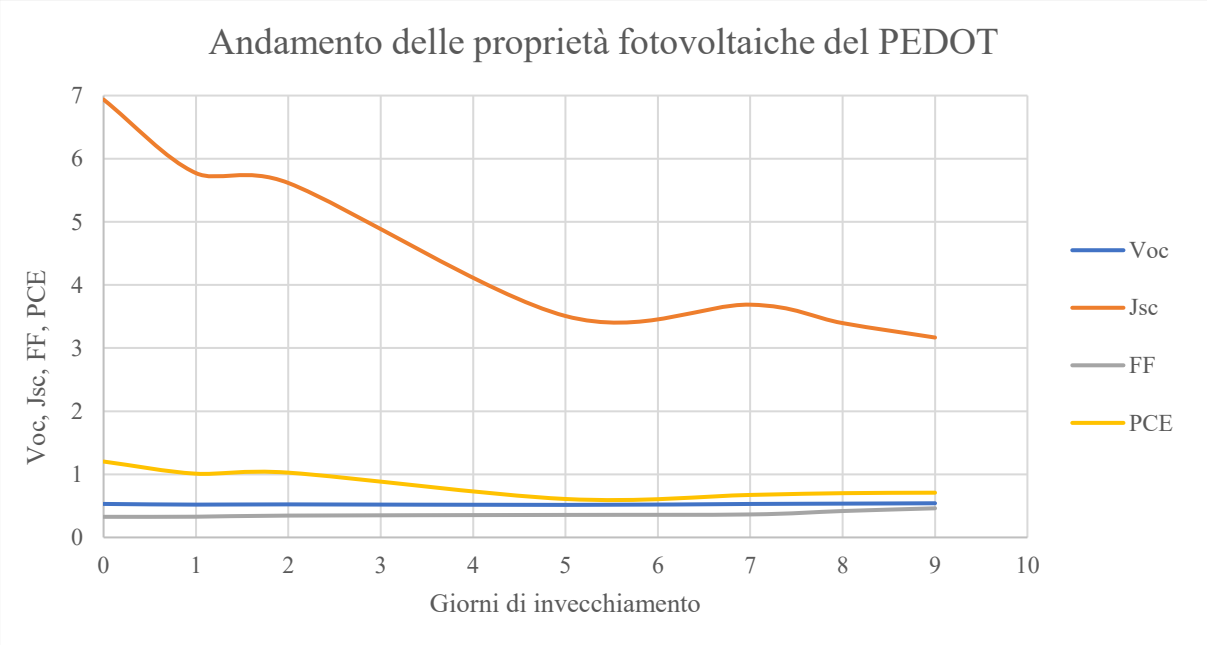

Figura 7 *Andamento delle proprietà fotovoltaiche delle celle basate sul PEDOT testate in laboratorio.*

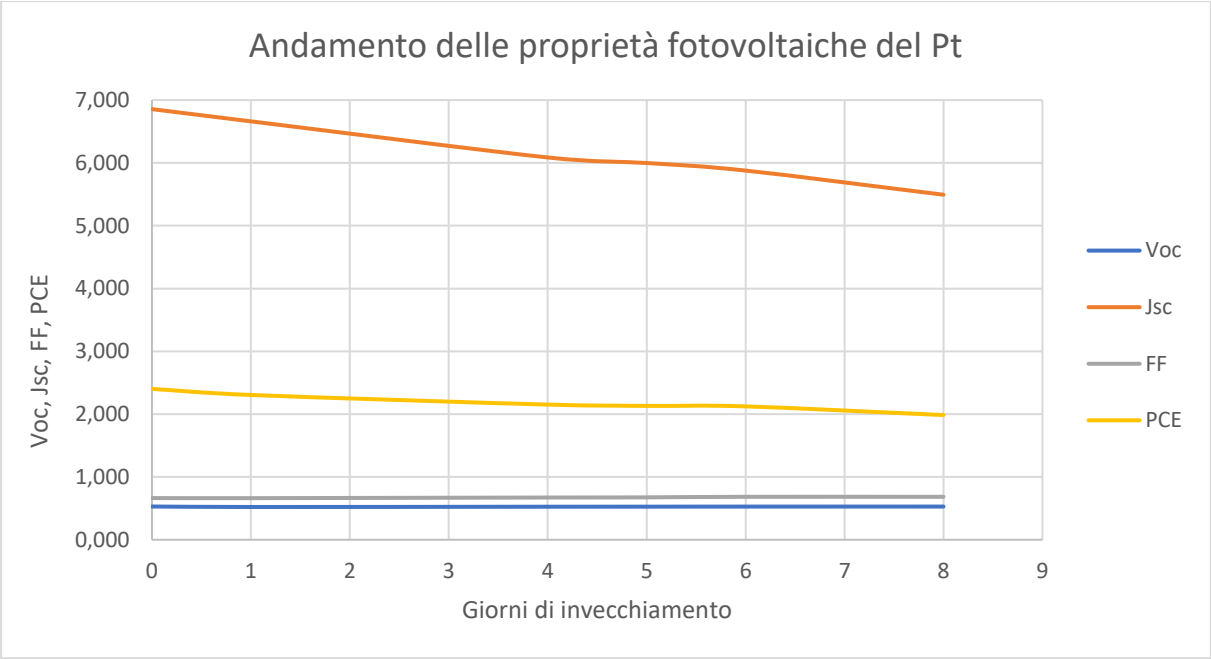

Figura 8 *Andamento delle proprietà fotovoltaiche delle celle basate sul Pt testate in laboratorio.*

Un altro fenomeno osservatosi nelle celle utilizzanti il PEDOT è una variazione della forma della curva I-V prodotta tramite le simulazioni. In principio infatti si può notare che le celle "giovani" possiedono un avvallamento nella curva. Andando avanti con l'invecchiamento questo avvallamento scompare. Questo fenomeno è stato attribuito alla natura di polimero del PEDOT. Infatti il PEDOT interagisce sempre più intimamente con l'elettrolita trasformando via via l'interfaccia tra i due. Invece il platino non presenta queste variazioni, il rapporto tra il metallo e l'elettrolita rimane inalterato all'invecchiare della cella. Questo fenomeno si può osservare in Figura 9.

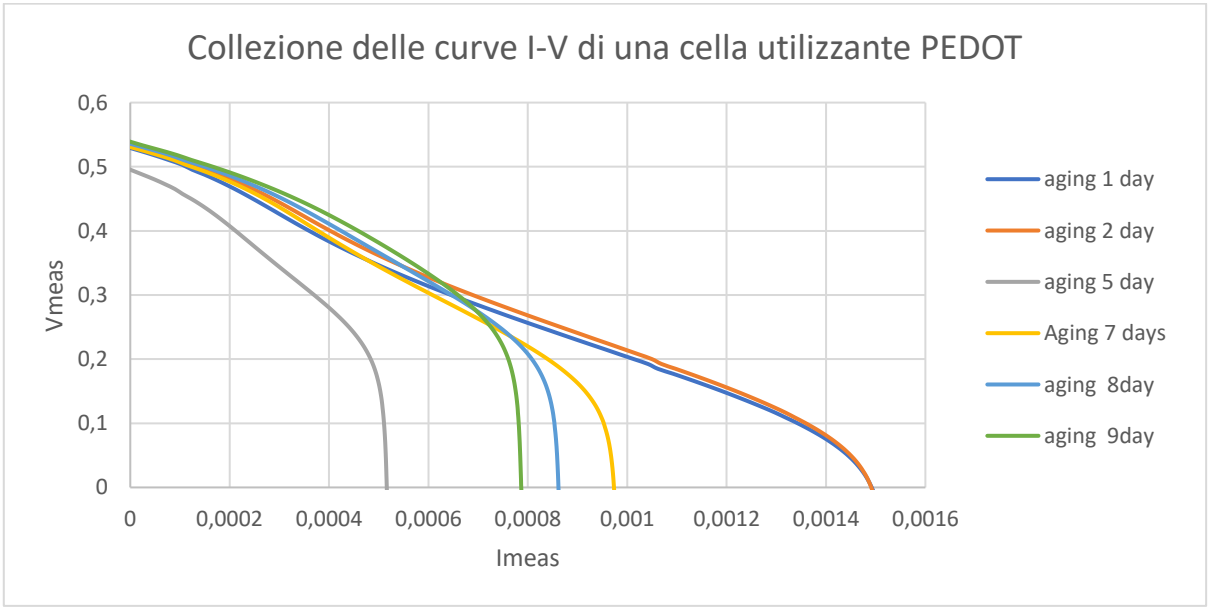

Figura 9 *Evoluzione delle curve J-V della cella utilizzante il PEDOT.*

VIII. Conclusioni

In conclusione, il PEDOT è un buon candidato per la sostituzione del platino nelle celle solari sensitizzate al colorante. La ricerca scientifica ha portato avanti innumerevoli prove e test che spaziano in tutte le proprietà delle DSSC confermando come il PEDOT sia versatile e prossimo alla sua applicazione su larga scala.

L'esperienza di laboratorio ha portato ad efficienze relativamente basse ma, considerando che il PEDOT non era stato trattato in nessun modo e che l'unico trattamento effettuato è stato quello con il perclorato di titano sugli anodi, le efficienze si avvicinano comunque ad una semplice cella utilizzante il platino.

Sommario

Acronyms and symbols

Acronyms & Symbols	Meaning
AFM	Atomic force microscope
ATO	Antimony tin oxide
CB	Conduction band
Cb	Carbon black
CCNT	Coiled carbon nanotube
CE	Counterelectrode
CNT	Carbon nanotube
CV	Cyclic voltammetry
DBSA	Dodecylbenzenesulfonic acid
DMSO	Dimethyl sulfoxide
DNA	Deoxyribonucleic acid
DSSC	Dye-sensitized solar cell
EDS	Energy dispersion spectra
EDX	Energy dispersive X-ray
EFG	Exfoliated graphite
EG	Ethylene glycol
FE-SEM	Field emission scanning electron microscope
FTIR	Fourier transform infrared
FTO	Fluorine tin oxide
GD	Graphene dot
GnP	Graphene nanoplatelet
GO	Graphene oxide
HEC	Hydroxyethyl cellulose
HFIP	Hexafluoro isopropanol
HNT	Halloysite nanotube
HOMO	Highers occupied molecular orbital
HR-TEM	High resolution transmission electron microscope
HTM	Hole transporting material
ILE	Ionic liquid electrolyte
Im	Imidazole
IPCE	Incident photo converted electron
ITO	Indium tin oxide
Jsc	Short circuit current density
LUMO	Lowest unoccupied molecular orbital
MFA	Microflower array
MWCNT	Multi walled carbon nanotube
NC	Nanocrystal
NCC	Nanocrystalline cellulose
NGR	Nitrogen doped graphene
NMR	Nuclear magnetic resonance
NW	Nanowire
OMLD	Oxidative molecular layer deposition
PAA	Polyacrylic acid
PC	Propylene carbonate
PCE	Power conversion efficiency
PEDOT	Poly(3,4-ethylenedioxythiophene)

PEDOT:PSS	poly(3,4-ethylenedioxythiophene) polystyrene sulfonate
PEDOT-TsO	Tosylate-doped PEDOT
PEG	Polyethylene glycol
PEO	Polyethylene oxide
PEP	Photo electrochemical polymerization
PET	Polyethylene terephthalate
PIL	Polymeric ionic electrolyte
PMMA	Poly(methyl methacrylate)
POM	Polyoxometalate
PPY	Polypirrole
PS	Polystyrene
PV	Photovoltaic
PVA	Polyvinyl alcohol
QSS-DSSC	Quasi-solid state dye-sensitized solar cell
rGO	Reduced graphene oxide
RMS	Root mean square
SDS	Sodium dodecyl sulphate
SEM	Scanning electron microscope
SNP	Silicon nanosphere
ss-DSSC	Solid-state dye-sensitized solar cell
SSP	Solid state polymerization
SWCNH	Singla walled carbon nanohorn
TA	Tube array
TCA	Tube coral array
TCO	Transparent tin oxide
TEM	Transmission electron microscope
TGA	Thermo gravimetric analysis
TiN NP	Titanium nitrate nanoparticles
TiN NR	Titanium nitrate nanorod
TiN NS	Titanium nitrate nanosphere
Voc	Open circuit potential
XPS	X-ray photoelectron spectroscopy
XRD	X ray diffraction
Z	Impedance
η	Efficiency

1 Introduction

In recent years, the main problems addressed are global warming and the energy demand. Combining the strong industrialization of recent decades with the increase in population, energy demand has increased sharply. It is clear, however, that this increase cannot be met by fossil fuels alone as they are limited. Great attention is therefore being paid to the development of renewable technologies, which strongly limit the impact of pollutants and the emission of carbon dioxide.

The main renewable sources are hydroelectric, solar, geothermal and biomass derived energy. The main energy source that has created the biggest expectations in an eco-sustainable future is solar energy, as the radiation incident on the Earth is considerable and it does not cause chemistry- or noise-related pollution forms.

To face to large use of fossil fuels and the issues concerning cost, recycling and disposal of photovoltaic panels, research groups are now working to produce a greener and more sustainable photovoltaic technology, replacing noble, rate and harmful elements, along with any other dangerous substances contained present in the devices. One of the most interesting option is given by dye-sensitized solar cells (DSSCs): they represent a markedly different scenario with respect to silicon, being composed of two conductive glasses, an oxide semiconductor, a dye, an electrolyte and a cathode.

In the first part of this Thesis, the current energy scenario is briefly presented, then the main photovoltaic technologies based on crystalline silicon (first generation), thin films (second generation) and hybrid materials (third generation) are presented. Subsequently, the technology involving DSSCs with all its components and working principle is described in detail. Afterwards, the main investigation techniques developed for DSSCs characterization are presented in order to ease document reading. The core of the bibliographic work is a review on the use of poly(3,4-ethylenedioxythiophene) (PEDOT) as a replacement for both Pt (the traditional cathodic component) and liquid/quasi-solid electrolytes based on redox shuttles (thus proposing PEDOT as a hole transporting material, HTM). The review first investigates PEDOT (Poly(3,4-ethylenedioxythiophene)) as cathode in DSSCs, describing the most significant advances published after the seminal paper in 2004; after that, the performance of PEDOT as HTM in solid-state DSSCs is described. After the review section, a brief report is presented, where the laboratory experience carried out during the last part of my Thesis is described.

2 Global energy scenario

The pandemic we are now facing has created a huge economic and health shock designed to reshape the global economy [1]. This situation highlights the opportunity to change trends and accelerate emerging ones by shifting the energy situation towards a more sustainable path. The forced stop brought by COVID-19 has highlighted the main long-term challenges, such as climate change.

The scenario presented in 2019 shows some encouraging aspects: the continuous and strong growth of renewable energy, driven by wind and solar sources. In fact, renewable energy saw a record increase of over 40% in primary energy growth in 2019 [1]. Coal, on the other hand, has fallen, for the fourth time in the last six years, to its lowest level in 16 years. Despite this, coal still accounted for 36% of global energy in 2018, compared to 10% by renewable energy. These data show that decarbonisation is still a long way off and that renewable energy needs to grow more and more rapidly.

Despite the encouraging aspects mentioned above, carbon emissions are the biggest concern in the global energy scenario. The trend in carbon emissions shows a slowdown of 0.5% in 2019, but this deceleration must be observed in the context of the large increase in emissions in 2018: +2.1% [1]. The hope of the energy sector was that the appalling increase in 2018 would be dampened by a drastic decrease in 2019. This fall in emissions did not happen, the average annual growth in carbon emissions in 2018 and 2019 was higher than its 10-year average.

These data show how much an environmentally sustainable restart from the stagnation brought by COVID-19 is necessary. The upheaval in the daily life of society has led to better air quality and low emissions: we can try to keep these better conditions as a standard for our world.

The International Energy Agency (IAE) estimates that global CO_2 emissions could fall by 2.6 gigatons by 2020. The challenge of reaching net zero in 2050 can only be achieved through a radical change in habits and consumption. In fact, a more responsible use of energy will help to reach net zero, and this energy will have to be a low-carbon form, e.g. from renewable sources, based on electrified systems, following carbon capture, use and storage (CCUS) guidelines, etc.

These data emerged from the analysis of 2019 global energy scenario:

- **Carbon emissions**: from energy use, they grew by 0.5%, less than the 10-year average (1.1% per year), while 2018 showed an unusual and very strong growth of 2.1% [1].
- **Oil consumption**: it grew with a value below the average of 0.9 million barrels per day (b/d or 0.9%) [1]. Demand for all liquid hydrocarbons (including biofuels) increased by 1.1 million b/d and exceeded 100 million b/d for the first time ever; the main request came from China, with a consumption of 680 000 b/d, followed by other emerging economies.
- **Natural gas**: its consumption increased by 78 billion cubic metres (bcm) or 2%, well below the abnormal growth recorded in 2018 (5.3%) [1]. Despite these figures, the share

of gas in primary energy increased up to a record of 24.4%. The demand for gas and its sudden increase was driven by the United States (with 27 billion m^3) and China (with 24 billion m^3). Russia and Japan showed declines (10 and 8 billion m^3, respectively). The United States also contributed massively to the growth in gas production, covering 2/3 of the 132 billion m^3. Australia and China also contributed massively to this growth.

- **Coal**: its consumption decreased by 0.6% and its share fell to the lowest level ever recorded in the last 16 years [1]. So far, coal use was located in China (1.8 Exajoules) and Indonesia (0.6 Exajoules). The biggest drops in consumption have been recorded in USA and Germany (-1.1 EJ and -0.3 Exajoules, respectively).
- **Renewables**: a big increase in their use was detected (including biofuels), a record in terms of energy consumption (3.2 EJ) [1]. This represented the biggest increase detected in 2019 among all the energy sources. Wind energy made the largest contribution (1.4 EJ), followed by solar energy (1.2 EJ). China is once again a major player, with 0.8 EJ followed by USA and Japan (0.3 and 0.2 EJ, respectively). Hydroelectric consumption increased by less than 0.8% on average.
- **Nuclear**: nuclear energy consumption increased by 3.2%, the fastest growth since 2004 [1]. China (0.5 EJ) and Japan (0.1 EJ) provided the largest increases).
- **Electricity**: its production increased by 1.3% when compared to the average of the last 10 years [1]. China currently accounts for 90% of net global growth. The share of renewable energy aimed at producing electricity for the first time surpassed that of nuclear power, from 9.3% to 10.4%, followed by natural gas. The share of coal, on the other hand, is the lowest contribution ever recorded (data set started in 1985).

Table 1 lists the data described above.

Table 1 *Primary energy fuel shares and contributions in 2019. Adapted and reprinted with permission from [1].*

Energy source	Consumption [exajoules]	Annual change [exajoules]	Share of primary energy [%]	Percentage point change un share from 2018 [%]
Oil	193.0	1.6	33.1	-0.2
Gas	141.5	2.8	24.2	0.2
Coal	157.9	-0.9	27.0	-0.5
Renewables*	29.0	3.2	5.0	0.5
Hydro	37.6	0.3	6.4	-0.0
Nuclear	24.9	0.8	4.3	0.1
Total	**583.9**	**7.7**		

*** renewable power (excluding hydro) plus biofuels**

In Figure 1, the trends in world consumption (left) and the global primary energy shares (right) are shown. It can be highlighted that, in both cases, the most rapid increases are those ascribed to renewables combined with natural gas. The consumption of hard coal, which is also growing, is still very significant.

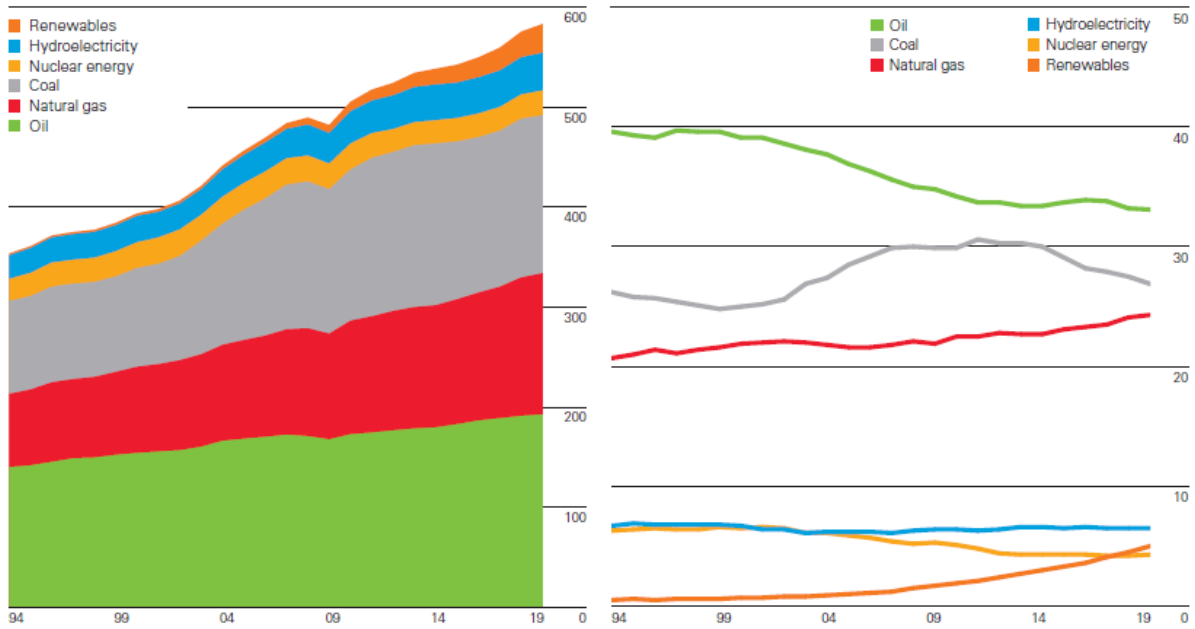

Figure 1 *World consumption (left) and shares of global primary energy (right). Reprinted with permission from [1].*

Figure 2 represents the breakdown of regional consumption in 2019 for the different energy sources.

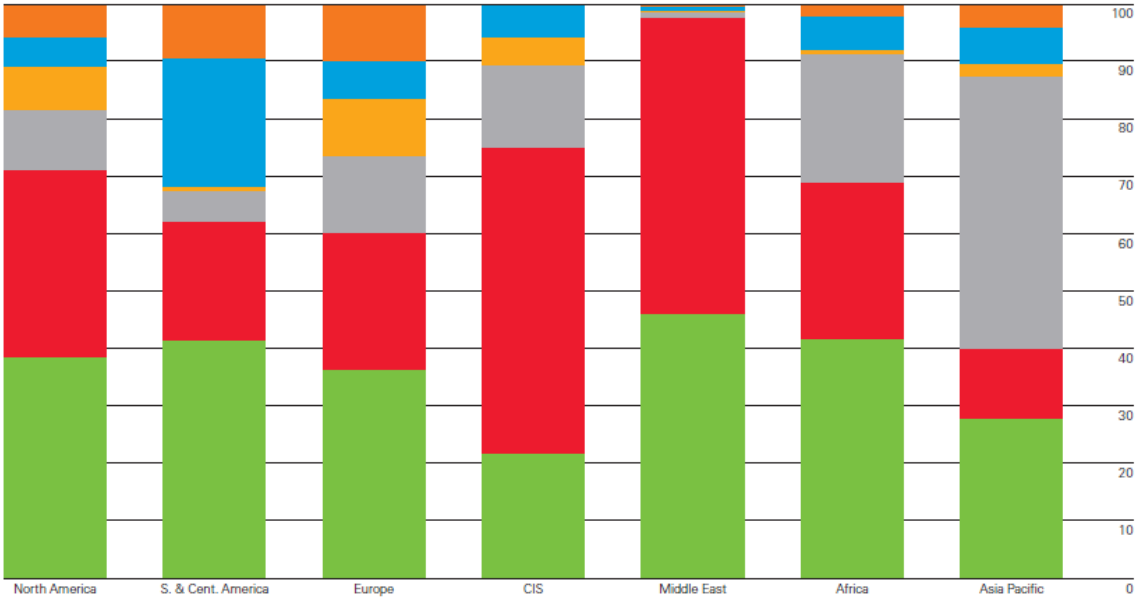

Figure 2 *Regional consumption pattern in 2019, colour referred to Figure 1 (left). Reprinted with permission from [1].*

From these data, it can be concluded that the drive for renewables is an open and necessary issue to reach net zero emissions by 2050 [1]. Photovoltaics and concentrated solar power systems represent a great opportunity to exploit the strong solar radiation that strikes the Earth every day, by a continuous radiation that can be exploited to the fullest extent of available technology.

An overview of the main existing photovoltaic technologies is given in the following sections.

3 Photovoltaics

Photovoltaics is the production of electricity converting photons in sunlight [2]. It is a direct method, where a semiconductor substrate generates electrons thanks to the excitation by photons with sufficient energy. As noted in the world energy production scenario, solar (photovoltaics plus concentrating solar) represents a good slice of the global sustainable energy production, and photovoltaic is mainly the protagonist.

In 1839, A. E. Becquerel discovered the photovoltaic effect, showing the basic principle of a solar cell [3]. Over the years, the technology has seen much improvement thanks to scientific research. Now, solar cells can be classified into three generations:

1) First generation: cells composed of monocrystalline or polycrystalline silicon-based substrates;
2) Second generation: use of silicon together with other semiconductors such as gallium arsenide (GaAs) and cadmium telluride (CdTe), an enhancement of the first generation;
3) Third generation: semiconductors are replaced with cheaper, hybrid and multijunction materials.

In the followings, the three photovoltaic generations will be investigated in more detail.

3.1 First generation solar cells

The first generation devices were discovered by Chaplin, Fuller and Perason in 1954; they used monocrystalline and polycrystalline silicon as semiconductor materials [2]. Above all, the monocrystalline conformation had better efficiencies than the polycrystalline one, because the latter had more defects that facilitated the recombination of electrons. Its band gap is 1.12 eV. This value allows the absorption of radiation with wavelengths between 0.35 and 1.2 μm, which correspond to about 40% of the total incident energy (absorption is in the infrared and in the visible).

This first generation technology is now a consolidated technology that achieves high efficiencies, even beyond 20%. Silicon cells are the most widespread in the photovoltaic market. However, production processes use a massive amount of hydrofluoric acid and exploit high temperatures; these factors represent a significant environmental impact. In addition to the use of high temperatures and acid, the process requires a high degree of purity (silicon for solar use with impurities between 10^{-7} and 10^{-9}), leading to a high cost, corresponding to 20-25% of the total cost of the whole device. In addition to the high cost of the device, production costs are also high because the minimum thickness that can be used for silicon is 100 μm, due to the fragility of the semiconductor material [4].

The silicon cell is a sandwich-type cell, with two layers of silicon at the ends [5]. A p-type conductive layer with a thickness ranging from 180 to 300 μm is made up of silicon doped with boron (atom acceptor for p-type junction). The other conductive layer is n-type and is made up of silicon doped with phosphorus compounds by means of gaseous diffusion. The n layer is an emitter of electrons with a much smaller thickness (about 1 μm), to prevent electrons from recombining before reaching the absorber layer.

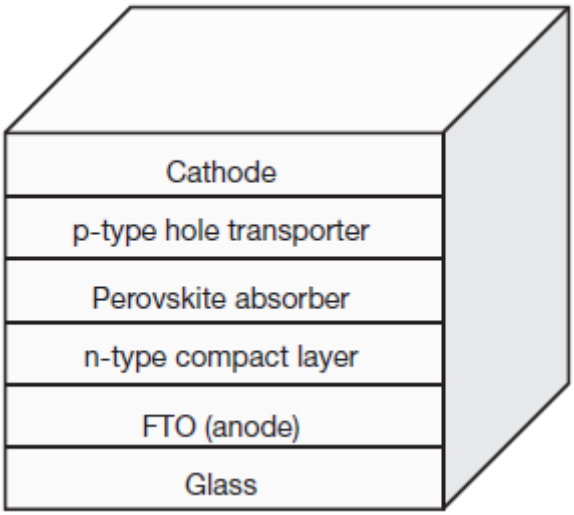

Figure 3 *First generation photovoltaic cell structure. Reprinted with permission from [5].*

3.2 Second generation solar cells

Second generation photovoltaic cells, or even thin-film cells, are designed to reduce material costs by using very thin semiconductor films. In this way less material is used.

These cells are mainly composed of indium, tellurium and cadmium deposited on glass or polymeric substrates. This technology is a p-i-n junction diode. The p-i-n layers are doped and are very thin. The intrinsic layer i absorbs light, transfers energy to the charge carriers and is used for current generation. In this case, the semiconductor materials are amorphous, doped and show poor electrical properties due to the presence of defects that act as recombination centres. In this type of cell, diffusion fails to guarantee the transport of electrons, therefore an electric field generated by the p-i-n junction is required, which allows the separation of electrons from the generated gaps and improves the charge transfer to the n and p layers [6].

The main materials used for second generation photovoltaic cells are:

- **Amorphous silicon**: can be prepared up to 5 μm thick, has a high absorption coefficient and can be deposited even at low temperatures. Amorphous silicon is not pure, it is doped with diborane (B_2H_6) or phosphine (PH_3), thus forming Si-H bonds. After a few hours of exposure, however, a sharp drop in efficiency can be observed due to the breaking of the Si-H bonds under strong irradiation. In this case, hydrogen molecules leave the material and amorphous silicon remains. This process leads to a drop in panel performance. As previously mentioned, amorphous silicon brings with it all the problems related to structural defects and recombination. The advantages of this cell are that it can be fabricated at low temperatures and can be integrated on surfaces such as roofs and facades of structures [4, 7, 8];
- **Cadmium telluride**: the efficiency of the cells using this semiconductor is around 10%. This conformation has a longer life than that with amorphous silicon, in fact it has a higher resistance at high temperatures. The biggest defect lies in cadmium, as it is a toxic material and must be disposed of correctly, which includes disposal costs [7];
- **Copper diselenide indium biselenide copper, indium and gallium diselenide (CIS, CIGS)**: these are all semi-crystalline semiconductors with a high absorption coefficient.

They do not present degradation problems, but are unstable in humid and hot environments. Indium is also a very rare material with a very variable price on the market [8].

3.3 Third generation solar cells

Through third generation solar cells, research has abandoned silicon, introducing cheaper and more environmentally friendly cells, prepared with abundant materials and whose processing does not require critical conditions of temperature, pressure, purity and impact. Third-generation photovoltaics currently have lower efficiencies than the first two categories, but in recent years there has been a rapid growth in certified efficiencies.

The main technologies used are:

- Dye-sensitized cells and quantum dots: the first one are exhaustively investigated in this Thesis, they mostly use semiconductors such as TiO_2 and use a thin layer of Pt as cathode; Pt replacement is possible by inserting polymers such as PEDOT, which is more economical and environmentally friendly. The latter, on the other hand, have optical characteristics that can vary by varying the size of the particles that make up the photoactive species. Quantum dots are semiconductors with low band prohibited (InP, CdSe, CdS) [2]. They can be adsorbed by the semiconductor through treatments and, when irradiated, can generate multiple excitations with the absorption of a single photon.
- Organic cells: organic materials are used with the aim of producing economical, flexible devices, compatible with different substrates and low temperature methods.
- Perovskite solar cells: "Perovskite" is the nomenclature for any material that adopts the same crystalline structure as calcium titanate: ABX3 [9]. There are several materials that adopt this structure, with a multitude of properties, including: insulating, piezoelectric, thermoelectric, semiconductor, conductive and superconductive. Perovskite solar cells are designed to improve the absorption of sunlight.

4 Dye-sensitized solar cells: device and working principle

4.1 Introduction

Dye synthesised solar cells (DSSCs), or also known as Grätzel cells, are photoelectrochemical devices used as alternatives to silicon-based ones. The first cell was tested in 1991 by O'Regan and Grätzel and achieved an efficiency of 7.1-7.9%, through a low-cost process with realistic energy-conversion efficiency in an industrial and civil context [10].

In DSSCs, the dye chemisorbed onto an oxide semiconductor absorbs photons from sunlight and inject an electron in the semiconductor. The electrolytic solution contained in the devices (usually composed by iodine-based I-/ I3- redox pair) regenerate the dye, reducing it; then, the electrolyte itself is reduced at the counter electrode (CE), through a Pt-catalyzed reaction.

The most widely used semiconductor is TiO2 (titania). It is a transparent semiconductor (it allows the passage of light) and has a good porous structure suitable for the chemisorption of a huge amount of the dye on its surface, increasing the contact between the two species; this is a crucial factor for a proper operation of DSSCs, as TiO_2 alone would only absorb ultraviolet light. Instead, the dye anchored on its surface allows the enlargement of the absorption spectrum in the visible and near-infrared portions on sunlight, increasing cell efficiency.

4.2 Components

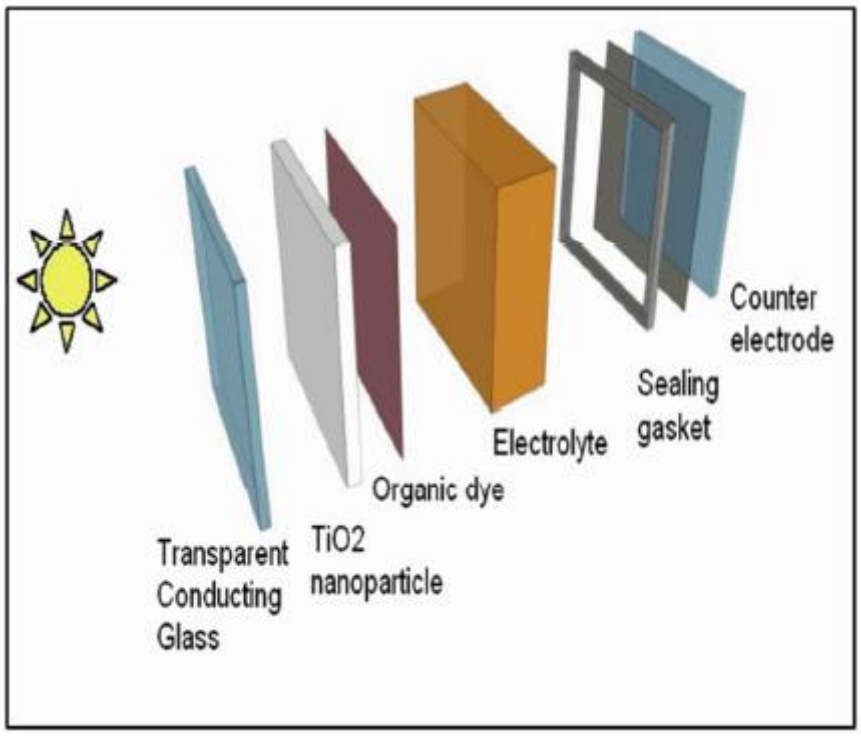

Figure 4 *Main components of a DSSC. Reprinted with permission from [2].*

4.2.1 Conductive substrate

DSSCs are manufactured on a conductive and transparent oxide (TCO) glasses, on both sides [11]. This type of substrate must allow light to easily pass through, facilitate charge transport

to the external circuit, have good transparency to light in the visible and infrared region and be stable at high temperatures (for the sintering process of the semiconductor up to 500 °C).

The most used TCO is fluorine-doped tin oxide (FTO), followed by indium-doped tin oxide (ITO). FTO shows:

- excellent thermal stability (up to 500 °C);
- good transparency;
- good adhesion to the substrate;
- chemical stability;
- better environmental compatibility with respect to ITO.

Conversely, as regards ITO, indium is a rare metal, is chemically less stable when in contact with the electrolyte and has a resistance that increases with temperature.

Glass is the most widely utilized support; alternatively, some polymers with high flexibility are available to fabricate flexible devices [2]. These polymers are not stable up to 450 °C (to carry out anode fabrication), therefore low temperature deposition methods were studied, but the resulting substrates showed imperfections and structural defects.

4.2.2 Semiconductors

The semiconductor materials used in DSSCs are mainly metal oxides, such as TiO_2, ZnO and SnO_2 [12]. Titanium dioxide is the most widely used semiconductor anode in DSSCs; it comes in various crystalline forms: anatase, brookite and rutile. Rutile is thermodynamically more stable, but anatase possesses high conductivity, which is why it is preferred in DSSCs.

Several deposition methods have been studied for the preparation of the TiO2 layer because the crucial factor for its good functioning is its morphology. In fact, the morphology is the main factor that influences the dye-loading, the electrode/electrolyte interface and the recombination phenomena. For this reason, TiO2 is often treated with TiCl4 [13]. Titanium dioxide is deposited in the form of nanoparticles with an average diameter of 20 nm and an average porosity of 55%. The high surface area of the high porosity allows better permeation of the electrolyte into the pores and thus better contact between the two phases.

In addition to the morphology, the high band gap also gives TiO_2 the supremacy of use in DSSCs. The conduction band of the titania is at a lower energy level than that of LUMO of the dyes used, this factor allows an easier electron injection. However, the band gap (3.2 eV) absorbs radiation with wavelengths below 380 nm, thus falling into the UV radiation spectrum. The absorption of UV radiation could lead to the formation of highly reactive vacation and oxidation reactions that could damage various components of the cell. For this reason, the presence of UV filters is essential. The glass and the conductive substrate deposited do not allow UV absorption.

4.2.3 Dye

The dye in the DSSC is necessary to allow the absorption of radiation, both in the visible and infrared region. The typical features of a dye (or sensitizer) are the following:

- absorb light over as wide a wavelength range as possible;
- stable when in contact with the electrolyte;
- stable under continuous illumination, it must not undergo degradation reactions;

- intermediate hydrophobicity, to prevent detachment in the presence of water and to ensure wettability in the presence of the aqueous electrolyte;
- forming bonds with the semiconductor surface, usually through groups such as $-H_2PO_3$ and -COOH;
- to guarantee a good pairing between:
    - LUMO (the lowest unoccupied molecular orbital of the dye) and the semiconductor conduction band;
    - HOMO (the highest occupied molecular orbital of the dye) and the semiconductor valence band;
- thermal stability.

The mechanism that sees the dye as protagonist is the following: a photon with enough energy is absorbed by a dye molecule, excites an electron, this electron passes from the highest occupied orbital to the lowest unoccupied one [12]. Therefore, a dye is as efficient when:

- molecules absorb as many incident photons as possible;
- photons are converted to electron-holes pairs;
- it can be chemisorbed as monolayer, to ensure electrons injection from dye to TiO_2.

High efficiencies in terms of PV performance, conversion yield and long-term stability are achieved with the dye based on polypyridyl complexes of ruthenium (Ru), developed by the Grätzel group.

The main dye used and studied over the last 20-30 years can be grouped into two large sets:

1) Ru complexes such as N3, N719, Z907 and black dye;
2) donor-acceptor metal-free organic dyes (D-A).

The first group includes Ru metal, which is expensive and requires complex and tricky purification processes [14]. The second group includes natural or synthetic dyes, that have the advantage of being metal-free and having an inexpensive preparation process.

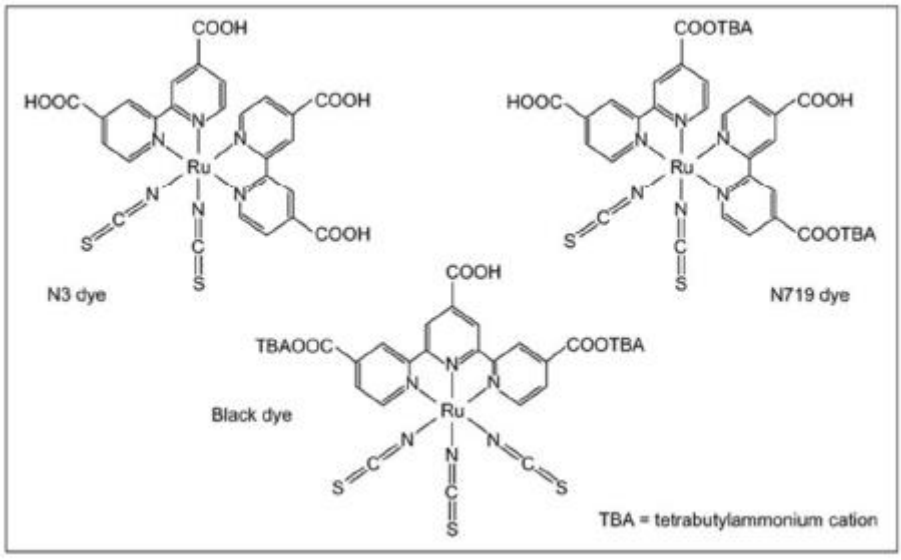

Figure 5 *Chemical structure of the main commercial dye. Reprinted with permission from [2].*

4.2.4 Electrolyte

The electrolyte plays a very important role in the DSSC, i.e. it regenerates the oxidized dye molecule through the transfer mechanism: the electrons from the external circuit arrive to the cathode and regenerate the electrolyte, this latter having previously reduced oxidized dye molecules [2]. The electrolyte is regenerated by the catalyst present at the counterelectrode.

The properties of a good electrolyte are as follows:

- chemically, thermally and electrochemically stable;
- good charge transport properties;
- the redox reaction of the electrolyte must regenerate the oxidised dye easily;
- must not be corrosive;
- the absorption spectrum of the electrolyte must not interfere with that of the dye.

An electrolyte can be classified according to its state of aggregation: solid, liquid or quasi-solid. Depending on whether it is solid or quasi solid, DSSCs will be called SS-DSSCs (solid-state DSSCs) or QSS-DSSCs (quasi solid-state DSSC).

The most commonly used **liquid electrolyte** is based on the redox pair I^-/I_3^- solubilized in an organic solvent. With this electrolyte, high efficiencies have been obtained as it is characterized by a high ionic conductivity, good solubility and high dielectric constant. However, the iodine redox shuttle shows limits: it absorbs in the visible region, corrodes the metal contacts and is volatile [15]. Other kinds of liquid electrolytes based on copper or cobalt have been studied. In general, cells assembled with liquid electrolytes can present problems of non-hermetic sealing, making the solvent evaporate even at ambient temperatures upon time.

The solid electrolyte allows the hole conduction through hopping within its solid matrix. Crystalline metallic semiconductors (copper based like CuI and CuSCN or nickel based like NiO), conductive polymers such as PEDOT or organic molecules have been studied and used [16]. PEDOT has aroused a lot of interest as it is a polymer that is easy to prepare and rather inexpensive; also, a cell with a solid electrolyte does not present the problem of solvent losses and evaporation at all. The second part of the literature review in this Thesis collects all the studies involving PEDOT as an electrolyte (or, better, HTM). The best efficiency obtained was 7.1%, lower than that obtained with a liquid iodine electrolyte [153]. The main problem with the solid electrolyte composed of PEDOT is that PEDOT does not adhere adequately to the dyed TiO_2 films, and the recombination between the semiconductor electrons and the electrolyte gaps can be high [145].

The quasi-solid electrolyte is very often present in the form of gels or membranes, to which inorganic nanoparticles or polymeric materials are added. The most commonly used polymers are polyethylene glycol (PEG) or polymethyl methacrylate (PMMA). The most commonly used inorganic nanoparticles are silicon dioxide and titanium dioxide [15]. These electrolytes have physical properties intermediate between liquid and solid states and present a compromise in terms of efficiency and durability.

4.2.5 Counterelectrode

The counterelectrode (CE) is the cell component that closes the circuit, collects the electrons coming from the external circuit and catalyses the electrolyte reduction. The need to catalyse the charge transfer is to overcome the resistances between FTO and the electrolyte.

The most commonly used material as CE is platinum, obtained by thermal decomposition of hexachloroplatinic acid (H_2PtCl_6) [17]. Platinum is a rare and very precious metal; in addition, the manufacturing cost is extremely high due to the high temperatures reached; for these reasons, scientific research is exploring new usable materials that are more eco-sustainable and less expensive.

Carbon CEs are good candidates. Carbon has a low cost and can also be derived from organic waste [112]. The excellent conductive properties of carbon combined with the possibility to produce different nanomorphologies, such as nanotubes [18], nanospheres, nanohorns, nanosheets, etc.: they represent a valid competitive material with Pt.

Alternatively, research is intensively pursuing the use of PEDOT as CE. PEDOT is a polymer and is the most widely used polymer as CE, often used with additives and doped with PSS. For example, PEDOT is often studied in combination with carbon, to combine the properties of the polymer with the conductive and morphological properties of carbon. Its characteristics, ease of production and low cost also make it competitive at an industrial level, to manufacture Pt-free DSSCs.

To this proposal, this Thesis also presents a literature review about the progress and results obtained from research groups working on PEDOT as CE for DSSCs.

4.2.6 Operating principle

The operating principle of the DSSC is based on two fundamental steps to convert sunlight into electrical energy:

1) excitation of electrons by absorption of solar radiation;
2) charge carriers separation [2].

Unlike classical solar cells, in DSSCs sunlight is harvested by means of dye molecules. These molecules are bound to the semiconductor material. After the absorption of sunlight takes place, electrical charge separation occurs at the dye-TiO_2 interface.

The operation of a DSSC is conceptually similar to the natural photosynthesis process in plants. In the case of DSSC technology, the dye has the role of chlorophyll, i.e. it absorbs solar radiation. The functioning scheme is as follows:

1. $TiO_2D + h\nu \rightarrow TiO_2D^*$
2. $TiO_2D^* \rightarrow TiO_2 + D^* + e^-(CB)$
3. $TiO_2D^* + 3I^- \rightarrow TiO_2D + I_3^-$
4. Electron transport in the external circuit
5. $I_3^- + 2e^-(Pt$ or PEDOT$) \rightarrow 3I^-$
6. $I_3^- + 2e^-(CB) \rightarrow 3I^-$
7. $TiO_2D^* + e^-(CB) \rightarrow TiO_2D$

The photoelectrochemical process that takes place in DSSCs can be summarised through the following steps:

A. **Absorption of sunlight and excitation of electrons in the dye molecules**. In this first step, photons with energy between 0.5 eV and 3.5 eV hit the conductive glass, TiO_2 electrode and penetrate until they meet the dye. Photons with energy equal to or greater than the dye molecule gap (HOMO-LUMO) produce an excitation of electrons, which are then promoted by HOMO to LUMO. Therefore, the passage of electrons from HOMO to LUMO depends on the gap of the dye itself and the energy of the incident photon (Figure 6). In fact, if the photon does not have sufficient energy, it will not cause the promotion of the electron.
B. **Injection of electrons into the TiO_2 layer and charge separation.** The excited electrons pass from LUMO to the conduction band (CB) of the semiconductor through the bonds between the dye and TiO_2. If a hypothetical unitary quantum efficiency is to be achieved, the orbits of Ti^{4+} and the dye should be perfectly matched. Once in the CB, the electrons are transported along the layer. An efficient process would have no effect of recombining the electrons with the dye. Once the electrons pass through the entire semiconductor film, they are collected in the transparent conductive film (the photoelectrode). This process of collecting electrons from the CB on the transparent conductive substrate takes place at a micro to millisecond scale. The oxidised dye is regenerated as it was in principle in a nanosecond range.
C. **Redox reaction between electrolyte and CE.** Dye molecules are oxidised and cannot spread within the TiO_2 layer because they are bound to it. These molecules are therefore reduced by the electrolyte in a nanosecond time. The redox shuttle typically used is I^-/I_3^-, in this case the reduction of the oxidised dye produces triiodide. After that, the triiodide spreads towards the CE. The electrons pass from the transparent conductive substrate to the external circuit and return to the CE side.

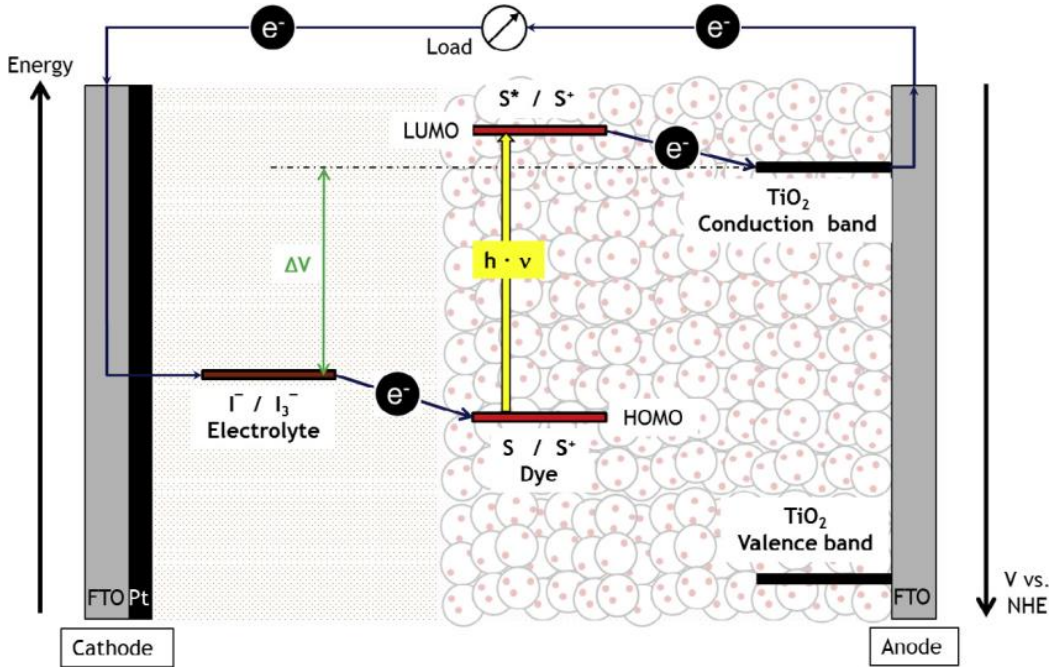

Figure 6 *Energy levels for the titania, the dye and the redox pair. Reprinted with permission from [19].*

Recombination effects. Recombination is the phenomenon occurring when the photoelectrons recombine with two different components: the electrolyte or the dye molecules. These reactions have the effect of reducing the electrical power output of a DSSC and typically occur during electron transport from the CB of TiO_2 to the adjacent TiO_2 particle within the semiconductor layer. The two recombination pathways are therefore declined as follows:

1) **Recombination with the oxidised dye**: it is in the micro-millisecond range and occurs at the contact sites between the dye and TiO_2;
2) **Recombination with the electrolyte**: it takes place in the range of milliseconds and is the most dominant process. The electrolyte permeates into the pores of the TiO_2 and this allows the formation of recombination sites. The way to avoid them would be to deposit a thin film of TiO_2 between the FTP and the porous nanocrystalline layer of TiO_2.

5 Experimental techniques to characterize DSSCs

In this section, the main tests that take place to characterize a DSSC are listed, in order to facilitate the reading of the Thesis.

5.1 Morphologies characterization

Since the CE morphology is a key factor for the cell performance, they are always studied and analysed using images collected by:

- field-emission scanning electron microscope (FESEM);
- transmissions electron microscope (TEM);
- atomic force microscope (AFM).

Depending on the type of CE, it is useful to analyse its surface morphology as the more porous the layer, the better the permeation of the electrolyte and the more active sites to catalyse redox shuttle reduction reaction. In fact, very often PEDOT is used in combination with carbon with different shapes, because it is possible to create particular conformations that greatly increase the surface area of the CE. In addition to carbon, PEDOT can be doped with various substances (here is the example of methanol) or treated with acids to increase its porosity and consequently the surface area.

In order to have an example of morphological changes and images of the CE layer, I list here an example where PEDOT is doped with methanol (MeOH) [87]. In addition to doping, synthetic methods are used to create two different conformations: PEDOT-MeOH tube array and PEDOT-MeOH coral. The morphology is improved compared to pure PEDOT because its surface (without doping or treatment) was smooth and not very porous. In this case the authors combined the two conformations to create the PEDOT-MeOH tube-coral array. Figure 7 shows how the FESEM images (in this case) can give an idea of how the product is actually true to expectations. In fact, in this case it can be seen the tube arrays and corals distinct and then joined together to form the desired CE. It will then be demonstrated through the photovoltaic performance analysis that the improvement of the morphology has a great influence on them.

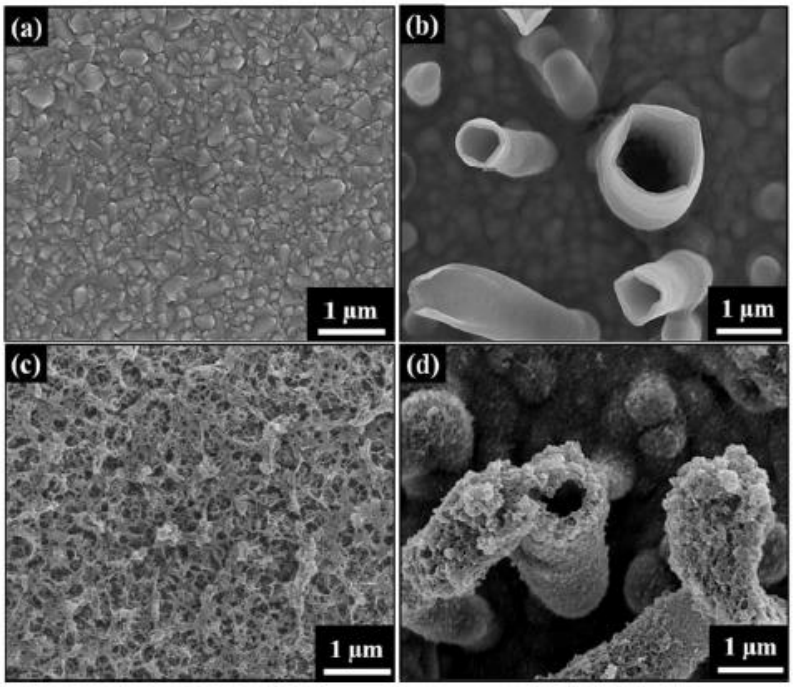

Figure 7 *Top-view of FE-SEM images of a) Pt, b) PEDOT-MeOH tube arrays, c) PEDOT-MeOH Coral and d) PEDOT-MeOH tube coral arrays. Reprinted with permission from [87].*

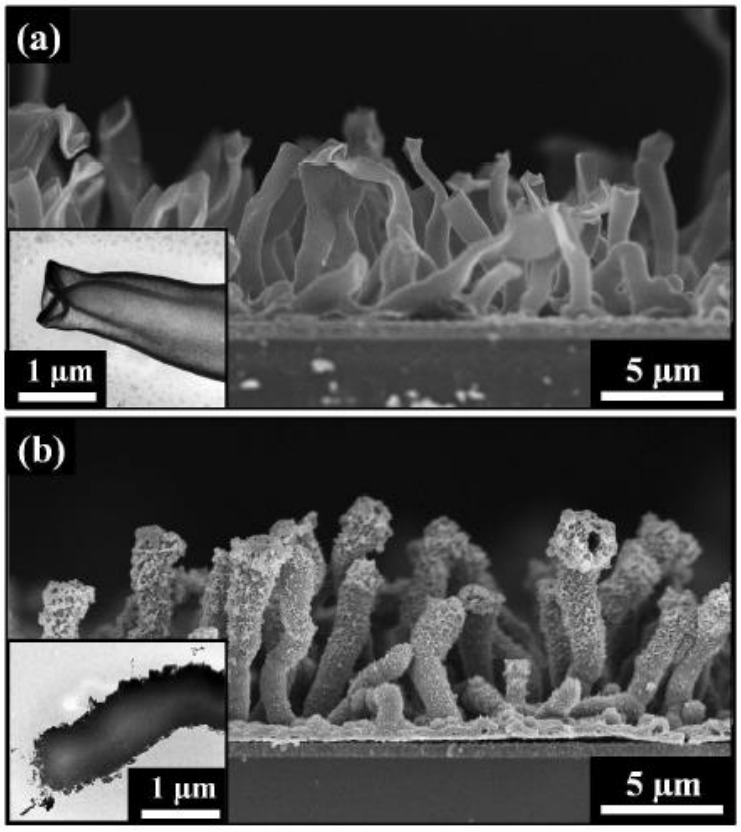

Figure 8 *Cross section FE-SEM images of a) PEDOT-MeOH tube arrays and b) PEDOT-MeOH tube coral arrays with their TEM images shown in the insets correspondingly. Reprinted with permission from [87].*

5.2 Cyclic voltammetry

Cyclic voltammetry (CV) is performed in order to explore the reaction kinetics of the electrolyte redox reaction and evaluate the electrocatalytic activity of the CE. The most commonly used electrolytic solution in the iodine I^-/I_3^- one, so it will be taken as an example with PEDOT as CE. The curves can also be made by varying the charge density.

A classic PEDOT CV curve with the iodine electrolyte appear as shown in Figure 9.

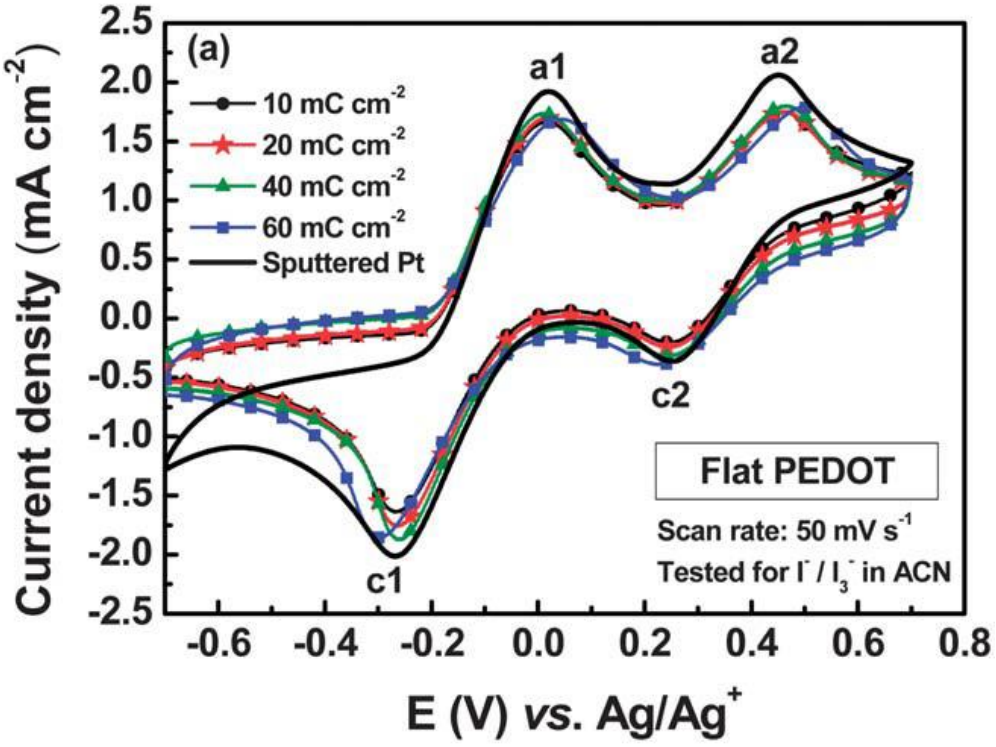

Figure 9 *Cyclic voltammetry of pure PEDOT CE with iodine electrolytic solution at different current density. Reprinted with permission from [66].*

Four redox reaction peaks or two pairs of redox peaks can be observed [66]. The peaks with more negative potential (that, in Figure 9, are called a1 and c1) are associated with the first reaction, the peaks with more positive potential (a2 and c2) are associated with the second reaction:

$3I^- \leftrightarrow I_3^- + 2e^-$

$2I_3^- \leftrightarrow 3I_2 + 2e^-$

If the CE activity has to be evaluated, reaction (1) should be considered, i.e. that concerning the most negative peaks of the CV curves. In particular, the magnitude of the peak current density in c1 is used to quantify the electrocatalytic ability of the CE in the DSSC. In quite all the literature studies, these values are those significant in the CV analysis:

- cathodic peak current density (J_{pc});
- anodic peak current density (J_{pa}, useful for the following parameter);
- separation between the two peaks (ΔE_p).

To have the best catalytic activity, J_{pc} should be as large as possible in absolute value and ΔE_p should be as small as possible. In this way, the CE electrocatalytic activity can be quantified.

By varying the charge density, these three parameters vary, and it give an idea of the electrocatalytic activity in different situations. For example, in Figure 9, by increasing the charge density, J_{pc} decreases and ΔE_p increases.

5.3 Electrochemical impedance spectroscopy

The EIS measurements are taken in such a way as to investigate the internal cell resistances and try to explain the photovoltaic parameters trend obtained. For example, the FF is very affected by internal resistances. The article by Kung et al. [66] is again taken as an example.

In EIS measurements, the cell resistance is projected into an equivalent circuit extracted from the Nyquist plot (Figure 10).

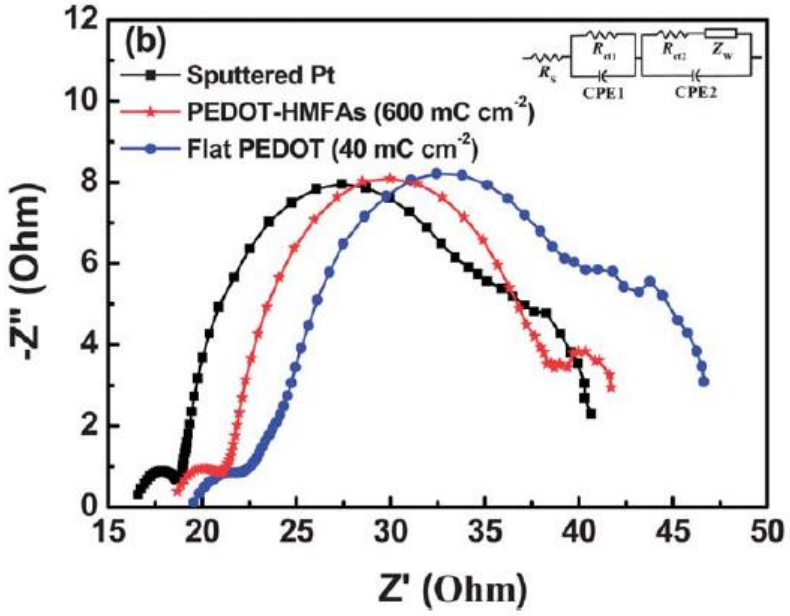

Figure 10 *EIS spectra of Pt, PEDOT and PEDOT-HMFAs (doped PEDOT studied in this article) at a light intensity of 100 mW cm^{-2}. Reprinted with permission from [66].*

These plots are composed of three semicircles that correspond, from right to left, to:

- the Warburg diffusion resistance of I^-/I_3^- in the electrolyte (Z_w);
- the charge transfer resistance at the TiO_2/dye/electrolyte interface ($R_{ct,2}$);
- the charge transfer resistance at the interface between the electrolyte and the CE ($R_{ct,1}$).

The series resistances of the DSSC (R_s) must then be added, these can be estimated by extrapolating the EIS spectrum intercept.

These parameters are then evaluated and compared with all CEs and, obviously, the lower the resistance, the better the corresponding cell will be and the better the photovoltaic parameters will be.

In particular, by analysing the performance of a cell with different CEs, it is possible to investigate in particular $R_{ct,1}$ and R_s.

5.4 Photovoltaic performance

Photovoltaic performance is evaluated by the photocurrent density-voltage (J-V) or current-voltage (i-V) curves of the DSSC using the CE under examination [19].

The parameters obtained from these tests are:

- I_{sc} or J_{sc} (short circuit current and current density, respectively), calculated at bias of 0 V;
- V_{oc} (open circuit voltage), measured when the current reaches 0 A;
- P_{max} (maximum power output) generated by DSSC when the product of the current for the voltage is maximum:

$$\mathrm{Pmax} = \mathrm{Imp} * \mathrm{Vmp}$$

- η, conversion efficiency of incident sunlight into electricity:

$$\eta = \frac{\mathrm{Pmax}}{Pin} = \mathrm{Imp} * \frac{\mathrm{Vmp}}{Pin} = \mathrm{Isc} * \mathrm{Voc} * \frac{\mathrm{FF}}{Pin}$$

- P_{in} (incident power) is the irradiance illuminated on the DSSCs;
- FF (fill factor) is a value between 0 and 1 that basically describes the shape of the I-V curve; a high value indicates the rectangular shape, which is the preferred one in the DSSCs:

$$\mathrm{FF} = \frac{\mathrm{Imp} * \mathrm{Vmp}}{Isc * Voc}$$

A standard light spectrum (AM1.5) is used to compare the performance of various cells. In Figure 11 a generic I-V obtainable from a DSSC is reported.

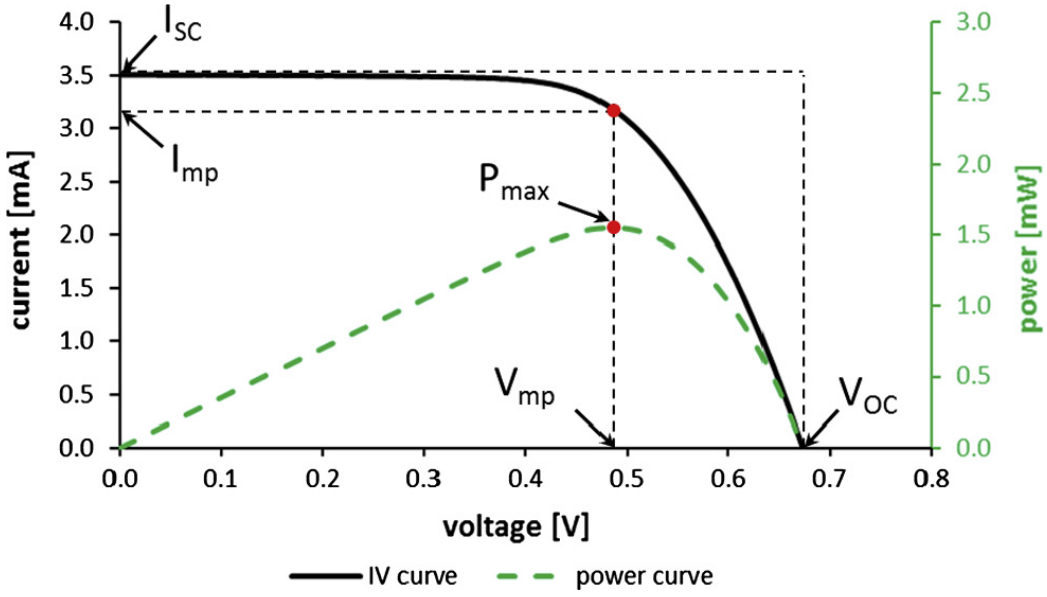

Figure 11 *Photocurrent-voltage characteristics of a DSSC. Reprinted with permission from [19].*

6 PEDOT as counter electrode in dye-sensitized solar cells

6.1 Saito et al.: chemically polymerized PEDOT as counter electrode in DSSCs (2002)

Saito et al. synthesized tosylate-doped PEDOT (PEDOT-TsO) and PEDOT:poly(styrene sulfonate) (PEDOT-PSS), then investigated the performance of these compounds as counter electrode (CE) in DSSCs [20]. PEDOT-TsO was synthesized adding the monomer 3,4-ethylenedioxythiophene into a Fe(III) tris-p-toluenesulfonate-imidazole dissolved in 1-butanol solution. After that, the solution was spin coated on an indium tin oxide (ITO) glass and heated. After this process, the polymerization took place and the polymer was treated and dried. PEDOT-PSS was dispersed in water and then filtrated, spin coated on ITO glass, heated and dried. The cell performance was studied through cyclic voltammetry (CV) and photocurrent-voltage (J-V) curves. The CV was useful to compare bare glass, platinum, PEDOT-TsO and PEDOT-PSS substrates. In the case of bare glass, the redox reaction was absent and there were no peaks in the curve. With PEDOT-PSS the oxidation current was lower with respect to the platinum substrate. An explanation may be the reduction of the active sites of PEDOT since PSS could preclude the access of the electrolyte to the PEDOT chain. Instead, the PEDOT-TsO promoted a regular exchange with the electrolyte. The photocurrent-voltage curves led to the DSSC parameters shown in Table 2.

Table 2 *Photovoltaic (PV) parameters for DSSCs assembled with TSO-doped PEDOT and reference electrodes. Adapted and reprinted with permission from [20].*

CE	V_{OC} [V]	J_{SC} [mAcm^{-2}]	FF	η [%]
PEDOT-TSO	0.67	11.2	0.61	4.60
PEDOT-PSS	0.68	11.0	0.28	2.10
PT	0.68	11.1	0.62	4.67

6.2 Saito et al.: the I^-/I_3^- reduction reaction on PEDOT (2002)

Saito et al. evaluated the relationship between the nature of the I^-/I_3^- redox reaction and the cathode of a DSSC (PEDOT-TsO and Pt) [21], working on devices prepared with an organic liquid electrolyte (OLE) or an ionic liquid electrolyte (ILE). Cell properties were investigated via CV and impedance measurements. All these studies also investigated the effect of thickness variation of the PEDOT film or the scan rate of the electrochemical test. Figure 12 shows the relationship between the anodic and cathodic peaks (obtainable through CV tests) and the square root of the scan rate. The relationship observed is linear. This trend confirms that the iodine species is little affected by the redox reaction on the cathode surface (both PEDOT-TsO and Pt).

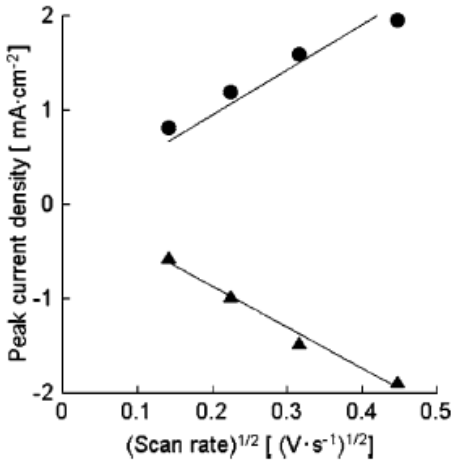

Figure 12 *Relation of anodic and cathodic peaks vs (scan rate)$^{1/2}$. Reprinted with permission from [21].*

Instead, the thickness of the electrode affected the I^-/I_3^- redox reaction, *i.e.* CV showed that higher thickness values improved the redox activity of the iodine-based shuttle. By impedance measurements, the authors found that the charge transfer resistance (R_{ct}) decreased with the increasing of the thickness of PEDOT-TsO. This was attributed to the increased surface area of the electrolyte and positively affected the PV parameters. A comparison between Pt and PEDOT-TsO electrodes showed that the second one had lower R_{ct}; this meant that PEDOT-TsO electrode could show higher performance than Pt electrode. The PEDOT-TsO CE with thickness of 2 μm showed higher V_{oc}, FF and efficiency than Pt and PEDOT-TsO cathodes with thickness of 70 nm. When OLE was used, the thickness of the electrode did not affect cell efficiency; conversely, ILE led to different PV parameters, as shown in Figure 13.

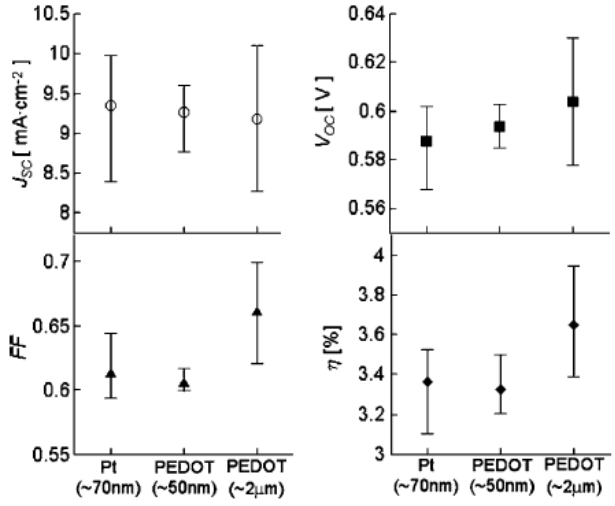

Figure 13 *Comparison of PV parameters for ILE-based DSSC using Pt and PEDOT-TsO cathodes. Reprinted with permission from [21].*

6.3 *Park et al.: thermal treated PEDOT-PSS as CE (2007)*

These authors fabricated DSSC using PEDOT:PSS as CE, investigated the PV properties, the efficiencies and then the surface morphology of thermal treated PEDOT:PSS [22]. DSSC were prepared with TiO_2 impregnated dye electrode and thermal treated PEDOT:PSS CE. There were not many differences between DSSC device working with PEDOT:PSS and with thermal treated one (Table 3). However, the heat treatment gave little effect on the performance of the cells. The authors also investigated the morphological change of the PEDOT:PSS film. After treatment at 45 °C for 120 min, the granular surface microstructure appeared and increased the surface area of the film. The highest efficiency of the cell (3.22%) was obtained with a test at 45 °C for 720 min.

Table 3 *PV characteristics of DSSCs using PEDOT-PSS as CE. Adapted and reprinted with permission from [22].*

	Treatment condition					
CE	**Temperature [°C]**	**Time [min]**	**V_{oc} [V]**	**J_{sc} [mAcm^{-2}]**	**FF**	**η [%]**
PEDOT:PSS	-	-	0.65	10.78	0.36	2.49
	45		0.60	10.77	0.37	2.40
	60		0.65	9.99	0.39	2.54
	80	20	0.65	10.35	0.36	2.46
	100		0.66	10.14	0.38	2.56
	120		0.66	9.87	0.38	2.48
	45		0.71	10.71	0.42	3.22
	60		0.63	10.87	0.41	2.78
	80	720	0.64	10.23	0.41	2.71
	100		0.63	11.26	0.35	2.51
	120		0.65	10.81	0.37	2.60
Pt	-	-	0.67	9.75	0.54	3.55

6.4 *Biancardo et al.: the first quasi-solid DSSC using a PEDOT:PSS cathode (2007)*

In this paper, the liquid electrolyte was replaced by a gel electrolyte and was tested in two different cells: one with Pt as CE and the second one with PEDOT:PSS as CE [23]. The gel electrolyte was polymethylmethacrylate (PMMA) dissolved in propylene carbonate (PC); this led to a homogeneous and transparent gel, with transport properties of a liquid and cohesive properties of a solid. The cell with the Pt CE was studied both with tape cast Pt and with air-brushed Pt. Option one showed better catalytic activity. PEDOT:PSS, on the other hand, showed performances very similar to the air-brushed Pt using the gel-polymer electrolyte. This means that the PEDOT:PSS counter electrode works better in a gel system than in a liquid one (Figure 14). The authors had no explanation for this observation, but suggested that the gel electrolyte could permit a better physical contact with the PEDOT:PSS layer.

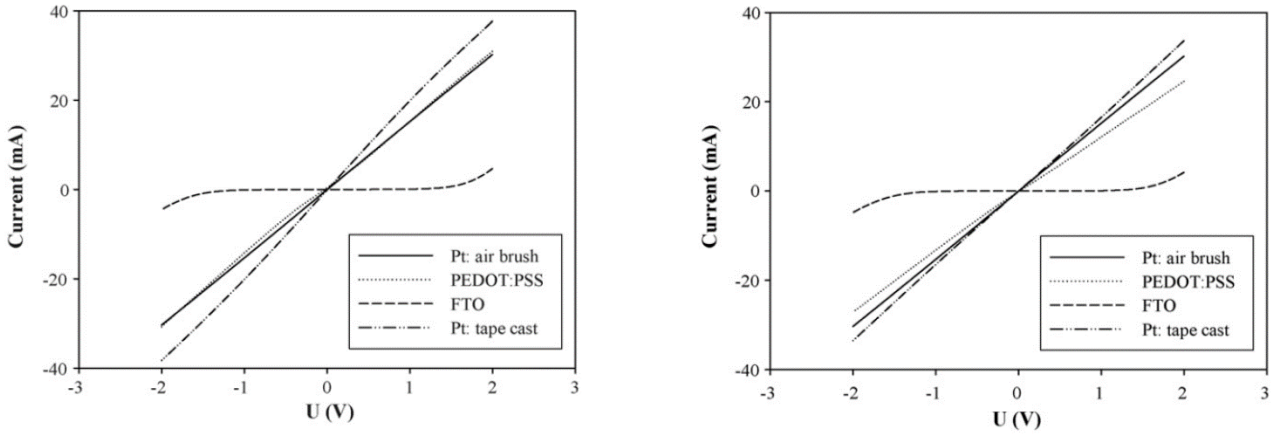

Figure 14 *Catalytic activities of counter electrodes measured in a symmetric model: (a) electrode/gel electrolyte/electrode, (b) electrode/liquid electrolyte/electrode [23].*

6.5 Xia et al.: the effect of doping ions in PEDOT (2007)

In this article, the author studied the influence of PSS, TsO and ClO_4 counterions on PEDOT [24]. PEDOT was synthesized by the classical way (chemical oxidation method) and by electrochemical polymerization. Photoelectrochemical properties were studied by current-voltage (I-V) characteristics using a solar simulator, film thickness was evaluated with surface profilometer and surface morphology was analysed with field emission scanning electron microscope (FESEM). By SEM analysis, the surface morphology of PEDOT in the presence of doping ions showed nonhomogeneous pattern for the chemical synthesized samples (Figure 15). The electropolymerized one with ClO_4^- showed a more porous structure and high surface area. So, electrochemical polymerized films showed more homogeneous morphologies. Table 4 summarizes all PV parameters obtained by different CEs. Bare fluorine doped tin oxide (FTO) gave poor performance, Pt CE gave the best one and PEDOT compound showed similar values to Pt.

Table 4 *Cell performance based on different CEs. Adapted and reprinted with permission from [24].*

CE	V_{oc} [mV]	J_{sc} [mA/cm^2]	FF	η [%]
Bare FTO	420	1.3	0.12	0.1
PT	682	9.8	0.65	4.3
'PEDOT-TSO	680	9.5	0.63	4.1
PEDOT-CLO$_4$	680	9.6	0.66	4.2
PEDOT-PSS	680	9.1	0.68	4.2
PEDOT-TSO	665	9.2	0.66	4.0

'PEDOT-TsO obtained by chemical oxidation method.

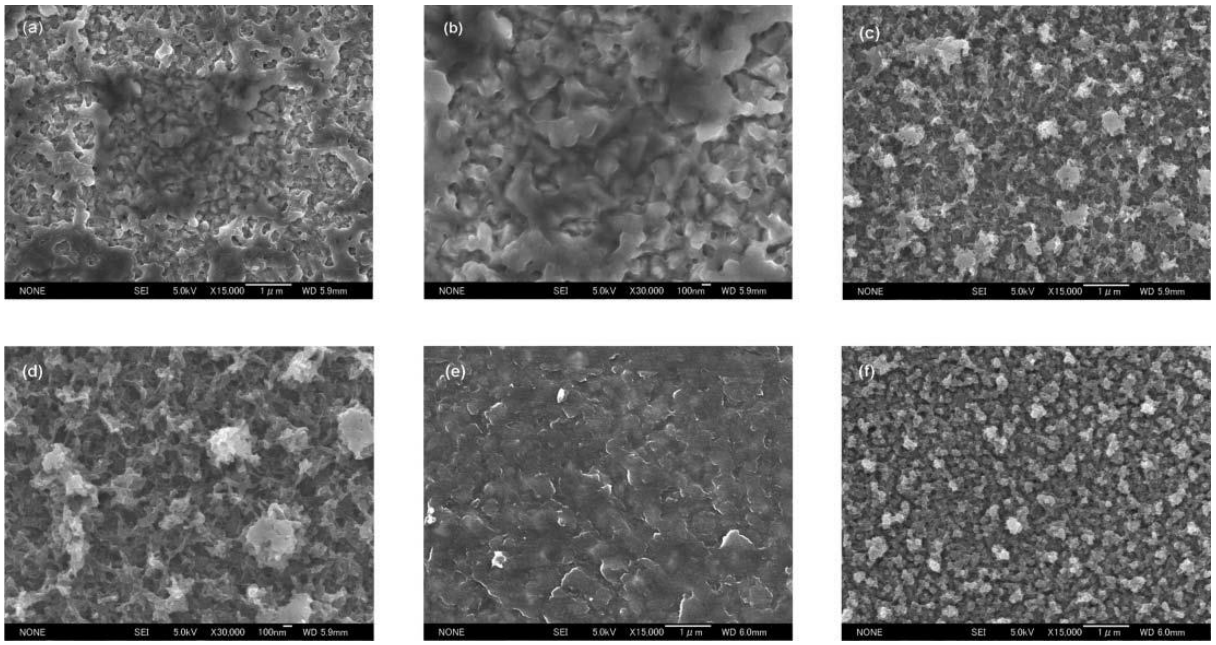

Figure *15 SEM images of chemically polymerized PEDOT-TsO and electropolymerized PEDOT: (a-b) chemically polymerized PEDOT-TsO; (c-d) electropolymerized PEDOT-ClO_4; (e) electropolymerized PEDOT-PSS and (f) electropolymerized PEDOT-TsO. Reprinted with permission from [24].*

6.6 Hong et al.: a graphene/PEDOT-PSS cathode (2008)

In this article, the authors investigated the effect of graphene inserted into the CE of a DSSC [25]; more in detail, the cathode was a transparent composite film composed by graphene/PEDOT-PSS on ITO. CV measurements identified trends like those of Pt as CE, while PEDOT:PSS alone showed worse efficiencies. This demonstrated that the electrode formed with the composite film possessed better electrocatalytic activity compared to the PEDOT:PSS one. I-V curves were studied using a composite film with 1 wt% graphene. The efficiency obtained was 4.5%, J_{sc} and V_{oc} parameters were very similar to those obtained with a cell with the Pt as CE (Table 5). However, the small differences between the values obtained with composite film CE and Pt CE limited cell performance. Finally, the authors studied how cell efficiency changed varying the amount of graphene from 0% to 1%. The cell efficiency in these tests increased from 2.3% to 4.5% and demonstrated that graphene inserted in the film improved cell performance.

Table 5 *PV performance of DSSCs with different CEs. Adapted and reprinted with permission form [**Errore. Il segnalibro non è definito.**].*

CE	J_{sc} [mAcm^{-2}]	V_{oc} [V]	FF	η [%]
PEDOT:PSS	10.99	0.72	28	2.3
Graphene/PEDOT-PSS	12.96	0.72	48	4.5
PT	13.05	0.72	68	6.3

6.7 First PEDOT CE synthesised in an ionic liquid (2009)

In this article, the authors investigated the first PEDOT CE synthesised in an ionic liquid (1-ethyl-3-methylimidazolium bis(trifluoromethanesulfonylamide)) and the first use of gold chloride as oxidant for PEDOT synthesis [26]. They compared the efficiencies obtained from

that cell with those obtained with a Pt CE. Then, the author tested both cells (PEDOT and Pt) with two different types of electrolytes, with the iodine-based redox shuttle dissolved in acetonitrile and ionic liquid. The results of such experiments are listed in Table 6. Cells with PEDOT as CE show efficiencies and performance comparable to those of Pt, thus making it possible to replace this rare metal.

Table 6 *PV performance of DSSCs using Pt and PEDOT as CE, with acetonitrile and ionic liquids. Adapted and reprinted with permission from [26].*

	Acetonitrile		**Ionic liquid**	
	Pt	**PEDOT**	**Pt**	**PEDOT**
J_{sc} [mA/cm^2]	14.43	14.61	10.23	10.53
V_{oc} [mV]	784	769	693	671
FF	0.70	0.70	0.71	0.68
η [%]	7.9	7.82	5.06	4.78

6.8 Balraju et al.: DSSCs based on modified TiO_2 electrode and PEDOT CE (2009)

The authors manufactured a FTO/TiO_2/dye/electrolyte/PEDOT cell and investigated how to increase the performance of the TiO_2 electrode [27]. The first approach was the electrode surface treatment with HCl. After that, they pre-annealed the electrode, thus increasing the J_{sc}. They also modified the FeTsPc dye by adding 10mM of TBP. The latter treatment made the dye even more soluble in organic solvents. Bare TiO_2 showed η of 3.08%, HCl treated TiO_2 showed η of 3.65% and HNO_3 treated TiO_2 showed η of 4.10%.

6.9 Jiang et al.: PEDOT-ClO_4 as CE (2009)

The authors prepared a counterelectrode consisting of PEDOT-ClO_4^-/TiO_2/FTO (prepared by a facile electrochemical deposition method) to promote electron-transfer at the ClO_4^--PEDOT/electrolyte interface [28]. The photoanode used was classic TiO_2 one. The best TiO_2 manufacturing conditions (for the cathode) was studied varying the time of deposition from 5 s to 35 s (voltage remained constant at 10 V). EIS measurements showed that Rct (charge-transfer resistance) decreased with the TiO_2 deposition time to a minimum of 2.12 Ωcm^2 for PEDOT-ClO_4^-(3.5 V15 s)/TiO_2(10 V5 s)/FTO. The same cathode showed the best PV performance (Table 7).

Table 7 *PV characteristics of DSSCs with different CEs. Adapted and reprinted with permission from [28].*

CE	**I_{SC} [mA]**	**J_{SC} [mAcm^{-2}]**	**V_{oc} [V]**	**FF**	**η [%]**	**P_{max} [mW]**
PT	2.84	11.85	0.771	55.87	5.11	1.23
PEDOT-ClO_4^- (3.5V15s)/ FTO	2.15	8.97	0.776	52.88	3.68	0.88
PEDOT-ClO_4^- (3.5V15s)/ TiO_2(10V5S)/FTO	2.68	11.16	0.770	55.63	4.78	1.15

PEDOT-ClO_4^- (3.5V15s)/ TiO_2(10V15S)/FTO	2.64	10.98	0.766	55.61	4.69	1.23
PEDOT-ClO_4^- (3.5V15s)/ TiO_2(10V35S)/FTO	2.58	10.74	0.752	53.41	4.31	1.04

6.10 *Sakurai et al.*: a PEDOT/TiO_2/FTO counter electrode (2009)

They studied the performance of DSSCs with ClO_4^--PEDOT/TiO_2/FTO (prepared by a facile electrochemical deposition method)as CEs and focused on morphological aspects [29]. This study was made because the TiO_2 part could positively change the interfacial electron transfer. After manufacture, the cell was studied by EIS, I-V and morphological characterizations. It was observed that the ClO_4^--PEDOT/TiO_2/FTO composition increased cell performance as $R_{CT,1}$ (charge transfer resistance at the cathode/electrolyte interface) turned out to be lower, with respect to TiO_2-free counterparts. The I-V values and EIS results are the same of the previous article (Table 7). The morphological characterisation was carried out to study the cross-section of the films (Figure 16): the thickness of PEDOT-ClO_4^- (3.5 V, 15 s)/TiO_2 (10 V, 35 s)/FTO CE was around 2 μm, which was like the thickness of TiO_2 (10 V, 35 s)/FTO layer. This is why the monomer EDOT penetrated completely onto the micro-cavities of the TiO_2 surface confirming that the insertion of TiO_2 on cathode side did not affect the film thickness.

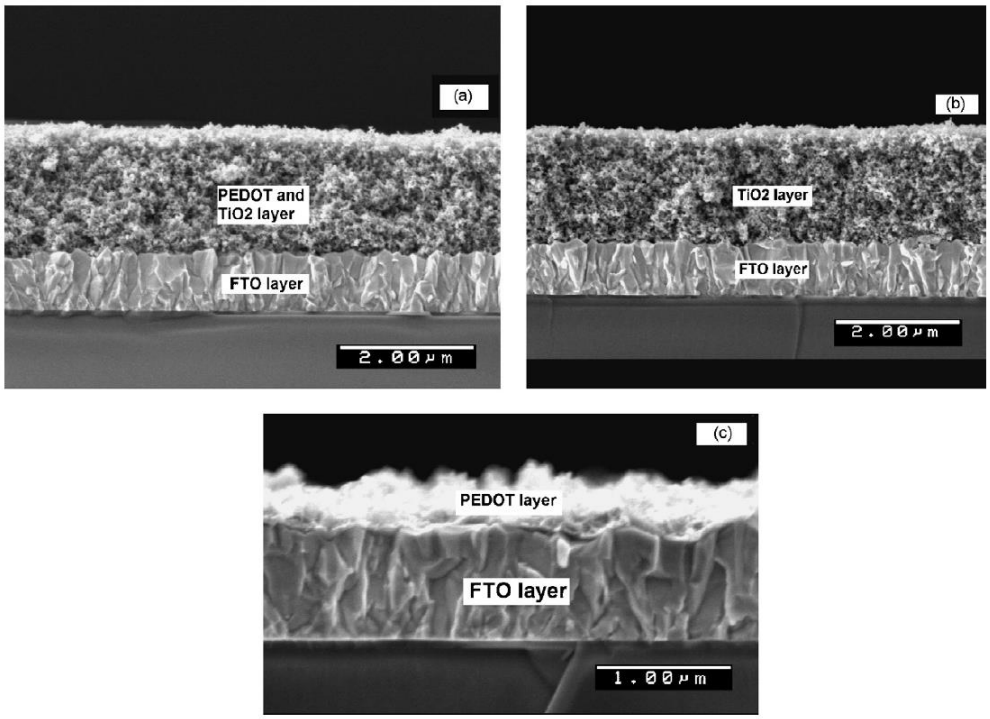

Figure 16 *Cross-section of a) PEDOT-ClO_4^- (3.5 V, 15 s)/TiO_2 (10 V, 35 s)/FTO; b) TiO_2 (10 V, 35 s)/FTO; c) PEDOT-ClO_4^- (3.5 V, 15 s)/FTO. Reprinted with permission from [29].*

6.11 Lee et al.: treated PEDOT as CE on dye-sensitized solar cells (2010)

Lee et al. studied PEDOT synthesized mixing imidazole with EDOT in various ratios. [30].The incorporation of imidazole led to a slower polymerization reaction of EDOT, decreasing the doping levels and avoiding the formation of nanoscopic drops that were characteristics when faster polymerization rate was adopted. CV measurements were carried out in order to study the behaviour of PEDOT CE and the relationship between ion diffusivity and cell reaction kinetics. The curve presented the familiar two oxidative peaks and two reductive peaks and were very similar to those obtained with a Pt-based system (Figure 17). A conversion efficiency of 7.44% was measured. Subsequently, the authors studied the effect of addition of multi-walled carbon nanotubes (MWCNT) to improve the performance of the DSSCs. MWCNT increased the catalytic activity and the adhesion with substrate. PEDOT with 0.6wt% MWCNT was studied coated on FTO and stainless steel: the cell performance grew up to 8.08% when a stainless steel support was used.

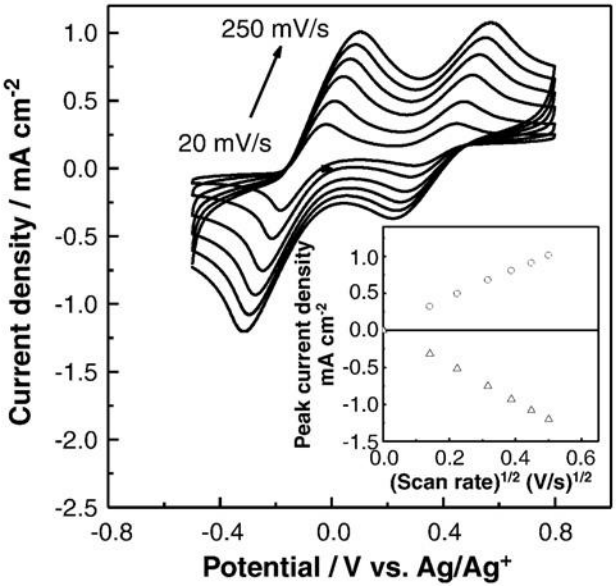

Figure 17 *CVs taken at various scan rates ranging from 20 to 250 Vs^{-1}. Reprinted with permission from [30].*

6.12 Pringle et al.: flexible PEDOT CEs and interface with ionic liquids (2010)

Pringle et al. studied the electrodeposition of PEDOT on conducting plastic substrates (ITO-PEN) at low electrodeposition time [31]. SEM analysis and profilometry confirmed the growth of the PEDOT film on ITO-PEN. It was immediately observed that, with a deposition time of 5 s, the film was more compact and denser. As the deposition time increased (up to 45 s), the surface became more granular and rougher (Figure 18). The authors deduced that this was the natural constitution of the PEDOT film, denser at the base and more porous at the top. CV measurement showed that PEDOT coated on ITO-PEN can catalyse the reduction of the redox pair in a manner comparable to that of the Pt electrode. The I-V curves also demonstrated the analogous of performance of cells fabricated with PEDOT-on-ITO-PEN, Pt/Ti-on-PEN and Pt-FTO. The data shown in Table 8 highlights the high efficiency obtained by the cells with ITO-PEN: the efficiency exceeded those achieved with platinum electrodes. Finally, the authors studied the effect of two different ionic liquid electrolytes: 1-ethyl-3-methyl imidazolium thiocyanate ([C_2mim][SCN]) and 1-ethyl-3-methylimidazolium tetracyanoborate

([C_2mim][$B(CN)_4$]). The less viscous electrolyte showed better performance with an efficiency of 5.7%.

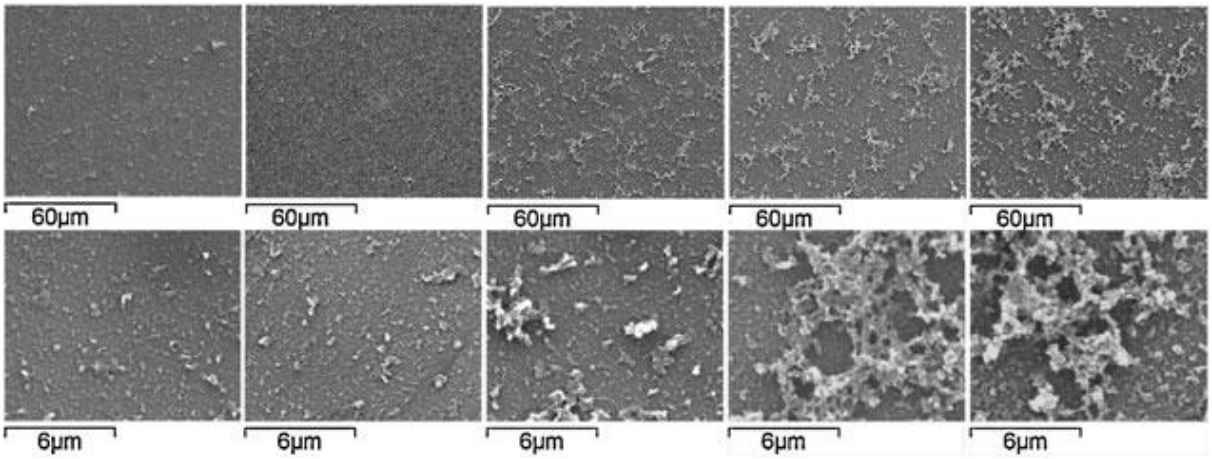

Figure 18 *SEM images of PEDOT on ITO-PEN grown for 5, 10, 15, 30 and 45s (from left to right). Reprinted with permission from [31].*

Table 8 *PV performance of DSSCs using PEDOT on ITO-PEN compared to Pt on FTO glass and Pt/Ti on ITO-PEN. Adapted and reprinted with permission from [31].*

Solvent	**Acetonitrile**			**[C_2mim][SCN] ionic liquid**			**[C_2mim][$B(CN)_4$] ionic liquid**		
Cathode	**Pt on FTO glass**	**Pt/Ti on PEN**	**PEDOT on ITO-PEN**	**Pt on FTO glass**	**Pt/Ti on PEN**	**PEDOT on ITO-PEN**	**Pt on FTO glass**	**Pt/Ti on PEN**	**PEDOT on ITO-PEN**
J_{SC} [mA/cm^2]	14.0	13.8	14.1	9.4	9.7	9.9	11.1	936	10.9
V_{oc} [mV]	783.2	805.3	787.1	682.8	718.9	698.7	656.7	664.6	713.8
FF	0.72	0.61	0.73	0.75	0.64	0.73	0.76	0.72	0.74
η [%]	7.9	6.79	8.0	4.8	4.5	5.0	5.6	4.6	5.7

6.13 Mozer et al.: A GORETEX-PEDOT system (2010)

Mozer et al. experimented the addition of a Goretex membrane between PEDOT and FTO to developed a compressible, flexible, highly conductive current-collecting electrode based on vapor-phase polymerized PEDOT on Goretex membrane [32].The Goretex membrane is coated with ~10 nm poly(maleic anhydride) using low-power plasma polymerization and afterwards sputter coated with a 40 nm layer of Au to reduce the sheet resistance. Au and plasma-polymerized layer prevents the membrane from being flooded by the oxidant vapor-phase used in the polymerization of PEDOT, thus allowing coating with PEDOT on only one side of the membrane. The authors tested the cell with gold, but stated that the noble metal could be replaced with a cheaper solution obtaining the same efficiencies. The overall thickness of the CE measured by SEM was in the range of 400-500 nm. This membrane proved to be perfect for both gaseous exchange and for contact with liquid electrolyte. Atomic force microscope (AFM) images revealed that the porosity of the GORETEX-PEDOT layer was comparable to that of the TiO_2 electrode (Figure 19). I-V measurements showed a maximum efficiency of 2.85%.

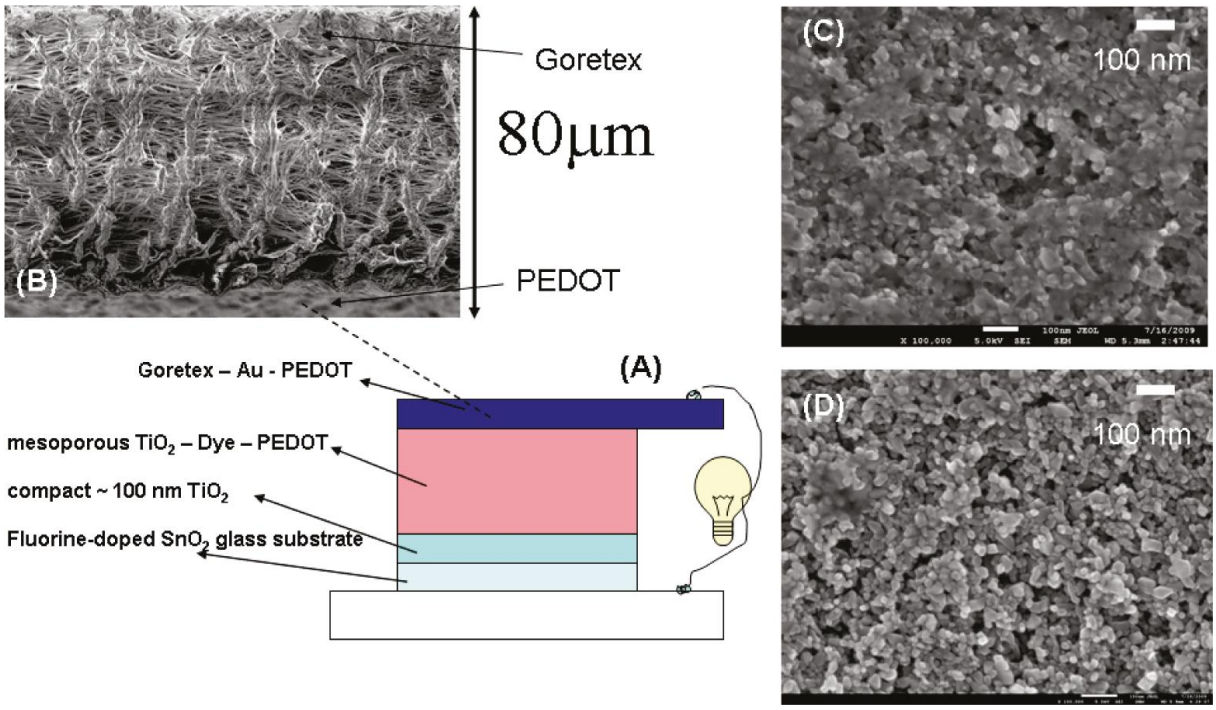

Figure 19 *(A) schematic representation of DSSC using Goretex-Au-PEDOT cathode. SEM images of (B) Goretex-Au-PEDOT cross-section. (C) morphologies after PEDOT deposition. (D) morphologies before PEDOT deposition. Reprinted with permission from [32].*

6.14 *Ahmad et al.: PEDOT based DSSCs (2010)*

Ahmad et al. reported electropolymerized PEDOT based DSSC [33]. After assembling the cell, the authors studied its performance. Through CV measurements, it was noticed that the curve showed the classic two oxidative peaks and two reductive peaks. These peaks intensity increased linearly with the scan rate. SEM analysis allowed to observe the surface of PEDOT, which exhibited homogeneous morphology and a high porosity with uniform grains (Figure 20). PV activities were investigated by comparing a cell using Pt and 3 cells with PEDOT. These three cells were differentiated by the polymerization time. The authors obtained values comparable to those of the Pt cell with PEDOT30 sample (polymerization time: 30 s, Table 9).

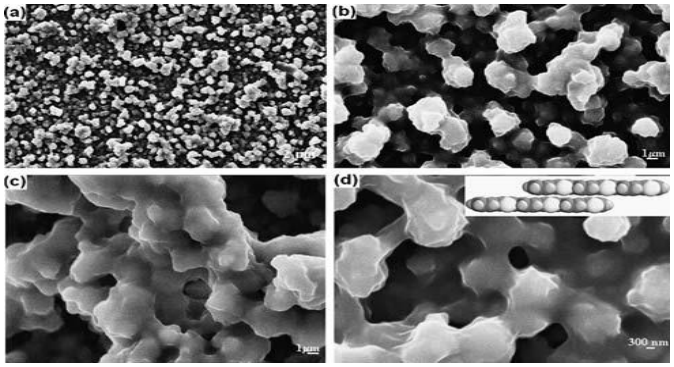

Figure 20 *SEM images of PEDOT films at (a) 200x103, (b) 500x103, (c) 500x103 and (d) 1000x103 times magnification and with different scale bar. Reprinted with permission from [33].*

Table 9 *PV performance of with various counter electrode. Adapted and reprinted with permission from [33].*

CE	V_{oc} [mV]	J_{sc} [mA/cm^2]	FF	η [%]
Thermal Pt	747	15.9	0.73	8.71
PEDOT30	693	15.0	0.76	7.93
PEDOT60	683	15.2	0.75	7.86
PEDOT120	673	15.5	0.75	7.87

6.15 Sakurai et al.: TiO_2/PEDOT-ClO_4^- double layer as CE (2011)

Sakurai et al. investigated the performance of DSSCs with TiO_2/PEDOT-ClO_4^- CEs to increase the conversion efficiency due to improvements in interfacial roughness and electron transfer [34]. The cathode was prepared by depositing a thin film of TiO_2 onto FTO glass and then depositing PEDOT-ClO_4^- via electro-polymerization. SEM and XRD analyses were made to measure the thickness of the TiO_2 and PEDOT layers and to investigate their crystalline structure. Through CV measurements, the authors noted that the double layer TiO_2/PEDOT-ClO_4^- decreased the reduction current density, thus increasing cell performance. EIS measurements were also made to evaluate the interface resistance between the electrolyte and the electrode (R_2). It can be noted that, using the TiO_2/PEDOT-ClO_4^- CE, R_2 decreased by at least half of that of the electrode with only PEDOT-ClO_4^-. PV performance measurements showed a maximum efficiency of 4.61% for the TiO_2/PEDOT- ClO_4^- electrode.

6.16 Zhang et al.: MWCNT-PEDOT based DSSC (2011)

Zhang et al. inserted MWCNT into the PEDOT matrix to improve morphology and performances [35]. The CE was synthesized with oxidative electropolymerization on FTO. The samples studied differ from each other by deposition charge (5, 25, 100, 200, 400 mCcm^{-2}). Through SEM analysis it can be noted that MWCNT-PEDOT showed higher porosity and that the thickness of the film increased with increasing deposition charge (Figure 21). The PV performances were studied by comparing different CE: Pt, 100 mCcm^{-2} MWCNT-PEDOT, 100 mCcm^{-2} PEDOT. Table 10 shows the values and you can see that the CE studied in this article shows even better performance of the electrode at Pt. Subsequently, CV measurements were made to investigate the electrocatalytic activity of the CE. It was shown that the catalytic activity of MWCNT-PEDOT in the conversion of the redox pair I_3^-/I^- was particularly high compared to that of the CE with only PEDOT. The high catalytic activity could depend on the increase of the electrochemically active surface, therefore on the effect of the MWCNT. EIS measurement also proved that the charge transfer resistance at the interface (R_{CT}) was lower in the MWCNT-PEDOT CE (33.1 Ω, for Pt: 37.6 Ω and for PEDOT: 35.2 Ω). This demonstrated once again that the addition of MWCNT enhances the electrochemically active surface.

Table 10 *DDSCs PV performance with various CE. Adapted and reprinted with permission from [35].*

CE	J_{sc} [mAcm^{-2}]	V_{oc} [V]	FF	η [%]
Pt	11.3	0.759	0.631	5.43
MWCNT-PEDOT	11.5	0.742	0.641	5.47
PEDOT	10.3	0.744	0.632	4.84

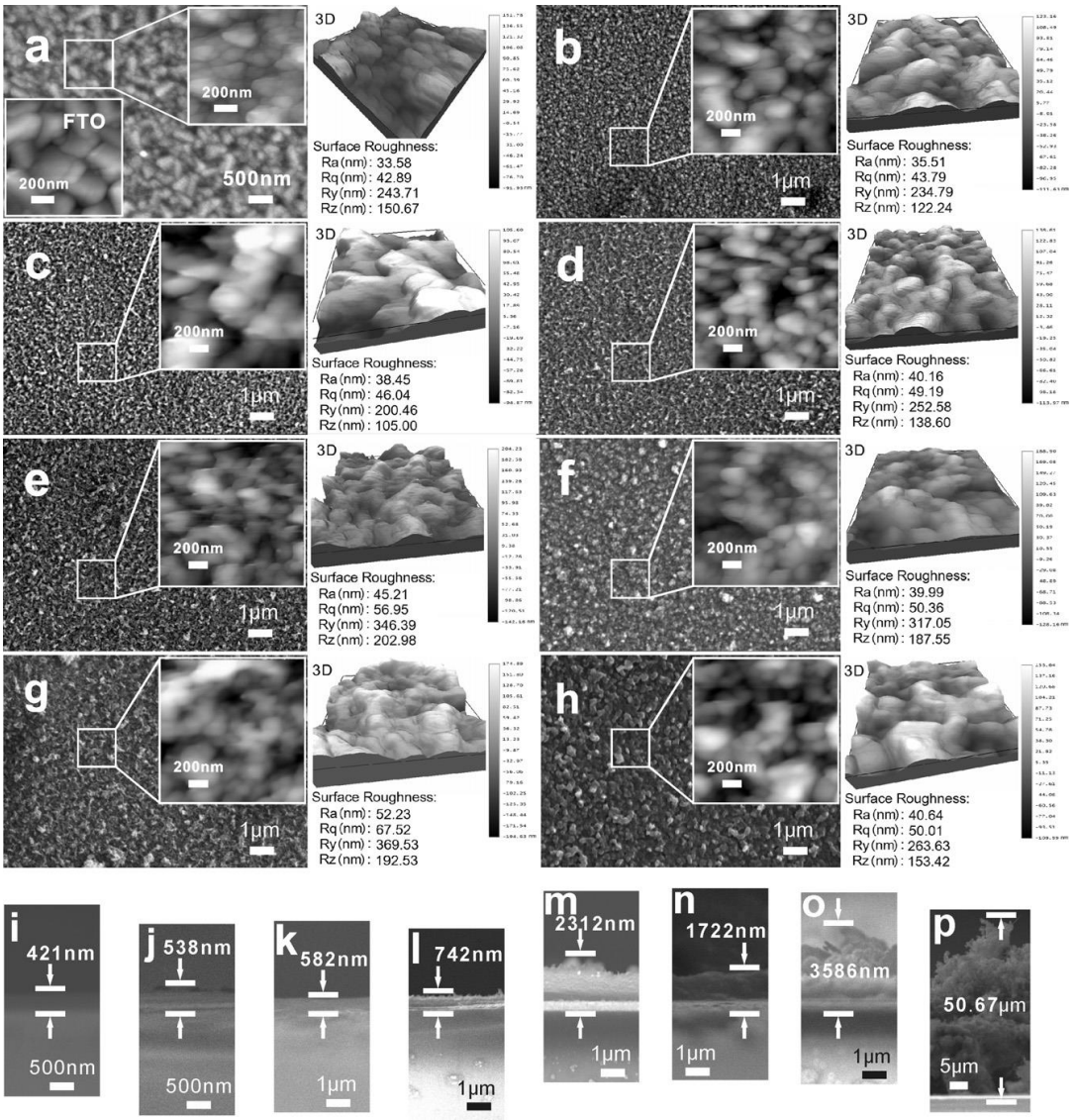

Figure 21 *SEM images, contact-mode AFM images (inset), corresponding 3D AFM images (on the right) and surface roughness parameters for the (a) Pt film, (b) 5 mC cm^{-2}, (c) 25 mCcm^{-2}, (d) 50 mCcm^{-2}, (e) 100mCcm^{-2}, (g) 200 mCcm^{-2}, (h) 400 mCcm^{-2} PEDOT–MWCNT film and (f) 10 mCcm^{-2} PEDOT film on FTO glass. The surface roughness parameters are labeled as follows: the arithmetical mean roughness (Ra), the root mean square roughness (Rq), the maximum peak (Ry) and the ten-point mean roughness (Rz). Cross-section SEM images of (i) bare FTO glass and of CEs with the various films on FTO glass: (j) 5 mC cm^{-2}, (k) 25 mCcm^{-2}, (l) 50 mCcm^{-2}, (m) 100 mCcm^{-2}, (o) 200 mCcm^{-2}, (p) 400 mCcm^{-2} PEDOT–MWCNT film and (n) 100 mCcm^{-2} PEDOT film. Reprinted with permission from [35].*

6.17 Kitamura et a.: a PEDOT:PSS and carbon black composite (2011)

Kitamura et al. have produced a CE composed of PEDOT:PSS with added carbon black (Cb) to improve its morphological properties [36]. It was observed that the product was a mesoporous material, with hybrid carbon black films inside it that improved its morphology. The composite electrode will be called PPCBF for ease. This CE was produced using the Layer-by-layer technique (LbL). The morphology was studied with a PPCBFs using 10 LbL cycles and various concentrations of carbon black. PPCBFs became more mesoporous as the carbon

black concentration increased (Figure 22). The authors then went on to analyse the PV performance by comparing it with that of an CE composed only of PSS on ITO glass and with that of a Pt CE. The cells were also studied how the deposition cycles of LbL layers varied. Increased deposition cycles improved cell performance. The best performance was achieved with PPCBFs made with 20 cycles with an efficiency of 4.70% only 8% lower than that of Pt (5.12%).

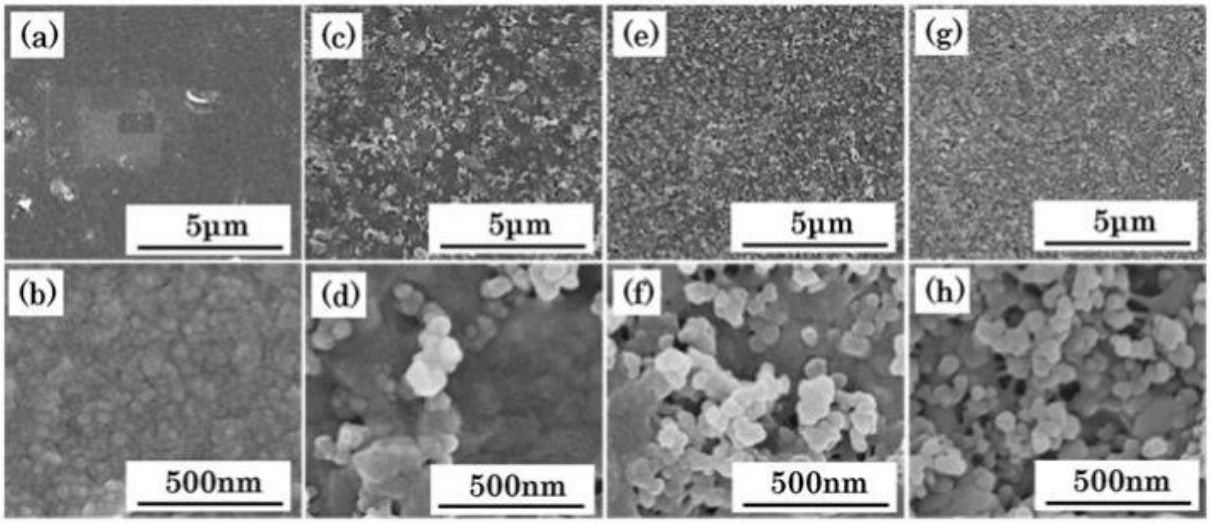

Figure 22 *FE-SEM images of PPCBFs with different Cb concentrations: (a), (b) 0 wt%, (c), (d) 0,1 wt%, (e), (f) 0,5 wt% and (g), (h) 0,75 wt%. Reprinted with permission from [36].*

6.18 Sudhagar et al.: CoS doped PEDOT:PSS (2011)

The authors reported the performance of a DSSC with PEDOT:PSS incorporated with CoS nanomaterial to improve the catalytic effect [37]. The CV tests were performed by comparing different CE: PEDOT:PSS, CoS-PEDOT:PSS, Pt and bare CoS. The cathodic peak current density is high in the CE composed of CoS-PEDOT:PSS, this also leads to an increase in electrocatalytic activity, confirming the beneficial effect of adding CoS. The model of the CoS-PEDOT:PSS curve was very similar to that of Pt (Figure 23). The PV performance was analysed by J-V analysis. CoS-PEDOT:PSS showed high efficiency (5.4 %), Pt (6.1 %). They also noted that the photocurrent density of CoS-PEDOT:PSS was higher than that of PEDOT:PSS one (13.2 $mAcm^{-2}$ and 11.6 $mAcm^{-2}$ respectively). The authors were able to confirm that the performance had improved and was comparable to that of Pt. Finally, the authors studied the effect of CoS concentration on catalytic activity. Electrochemical impedance analyses showed that the Rct resistance increased in CE CoS-PEDOT-PSS compared to CE PEDOT:PSS resistance (6.15 Ωcm^2 and 2.65 Ωcm^2 respectively). However, the diffusion resistance of Nerst has decreased drastically (39 Ωcm^2 and 85.5 Ωcm^2).

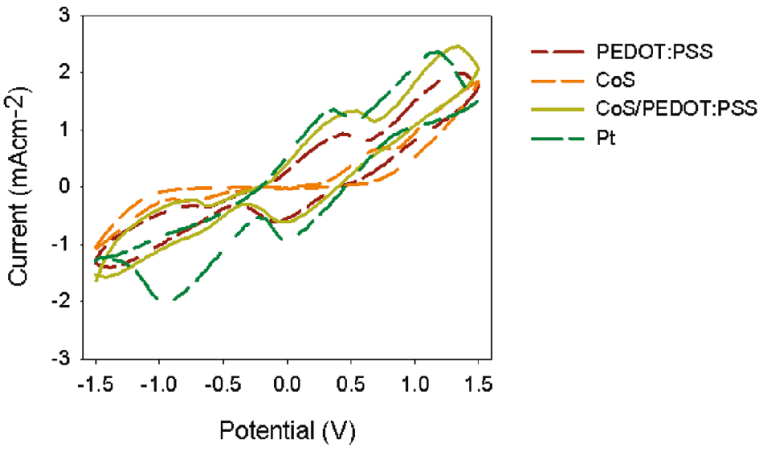

Figure 23 *Cyclic voltammograms of pristine PEDOT:PSS, CoS, CoS/PEDOT:PSS and Pt electrodes. Reprinted with permission from [37].*

6.19 Shin et al.: Carbon nanotubes/PEDOT (2011)

Shin et al. studied a structure composed by carbon nanotubes coated with a layer of PEDOT (CNT/PEDOT) to improve the morphology [38]. Figure 24 shows the synthesis mechanism of CNT/PEDOT core/shell nanotubes. Nanotubes were synthesized using dodecylbenzenesulfonic acid (DBSA) as surfactant.

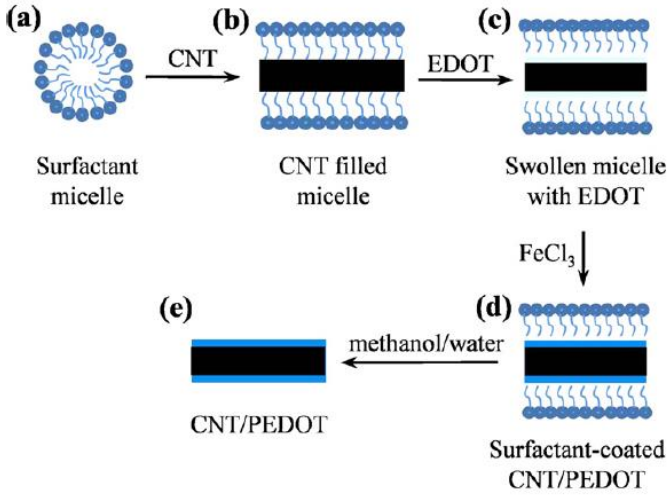

Figure 24 *Schematic illustration of the synthesis of CNT/PEDOT CE. Reprinted with permission from [38].*

Transmission electron microscope (TEM) images showed that the nanostructures formed properly, the surface of the CNTs was completely covered by a 2-6 nm thick layer of PEDOT. J-V measurements were made by comparing three different CEs: CNT, PEDOT, CNT/PEDOT. The results are shown in Table 11. It could be noted that the J_{sc} in the CE CNT/PEDOT fell to 9.0 $mAcm^{-2}$ but the V_{oc} and the FF increased considerably obtaining the highest efficiency of 4.62%.

Table 11 *PV parameters of CNT, PEDOT, CNT/PEDOT CEs. Adapted and reprinted with permission from [38].*

CE	J_{sc} [mAcm^{-2}]	V_{oc} [mV]	FF	η[%]
CNT	12.2	623	0.51	3.88
PEDOT	9.7	628	0.71	4.32
CNT/PEDOT	9.0	702	0.73	4.62

6.20 Trevisan et al.: nanostructured PEDOT nanotubes (2011)

The authors demonstrated how nanostructured PEDOT increases the efficiency of a DSSC [39]. The study was done by comparing two cell types: cell A: thickness of TiO_2 layer 19 μm and filled with the redox couple I^-/I_3^- in acetonitrile:valenothrile; cell B: thickness of TiO_2 layer 12 μm and the electrodes were prepared with methoxypropionitrile as solvent. The A cell showed better performance than the B cell. By the results shown in Table 12 you can see that the values of V_{oc}, J_{sc}, FF are higher in cell A rather than in cell B, regardless of the CE. The authors observed that the main difference in performance in cells A was FF (and consequently η); in descending order it was observed that Pt>PEDOT-NT>PEDOT. In the case of cell B, the tests were done with the CEs Pt and PEDOT-NT and the same trend was observed. With EIS measurements, this difference could be justified by the increase of the resistance in series R_{series} ($R_{series}=R_s+R_{ce}+R_d$). The CE contribution is in the sum R_s+R_{ce} and it was noted that for the cell type A this sum was lower in the counter electrode to Pt. In type B cells it was noted that the Rs was less in the case of Pt CE, but this difference could not compensate for the high catalytic activity of the CE composed of PEDOT-NT.

Table 12 *PV performance of DSSCs with various CEs and constructions way. Adapted and reprinted with permission from [39].*

CE	Cell Type	V_{oc} [V]	J_{sc} [mAcm^{-2}]	FF	η [%]
Pt	**A**	0.74	16.21	0.71	8.5
PEDOT NT	**A**	0.72	16.24	0.70	8.3
PEDOT flat	**A**	0.73	15.83	0.69	7.9
Pt	**B**	0.69	13.63	0.62	5.9
PEDOT NT	**B**	0.68	13.13	0.68	6.3

6.21 Yue et al.: PEDOT:PSS/carbon CE performance (2011)

The authors tested PEDOT:PSS/carbon conductive composites [40]. The particularity of this cell is the heterojunction replacing the redox pair I^-/I_3^-: [6,6]-phenyl-C61-butyric acid methyl ester (PCBM)/poly(3-hexylthiophene) (P3HT). Figure 25 shows the structure of the cell.

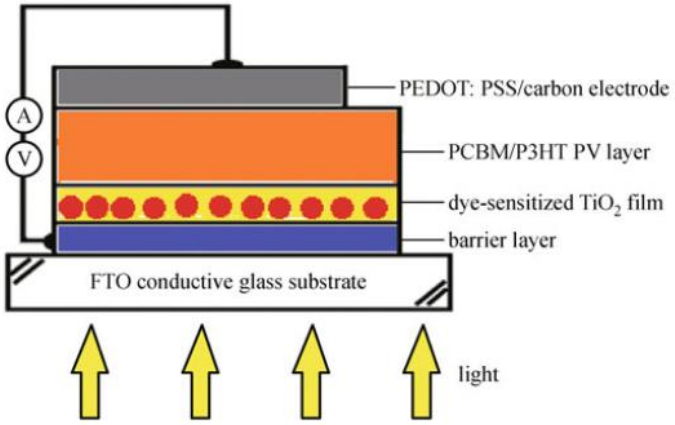

Figure 25 *schematic diagram of the PEDOT:PSS/carbon and TiO_2/dye/PCBM/P3HT/PEDOT:PSS/carbon solar cell. Reprinted with permission from [40].*

The authors also studied the influence of temperature by carrying out two tests: Series 1, the cell was annealed under vacuum conditions; Series 2, the cell was annealed under atmospheric conditions. It was noted that conductivity increased in both series by increasing the heating temperature with maximum values at T of 80 °C: 1,728 and 1,720 Scm^{-1} respectively. In all tests the results of series 1 were better than series 2 and the authors justified these results by thinking that the vacuum environment had less H_2O and O_2, so less impact on the electrode. The J-V curves showed that PEDOT:PSS/carbon had better performance than Pt, with efficiencies of 4.11% and 3.42% respectively.

6.22 Thompson et al.:Monolithic carbon/PEDOT DSSC based (2012)

Thompson et al. studied a monolithic DSSC [41]. The diagram can be seen in Figure 26. The cell consisted of a TiO_2 working electrode and a graphite/carbon layer as CE. The EDOT monomer was electrodeposited on the CE and electropolymerization to PEDOT was activated. The effect of the thickness of the carbon film was also studied, printing different layers and studying the variation in the resistance of the sheet. It was observed that with one carbon layer, and without PEDOT, the resistance was variable. When PEDOT was deposited, the resistance remained constant, confirming what was expected: the deposit of PEDOT evened out the CE surface, making it smoother. By increasing the number of layers, the resistance increased dramatically. The final thickness after the deposition of PEDOT on a carbon layer was: 18 µm. I-V measurements confirmed that the deposition of PEDOT on carbon increased efficiency compared to a carbon-only cell (5.2% and 2.3% respectively).

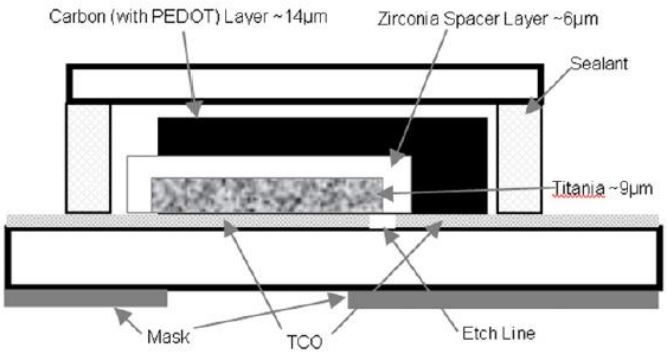

Figure 26 *Schematic view of a monolithic cell. Reprinted with permission from [41].*

6.23 Xu et al.: different TiN:PEDOT-PSS CEs (2012)

The authors studied the performance of three different CEs, all composed by TiN and PEDOT-PSS (TiN:PEDOT-PSS) but built with different shapes to enhance the catalytic sites [42]. The first electrode was made up of titanium nitride nanoparticles (TiN(P)), the second of TiN nanorods (TiN(R)) and the last of TiN mesoporous spheres (TiN(S)). Through an analysis of the surface morphology it was observed that TiN(P) was better dispersed on the surface of the PEDOT-PSS, benefiting electronic conduction (Figure 27). CV tests were carried out with the CEs in question and Pt CE. It was noted that TiN(R):PEDOT-PSS and TiN(P):PEDOT-PSS had properties comparable to those of Pt. The J-V tests confirmed the excellent performance of TiN(R):PEDOT-PSS and TiN(P):PEDOT-PSS CEs which reported an efficiency of 7.06% and 6.89% respectively, higher than that of Pt which was 6.57% (TiN(S):PEDOT-PSS reported 6.19%). EIS measurements also demonstrated the superiority of TiN(R):PEDOT-PSS and TiN(P):PEDOT-PSS CEs. These electrodes reported much lower charge-transfer resistances than Pt and TiN(S):PEDOT-PSS Electrode (R_{ct} TiN(P):PEDOT-PSS=0.28 Ωcm^2, R_{ct} TiN(R):PEDOT-PSS=0.51 Ωcm^2 R_{ct} Pt=1.06 Ωcm^2, R_{ct} TiN(S):PEDOT-PSS=1.14 Ωcm^2).

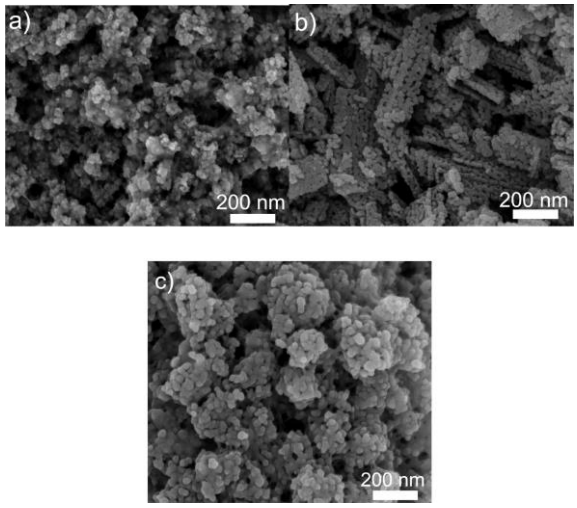

Figure 27 *SEM images of TiN:PEDOT-PSS: (a) TiN(P):PEDOT-PSS, (b) TiN(R):PEDOT-PSS and (c) TiN(S):PEDOT-PSS. Reprinted with permission from [42].*

6.24 Balis et al.: QSS-DSSC with gel electrolyte and PEDOT (2012)

The authors investigated the performance of a cell based on PEDOT and a gel electrolyte, so as to confirm that the gel was more efficient than the liquid electrolyte with PEDOT CE [43]. The electrolyte used was a precursor of Ureasil. The cell under examination was therefore an almost solid state QSS-DSSC. The parameters of a QSS-DSSC were compared with Pt and PEDOT. A fundamental thing was that the thickness of the PEDOT was very large compared to that of Pt, but it still had very good catalytic and electron conduction properties. J-V tests showed that the efficiency of the cell using PEDOT was 15% lower than that using Pt (6.4% and 6.9% respectively).

6.25 Yue et al.: PEDOT:PSS with graphite and carbon black (2012)

In this article a CE composed of PEDOT:PSS mixed with graphite and carbon black (PEDOT:PSS/C) has been introduced to enhance the cathode activity [44]. The electrode in question was studied with CV measurements noting larger current density peaks (both oxidation and reduction) than those of a normal Pt electrode (Figure 28). These results showed that PEDOT:PSS/C could have a lower resistance and higher conductivity, thus increasing the performance of the cell. EIS measurements found that the resistances varied with temperature and reached a minimum of Rct = 7.58 Ωcm^2 at 80 °C. However, Pt showed lower resistances at this temperature (Rct = 3.23 Ωcm^2). The conductivity was studied showing the same Rct trend and presenting a maximum of 1.720 Scm^{-1} at 80 °C. The J-V measurements showed that the CE composed by PEDOT:PSS/C had PV parameters very similar to Pt, however the efficiency was lower η(PEDOT:PSS/C) = 7.01 %, η(Pt) = 7.78%.

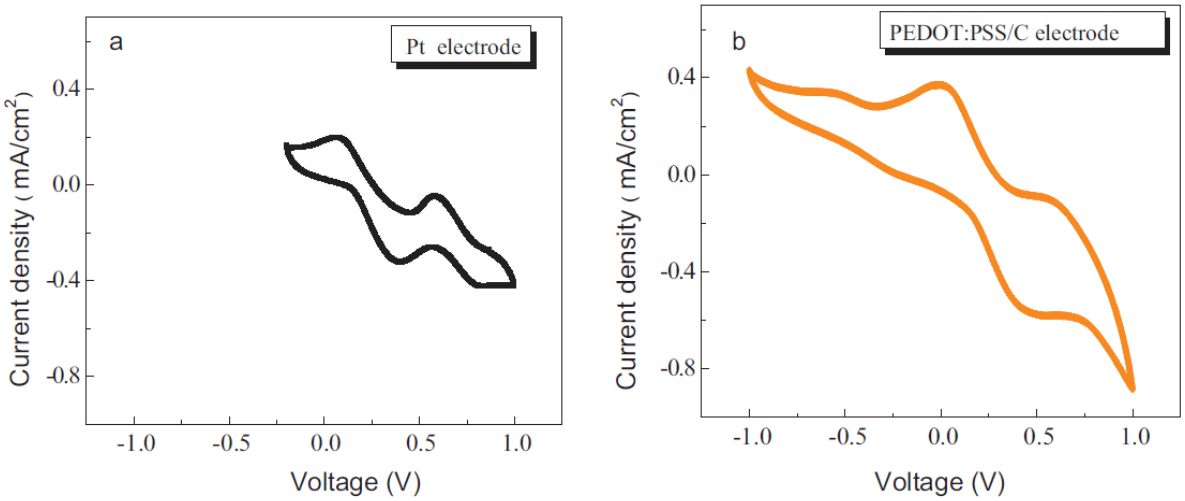

Figure 28 *CV for (a) Pt and (b) PEDOT:PSS/C. Reprinted with permission from [44].*

6.26 Kim et al.: PEDOT:PSS CE and different polymer electrolytes (2012)

The authors studied how to increase the photovoltaic performance of some DSSCs using PEDOT:PSS and various polymers as electrolyte [45]. The polymers in question are PEO, PEG, PMMA and PVAc. These performances were studied through a solar simulator and EIS. The results showed that the efficiencies were: 4.08% for PEO, 3.87% for PEG, 0.49% for PMMA and 0.20% for PVAc. To compare these efficiencies, the authors did the same studies with a DSSC with the CE composed by Pt and found that the efficiencies were all around 5.7% ± 0.1. Subsequently, they went to research why, for polymers PMMA and PVAc, the performance decreased so much through EIS measurements. They noted that the charge transfer resistance of the electrode PEDOT:PSS/polymer electrolyte interface was very high for PMMA and PVAc polymers. These results demonstrated the low PV performance values for these cells. They concluded by confirming that the choice of polymer used greatly affected the PV characteristics and probably the low conductivity of these polymers went against them.

6.27 Yue et al.: Application of PEDOT:PSS/Polypyrrole (2012)

Yue et al., have tested PEDOT:PSS and Polypyrrole (PPy) (PEDOT:PSS/ PPy) composite to enhance the cell performance [46]. EIS measurements were made to investigate internal resistances and the authors were able to confirm that the cell had a very low interfacial charge transfer resistance (Rct) compared to the other cells (Table 13). The CV measurements confirmed the hypothesis of the higher electrocatalytic activity of CEs composed of: PEDOT:PSS/PPy. The best operating temperature conditions were also studied to study the conductivity and resistance of the CE. It was observed that the best performances were obtained at 80 °C and with a conductivity of 1.563 S/cm and a resistance of 0.64 Ωcm. Photovoltaic performance was studied by comparing the electrodes: PEDOT:PSS, PPy, PEDOT:PPS/ PPy and Pt. From Table 13 it can be seen that the performance of PEDOT:PSS/ PPy is comparable to that of Pt, while the other two CE have much lower performance.

Table 13 *PV performance of DSSCs composed by: PEDOT:PSS, PPy, Pt and PEDOT:PSS/PPy CEs. Adapted and reprinted with permission from [46].*

CE	V_{oc} [V]	J_{sc} [mAcm^{-2}]	FF	η [%]	R_{ct} [Ωcm^2]
PEDOT:PSS	0.73	12.53	0.69	6.31	22.32 ± 0.02
PPy	0.72	11.15	0.65	5.23	29.32 ± 0.02
Pt	0.76	14.75	0.69	7.73	2.1 ± 0.02
PEDOT:PSS/PPy	0.75	14.27	0.71	7.60	4.3 ± 0.02

6.28 Maiaugre et al.: high performance TiO_2 nanoparticle:PEDOT-PSS (2012)

Maiaugree et al. studied the performance of a DSSC with a CE made up of TiO_2 nanoparticles mixed with PEDOT-PSS, assuming that a morphological improvement would benefit performance [47]. The SEM images showed that the surface of the pure PEDOT-PSS was very smooth and when mixed the TiO_2 became rough (Figure 29). The DSSC showed very high performance, with an efficiency of 8.49%, higher than Pt sputtered (7.5%). This performance improvement was related to the addition of TiO_2 nanoparticles.

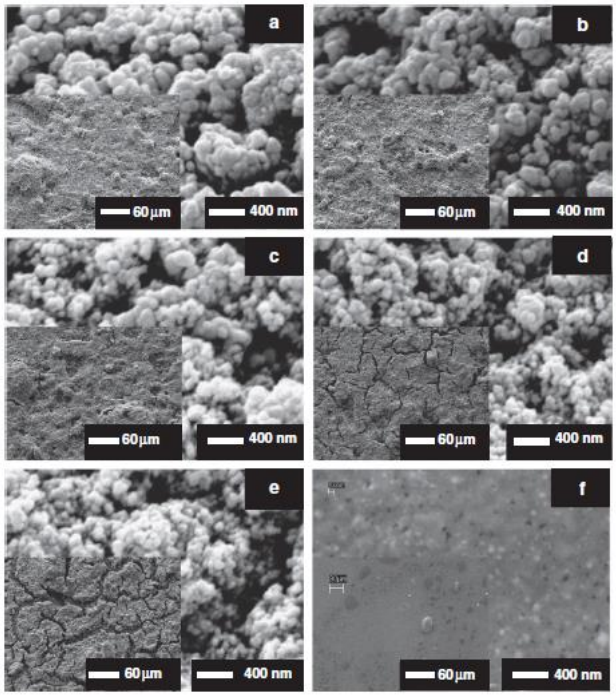

Figure 29 *SEM images of PEDOT:PSS mixed with TiO_2 in different weight amount: (a) 100 wt% TiO_2, (b) 70 wt% TiO_2, (c) 50 wt% TiO_2, (d) 30 wt% TiO_2, (e) 10 wt% TiO_2, (f) pure PEDOT:PSS. Reprinted with permission from [47].*

6.29 Xiao et al.: PEDOT- MWCNT composite (2012)

In this article, the authors studied PEDOT-coated MWCNT by electropolymerization in order to improve the morphology of the cathode [48]. They were compared: MWCNT, PEDOT, FTO naked. Through FE-SEM images, the fibrous morphology of the CE was observed, and it was also noted that the thickness of the PEDOT increased with increasing duration of electropolymerization (Figure 30). EIS measurements made it possible to observe and measure the resistances inside the devices. Rct was low for CE PEDOT and PEDOT/MWCNT (1.27 Ωcm^2 and 1.06 Ωcm^2). This showed that the PEDOT itself had superior electrocatalytic activity. Finally, the efficiencies obtained were very high for PEDOT/MWCNT and PEDOT, even more than one cell with Pt (7.03%, 6.39% and 5.88% respectively).

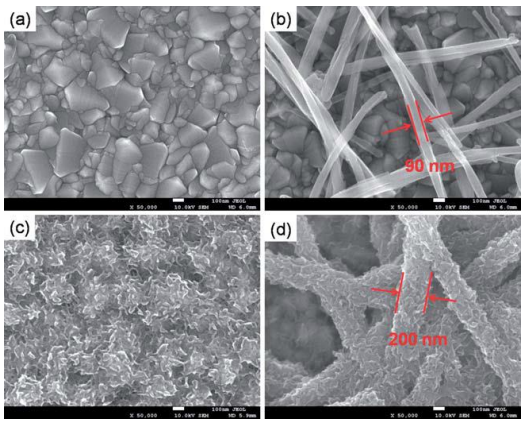

Figure 30 *FE-SEM images of (a): FTO glass, (b) MWCNT, (c) PEDOT and (d) PEDOT/MWCNT. Reprinted with permission from [48].*

6.30 Lee et al.: best efficiency achieved with PEDOT (2012)

Lee et al. studied the performance of PEDOT nanofibres (PEDOT-NF) [49]. To increase the dispersion of PEDOT-NF they added dimethylsulphoxide (DMSO 5 wt%) to the resulting solution. They then compared the performance of PEDOT-NF with and without DMSO (PNFD and PNFD respectively). CV measurements showed that the peak potential separation value (ΔEp) of PNFD was lower than PNFD (0.44 V and 0.49 V), indicating the best electrocatalytic activity towards the I^-/I_3^- redox reaction. These results also coincided with EIS measurements, which showed lower resistance to charge transfer (Rct), thus increasing cell efficiency. In general, compared to bulk PEDOT, performance was better, achieving the best performance ever. As can be seen in Table 14, very high efficiencies were achieved, even higher than Pt, confirming that PEDOT-NF had better electrochemical characteristics.

Table 14 *PV performance of DSSCs with various CEs. Adapted and reprinted with permission from [49].*

CE	V_{oc} [mV]	J_{sc} [mAcm^{-2}]	FF %	η %
Pt	747	15.8	73.0	8.6
PNF	717	15.7	73.4	8.3
PNFD	724	17.5	72.6	9.2
Bulk PEDOT	669	14.8	68.8	6.8

6.31 Zhang et al.: high performance PEDOT:PSS $CuInS_2$ (2012)

In this article the authors studied a CE composed by $CuInS_2$ nanocrystals (NCs) incorporated with PEDOT:PSS [50]. The SEM images showed that the $CuInS_2$ NCs were hexagonal-plate and that PEDOT:PSS adhered to the boundaries of the NCs, increasing homogeneity and adhesion to the FTO. PV performances were researched, and it was shown that this CE had good parameters, reaching the efficiency of 5.5% (comparable to that of the Pt, 5.51%). The CV and EIS measurements both showed that the catalytic activity was very good (comparable to that of the Pt) and that the cell internal resistances were modest (Rct=2.11 Ω and Rs=14.02 Ω), thus confirming the high efficiency value, J_{sc}, V_{oc} and FF (5.5%, 16.01 mAcm^{-2}, 0.7 V and 58.1% respectively).

6.32 Xiao et al.: PEDOT via Pulse potentiostatic electropolymerization (2012)

Xiao et al. studied how the different synthesizing techniques of PEDOT modified the performance when used as CE in a DSSC [51]. They investigated three methods of electropolymerization: CV, Constant Potential (I-t) and pulse constant potential (pulse potentiostatic). FE-SEM images showed that, using the CV method, the layer surface was flaky and nonuniform, instead with the I-t method and potentiostatic pulse was continuous and uniform. In addition, PEDOT particles became smaller and smaller when the method switches from I-t to the powerful pulse potentiostatic one. The pulse frequency also affected particle growth: the higher the pulse frequency the smaller the particle diameter. The best condition (nano-meadows morphology) was obtained under 1.2 V pulse-on potential, 0.2 V pulse-reversal potential, 1 s pulse-on period, 0.5 s pulse-reversal period and total 900 duration time (Figure 31,

P-7x10,000 and P-7x1,00,000). CV measurements showed that the PEDOT P-7 CE had excellent electrocatalytic activity thanks to the high oxidation and reduction densities obtained. EIS measurements also confirmed that this electrode had high electrocatalytic performance, with a R_{ct} of 1.27 Ωcm^2, lower than that of Pt (1.56 Ωcm^2). The PV performances obtained are summarized in Table 15. The PEDOT P-7 CE proved to be clearly better than the Pt except in Voc (however very similar), while the other CEs showed lower performance, thus demonstrating that the electrode manufacturing method has a great influence on performance.

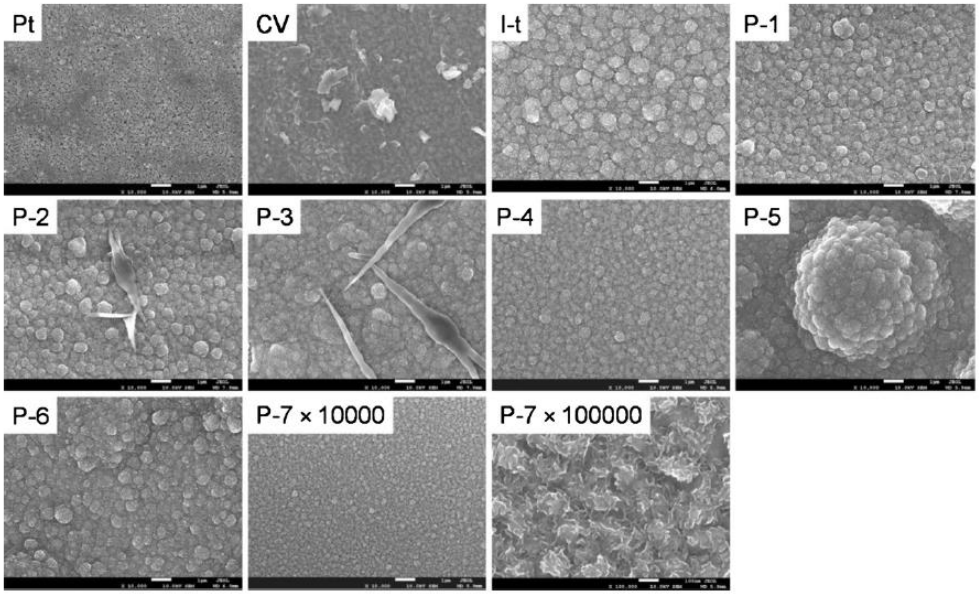

Figure 31 *SEM images of Pt, CV PEDOT, I-t PEDOT and pulse potentiostatic CEs. Reprinted with permission from [51].*

Table 15 *PV performance of Pt, CV PEDOT, I-t PEDOT and pulse potentiostatic PEDOT CEs. Adapted and reprinted with permission from [51].*

CE	V_{oc} [mV]	J_{sc} [mA/cm^2]	FF	η %
Pt	751	11.39	0.67	5.75
CV	738	11.30	0.59	4.95
I-t	745	12.32	0.62	5.69
P-7	747	12.84	0.66	6.40

6.33 Xiao et al: PEDOT deposited on Ti network (2012)

Xiao et al. studied the performance of an CE composed of electrodeposited PEDOT on a network of Ti (PEDOT/Ti) [52]. The range of potential used can control the growth of the electropolymerization PEDOT arrays, through SEM images it was observed that it was better to work at low voltages "low E" of 0.2 V and "scan rate" of 0.05 Vs^{-1}. EIS measurements showed that the resistance decreased as the voltage decreased, reaching a minimum of 73.44 ± 0.03 Ωcm^2 for Rs and 34.34 ± 0.02 Ωcm^2 for Rct. The best performances were: Voc=0.718 V, Jsc=7.06 $mAcm^{-2}$, FF=0.687 and η=6.33%.

6.34 Jeon et al.: QSS-DSSC based on Polymeric electrolyte ionic liquid ad PEDOT (2013)

In this paper, the authors studied a quasi-solid-state DSSCs assembled with a polymeric ionic liquid electrolyte (PIL) (in this case Poly(1-methyl 3-(2-acryloyloxypropyl) imidazolium iodide)) and PEDOT-NF CE [53]. TEM images showed that PEDOT-NF had a very small diameter (10-50 nm) and a smaller grain boundary than bulk PEDOT, resulting in more efficient electron transfer. Then, the authors, studied how the conductivity of gel polymer electrolytes changed as a function of Poly(1-methyl 3-(2-acryloyloxypropyl) imidazolium iodide) (PMAPII) content. The conductivity increased with the increase of the PMAPII content up to 16 wt%, then decreased, reaching a value of $4.9*10^{-3}$ Scm^{-1}. The best performances achieved were with 16 wt% of PMAPII: Jsc: 14.7 [$mAcm^{-2}$], Voc: 0.79 [V], FF:0.7 and η:8.12%.

6.35 Erten et al.: Ruthenium-PEDOT:PSS (2013)

Erten et al. investigated the PV properties of a cell composed of a PEDOT:PSS CE and RuII(4,7-diphenyl-1,10-phenanthroline-disulfonic acid disodium salt)-bis(2,20-bipyridine), [Ru(L1)(bpy)2](PF6)2 (K403) in aqueous solution as it guaranteed advantages in the manufacture of DSSC [54].The performance of this cell was very low: V_{oc}: 364 [mV], J_{sc}: 1.3 [$mAcm^{-2}$], FF: 0.64 and η: 0.29%.

6.36 Ellis et al.: PEDOT from aqueous micellar electrodeposition (2013)

The authors produced DSSCs composed by PEDOT as CE and sodium dodecyl sulphate (SDS) and water as solvent for electrochemical polymerization [55]. The cells were blue-coloured, the more intense the colour the longer the deposition time had been (PEDOT_175s, PEDOT_250s and PEDOT_400s). Electropolymerization was performed on both FTO and flexible plastic, to test the DSSC also for flexible and modellable applications. In both cases the PEDOT film was homogeneous. The EIS measurements showed that as the thickness increased, the R_{ct} resistance increased. However, all measured R_{ct} resistance were smaller than the Pt (R_{ct} PEDOT_400s=0.26 and R_{ct} Pt=5.5 Ωcm^2). The PV performances showed that the cells based on PEDOT CE showed higher efficiencies than that one based on Pt, reaching values of 6.2% (PEDOT_175s) and 5.0% (Pt).

6.37 Chiang et al.: High-efficient PEDOT:PSS (2013)

Chiang et al. reported new methods in order to increase the performance of the PEDOT:PSS film, after that they tried to combine a layer of PEDOT over the layer of PEDOT:PSS to combine the catalytic properties with those of a good CE [56]. The PH-1000 (PEDOT:PSS aqueous solution/suspension) was added to 10% (in volume) of EG (ethyleneglycol) then 5% (in volume) of HFIP (hexafluoro-isopropyl alcohol) was mixed (PEDOT:PSS/H2O/EG/HFIP). PH-1000 mixed with 10% EG (PEDOT:PSS/H2O/EG) was prepared for comparison. The conductivity of the M-PEDOT:PSS film (PEDOT:PSS/H2O/EG/HFIP) was much higher than that of PEDOT:PSS-E (PEDOT:PSS/H2O/EG) (1638 S/cm and 353 S/cm respectively), thus demonstrating that the best compound was M-PEDOT:PSS. SEM images showed that M-

PEDOT:PSS films consisted of packing with spherical particle. The spherical particles were smaller, more homogeneous and better ordered than PEDOT:PSS-E one. When the PV performance of M-PEDOT:PSS was investigated as CE the authors realized that it could not be a good electrode and a catalyst simultaneously. A layer of PEDOT was inserted above the M-PEDOT:PSS (Figure 32) and the performances were studied again, obtaining excellent results. In fact, the efficiency of PEDOT/M-PEDOT:PSS reached the value of 7.29% (7.62% efficiency of Pt).

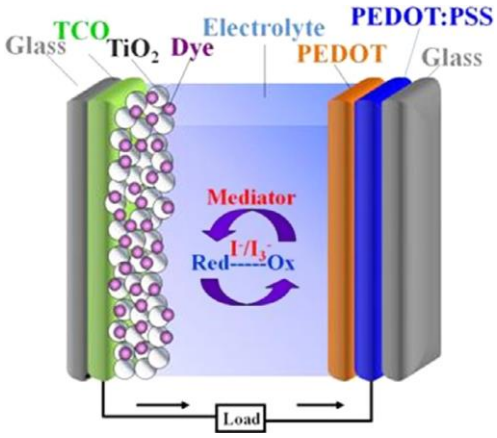

Figure 32 *The architecture of DSSC device based PEDOT/ M-PEDOT:PSS. Reprinted with permission from [56].*

6.38 Chou et al.: PEDOT:PSS with different annealing temperature (2013)

Chou et al. tested the influence of annealing temperature on PEDOT:PSS used as CE in DSSC [57]. The morphology of the PEDOT:PSS film evolved from drop-like dispersed randomly into earthworm-like bars dispersed homogeneously. The tested temperatures were 80 °C, 100 °C and 120 °C. Cell efficiencies increased as the annealing temperature increased to a maximum of 6.08%, efficiency comparable to that of a Pt CE.

6.39 Nagarajan et al.: PEDOT on exfoliated graphite (2013)

Nagarajan et al. tested for the first time a CE composed of PEDOT on exfoliated graphite (EFG) [58]. HR-TEM (high resolution TEM) results showed that EFG sheets were crystalline with internal cracks, but when PEDOT was inserted, the composite became flexible without showing cracks. The flexibility was attributed to the fibres of PEDOT that reinforced the surface giving it more elasticity. SEM images showed that the CE possessed a high surface area and a highly porous structure, indicating good catalytic activity. The PV performances were tested on four cells with four different CEs: EFG, PEDOT/FTO, PEDOT/EFG, Pt/FTO. Table 16 shows that the CE of PEDOT/EFG achieved the best performance. EIS measures confirmed that internal cell resistance decreased dramatically with the PEDOT/EFG CE, allowing the FF to increase (from 0.23 in the pristine EFG to 0.72 in the PEDOT/EFG). CV tests were carried out on the same electrodes, demonstrating how the pristine EFG showed very low catalytic activity but when the PEDOT the catalytic reduction current was incorporated drastically increased, showing excellent electrocatalytic performance.

Table 16 *PV performance of various CEs in DSSC. Adapted and reprinted with permission from [58].*

CE	V_{oc} [V]	J_{sc} [mA/cm^2]	FF %	η %
EFG	0.75	10.1	0.23	1.78
PEDOT/FTO	0.75	9.04	0.69	4.81
PEDOT/EFG	0.77	10.2	0.72	5.78
Pt/FTO	0.79	9.01	0.63	4.49

6.40 Yun et al.: Effect of MWCNT concentration in PEDOT:PSS CE (2013)

Yun et al. tested the effect of MWCNT concentration in PEDOT:PSS as CE in DSSCs devices [59]. They confirmed that the maximum concentration of MWCNT was 0.3wt% thus obtaining the highest efficiency of 6.0%, J_{sc} of 12.4 mAcm^{-2} and FF 62.8%. EIS measurements confirmed that internal cell resistance decreased as the MWCNT concentration increased to a minimum of R_s=17.0 Ωcm^2 per 0.3 wt% in PEDOT:PSS. However, the efficiencies were lower than that one of a classic Pt/FTO cell (η=7.1%).

6.41 *Yue et al.: PEDOT:PSS with different annealing (2013)*

The authors tested PEDOT:PSS and graphite carbon mixture as CE in DSSC, also examining the effect of temperature and heat treatments [60]. The SEM images showed that before the carbon graphite was inserted the surface was smooth and with low roughness. After the insertion of graphite carbon, the surface was coarser and with a high surface area, improving the properties of the CE. CV and EIS measurements were made, finding that the CE had much higher current density at the I_3^- reduction peak than Pt Electrode. This can result in a faster reaction rate. R_{ct} for I^-/I_3^- redox reaction was lower for PEDOT:PSS than for Pt. Two different sets of electrodes were investigated: annealed in vacuum (series 1) and annealed in atmosphere (series 2). It was observed that for both series the maximum conductivity and the minimum sheet resistance were obtained at 80°C (1.73 S/cm and 1.72 S/cm, 11.94 Ωsq and 11.94 Ωsq for series 1 and series 2 respectively). Finally, PV performances were studied for different annealing temperatures (40, 60, 80, 100, 120 and 140 °C), obtaining the best performance always at 80 °C (Table 17).

Table 17 *PV performance for different annealing temperature. Adapted and reprinted with permission from [60].*

Temperature °C	V_{oc} [V]	J_{sc} [mAcm^{-2}]	FF	η %
40	0.74	11.8	0.54	5.0
60	0.80	12.7	0.66	6.7
80	0.81	13.6	0.69	7.6
100	0.75	12.4	0.61	5.5
120	0.72	12.2	0.60	5.4
140	0.74	12.0	0.60	5.3

6.42 Yuan et al.: POM-doped PEDOT film (2013)

Yuan et al. manufactured a hybrid film consisting of a mixture of polyoxometalate (POM)-(K8[Siw11o39] 13H_2O) and PEDOT (SiW_{11}-PEDOT) via electropolymerization in aqueous

solution [61]. Then, the authors investigated three types of CEs: Siw11-PEDOT, PEDOT-only and Pt. They achieved remarkable performance for the SiW_{11}-PEDOT CE, with an efficiency of 5.81%, comparable to that of the Pt (η_{Pt}: 5.94%). After that, the authors tried to insert a precursor: 3-Aminopropyltriethoxysilane (APS). This precursor raised the performance, reaching an efficiency of 5.93%, close to that of the Pt. FESEM images showed that SiW_{11}-PEDOT had denser surface films compared to PEDOT-only. PEDOT-only also featured a network structure while SiW_{11}-PEDOT film displays a lotus leaf-like surface, with microstructure of small mastoid shapes regularly intermingled. The thickness of the Siw11-PEDOT is 13 μm, while that of the PEDOT-only is 1.6 μm. Both CV and EIS measurements demonstrated the excellent electrocatalytic activity of the SiW_{11}-PEDOT CE.

6.43 Yue et al.: Graphene/PEDOT:PSS mixture (2013)

Yue et al. tested a CE consisting of a mixture of PEDOT:PSS and graphene (graphene/PEDOT:PSS) [62]. The morphology of graphene/PEDOT:PSS film allowed to understand how graphene improved the CE performance, in fact the surface of the composite film possessed many clusters and had a very high surface area, excellent property for the adsorption of liquid electrolyte. Fourier transform infrared (FTIR) analysis confirmed that graphene/PEDOT:PSS composite film was successfully prepared by the one-step method to electrochemical deposition. CV measurements showed two pairs of similar redox peaks for graphene/PEDOT:PSS CE and Pt CE. In this case, the magnitude of cathodic reduction peaks current (I_{pc}) and cathodic peaks potential (V_{pc}) are directly proportional to the ability to reduce I_3^- species. The measurement was made with various weights of graphene, confirming that the maximum concentration was 0.05 wt%, thus obtaining the highest I_{pc} (3.93 $mAcm^{-2}$ in absolute value) and the lowest V_{pc} (0.2 V in absolute value). EIS measurements also confirmed that the R_{ct} resistance decreased as graphene concentration increased to a minimum of 2.74 Ωcm^2 per 0.05 wt% graphene. Finally, the PV performances were investigated, obtaining remarkable values for the CE containing 0.05wt% of graphene: V_{oc}: 0.77 [V], J_{sc}: 15.7 [$mAcm^{-2}$], FF: 0.65 and η: 7.86 [%].

6.44 Song et al.: Silicon Nanoparticles in PEDOT:PSS (2013)

Song et al. investigated the effect of silicon nanoparticles inserted into PEDOT:PSS (SiNPs/PEDOT:PSS) used as CE in DSSC devices [63]. PV performances showed that efficiencies of 5.7% were obtained, slightly lower than a classic Pt cell (6.6%). The CV and EIS measurements showed the good electrocatalytic activity of the composite layer, showing how R_{ct} decreases with the insertion of the SiNPs and how CV curve was enhanced. SEM images also showed that after the insertion of Si NPs the surface became rougher, thus the contact with the electrolyte was increased and the ion exchange was facilitated.

6.45 Yin et al.: PEDOT via solid-state polymerization (2013)

Yin et al. manufactures via solid-state polymerization (SSP) of PEDOT (SSP-PEDOT) a CE for DSSC device [64]. SEM images showed that the surface was rough and composed of nanostructures that gave high surface area, an advantage for triiodide reduction. The CV curves

showed two typical pairs of oxidation/reduction Peaks, very similar to those of Pt. The EIS measures confirmed that the CE produced via SSP could give high performance to the DSSC, the internal resistance was relatively low, very similar to that of the Pt. Finally, PV performance was investigated with an efficiency of 7.04%, Voc [V]:0.710, Jsc [$mAcm^{-2}$]: 16.26 and FF:0.61 (η_{Pt}:7.35%).

6.46 Maiaugree et al.: A Ni composite PEDOT:PSS (2013)

Maiaugree et al. specifically focused on the use of nickel mixed with PEDOT:PSS (Ni/PEDOT:PSS) to manufacture a CE used in DSSC technology [65]. Using SEM images, they observed that the PEDOT:PSS was completely incorporated into Ni and the surface of the layer had a rough nanometric surface, enhancing the surface area of the CE. PV performance showed that the cell manufactured with Ni/PEDOT:PSS CE had an efficiency of 2.25%. The authors then tried to replace pure Ni with Ni sulphate ($NiSO_4$) thus forming the CE $NiSO_4$/PEDOT:PSS. Performance increased slightly to an efficiency of 3.05%.

6.47 Kung et al.: PEDOT microflower arrays (2013)

Kung et al. studied a PEDOT hollow microflower arrays CE, using ZnO microflower arrays (MFAs) as template [66]. As a first step, ZnO-MFAs was deposited on FTO. Then, the coating with PEDOT was done, thus forming PEDOT/ZnO-MFAs. In doing so, PEDOT took the microflower arrays form. Finally, through a treatment with HCl, the ZnO was removed, thus obtaining PEDOT-HMFAs. The authors noted that immediately, after treatment with HCl, the petals of the structure were thinner, thus porosity and the surface area of the layer increased. CV was performed, and to understand the electrode performance you can observe the cathode peak current density (J_{pc}) Figure 33. It can be observed that for each charge densities of electrodeposition were significantly lower in absolute value than the Pt, affirming its electrocatalytic superiority. The authors also investigated the long-term stability of various CEs: PEDOT-HMFAs, flat PEDOT, Pt. After 200 potential cycles: in the case of Pt J_{pc} decreased by 23%, for flat PEDOT 16% and 8% for PEDOT-HMFAs confirming also in this case the greater stability of both electrodes composed by PEDOT. They achieved very high performances, almost comparable with those of the Pt, in fact the efficiency obtained with PEDOT-HMFAs was 7.20% (η_{Pt}:7.61%).

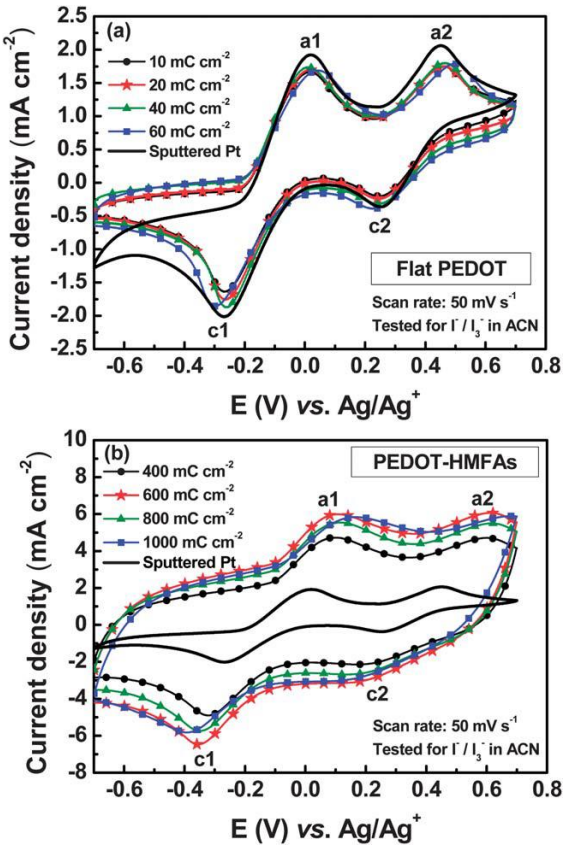

Figure 33 *CV curves of (a) the flat PEDOT CE obtained with various charge densities and of the Pt CE; (b) CV curves of the PEDOTHMFAs CE obtained with various charge densities and the Pt CE. Reprinted with permission from [66].*

6.48 Guan et al.: Aligned CNT-PEDOT:PSS composite film (2013)

In this elaboration, Guan et al. tested for the first time an aligned CNT-oriented composite film by coating PEDOT:PSS onto CNT sheets (Figure 34) [67]. This aligned composite film featured very high electrocatalytic activity, much higher than the bare CNT, Bare oriented PEDOT:PSS, randomly dispersed CNT-PEDOT:PSS, and Pt. The structure formed by CNTs had multi-walled shape, with a diameter of about 10 μm. Subsequently, PEDOT:PSS was spin-coated on the CNT sheet, forming a high-quality film and high electrocatalytic performance CE. CV was performed on the following CEs: bare aligned CNT, bare oriented PEDOT:PSS, randomly and aligned oriented CNT-PEDOT:PSS and Pt. Neither the oriented PEDOT:PSS CE nor the aligned CNT CE show the two pairs of Ox-Red peaks thanks to their low catalytic activity. The Pt and the randomly/aligned CNT-PEDOT:PSS showed the classic pairs of peaks. The V_{pp} value of the aligned CNT-PEDOT:PSS was 0.38 V, much lower than dispersed randomly and Pt (0.67 V and 0.47 V respectively). The J-V curves showed the PV performance of the DSSCs. From Table 18 it is clear that the aligned CNT-PEDOT:PSS is superior to all other electrodes, confirming that the order and conformation produced was actually better, even better than the Pt. EIS measurements also confirmed that both series and R_{ct} resistances were much lower in the aligned CNT-PEDOT:PSS CE, confirming the high efficiency and FF values.

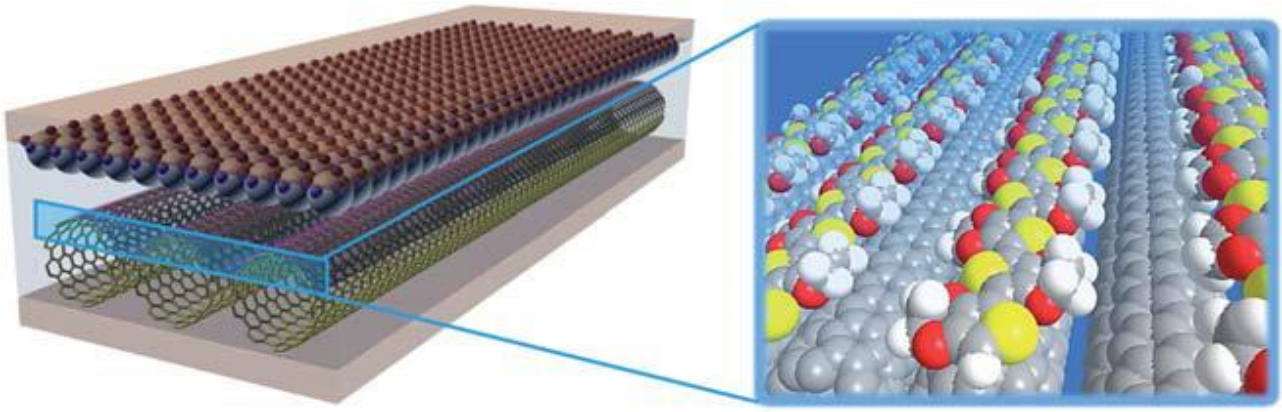

Figure 34 *Schematic view of the oriented PEDOT:PSS on aligned CNTs. The red, white, yellow and grey colors correspond to the elements O, H, S and C elements. Reprinted with permission from [67].*

Table 18 *PV performance of various CEs applied to a DSSC devices. Adapted and reprinted with permission from [67].*

CE	V_{oc} [V]	J_{sc} [mA/cm^2]	FF	η %
Aligned CNT-PEDOT:PSS	0.731	16.1	0.71	8.3
Random CNT-PEDOT:PSS	0.720	14.4	0.39	4.0
Oriented PEDOT:PSS	0.723	14.5	0.33	3.4
Aligned CNT	0.733	13.5	0.50	5.0
Pt	0.728	16.2	0.64	7.5

6.49 Li et al.: TiS_2/PEDOT:PSS composite material (2013)

Li et al. studied a composite CE formed by TiS_2/PEDOT:PSS [68]. Various types of CEs were studied using FE-SEM images: bare TiS_2, bare PEDOT:PSS, Pt and TiS_2/PEDOT:PSS composite films. It was observed that the Pt was flat, with small and uniform particles of Pt scattered on the surface. Bare TiS_2 had flaky TiS_2 particles with size of about 1μm, giving little contact with the ITO. Bare PEDOT:PSS was very smooth and compact, not favourable properties for the contact with electrolyte. TiS_2/PEDOT:PSS, on the other hand, had high roughness and a very high surface area, proof of its electrocatalytic superiority. The authors noted that by upgrading the TiS_2 to the PEDOT:PSS coffin, the performance of the CE increased, but instead increasing the amount of TiS_2 in the TiS_2/PEDOT:PSS CE there was no improvement, the best quantity was 10wt%. A maximum efficiency of 7.04% was achieved for 10 wt% TiS_2/PEDOT:PSS CE, 3.24 bare TiS_2, 3.91 bare PEDOT:PSS and 7.65 for Pt.

6.50 Yue et al.: PEDOT and Pt composite film (2014)

Yue et al. tested a composite CE consisting of PEDOT and Pt, then compared the performance of this CE with those of pure Pt and pure PEDOT noting that the two substances had a synergistic effect by increasing performance when mixed [69]. The SEM images were analysed for PEDOT and PEDOT/Pt. The film had a mound-like surface morphology with cluster aggregates. The second had an excellent surface area and an orderly network structure, thus increasing the penetration of the liquid electrolyte and thus creating highly electrocatalytic CE

activity. CV measures were performed, and all curves had the two pairs of ox-red peaks. The critical values for this test were the cathodic peak potential (E_p) and current density (I_{pc}). The more positive E_p, the smaller the overpotential to reduce redox torque and the stronger the electrocatalytic activity. E_p: Pt(-0.186 V) < PEDOT(-0.147 V) < PEDOT/Pt(-0.125 V), I_{pc}: Pt(2.94 mA) < PEDOT(3.14 mA) < PEDOT/Pt(3.59 mA). EIS analysis showed that the resistance R_s was similar for all three electrodes (about 3.10Ω), whereas the R_{ct} resistance was much lower in PEDOT/Pt than in PEDOT and Pt (1.31, 1.49 and 1.89 Ωcm^2 respectively), revealing a synergetic effect of the Pt and PEDOT on the electrocatalytic activity of the hybrid CE. PV performance finally confirmed these assumptions, showing high efficiencies for all electrodes, but the one with the highest efficiency was PEDOT/Pt:7.86% (6.95% and 6.29% for Pt and PEDOT respectively).

6.51 Li et al.: PEDOT doped with various ionic liquid (2014)

Li et al. used PEDOT films doped with various ionic liquids (more precisely anionic and cationic liquids) [70]. Ionic liquids containing imidazolium cations: 1-ethyl-3-methylimidazolium tetrafluoroborate ($EMIBF_4$), 1-hexyl-3-methylimidazoliumtetrafluoroborate ($HMIBF_4$), and 1-dectyl-3-methylimidazoliumtetrafluoroborate ($DMIBF_4$). Ionic liquids containing different anions: $HMIBF_4$, 1-hexyl-3-methylimidazoliumhexafluorophosphate ($HMIPF_6$), 1-hexyl-3methylimidazoliumtrifluoromethansulfonate ($HMISO_3CF_3$) and 1-hexyl-3methylimidazoliumbis(trifluoromethylsulfonyl)imide (HMITFSI). Especially HMITFSI-doped PEDOT was an innovation, because it demonstrated very high efficiencies reaching the value of 8.87%. The conductivities of the various CEs were measured, observing that for $EMIBF_4$, $HMIBF_4$ and $DMIBF_4$ the conductivities were: 10.7, 12.4 and 12.8 $mScm^{-1}$. It was inferred that conductivity, therefore the ability to donate electrons, increased as the length of the alkyl chain increased. The conductivity of $HMIBF_4$, $HMIPF_6$, $HMISO_3CF_3$, and HMITFSI was tested by finding these values: 11.6, 16.4, 14.4, and 17.9 $mScm^{-1}$ respectively. The FE-SEM of $EMIBF_4$-doped PEDOT, $HMIBF_4$-doped PEDOT and $DMIBF_4$-doped PEDOT images were studied and it was observed that porosity and roughness increased with increasing catalytic length. With anionic liquids it was observed that the surface was always microstructured, with high roughness and with high porosity. CV and EIS measures confirmed the superiority of HMITFSI-doped PEDOT over the other CE. The PV performances are summarized in Table 19. An extraordinarily high efficiency was obtained with HMITFSI-doped PEDOT CE.

Table 19 *PV performance of DSSCs with various CEs. Adapted and reprinted with permission from [70].*

CE	V_{oc} [mV]	J_{sc} [$mAcm^{-2}$]	FF	η %
Pt	727	14.46	0.68	8.08
Bare PEDOT	728	12.52	0.68	6.19
$EMIBF_4$-doped PEDOT	718	13.59	0.68	6.69
$HMIBF_4$-doped PEDOT	724	15.79	0.68	7.78
$DMIBF_4$-doped PEDOT	722	14.53	0.68	7.20
$HMIPF_6$-doped PEDOT	734	16.21	0.69	8.28
$HMISO_3CF_3$-doped PEDOT	725	15.66	0.69	7.82
HMITFSI-doped PEDOT	722	17.74	0.69	8.87

6.52 Chen et al.: Well-known PEDOT CE (2014)

Chen et al. experimented a DSSC based on well-known PEDOT polymer CE [71]. They also studied the CE at different annealing temperatures (40, 60, 80 °C). At the lowest temperature (40 °C), the polymer had a porous structure with small particles of 50-80 nm diameter. At 60 °C the morphology was similar but increasing the T up to 80 °C we observe that it changed slightly: it had a more uniform and flat shape. They deduced that as the T grew, the film became flatter and thinner and adhered better to the FTO. The absorbance spectra showed that the polymer was a longer wavelength (360-471 nm), compared to monomer (318-403 nm), then the author observed broad peak at near-IR region (770 nm) that were attributed to partially oxidized areas of the conductive polymer. Increasing the temperature, they found higher abs values. The PV performances extrapolated from the J-V curves showed that the authors found the best performance with the PEDOT annealed at 60°C: Voc=793 [mV], Jsc=9.0 [$mAcm^{-2}$], FF=0.69 and η=4.9% (η_{Pt} =5.1%).

6.53 Rhee et al.: Hybrid PEDOT doped MWCNTs film (2014)

Rhee et al. introduced a hybrid material consisting of PEDOT:PSS and MWCNTs (PEDOT:PSS-MWCNTs), the film was prepared via cyclic voltammetry [72]. SEM images showed that the hybrid film had many MWCNTs on the surface that increased the surface area, helping to improve the electrocatalytic active area and CE activity. The CV measurements showed the typical pattern with two pairs of peaks. PEDOT:PSS-MWCNTs had larger oxidative current (0.5 mA): crucial factor for good electrocatalytic effect and fast electron transport. The PV performances were good, reached an efficiency of 6.67 %, higher than that of the Pt (6.25%). The EIS tests confirmed that the R_{Ct} resistances, crucial for the FTO/CE/Electrolyte contact, were lower than those of the Pt, thus confirming the electrocatalytic superiority of the PEDOT:PSS-MWCNTs CE.

6.54 Gao et al.: PEDOT electropolymerization in aqueous phase (2014)

The authors studied PEDOT CEs manufactured via electropolymerization in aqueous phase method with different polymerization times [73]. SEM images showed that as the polymerization time increased the porosity of the film increase, thus increasing also the surface area with a maximum time of 40 s. The CV curves and EIS measurements confirmed that the best time was always 40 s, finding the higher values of current density and lower values of overpotential. Especially the R_{ct} was low, with a minimum value of 3 Ω (always at 40 s), increasing or decreasing the polymerization time the resistance increased. The PV performances extrapolated from the J-V curves showed that the PEDOT-40s CE was the best, even better than the Pt (Voc=0.68 [V], Jsc=16.66 [$mAcm^{-2}$], FF=0.57 and η=6.46% for PEDOT-40s and Voc= 0.68 [V], Jsc=15.27 [$mAcm^{-2}$], FF=0.61 and η=6.33% for Pt).

6.55 Park et al.: PEDOT doped with Iron sulfonate compound (2014)

Park et al. manufactured a conductive polymer consisting of PEDOT doped with iron(III) tris-p-toluenesulfonate (PEDOT:Tos) and combined with a redox shuttle cobalt(III/II) tris(2,2 -bipyridine) ($[Co(bpy)_3]^{3+/2+}$) [74]. The authors tested three different CEs: Pt/FTO, PEDOT:Tos/FTO glass and PEDOT:Tos/glass; the efficiencies obtained through the J-V curves were as follows: 6.1%, 6.5% and 6.3% respectively. Testing the same CEs with the classic redox pair I^-/I_3^- it was noted that the efficiencies were significantly lower: 4.7%, 3.5% and 0.98%. The low electrocatalytic activity was explained by the low capacity to activate the charge-transfer between the PEDOT and the I_3^- species. As it seemed with the Co, there weren't these problems. Using CV measurements, it was noted that E_p was 0.25V for PEDOT:Tos/FTO glass, 0.47 V for PEDOT:Tos/glass and 0.49 V for Pt/FTO glass. The lower the value of E_p, the higher the electrocatalytic activity, the PEDOT:Tos/FTO glass thus demonstrated the strong activity. The EIS measures also confirmed that the PEDOT Ces had much smaller Rcts than the Pt (2.7 and 1.1 Ωcm^2 for PEDOT:Tos/FTO glass and PEDOT:Tos/glass, 10.9 Ωcm^2 for Pt/FTO glass) confirming the superiority of PEDOT as CE in DSSC.

6.56 Song et al.: PEDOT doped Molybdenum sulphide (2014)

Song et al. studied an CE composed of MoS_2 mechanically mixed with PEDOT (MoS_2/PEDOT) [75]. The MoS_2 was manufactured to have two samples: one was a powder with big particle dimension 10-100nm (M1), the other treated with additives to control the size (M2). The SEM images showed that M2 had clusters of small size 30-40 nm, thus being the best candidate for the CE. Indeed, the J-V measurements showed that the CE composed of MoS_2(M2)/PEDOT compared to MoS_2(M1)/PEDOT, however not as high as those of Pt (Table 20). EIS measurements showed that both R_s and R_{ct} resistances were lower in MoS_2/PEDOT than in Pt. Evidently the reduced PV performances are given by a reduced electrocatalytic activity of the CE MoS_2/PEDOT regarding that of the Pt.

Table 20 *PV performance of DSSCs with various CEs. Adapted and reprinted with permission from [75].*

CE	V_{oc} [V]	J_{sc} [mA/cm^2]	FF %	η %
MoS_2(M1)/PEDOT	0.68	14.0	0.50	4.7
MoS_2(M2)/PEDOT	0.68	14.55	0.58	5.7
Pt	0.73	15.26	0.59	6.6

6.57 Koussi-Daoud et al.: PEDOT doped Au (2014)

Koussi-Daoud et al. studied a CE consisting of a composite film of PEDOT and gold nanoparticles (AuNPs-PEDOT) [76]. The results of the J-V test are summarized in Table 21, it was immediately noticed the increase in performance when AuNPs were added to pure PEDOT, especially Jsc and efficiency, which increase by 130%. CV was performed in order to verify the electrocatalytic activity. The peak-potential separation was 470mV for AuNPs-PEDOT and 650 mV for PEDOT alone. The decrease in peak-potential separation measured between PEDOT and AuNPs-PEDOT suggested faster electron transport when the AuNPs was present.

Table 21 *PV performance of DSSCs with various CEs. Adapted and reprinted with permission from [76].*

CE	V_{oc} [V]	J_{sc} [mAcm^{-2}]	FF	η %
Pt	0.71	3.3	0.59	1.3
PEDOT	0.70	3.6	0.56	1.4
PEDOT-AuNPS	0.71	7.6	0.60	3.2

6.58 Song et al.: PEDOT:PSS doped silica (2014)

Song et al. tested an CE composed of Silica (SiO_2) nanoparticles and PEDOT:PSS (SiO_2/PEDOT:PSS) (the conformation of the cell is a bifacial cell, receive the light from both sides Figure 35) [77]. First, the optical properties were investigated, confirming that the amount of SiO_2 and the thickness of the layer affected the transmission, more SiO_2 and less thickness improved the transmission in the long wavelength range. SiO_2/PEDOT:PSS showed better performance than PEDOT:PSS with an efficiency of 4.61%.

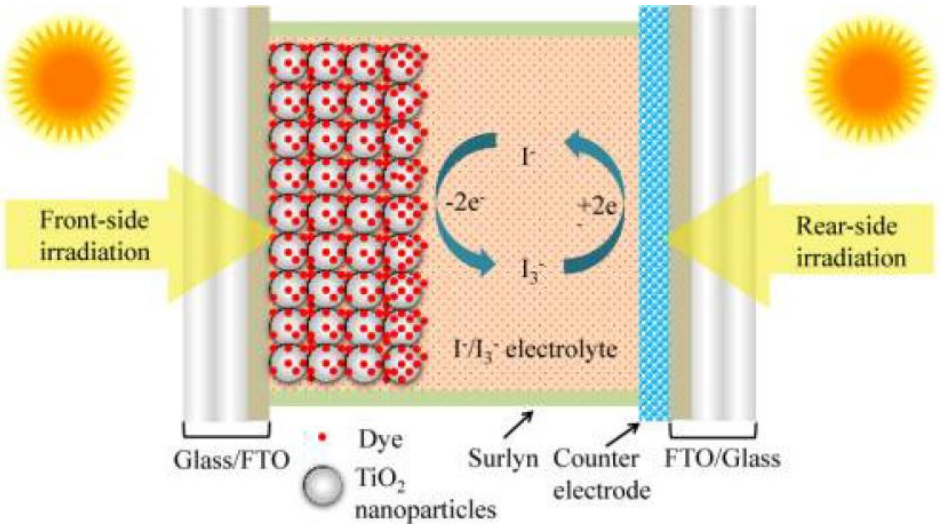

Figure 35 *Schematic structure of a bifacial DSSC device. Reprinted with permission from [77].*

6.59 Tsai et al.: PEDOT:PSS doped with SiC nanoparticles (2014)

Tsai et al. studied a CE composed of PEDOT:PSS doped with silicon carbide nanoparticles (SiC-NPs), (SiC-NPs/PEDOT:PSS) for a DSSC device [78]. FE-SEM images were performed on several CEs: Pt, pure PEDOT:PSS, pure SiC and SiC-NPs/PEDOT:PSS composite film. The Pt film showed uniform surface covered with many uniform Pt particles. Pure SiC had a porous but disconnected surface. Pure PEDOT:PSS had a very smooth and compact morphology. Instead, when SiC-NPs was added to PEDOT:PSS the surface became porous and with a high surface area, better adhesion to ITO. The authors also tested CEs with larger amounts of SiC-NPs: 1, 3, 5 wt%. They noticed that increasing SiC-NPs increased the porosity. PV performance confirmed that 5 wt% SiC-NPs/PEDOT:PSS had better η, almost comparable with Pt: 7.25 and 7.98% respectively. The CV measurements confirmed the good electrocatalytic activity of 5 wt% SiC-NPs/PEDOT:PSS, obtaining for Pt, PEDOT:PSS and 5 wt% SiC-NPs/PEDOT:PSS cathodic peak current density (J_{cp}) of 1.62, 0.4, 1.51 mAcm^{-2} respectively and peak separation

(ΔE_p): 318, 446 and 425 mV respectively. EIS analysis showed that SiC-NPs increased Rs resistance and therefore increased contact with ITO. The R_{ct} resistances instead were a bit higher in 5 wt% SiC-NPs/PEDOT:PSS compared to Pt, confirming the slightly lower PV performance values.

6.60 Liu et al.: Double layer PEDOT:PSS/PEDOT (2014)

Liu et al. tested a CE for a DSSC composed of PEDOT:PSS on polyethylene terephthalate (PET) substrate, to increase the performance of the CE they also electropolymerized a layer of PEDOT over the PEDOT:PSS (Figure 36) [79]. The nomenclature used will be: PEDOT/PET (CE without surface electropolymerized PEDOT), EP/PEDOT/PET (CE with surface electropolymerized PEDOT film). The cells were tested with TiO_2 as electrode and compared with a PET/Pt-Pt/PET cell. The SEM images confirmed that PEDOT/PET did not have a surface rough enough for the role. Instead EP/PEDOT/PET showed high roughness and surface area. EIS measurements showed that the internal resistance, extracted from Tafel diagrams and displayed in the equivalent circuit, were higher for CEs containing PEDOT, than for Pt. The PV performance confirmed that PEDOT/PET had low efficiencies (0.93% for 1 Sun, 1.40% for 0.2 Sun), while EP/PEDOT/PET showed higher efficiencies (4.84% for 1 Sun, 6.54% for 0.2% Sun) however not as high as Pt (6.70% for 1 Sun, 6.95% for 0.2 Sun). Finally, the authors confirmed that adding a layer of PEDOT on PEDOT:PSS improved the performance of the DSSC.

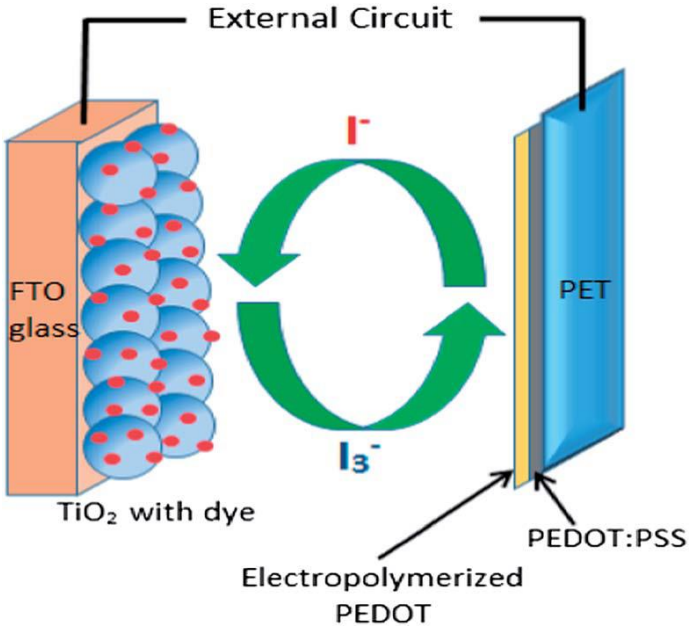

Figure 36 *Configuration of FTO/TiO_2/I⁻-I_3^-/PEDOT/PEDOT:PSS/PET DSSC. Reprinted with permission from [79].*

6.61 Park et al.: PEDOT inverse opal structure on polystyrene template (2014)

Park et al. studied an inverse-opal PEDOT CE for DSSC device [80]. This structure is very particular as it allows to produce a porous and orderly electrode, almost a crystalline structure. Two structures were then prepared: an inverse-opal-structured PEDOT (IO-PEDOT) CE by electropolymerization of the EDOT on the polystyrene (PS) pattern. The PS opal template was assembled and prepared in an aqueous solution of PEDOT:PSS. SEM images showed that the aqueous phase deposition was much more orderly, uniform and crystalline. This surface was compared to that of the classic PEDOT (c-PEDOT) and an increase in porosity and crystallinity was noticed. CV measurements were performed, IO-PEDOT showed the highest cathodic peak current compared to c-PEDOT and Pt (-1.6, -1.1 and -0.9 $mAcm^{-2}$ respectively) confirming the superior electrocatalytic activity. EIS measurements also showed that the film conformation decreased internal resistances. Particularly R_{ct} was very low: 0.16, 2.02 and 0.21 Ωcm^2 for IO-PEDOT, c-PEDOT and Pt respectively.

6.62 Song et al.: Nanomaterial-PEDOT:PSS (2014)

Song et al. investigated the effect of adding nanomaterials to PEDOT:PSS to create a composite CE in a DSSC [81]. They tested three different nanomaterials: Silicon (Si), TiO_2 and Silica (SiO_2). The specific surface area of these three nanomaterials follows this trend: $SiO_2 > TiO_2 >$ Si, so the authors expected to find better performance in this order: SiO_2/PEDOT:PSS>TiO_2/PEDOT:PSS>Si/PEDOT:PSS. The PV performance followed that trend, in Table 22 you can see how SiO_2/PEDOT:PSS presents high performance but TiO_2/PEDOT:PSS presents higher V_{oc} and J_{sc}. The higher V_{oc} value was explained thanks to the large conduction band of TiO_2, which helped to improve this aspect. EIS measurements confirmed that the CE composed of SiO_2/PEDOT:PSS had lower R_{ct} and R_s than the other CEs. These results are reflected in the high catalytic activity of the composite. SEM images showed that all three films were mesoporous, with a higher surface area than the PEDOT:PSS pristine, resulting in better electrocatalytic activity. Finally, the surface roughness was studied finding the following values: 6.0, 18.8 and 39.8 nm for PEDOT:PSS, TiO_2/PEDOT:PSS and SiO_2/PEDOT:PSS respectively.

Table 22 *PV performance of various CEs. Adapted and reprinted with permission from [81].*

CE	V_{oc} [V]	J_{sc} [mA/cm^2]	FF %	η %
PEDOT:PSS	0.71	15.0	39.7	4.2
Si/PEDOT:PSS	0.73	14.5	53.8	5.7
TiO_2/PEDOT:PSS	0.75	15.9	57.0	6.8
SiO_2/PEDOT:PSS	0.71	14.9	65.2	6.9

6.63 Chang et al.: PEDOT:PSS doped Ni NPs (2014)

Chang et al. incorporated thepoly(oxyethylene)-segmented imide (POEM) dispersed Ni-NPs into the structure of the PEDOT:PSS, to form a Ni-NPs/PEDOT:PSS CE for a DSSC [82]. Through SEM images, it was observed that both the Pt and the PEDOT:PSS pristine had smooth surfaces so by atomic force microscopy (AFM) were also analysed. It was observed that the

root means square roughness (R_{rms}) of Pt and PEDOT:PSS was: 135.54 and 45.32 nm respectively. So, the Pt had more porosity and mean path than the PEDOT:PSS. As far as Ni-NPs/PEDOT:PSS was concerned, SEM images showed high surface area, very high roughness and porosity. AFM images confirmed that R_{rms} of Ni-NPs/PEDOT:PSS was 2.73 μm, so much higher than the other two CEs. PV performance was investigated through J-V curves and it was observed that Ni-NPs/PEDOT:PSS had high performance, even higher than Pt (Table 23). EIS measurements showed that the Pt had both Rs and R_{ct} resistances lower than Ni-NPs/PEDOT:PSS, confirming its high electrocatalytic activity and J_{sc}. In fact, a higher value of R_{ct} affects a lower electrocatalytic ability and a higher value of Rs is reflected in a lower J_{sc}. Finally, CV tests were performed. The J_{pc} of PEDOT:PSS was not detectable, while those of Pt and Ni-NPs/PEDOT:PSS yes, the Pt had J_{pc} higher than Ni-NPs/PEDOT:PSS, confirming again the J_{sc} values.

Table 23 *PV performance of various CEs. Adapted and reprinted with permission [82].*

CE	V_{oc} [V]	J_{sc} [mAcm^{-2}]	FF %	η %
Pt	0.70	15.80	0.69	7.63
PEDOT:PSS	0.68	12.96	0.49	4.36
Ni-NPs	0.67	4.19	0.08	0.24
Ni-NPs/PEDOT:PSS	0.74	15.56	0.68	7.81

6.64 Kim et al.: PEDOT via oxidative molecular layer deposition (2015)

Kim et al. experimented a layer of PEDOT about 20nm thick on mesoporous indium tin oxide (m-ITO) as CE for a DSSC [83]. They deposited the PEDOT via oxidative molecular layer deposition (oMLD). They immediately noticed that the obtained network had good properties, such as high surface area, good electron transport and high porosity. Through J-V measurements they obtained an efficiency of 7.18%, comparable with that of Pt (7.26%) but obtained from a Pt-free and low-cost cell.

6.65 *Ma et al.: Innovative method to enhancing NiS/PEDOT performance (2015)*

Ma et. al investigated a method to increase the performance of a DSSC using NiS/PEDOT as CE [84]. This method consisted of placing an aluminium foil as a reflector. This foil allowed front/rear irradiation of the cell and increased performance. Initially, the properties of the layer were investigated using SEM images. NiS/PEDOT had an interesting smooth morphology, with NiS particles integrated into the PEDOT network. This structure increased the electron transport path in the electrode. CV and EIS measurements were performed. Both analyses showed that NiS/PEDOT was a good candidate as CE, as it had good electrocatalytic activity and low resistance (lower than Pt and pure NiS and PEDOT). The PV performance confirmed the results obtained in previous analyses. Obtaining for NiS/PEDOT a high efficiency (7.77%). The authors finally tested the method to increase performance by adding aluminium foil as a reflector. This method allowed to increase the efficiency up to a value of 8.47% (all the values obtained are reported in Table 24).

Table 24 *PV performance of various CEs irradiated Front, Rear and Front&Rear. Adapted and reprinted with permission from [84].*

CE	V_{oc} [V]	J_{sc} [mAcm^{-2}]	FF	η %
Pt front&rear	0.733	15.81	0.63	7.30
Pt front	0.739	15.33	0.63	7.14
Pt rear	0.723	9.46	0.62	4.24
NiS front&rear	0.719	14.87	0.60	4.61
NiS front	0.712	14.54	0.56	5.80
NiS rear	0.704	10.67	0.55	4.13
PEDOT front&rear	0.730	16.81	0.59	7.24
PEDOT front	0.730	14.85	0.57	6.18
PEDOT rear	0.728	11.34	0.55	4.54
NiS/PEDOT front&rear	0.751	18.19	0.62	8.47
NiS/PEDOT front	0.746	16.79	0.62	7.77
NiS/PEDOT rear	0.734	12.96	0.62	5.89

6.66 Xia et al.: PEDOT deposited on antimony tin oxide (2015)

Xia et al. tested a PEDOT CE and then deposited it on antimony tin oxide (ATO) [85]. Different CEs were tested for comparison: Pt, ATO, PEDOT, PEDOT/ATO. SEM images showed that the ATO layer was composed of nanoparticles with a size of about 20 nm and a thickness of 190 nm. its porous structure gave it a very high surface area and by depositing the PEDOT it could be confirmed that the conformation improved the performance of the CE. The following efficiencies were obtained: 7.54, 7.47, 6.09 and 2.07% for Pt, PEDOT/ATO, PEDOT and ATO respectively. It was therefore confirmed that the PEDOT/ATO conformation was clearly the best, even better than Pt. CV measurements were carried out and it was observed that the ATO electrode had no peaks. Instead, the ratio between anodic and cathodic (I_{pa}/I_{pc}) peaks was 1.18, 7.40 and 1.30 for PEDOT/ATO, Pt and PEDOT. The closer to one the better the electrocatalytic activity will be, demonstrating once again that PEDOT/ATO had the best performance. EIS analysis also confirmed the superiority of the PEDOT/ATO CE, showing that the internal R_{ct} and Rs resistances were significantly lower than the other electrodes.

6.67 Yeon et al.: enhancing performance of PEDOT:PSS (2015)

Yeon et al. investigated a method to increase the properties of PEDOT:PSS CE by treating it with HNO_3 at room temperatures [86]. First, it was noted that treating the CE with HNO_3 instead of H_2SO_4 had the same effect on the CE, and that it was not necessary to treat it at high temperatures as 120 °C if HNO_3 was used. PEDOT:PSS conductivity was investigated by comparing PEDOT:PSS pure and PEDOT:PSS treated with 14 M of HNO_3 for 10 min. It was observed that conductivity increased from 1600 Scm^{-1} to 3964 Scm^{-1}, thus confirming that treatment with acid increased the properties of the CE. AFM images showed that the morphology of PEDOT:PSS was undergoing major changes. The roughness increased considerably, the roughness (Rq) before treatment had a value of 1.23 nm and then 1.85 nm. PV performance showed that the treated PEDOT:PSS had good electrocatalytic capabilities demonstrating an efficiency of 8.61% (η_{Pt}: 10.36%).

6.68 Lin et al.: PEDOT tube-coral array morphology (2015)

Lin et al. tested a PEDOT CE doped with methanol MeOH (PEDOT-MeOH) with different surface morphology [87]. The three morphologies were: PEDOT-MeOH tube array (TA), PEDOT-MeOH coral (C) and PEDOT-MeOH tube-coral array (TCA). The SEM images showed exactly what schematically shown in Figure 37, PEDOT-MeOH TA had tube arrays grown directly on the FTO, with an average diameter of 700 nm and an average length of 5 µm. PEDOT-MeOH C similarly showed morphology with very high porosity and surface area. Finally, PEDOT-MeOH TCA combined the two morphologies in a very porous layer distributed on the tube arrays (average diameter 500 nm and average length 5 µm). The PV performances are summarized in Table 25, it can be observed that PEDOT-MeOH TCA obtained amazing values, exceeding the Pt. To support the obtained values of FF and Jsc, CV measurements were made. In fact, it was observed that the Jpc value of the PEDOT-MeOH TCA was much higher than the others, confirming the high performances and demonstrating that the CE actually possessed very high catalytic activity (1.58, 1.13, 1.48, and 1.80 mAcm-2 for Pt, PEDOT-MeOH TA, PEDOT-MeOH C and PEDOT-MeOH TCA respectively). EIS analysis also confirmed that the cell with PEDOT-MeOH TCA possessed lower internal resistances than all other CEs tested, including Pt.

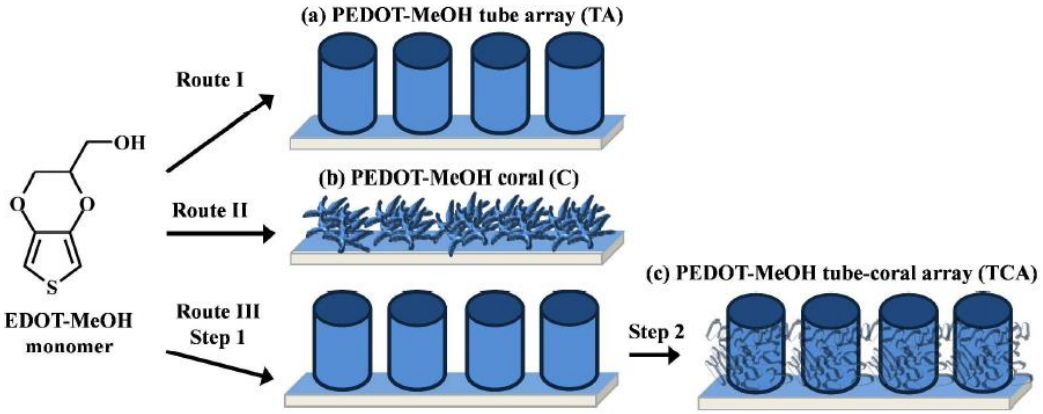

Figure 37 *Schematic view of different PEDOT-MeOH films and their spacial conformation. Reprinted with permission from [87].*

Table 25 *PV performance of various CE. Adapted and reprinted with permission from [87].*

CE	V_{oc} [mV]	J_{sc} [mA/cm^2]	FF	η %
Pt	748.00	17.81	0.67	8.94
PEDOT-MeOH TA	709.29	17.22	0.64	7.85
PEDOT-MeOH C	723.11	17.57	0.65	8.23
PEDOT-MeOH TCA	746.36	18.22	0.67	9.13

6.69 Wang et al.: PEDOT:PSS doped manganese monoxide (2015)

Wang et al. tested an innovative CE composed of PEDOT:PSS and manganese monoxide (MgO/PEDOT:PSS) [88]. The function of a CE is to accept the electrons coming from the external circuit, let the electrolyte to be reduced permeate and start the reduction. MgO is an

insulator, so it can never be an electron collector, but it can help in the adsorption of the I_3^- species. To work at its best, the CE must also have a good conductor, for this role PEDOT:PSS is perfect. Therefore, it will be important to mix the two components because you don't have to obstruct the electrons or the electrolyte. Various mixtures with various quantities have been studied and the best one that offered the highest performance was 64:1 fraction by weight of MgO/PEDOT:PSS obtaining (Voc=0.733 [V], Jsc=23.8 [$mAcm^{-2}$], FF=0.427 and η=7.45%). EIS measurements were carried out and it was observed that also in this case the best ratio was 64:1, as you had lower R_{ct} (40 Ω).

6.70 Lan et al.: PEDOT:PSS graphene doped and treated with acid (2015)

Lan et al. studied a CE composed of PEDOT:PSS and reduced graphene (rGO) (rGO/PEDOT:PSS) [89]. After that, they tested whether treatment with sulphuric acid (H_2SO_4) increased the catalytic activity of the counter electrode and consequently the PV performance. The nomenclature used will be as follows: PEDOT-PSS for the CEs composed of PEDOT:PSS pure, S/PEDOT:PSS for the acid-treated CE, rGO/PEDOT:PSS, S/rGO/PEDOT:PSS for the acid-treated electrode under examination. The TEM images showed that all electrodes had a very high amount of nanocracks and after the addition of rGO the nanocracks became higher. After the sulfuric acid treatment, the transparency of all CEs increased, and the surfaces became more homogeneous. The CV measurements showed that all CEs had the same trend, with two peaks of anodic current and two peaks of cathodic current. After acid treatment the cathodic current peak value increased, so the sulphuric acid decreased peak-to-peak separation, thus increasing cell performance. An efficiency of 7.065% was obtained for S/rGO/PEDOT:PSS, the other CEs obtained an efficiency of about 3%.

6.71 Jafari et al.: PEDOT:PSS/TiO_2 cathodes (2015)

Jafari et al. studied the performance of a PEDOT:PSS/TiO_2 CE in DSSC [90]. The SEM images showed that after the addition of TiO_2 the surface showed a higher roughness and consequently a larger surface area. The PV performance was investigated, and very low performance was obtained for the PEDOT:PSS/TiO_2 CE. In fact, it reached an efficiency of 0.73%, the Pt electrode tested as a comparison reached an efficiency of 1.2%. To explain the low cell performance, CV tests were performed. It was observed that the PEDOT:PSS/TiO_2 CE had high cathodic current density (49 μA) when compared to pure PEDOT:PSS. However, this value is low compared to that obtained with Pt (111 μA).

6.72 Wan et al.: PEDOT:PSS mixed with graphene (2015)

Wan et al. studied a CE composed of PEDOT:PSS mixed with graphene (PEDOT:PSS/graphene) via aqueous dispersion [91]. First, they analysed the TEM images comparing the pure PEDOT:PSS with the PEDOT:PSS/graphene, they observed that the former (prepared with the same polymerization method) showed the microgrid shapelessly. Instead, PEDOT:PSS/graphene had nanocomposite shapes, the graphene sheets surrounded

homogeneously the PEDOT:PSS. The PV performance extrapolated from the J-V graphs showed that the maximum efficiency obtained was 4.66%, that of Pt, studied for comparison was 5.94%. Both CV and EIS measurements showed that the Pt had better catalytic activity because: it had large reduction and oxidation current densities and R_{ct} resistance lower than PEDOT:PSS/graphene.

6.73 Chen et al.: PEDOT and nitrogen-doped graphene (2015)

Chen at al. tested a CE composed of nitrogen-doped graphene (NGr) and PEDOT to combine the high porosity of PEDOT with the high conductivity of NGr, and by obtaining a highly transparent CE they tried to measure its efficiency by illuminating the front and back side [92]. FE-SEM images showed that the PEDOT was completely decorated with honeycomb-like NGr structures as expected. The authors also performed an energy dispersive spectra (EDS) in order to map all the elements present in the composite layer and observed: sulphur, nitrogen and carbon, i.e. all the correct elements for an NGr/PEDOT film. Different conformations of NGr/PEDOT CE were tested, i.e. they tried to insert more layers, investigating which was the best quantity, it was obtained that the best conformation was the one with 2 layers, it had higher efficiencies, through CV and EIS measurements it was known that it had lower ΔE_p and lower internal resistances. A high efficiency of 8.30% was obtained. When backlighting, it was observed that the best was still the two-layer CE. In Table 26 you can see the results obtained through the study of the PV performance of front-rear sides.

Table 26 *PV performance of Pt front. PEDOT front, NGr front 2 layers NGr/PEDOT front and the same CEs for rear sides. Adapted and reprinted with permission from [92].*

CE	V_{oc} [mV]	J_{sc} [mAcm^{-2}]	FF	η %
Pt front	784.1	14.93	0.70	8.17
PEDOT front	711.6	13.96	0.70	6.96
NGr front	693.8	14.08	0.67	6.54
2layer NGr/PEDOT front	739.2	15.60	0.72	8.30
Pt rear	751.7	10.60	0.72	5.76
PEDOT rear	711.4	6.05	0.75	3.24
NGr rear	677.9	6.15	0.73	3.05
2layer NGr/PEDOT rear	735.9	10.80	0.77	6.10

6.74 Lin et al.: PEDOT mixed with CNT coated on ECP (2015)

Lin et al. manufactured flexible and low-cost CE composed of plasma-etched carbon nanotubes/polypropylene (ECP) decorated with PEDOT mixed with CNT [93]. ECP was used to replace TCO at the base and PEDOT/CNT as a catalyst for I_3^- species reduction and electron reception from the external circuit. The PV performance of the 40wt% CNT CE provided an efficiency of 6.82, comparable to that of a Pt CE (7.20%) with a similar cell shape.

6.75 Sekkaparatti et al.: reduced graphene oxide/polypyrrole/PEDOT (2015)

Sekkarapatti Ramasamy et al. studied a reduced graphene oxide/PPy/PEDOT (RGO/PPy/PEDOT) composite film as CE in a DSSC [94]. In situ polymerization and electropolymerization was used. First the RGO/PPy film was deposited on FTO by spin coating, followed by reduction heat treatment. This heat treatment could damage the PPy, but the authors observed that the actual role of PPy was to connect black bone to facilitate film uniformity. Then, PEDOT was electropolymerized on the surface, all these elements should have a synergistic cooperation in increasing cell performance. TEM images showed that the RGO/PPy/PEDOT film had marked PEDOT nanostructures combined with graphene sheets. UV-Vis transmittance spectra showed that the RGO/PPy film had good transparency (400-800 nm); this factor could only benefit the CE, as the more and more transparency the higher the efficiency of an excited solar cell under radiation. CV was carried out and it was observed that the RGO/PPy/PEDOT CE had excellent electrocatalytic activity. The PV performance showed these results: V_{oc}=0.76 [V], J_{sc}=17.0 [mAcm^{-2}], FF=0.55 and η=7.1% for RGO/PPy/PEDOT CE, while V_{oc}=0.78 [V], J_{sc}=19.2 [mAcm^{-2}], FF=0.62 and η=9.3% for Pt.

6.76 Han et al.: PEDOT a and the effect of EDOT monomer concentration (2015)

Han et al. investigated the influence of EDOT monomer concentration on the performance of the CE composed of PEDOT-ClO_4^- electropolymerized in situ [95]. The influence of monomer concentration is reflected on growth, morphology, conductivity and catalytic activity. SEM images showed that PEDOT generally exhibited porous surface but by increasing the monomer concentration from 0.01 M to 0.2 M the morphology was flatter, the thickness increased: 1.55, 2.46, 2.66 and 2.73 μm for PEDOT-0.01, PEDOT-0.05, PEDOT-0.1 and PEDOT-0.2 (PEDOT-molar concentration of EDOT). By increasing the amount of monomer, it was observed that the conductivity decreased. It is well known that the conductivity of an organic polymer is correlated with the doping level, therefore with the same amount of $LiClO_4$ the PEDOT with lower initial EDOT concentration had the highest conductivity, resistivity tests confirmed this thesis. CV measurements were carried out and it was observed that ΔEp increased with increasing EDOT concentration, so the polymerized PEDOT with lower EDOT concentration had better electrocatalytic activities. EIS measurements showed that R_{ct} increased with increasing EDOT concentration from 2.9 for PEDOT-0.01 Ω to 5.9 Ω for PEDOT-0.2, so the polymerized PEDOT with lower EDOT concentration had better charge transfer rate. PV performance confirmed that the best CE was the one cured with 0.05M of EDOT it showed: Voc=0.731 [V], Jsc=14.18 [mAcm^{-2}], FF=0.68 and η=7.42%.

6.77 Kim et al.: High-performance PEDOT-b-PEG (2015)

Kim et al. studied Poly(3,4-ethylenedioxythiophene)-b-poly(ethylene glycol) (PEDOT-b-PEG) CE [96]. The manufacturing was carried out at room temperature and the CE showed excellent properties such as: high transparency, good performance and low resistance to charge transfer. The efficiency obtained was 8.45%, higher than that of Pt (8.25%) and PEDOT NF (7.83%). It was observed that PEDOT-b-PEG was highly transparent, through the optical transmittance measured by the UV-VIS spectrum it was observed that it was very similar to Pt, with an optical

transmittance greater than 80% in the visible range. R_{ct} was also studied and it was observed that PEDOT-b-PEG had lower R_{ct} than PEDOT NF and Pt demonstrating a better catalytic activity.

6.78 Koussi-Daoud et al.: PEDOT with Cobalt co-mediator (2015)

Koussi-daoud et al. studied a cobalt complex used with a ligand bearing an EDOT substitute (Co(EtPy)23+/2+), it was used as a co-mediator in the electrolytic solution of a DSSC, PEDOT is the constituent of the counter electrode [97]. Being an article not purely based on PEDOT, the PV performance obtained is reported: Voc=0.92 [V], Jsc=8.4 [$mAcm^{-2}$], FF=0.67 and η=5.1%.

6.79 Jeong et al.: PEDOT:PSS doped with reduced graphene oxide (2015)

Jeong et al. studied the electrocatalytic and charge transfer properties of a CE composed of PEDOT:PSS doped with rGO [98]. To compare the results obtained, they also studied cells with PEDOT:PSS and Pt. FE-SEM images showed that adding 10 wt% rGO to PEDOT:PSS (rGO/PEDOT:PSS) increased the surface area and porosity of the layer, with a final thickness of 50 nm. CV measurements showed that rGO/PEDOT:PSS CE had better electrocatalytic activity because it had higher current density than both PEDOT:PSS and Pt. It was found that the addition of rGO improved the activity and morphology of the composite layer. EIS measurements showed that both CEs containing PEDOT:PSS had both Rs and Rct higher than Pt, probably due to the lower conductivity of PEDOT:PSS compared to Pt. Table 27 shows the values of EIS measurements and PV performance. It can be noted that despite the higher resistances the rGO/PEDOT:PSS showed better efficiencies than the other CEs, however a low Jsc compared to Pt, probably due to the higher resistances, which disadvantage the charge transfer.

Table 27 *PV performance and EIS results fo Pt, PEDOT:PSS and rGO/PEDOT:PSS CEs. Adapted and reprinted with permission from [98].*

CE	V_{oc} [V]	J_{sc} [$mAcm^{-2}$]	FF	η %	R_S [Ω]	R_{CT} [Ω]
PEDOT:PSS	0.67	8.8	0.41	2.4	18.03	15.83
rGO/PEDOT:PSS	0.73	10.4	0.68	5.1	20.35	11.90
Pt	0.68	10.9	0.63	4.6	17.94	1.74

6.80 Lee et al.: PEDOT:PSS doped with graphene dots (2015)

Lee et al. tested a CE composed of PEDOT:PSS and graphene dots (GD-PEDOT:PSS) [99]. GDs was incorporated via hydrothermal technique into PEDOT:PSS polymer. SEM images showed that PEDOT:PSS without GDs had a smooth morphology, therefore unsuitable for redox reactions. Instead, the GD-PEDOT:PSS had an irregular structure with island-like structure and high roughness, therefore with better chances to conduct redox reactions, therefore, to let the electrolyte permeate inside it. The resistance sheet of the CE was measured, and it was found that for the GD-PEDOT:PSS was $1.5*10^{-4}$ Ωcm, instead for the PEDOT:PSS

also was $9.6*10^{-4}$ Ωcm, the authors expected a good conductivity and roughness. The PV performance extrapolated from the J-V graphs showed that it reached an efficiency of 7.36%, Voc=718 [mV], Jsc=7.36 [$mAcm^{-2}$], FF=0.70. The PEDOT:PSS instead obtained the following results: : Voc=668 [mV], Jsc=12.82 [$mAcm^{-2}$], FF=0.60 and η=5.14%. CV analysis showed that the GD-PEDOT:PSS had higher cathode current density than the PEDOT:PSS and also lower ΔE_p. EIS analysis also showed that R_{ct} of the GD-EDOT:PSS was lower than that of pure PEDOT:PSS (7.92 and 10.38 Ω respectively). The best results obtained in PV performance were then explained.

6.81 Liu et al.: PEDOT:PSS-graphene oxide as protective material for Ag nanowires (2016)

Liu et al. tested an electrode composed of graphene oxide (GO) as a protective material for silver nanowires (AgNWs) and a small dosage of PEDOT:PSS to increase the efficiency and protection of silver [100]. GO and PEDOT:PSS were inserted to protect the AgNWs because when the latter met the liquid electrolyte it corroded almost immediately, leading to a very short life of the cell itself. It was observed from the TEM images that it was possible to efficiently cover the silver through the GO and then later the PEDOT:PSS layer slightly increased the surface area and porosity, but it protected the AgNWs itself. The PV performance was studied with different amounts of PEDOT:PSS, the best efficiency (2.33%) was obtained with a GO/PEDOT:PSS ratio of 1:0.25.

6.82 Xu et al.: TiO_2/SnO_2 and PEDOT:PSS (2016)

Xu et al. developed a TiO_2 CE with SnO_2 as a binder to build a porous template on which to deposit PEDOT:PSS by coating, thus forming a TiO_2/SnO_2/PEDOT:PSS (TSP) CE [101]. The TiO_2 nanoparticles were placed in an aqueous solution with $SnCl_4$, then coated on a conductive substrate and heated to 150 °C to form a conductive layer as a template on which to deposit the PEDOT:PSS. It was observed that SnO_2 improved contact with the substrate. The resulting composite layer had good conductivity, nano-porous structure and mechanical strength. CV measurements were made on TSP CE and compared with pure PEDOT:PSS and pure TiO_2/SnO_2. The latter had no catalytic activity, whereas PEDOT:PSS did. It was observed that the current density of the TSP was higher than the PEDOT:PSS and the peak separation range was also lower than that of the PEDOT:PSS (4.35 and 1.24 $mAcm^{-2}$, 459 and 512 mV respectively). These two values, a higher and a lower one, demonstrate excellent electrocatalytic activity and fast electron transport. The PV performance confirmed the superiority of the TSP CE obtaining an efficiency of 6.54%, higher than that of PEDOT:PSS pure 4.79%.

6.83 Kim et al.: Ag nanoparticles embedded to PEDOT (2016)

Kim et al. studied a CE composed of Ag nanoplates (AgNPs) embedded to PEDOT (AgNPs/PEDOT) [102].The authors noted that by controlling the amount of AgNPs (i.e. the ratio AgNPs:PEDOT) the conductivity and surface area of the CE could be controlled. AgNPs were first deposited on non-conductive glass and on top of the EDOT, which was then

polymerized at room temperature. It was observed that the best amount of AgNPs was 0.60 wt%. CV measurements were carried out on AgNPs/PEDOT 0.60 wt% CE, on PEDOT pristine. It was observed that AgNPs/PEDOT had better electrocatalytic activity (higher cathodic current density and smaller peak separation). In Table 28 are listened the obtained PV performance of different CEs with different amounts of AgNPs, it can be noted that AgNPs/PEDOT 60 wt% CE is the most efficient. The EIS measurements reported consistent results with those of the CV measurements, i.e. AgNPs/PEDOT CE was the best, in terms of electrocatalytic activity and conductivity.

Table 28 *PV performance of AgNPs/PEDOT CEs with different amount of AgNPs. Adapted and reprinted with permission from [102].*

CE	V_{oc} [V]	J_{sc} [mAcm^{-2}]	FF %	η %
0 wt%	0.82	11.79	56.88	5.50
0.06 wt%	0.80	12.21	59.17	5.80
0.6 wt%	0.81	12.00	61.73	5.99
1.20 wt%	0.80	12.66	58.30	5.90

6.84 Zheng et al.: PEDOT doped with F_3O_4 nanoparticles (2016)

Zheng et al. studied a composite film composed of PEDOT and F_3O_4 nanoparticles (F_3O_4/PEDOT) and used as CE in a DSSC, they also studied the performance trend with the amount of F_3O_4 [103]. The tests were performed by varying the amount of F_3O_4 from 0 mg/(ml of precursor solution) to 3. The best performance was obtained with 2 mg/(ml of precursor solution) (F_3O_4/PEDOT-2): V_{oc}=0.740 [V], J_{sc}=18.6 [mAcm^{-2}], FF=0.630 and η=8.69%. It was observed that with little F_3O_4 the film was thin, and the performance was poor, instead increasing the amount of F_3O_4 the performance increased to a maximum when using F_3O_4/PEDOT-2. CV measurements showed that actually the F_3O_4/PEDOT-2 had better catalytic activity, in fact the cathodic current density followed this trend: 0.999, 0.906, 0.802, 0.836 and 0.80 4mAcm^{-2} for F_3O_4/PEDOT-2, PEDOT, Pt, Fe $F_3O_4$3O4/PEDOT-1 and F_3O_4/PEDOT-3.

6.85 Anothumakkool et al. PEDOT impregnated with cellulose (2016)

Anothumakkool et al. studied a CE composed of PEDOT impregnated with cellulose paper (PEDOT-p-5) [104]. The obtained layer had very low sheet resistance (4 Ω/sq), such resistance is obtained from a 40 μm film. The conductivity of the CE was also measured, and it was noted that it was very high (357 S/cm), stable under environmental conditions and very flexible. The catalytic activity was monitored by CV and EIS measurements and a current density of 7.12 mA/cm^2 and a low Rct charge transfer resistance (4.6 Ω) were measured (the same values for Pt are: 2.40mAcm^{-2} and 9.4 Ω respectively). An efficiency of 6.1% was obtained, comparable with that of Pt (6.9%).

6.86 Seo et al.: PEDOT:PSS and TiO_2 nanoparticles (2016)

Seo et al. studied a composite CE based on PEDOT:PSS and TiO_2 nanoparticles and verified how PV performance varied with the amount of TiO_2 inserted [105]. AFM images showed that after the addition of nanoparticles, the surface of PEDOT:PSS increased in roughness and porosity, thus also increasing the surface area, indicating an increase in catalytic performance. CV tests showed that as the amount of TiO_2 increased, the cathodic current density increased to a maximum when 200 mg of TiO_2 was inserted. EIS tests also confirmed that 200 mg was the best compromise for lower resistance and impedance. In fact, with this amount the resistive part of Z (impedance) decreased from 28.72 to 3.143 Ω. The PV performance confirmed the results obtained from the previous tests, obtaining these values: Voc=0.72[V], Jsc=16.39 [$mAcm^{-2}$], FF=0.72 and η=8.27%, the Pt (taken as reference) obtained: Voc=0.73 [V], Jsc=14.75 [$mAcm^{-2}$], FF=0.71 and η=7.59%.

6.87 Belekoukia et al.: PEDOT and exfoliated graphene (2016)

Belekoukia et al. tested a CE composed of PEDOT and graphene produced by electrochemical exfoliation of graphite [106]. PEDOT was necessary because graphene alone could not have good electrochemical qualities and achieve good efficiency. SEM images showed that when PEDOT was electrodeposited on graphene the composite took on a dark blue colour and transparency was partially lost. However, PEDOT deposited nano-structured the film, increasing the surface area. The I-V curves were studied in order to extrapolate the PV performance, an efficiency of 8.0% was obtained; compared to 0.6% of Ex-Gr (pure exfoliated graphene), 4.6% of pure PEDOT and 7.7% of Pt. A synergy was observed between PEDOT and Ex-Gr because they alone could not achieve sufficient efficiency, but together they achieved an efficiency even greater than that of Pt.

6.88 Sumishita et al.: PEDOT:PSS and single wall carbon nanohorns (2016)

Sumishita et al. produced a CE composed of single wall carbon nanohorns (SWCNH) and PEDOT:PSS by spin coating method [107]. TEM images showed that SWCNH tended to form spherical or boundless aggregates with a diameter of about 10 nm. The best performing CE was 0.3 wt% SWCNH on PEDOT:PSS. Through this conformation we had better interface properties, more stable mechanical properties and larger surface area. The CV measurements showed the classic curves with redox peak pairs. PEDOT:PSS/SWCNH CE showed higher cathodic current density than pure PEDOT:PSS and pure SWCNH, also in this case 0.3 wt% of SWCNH had the best values, confirming this quantity as the best, in fact an increase of wt% had a negative effect on the electrocatalytic activity. Finally, the PV performance extrapolated from the J-V curves showed a maximum efficiency of 4.70% with the PEDOT:PSS/SWCNH at 0.3 wt% (η_{Pt}=5.55%).

6.89 Huang et al.: PEDOT:PSS doped molybdenum di-selenide nanosheets (2016)

Huang et al. tested a CE composed of molybdenum di-selenide nanosheets and PEDOT:PSS ($MoSe_2$NS/PEDOT:PSS) via drop-coating method [108]. It was demonstrated that $MoSe_2$ NS increased both the active catalytic sites and the charge transfer path from the conductive layer of the CE to its interface. Combining the properties of $MoSe_2$ and PEDOT:PSS resulted in an efficiency of 7.58%, slightly less than that of a conventional Pt cell (7.81%). The SEM images showed that the substrate had good roughness and a high surface area. Both CV and EIS tests showed that the CE produced had good electrocatalytic activity. Finally, the authors tried to deposit the same CE on a flexible titanium (Ti) foil. It was observed that the performance also increased and exceeded that of a conventional Pt cell ($MoSe_2$NS/PEDOT:PSS efficiency on Ti: 8.51%, Pt efficiency on Ti: 8.51%).

6.90 Mustafa et al.: new PEDOT, oxide graphene and TiO_2 material (2017)

Mustafa et al. produced a CE which consisted of a combination of: PEDOT, graphene oxide (GO) and TiO_2 forming the composite: PEDOT-GO/TiO_2 [109]. The morphology was studied by FESEM analysis and it was observed that: PEDOT showed dense, granular and wrinkled morphology; PEDOT-GO had uniform morphology with paper-like sheet resembles contributing to an increase in surface area; PEDOT-GO/TiO2 showed a porous surface with spherical nanoparticles and paper-like sheet morphology. CV measurements showed that PEDOT-GO/TiO_2 had much higher cathodic current densities than PEDOT-GO and Pt (-5.49, -3.57 and -3.54 $mAcm^{-2}$), thus confirming its superiority in electrocatalytic activity. Table 29 shows the results of J-V tests and EIS measurements. The PEDOT-GO/TiO_2 CE is the best both in terms of PV efficiency and internal resistances (R_s and R_{ct}).

Table 29 *PV performance and EIS results of various CEs. Adapted and reprinted with permission from [109].*

CE	V_{oc} [V]	J_{sc} [mA/cm^2]	FF %	η %	R_S [Ω]	R_{CT} [Ω]
GO	0.05	1.728	15.28	0.001	44.7	5150
PEDOT	0.30	1.872	26.86	0.015	30.7	143
PEDOT-GO	0.65	2.026	51.84	0.683	30.6	21
PEDOT-GO/TiO_2	0.65	3.967	45.22	1.166	22.2	9
Pt	0.59	3.710	33.21	0.727	175.8	19

6.91 Li et al.: PEDOT honeycomb-like (2017)

Li et al. synthesized a PEDOT CE honeycomb-like PEDOT using a PMMA mould [110]. The nomenclature used later will be: h-PEDOT-1 (PEDOT-like honeycomb manufactured with 6wt% PMMA), h-PEDOT-2 (PEDOT-like honeycomb manufactured with 8wt% PMMA), h-PEDOT-3 (PEDOT-like honeycomb manufactured with 10wt% PMMA) and f-PEDOT (flat PEDOT). FE-SEM images showed that PMMA-2 (8wt%), for example, had a diameter of 150-200 nm and a thickness of 150 nm. After depositing the PEDOT and removing the PMMA-2

the remaining thickness was 80nm with honeycomb-like morphology and high surface area. CV measurements showed that the order of cathode current densities was as follows: h-PEDOT-2>h-PEDOT-2>h-PEDOT-1>f-PEDOT. Thus, the h-PEDOT-2 conformation was the most electrochemically active. The ΔE_p also followed the same (inverse) pattern. EIS measurements also confirmed that the sample with lower internal resistance was the h-PEDOT-2. The results obtained through the PV performance for h-PEDOT-2 were: Voc=768 [mV], Jsc=17.72 [$mAcm^{-2}$], FF=0.67 and η=9.12%, and were the highest ever among all the different types of CE tested and mentioned in the article.

6.92 *Liu et al.: best electropolymerization condition for PEDOT and rGO/PEDOT (2017)*

Liu et al. produced a CE composed of PEDOT by studying how the polymerization time, voltage and concentration of EDOT influenced the performance of a DSSC using such a CE; after understanding the best cell conformation they tested how performance would increase if rGO was inserted as a conductive material [111]. SEM images showed that the PEDOT morphology had 3D network-like structures with nanoparticle aggregates that provided a good surface area. First, the voltage in the electropolymerization phase was varied from 10 V to 60 V, observing how the 20 V voltage obtained the best result, at efficiency levels (6.006%). By increasing the voltage Jsc decreased, presumably because the thickness of the PEDOT increased too much and increased the resistance to charge transfer. The same tests were carried out with different polymerization times (from 5 min to 30 min) with 20 V. The best time was 10min always achieving an efficiency of 6.006%. Increasing the concentration of EDOT decreased the conductive resistance therefore: if the concentration had been too high the film would have been too thick, instead if the concentration had been too low the performance would also have been low. The best concentration was 0.02 M obtaining 6.401%. Then the rGO was inserted, thus forming the rGO/PEDOT complex. By incident photon to converted electron (IPCE) measurements it was observed that by using rGO/PEDOT the IPCE increased over the entire visible spectrum. CV measurements showed that rGO/PEDOT was catalytically more active than other electrodes (Pt and PEDOT). EIS measurements also confirmed that both R_s and R_{ct} were lower than Pt and PEDOT. Finally, an efficiency of 7.115% was obtained, higher than that of Pt, confirming the results obtained through the CV, IPCE and EIS tests.

6.93 Moolosan et al.: PEDOT:PSS with carbon derived by carbonized human hair (2017)

Moolsarn et al. studied a CE composed of PEDOT and carbon from human hair carbonized at 700 °C (C-P) [112]. They tested different CEs in which different amounts of carbon were used: 0.2, 0.4, 0.6 and 0.8 g. The composition of human hair was first studied: friend acid, keratin, melanin and protein. All these molecules are composed of basic components such as: carbon, oxygen, nitrogen, hydrogen and sulphur. Through the X-Ray diffraction (XRD) spectra it was observed that after carbonization at 700 °C some nitrogen, oxygen and sulphur residues remained, so the temperature was not high enough to expel all heteroatoms. Both EIS and CV measurements showed good catalytic activity (through cathodic current density and Rct measurements), but not as good as Pt. Through the PV performances and the above-mentioned

tests, the best composition obtained was the one with 0.6g of coal, obtaining the following values: Voc=0.76 [V], Jsc=14.85 [mAcm^{-2}], FF=0.58 and η=6.54%.

6.94 Edalati et al.: Heuristic method for PEDOT:PSS production (2017)

Edalati et al. studied the effect of a heuristic technique for the deposition of PEDOT:PSS used as CE in a DSSC [113]. This technique consists in the deposition of PEDOT, a treatment by HNO_3 and a doping with metal particles that led to a dispersion of the latter on the surface of PEDOT:PSS coated on FTO. Energy Dispersive X-ray (EDX) spectroscopy was performed both on the PEDOT:PSS produced by the above-mentioned method and on pure PEDOT:PSS. It was noted that the modified PEDOT:PSS had a high percentage of Cu and Fe particles. The SEM images showed that the PEDOT:PSS had a very smooth surface and that instead through the addition of metals and the treatment with HNO_3 it became rough, thus increasing both the catalytic sites and the transport. The PV performance showed that the modified PEDOT:PSS was better than the pure Pt (3.9, 1.8, 5.1% efficiency respectively).

6.95 Wu et al.: PEDOT doped with different metal (2017)

Wu et al. studied the effect of metal doping (Mn^{2+}, Co^{2+}, Ni^{2+} and Cu^{2+}) on PEDOT and performance when PEDOT-M^{2+} was applied as CE in a DSSC [114]. The SEM images showed that the pure PEDOT had irregularly sized, nearly molten particles with no channels for charge transfer. PEDOT- Co^{2+} and PEDOT- Ni^{2+} did not have the molten state and had channels between the particles. PEDOT- Cu^{2+} and PEDOT- Mn^{2+} had particles of various sizes (from 100 nm to 2.0 μm) with channels that also increased porosity and surface area. The EDS technique was used to determine that PEDOT had been correctly doped with the correct transition metals. Table 30 shows that PEDOT- Mn^{2+} is the best in terms of performance. Finally, CV, EIS and Tafel polarization tests were conducted to confirm the superiority of PEDOT- Mn^{2+} and confirm the trend of V_{oc} and J_{sc} values. In general, in all tests (CV, EIS and Tafel polarization) the trend of the obtained values (cathodic current density, peak-to-peak separation, R_{ct} and exchange current J0) follows this order: PEDOT- Mn^{2+} -> PEDOT- Ni^{2+} -> PEDOT- Co^{2+} -> PEDOT- Cu^{2+} confirming that the PEDOT-Mn^{2+} had the best activity and reversibility.

Table 30 *PV performance of various PEDOT-M^{2+} CEs and PEDOT CE. Adapted and reprinted with permission from [114].*

CE	V_{oc} [V]	J_{sc} [mAcm^{-2}]	FF	η %
PEDOT	0.642	8.69	0.66	3.26
PEDOT-Cu^{2+}	0.696	8.19	0.66	3.78
PEDOT-Ni^{2+}	0.702	9.06	0.69	4.36
PEDOT-Co^{2+}	0.717	9.75	0.69	4.81
PEDOT-Mn^{2+}	0.738	10.25	0.69	5.19

6.96 Maiaugree et al.: PEDOT:PSS doped with nickel sulphide nanoparticles (2017)

Maiaugree et al. studied a CE composed of PEDOT:PSS and nickel sulphide nanoparticles (NiS(NPs)/PEDOT:PSS) [115]. All tests were performed with these amounts of NiS(NPs): 0.1-0.2-0.3-0.4 g.SEM images revealed that the addition of NiS(NPs) increased the surface area of the layer and therefore also the porosity. The CV tests showed that the CE composed of 0.3g NiS(NPs) was the most promising, showing higher cathode current density (but not higher than Pt). EIS measurements also confirmed that R_{ct} decreased as the amount of NiS(NPs) increased to a minimum of 0.46 Ω with 0.3 g NiS(NPs). When 0.4 g was added, the resistances increased again, probably due to the weak anchorage of PEDOT:PSS on the FTO. The J-V curves showed, as expected, that NiS(NPs)/PEDOT:PSS with 0.3 g NiS(NPs) had the best performance reaching an efficiency of 8.18% (the Pt efficiency, measured by comparison, was 8.62%), very close to the Pt efficiency.

6.97 Li et al.: Effect of the sheet resistance on PEDOT-TsO (2017)

Li et al. studied the effect of sheet resistance on the PV performance of a cell using PEDOT-TsO as CE, through reductions and oxidations of the CE [116]. First, the SEM images showed that PEDOT-TsO showed a homogeneous film with a pore size of 10-20 nm. After a reduction treatment with hydrazine the pores widened to 200-300 nm. A subsequent oxidation treatment using iodine vapour further increased the pore size up to 300-500 nm confirming that the treatments influenced the CE and increased the porosity, thus theoretically decreasing the sheet resistance. In Table 31 are collected the results obtained through the PV performance of cells using CEs reduced and re-oxidized at different times. The sheet resistance decreases, increasing the Voc and Jsc, confirming that it is a fundamental parameter for the performance of a DSSC.

Table 31 *PV performance of various Hydrazine-Iodine treated CEs and Pt and relative sheet resistance. Adapted and reprinted with permission from [116].*

CE	Sheet R [Ω/sq]	V_{oc} [mV]	J_{sc} [mAcm^{-2}]	FF	η %
Pt	-	752	14.44	0.65	7.05
PEDOT-TsO	10E2.1	723	14.25	0.48	4.93
hydrazine-1 min	10E3.3	738	13.62	0.45	4.53
hydrazine-30 min	10E4.2	726	16.42	0.43	4.16
hydrazine-12 h	10E5.4	754	12.97	0.43	4.21
hydrazine-24 h	10E6.0	749	12.47	0.42	3.91
hydrazine-48 h	10E6.5	752	11.07	0.42	3.51
iodine-3 min	10E5.3	759	12.34	0.48	4.54
iodine-10 min	10E4.3	759	13.29	0.47	4.69
iodine-40 min	10E3.4	759	13.88	0.58	6.14
iodine-12 h	10E3.0	745	14.49	0.64	6.86

6.98 Gemeiner et al.: PEDOT:PSS screen-printed with HEC (2017)

Gemeiner et al. studied an CE composed of PEDOT:PSS and structured by hydroxyethyl cellulose (HEC) [117]. The structural, optical, electrical and electrochemical properties of the CE were studied. The samples with 0.03 wt% HEC reached conductivity of 80 Scm^{-1} and a thickness of 200 nm with maximum transparency of 60% in the VIS region. CV measurements showed that it was also the best CE in terms of catalytic activity but had too high overpotential (1.22 V compared to Pt: 0.69 V). It was observed that decreasing the concentration of HEC also decreased the overpotential. The best PV performance was always obtained with the CE at 0.03wt% of HEC: Voc=0.68 [V], Jsc=13.46 [$mAcm^{-2}$], FF=0.41 and η=4.21%. The authors also stated that by adding nanomaterials such as MWCNT or TiO_2 the PV performance could increase significantly, as those obtained were not very high.

6.99 Thuy et al.: High-efficient PEDOT CE on FTO (2017)

Thuy et al. studied the best PEDOT/FTO ratio according to the PV performance obtained; Pt was used as reference [118]. The tests were done on the following ratios: 4:6, 6:4, 8:2 and 9:1 and on Pt. The best performance was obtained with the 9:1 PEDOT/FTO CE: Voc=0.665 [V], Jsc=16.8 [$mAcm^{-2}$], FF=0.65 and η=7.32%. The Pt obtained the following values: Voc=0.645 [V], Jsc=15.9 [$mAcm^{-2}$], FF=0.65 and η=6.73%. The latter, through IPCE measurements, had wavelength ranges around 300-800 nm. The EIS measurements confirmed that 9:1 PEDOT/FTO had lower Rct in absolute (1.00 Ω).

6.100 Li et al.: PEDOT/MWCNT high-efficiency CE with PMMA template (2017)

Li et al. tested a transparent CE applied to a double-sided DSSC, composed of PEDOT/MWNCT using a PMMA template [119]. Five types of CEs were tested: flat PEDOT (f-PEDOT), flat PEDOT/MWCNT (f-PEDOT/MWCNT), honeycomb-like PEDOT (h-PEDOT), honeycomb-like PEDOT/MWCNT (h-PEDOT/MWCNT) and Pt. SEM images showed that the honeycomb-like conformation had been performed correctly. After PMMA removal the thickness of h-PEDOT/MWCNT 280nm. They studied the best volume of MWCNT and found that it was 5.0 μL. CV measurements showed that the h-PEDOT/MWCNT CE had better catalytic activity. From Table 32 it can be seen that also from EIS measurements the order of catalytic activity was h-PEDOT/MWCNT > h-PEDOT> Pt> f-PEDOT/MWCNT> f-PEDOT. The best performance was obtained for the h-PEDOT/MWCNT CE with an efficiency of 9.07%.

Table 32 *Front and rear PV performances, EIS and CV resultrs of: Pt, (A) f-PEDOT, (B) f-PEDOT/MWCNT, (C) h-PEDOT and (D) h-PEDOT/MWCNT. Adapted and reprinted with permission from [119].*

CE	Illumination	Epp [mV]	Rct [Ωcm^2]	V_{oc} [mV]	J_{sc} [mA/cm^2]	FF	η %
Pt	Front	597	0.47	760	15.60	0.65	7.71
	Rear			714	7.84	0.67	3.75

A	Front	664	0.53	761	15.42	0.64	7.51
	Rear			705	7.39	0.67	3.49
B	Front	615	0.32	771	15.69	0.67	8.10
	Rear			721	8.12	0.69	4.04
C	Front	646	0.28	776	16.03	0.66	8.21
	Rear			756	8.76	0.70	4.64
D	Front	626	0.19	792	17.09	0.67	9.07
	Rear			757	10.76	0.69	5.62

6.101 Mustafa et al.: PEDOT/ TiO_2 doped with various substances (2017)

Mustafa et al. tested several CEs based on PEDOT/TiO_2 and: rGO, nanocrystalline cellulose (NCC), MWCNT [120]. It was observed that the CEs using rGO and MWCNT had high electrical conductivity and surface area while NCC provided a very high transparency, important to produce a good dye sensitized cell. In addition to the advantages listed above, these CEs are Pt-free and low cost. PEDOT-NCC/TiO_2 achieved higher efficiency than the others (PEDOT-rGO/TiO_2 and PEDOT-MWCNT/TiO_2): 2.10, 1.11 and 1.29%. PEDOT-NCC/TiO_2 CE had R_{ct} of 10.4 Ωcm^2 and high cathodic current density of -2.96 $mAcm^{-2}$ compared to PEDOT-rGO/TiO_2 and PEDOT-MWCNT/TiO_2 CEs.

6.102 Ahmed et al.: PEDOT:PSS doped with Zeolites (2018)

Ahmed et al. produced a CE composed of Zeolitic-Imidazolate-Framework (ZIF-8) and PEDOT:PSS and tested it in a DSSC [121]. Different concentrations of ZIF-8 were tested: 1, 3 and 5 wt%. It was noted that as the concentration of ZIF-8 increased, the average roughness became: 36, 50, 577 nm respectively. The thickness increased: 530, 585 and 630 nm respectively. CV tests showed that ZIF-8/PEDOT:PSS at 3% had higher catalytic activity (through measurements of cathodic current density and peak separation). EIS measurements also showed that up to 3% R_{ct} decreased to a minimum of 3.8 Ω and then increased, probably due to an aggregation of ZIF-8 particles. PV performance showed that the 3% CE reached an efficiency of 7.02%, very close to that of Pt.

6.103 Kim et al.: PEDOT:PSS and graphene nanoplatelets (2018)

Kim et al. produced a CE composed of PEDOT:PSS (for brevity called PP) and graphene nanoplatelets (GnPs) with different concentrations and tested it on a DSSC [122]. The GnPs were dispersed by sonication in water-ethanol solution, the following amounts were dispersed in wt%: 0.02, 0.1, 0.5, and 1 (later called PPGx, where x was:7, 2, 3,4 for 0.02, 0.1, 0.5, and 1 respectively). Once GnPs was mixed by sonification it exfoliated and fractured into very small pieces. In this way it could easily be deposited by an e-spry technique on all surfaces. EDX, X-ray photoelectron spectroscopy (XPS) and Raman spectroscopy measurements were made to better understand the nature of the CE and the compound obtained. The electrochemical

capabilities obtained by EIS, CV and J-V graphs were then tested. The EIS measurements showed lower and lower R_{ct} resistances as the GnPs concentration increased, reaching an extraordinarily low R_{ct} for PPG4: 0.07 Ωcm^2. Also, the CV measurements reported the PPG4 as the best compromise, it had very high cathodic current density showing an extraordinary catalytic activity. The PV performance obtained through the J-V graphs showed an efficiency of 8.33% for PPG4, much higher than the others and higher than Pt (7.99%).

6.104 Yun et al.: PEDOT:PSS and MWCNT with different diameter and purity (2018)

Yun et al. studied the effect of the purity of MWCNT on the performance and physical, chemical and electrical properties of an MWCNT/PEDOT:PSS (for brevity MWPE) CE [123]. There were four MWCNTs, characterised by their diameter and purity: TMC100-05, TMC100-10, TMC220-05 and TMC200-10 with purity and diameter in ascending order. XPS measurements were taken to investigate the atomic composition of the four electrodes. Subsequently the sheet resistance was measured, noting that as the purity and diameter of the MWCNT increased, the resistance decreased by three orders of magnitude, from 140 kΩ/sq for the TMC100-05 to 2.94 kΩ/sq for the TMC200-10. Optical transmittance was also investigated, and it was observed that the TMC220-05 exhibited the best transmittance in the visible region. As expected, the CE itself (composed with TMC220-05) showed the best performance with the following values: Voc=807.5 [mV], Jsc=12.9 [$mAcm^{-2}$], FF=0.49 and η=4.2%. The authors also investigated how the performance varied if the CE was treated with HCl-methanol and observed that the performance increased, especially Jsc and Voc. The CE using the TMC220-05 treated with HCl-methanol obtained the following performance: Voc=813 [mV], Jsc=12.9 [$mAcm^{-2}$], FF=0.55 and η=5.8%.

6.105 Kim et al.: PEDOT nanofibers doped with iodide compound as CE in DSSC (2018)

Kim et al. synthesized a CE composed of nanofibrous PEDOT (PEDOT NFs) and tried to improve its cooperation with the electrolyte by means of dimethyl imidazolium iodide (DMII) doping as a charge transport aid [124]. DMII doping increased the mobility of the PEDOT NFs by increasing its conductivity by about 18 times due to better aggregation, linearization and crystallinity. It was assumed that DMII would act in the polymerization phase by reducing the concentration of dodecyl sulfate ions (DS^-). Through EIS measurements it was observed that the resistance to charge transfer was reduced giving a high efficiency to the DSSC using PEDOT NFs doped with DMII (8.52%), the efficiency obtained with Pt was lower (8.25%), confirming that PEDOT is a good substitute for Pt-free cells.

6.106 Ma et al.: PEDOT in comparison with Pt/PEDOT (2018)

Ma et al. studied two CEs composed of flexible PEDOT and composite Pt/PEDOT [125]. SEM images showed that PEDOT had a porous structure and Pt had particle aggregates on the ITO substrate. The PV performance was immediately tested, and the following efficiencies were

obtained: 7.56% for Pt and 6.77% for PEDOT. In order to increase the cell performance, it was studied how the polymerization time influenced the behaviour of PEDOT. The times 40, 80, 120 and 160 s were tested. The SEM images showed that by increasing the curing time to 80 s, a more porous network was created, but by increasing the time even more porosity was lost. In addition, by increasing the time the colour of the CE varied from light blue to darker and darker blue, confirming the increase in thickness and a consequent loss of transparency. Both the CV and EIS tests showed that with the deposition time of 80 s the best results and lowest resistance were obtained, reaching an efficiency of 7.18%. Finally, Pt/PEDOT CE was tested, observing that the performance improved even more: Voc=776 [mV], Jsc=15.51 [$mAcm^{-2}$], FF=0.66 and η=7.90%.

6.107 Ma et al.: Advantages of PEDOT/rGO CE (2018)

Ma et al. tested PEDOT/rGO and PEDOT/GO on FTO as CE in DSSC [126]. The SEM and FE-SEM images showed how PEDOT had a dense and compact morphology. When GO was added, evenly distributed agglomerates of GOs could be seen that once they were reduced, they disappeared, indicating a good combination of PEDOT and rGO. CV analyses showed that PEDOT/rGO showed higher catalytic activity than the others (by measuring cathodic current density and peak-to-peak separation). EIS analyses also showed that R_{ct} decreased dramatically from 66.95 $ohmcm^2$ for PEDOT to 18.17 $ohmcm^2$ for PEDOT/rGO, resulting in better electronic transport and higher efficiency. The PV performances summarized in Table 33 were studied by modulating the polymerization time of the PEDOT/rGO from 100 s to 250 s, to understand its dependence. The best performance was obtained for the PEDOT/rGO-150s.

Table 33 *PV performance of various CEs. Adapted and reprinted with permission from [126].*

CE	V_{oc} [V]	J_{sc} [$mAcm^{-2}$]	FF	η %
Pt	0.78	17.03	0.63	8.33
PEDOT-150s	0.78	15.23	0.58	6.88
PEDOT/GO-150s	0.76	16.14	0.60	7.37
PEDOT/rGO-100s	0.76	15.24	0.66	7.56
PEDOT/rGO-150s	0.73	15.82	0.67	7.79
PEDOT/rGO-200s	0.75	15.42	0.67	7.64
PEDOT/rGO-250s	0.76	15.29	0.64	7.48

6.108 Vasanth et al.: PEDOT:PSS (2018)

Vasanth et al. studied PEDOT:PSS on FTO CE deposited by micro contact printing by means of a Polydimethylsiloxane (PDMS) print [127]. The performance obtained by this technique was studied using a Keithly 2420A electrometer. The J-V curves were compared to the Pt curves, obtaining an efficiency of 1.47%, Voc of 0.75V, Isc of 3.29 $mAcm^{-2}$ and FF of 60%.

6.109 Di et al.: PEDOT doped with phosphate compound (2018)

Di et al. studied the effect of various phosphate compounds ($Ni_3(PO_4)_2$, $Co_3(PO_4)_2$ and Ag_3PO_4) combined with PEDOT to create a composite material to be used as CE in a DSSC [128]. First, XRD tests were carried out to study the obtained compounds and have a confirmation. After the XRD tests the microscopic properties of the composite materials obtained through SEM images were investigated. It was observed that the phosphate particles were surrounded by the polymer. The polymer matrix in this case was very important because it provided, through its good conduction, a fast charge transport. The best compound (both in terms of PV performance and through CV and EIS tests) was PEDOT-$Ni_3(PO_4)_2$, with an efficiency of 6.412% and R_{ct} of 1.61 Ωcm^2.

6.110 Maiaugree et al.: PEDOT:PSS doped with perovskite (2018)

Maiaugree et al. studied a CE composed of a Co-doped $SrTiO_3$ NPs and PEDOT:PSS polymer (STCo NPs/PEDOT:PSS) material [129]. In order to better understand the effect of $SrTiO_3$ several CEs were studied with different amounts of the latter: $SrTi_{1-x}Co_xO_3$, where x=0, 0.025, 0.05, 0.075 and 0.1, synthesized by hydrothermal method. The SEM images showed that the film had an agglomerated cubic shape, the NPs were about 50-150 nm in size and the surface was generally very porous and rough. The CV measurements were carried out in such a way as to investigate CE activity, and it was obtained that STCo NPs/PEDOT:PSS CE with x=0.075 had the lowest reduction peak, resulting in higher catalytic activity. The film resistance was also studied in order to have another useful parameter for the choice of CE. It was noted that the resistance decreased as the Co content increased, with a maximum for x=0 of 3249 Ω up to a minimum for x=0.075 of 121 Ω. The EIS measurements also showed lower series and charge transfer resistances in the case of STCo NPs/PEDOT:PSS with x=0.075. Through the PV performance obtained it was concluded that the best CE was STCo NPs/PEDOT:PSS with x=0.075, which obtained the following values: : Voc=0.71 [V], Jsc=21.22 [$mAcm^{-2}$], FF=0.55 and η=8.39%.

6.111 *Yun et al.: PEDOT:PSS and Coiled carbon nanotubes composite material (2018)*

Yun et al. manufactured a CE composed of PEDOT:PSS and coiled carbon nanotubes (CCNT); later they tested how a treatment with HCl-methanol increased the characteristics of a DSSC using this electrode [130]. The TEM images showed how pure CCNT possessed helical carbon nanomaterials of different sizes. Once inserted together with PEDOT:PSS the resulting morphology was uniform and smooth, with a consequent decrease of conductivity and an increase of the resistance sheet ($7x10^5$ Ω/sq). For this reason, the posthumous treatment with HCl-methanol was performed. It was observed that a large portion of PSS was removed (PSS has a proven insulating effect), the layer decreased in thickness and the sheet resistance decreased by about one hundred times. It was demonstrated that the conformation treated with HCl-methanol and 0.4 g of coil was the best. PV performance showed that CCNT/PEDOT:PSS_0.4coil was 5.3% efficient and FF 46.4%.

6.112 Ahmed et al.: SiN_4/MoS_2 and PEDOT:PSS (2018)

Ahmed et al. tested a CE composed of PEDOT:PSS used as a binder for the composite SiN_4/MoS_2 [131]. Tests XDR and XPS were conducted to confirm that the composite SiN_4/MoS_2 had the right shape and composition, and it was observed that the composite had been successfully prepared. The same tests were carried out when PEDOT:PSS was incorporated, observing that there was an increase in porosity, also due to the unevenly distributed SiN_4/MoS_2 agglomerates on the surface. The thickness increased from 94 nm for pure SiN_4/MoS_2 to 550 nm for SiN_4/MoS_2/PEDOT:PSS, the Pt thickness (taken for comparison) was 571 nm, therefore comparable. CV measurements were performed by increasing the amount of SiN_4/MoS_2 from 1% to 10% by weight. It was observed that the properties increased as the latter increased. In fact, the best results in terms of cathodic current density and peak separation were 10% SiN_4/MoS_2/PEDOT:PSS and 5% SiN_4/MoS_2/PEDOT:PSS. Even the EIS tests showed how R_{ct} decreased as the SiN_4/MoS_2 content increased. Finally, the PV performance showed an efficiency of 7.22% for 10% SiN_4/MoS_2/PEDOT:PSS and 7.21% for 5% SiN_4/MoS_2/PEDOT:PSS, very similar to that of Pt (7.50%).

6.113 Wang et al.: Carbon/PEDOT CE and T^-/T_2 electrolyte (2019)

Wang et al. studied the combined effect of a liquid electrolyte (smectic T^-/T_2 containing [C12MIm][T]/T_2/TBP/$LiClO_4$ in the molar ratio of 2 : 1 : 0.1) and a carbon composite CE/PEDOT nanoparticles [132]. The electrolyte ($C_{12}T$) was also studied doped ($C_{12}T_{add}$). SEM images showed that the carbon had spherical morphology with spheres of an average diameter of 35 nm, giving a high surface area. When PEDOT was inserted the layer, thickness became 800nm, with the carbon uniformly dispersed in the PEDOT matrix. In Table 34 you can see the results of the J-V tests. The PV performance increased from $C_{12}T$ to $C_{12}T_{add}$. When inserting the PEDOT into the CE, a considerable increase in FF was noted (using $C_{12}T_{add}$). The trends of the values were studied even when the temperature varied. In fact, in the Figure 38 by increasing the T from 30 to 60 °C there is a maximum of around 40 °C for Jsc, FF and η. The EIS measurements showed that the carbon/PEDOT (CP) CE and $C_{12}T_{add}$ had much lower resistances than all the other conformations, thus confirming that the collaboration between electrolyte and electrode was very good.

Table 34 *PV performance of Pt, C and CP CEs with $C_{12}T$ and $C_{12}T_{add}$ electrolytes. Adapted and reprinted with permission from [132].*

CE	V_{oc} [V]	J_{sc} [mA/cm^2]	FF %	η %
Pt-$C_{12}T_{add}$	0.621	14.0	0.455	3.96
C- $C_{12}T_{add}$	0.621	15.1	0.488	4.57
CP- $C_{12}T_{add}$	0.642	15.8	0.568	5.76
CP- $C_{12}T$	0.617	11.8	0.527	3.83

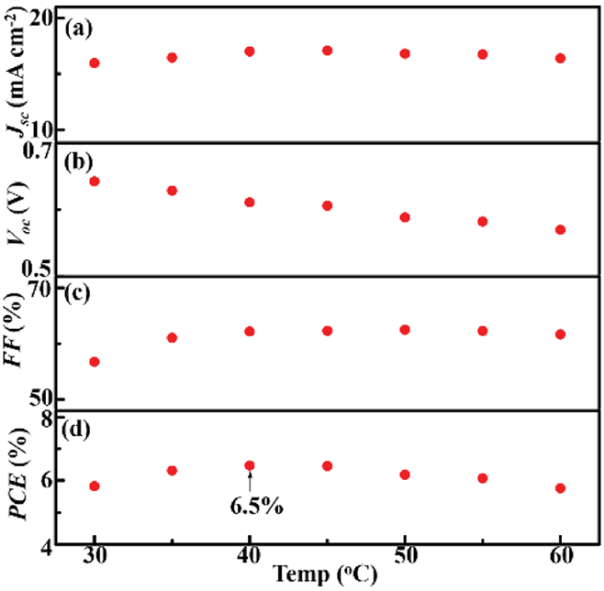

Figure 38 *Dependence on the temperature of the properties: (a) Jsc, (b) Voc, (c) FF%, (d) η. Reprinted with permission from [132].*

6.114 Basri et al.: PEDOT and polyvinyl alcohol (2019)

Basri et al. built a new CE composed of polyvinyl alcohol (PVA) nanofibers and PEDOT, all prepared via electrospinning and electropolymerization [133]. The FE-SEM images showed that PVA had very fine fibres with an average diameter of 76 nm. A small diameter increases conductivity considerably, so this morphology was suitable for application in DSSCs. Once the PEDOT had been inserted by electrodeposition it was observed that it covered the entire surface of the PVA. PVA/PEDOT nanofibers present a very porous cauliflower-like network with a large surface area. Table 35 summarises the values obtained from the CV, EIS and J-V tests. It can be observed that I_{cp} (cathodic peak current) is much higher in the case of PVA/PEDOT CE. Similarly, E_{pp} is lower than the other CEs (a high I_{cp} value and a low E_{pp} value confirm good catalytic activity). EIS measurements reported that the R_{ct} resistance, relative to charge transport in the electrode/electrolyte interface, was lower in the case of PVA/PEDOT CE, again confirming the superiority of the latter. Finally, the PV performance was considerably higher, even compared to Pt.

Table 35 *PV performance, EIS and CV results for various CEs. Adapted and reprinted with permission from [133].*

CE	V_{oc} [V]	J_{sc} [mAcm^{-2}]	FF %	η %	I_{cp} [mA]	E_{pp} [V]	R_{CT} [Ω]
PVA NFs	0.16	0.66	16.10	0.017	-0.79	0.34	40.90
PEDOT	0.66	4.05	52.00	1.39	-0.19	0.63	0.59
PVA/PEDOT NFs	0.61	7.73	46.93	2.11	-0.072	0.82	0.21
Pt	0.59	3.68	52.50	1.14	-0.15	0.57	2.83

6.115 Shenouda et al.: a PEDOT:PSS CE (2019)

Shenouda et al. studied a PEDOT:PSS CE for a DSSC [134]. The morphology was investigated using an AFM and it was observed that the layer was composed of spherical clusters with an average diameter of 214.04 nm. The PV behaviour was studied with an intensity range from 10 to 13 0mWcm^{-2}, demonstrating a constant FF at 0.5. The DSSC using PEDOT:PSS as CE proved to be a good candidate, especially good for the absence of Pt and low production costs.

6.116 Wan Khalit et al.: New PEDOT, rGO and alumina material (2019)

Wan Khalit et al. tested a new CE composed of PEDOT, rGO and alumina (PEDOT/Al_2O_3-rGO) prepared by two-step deposition: deposition of Al_2O_3-rGO by cyclic voltammetry and deposition of PEDOT on Al_2O_3-rGO by chronoamperometry [135]. The FTIR and XRD tests were performed in order to determine whether the functional groups and crystalline phases had formed successfully and so it was. The FESEM images showed that the PEDOT/Al_2O_3-rGO composite layer had a wrinkled paper-like structure typical of PEDOT and a coral-like structure typical of PEDOT, with distributed alumina nanoparticles increasing the presence of active sites. Overall, the layer showed high porosity, resulting in a high surface area. Table 36 shows the results of the CV, EIS and PV performance tests. The PEDOT/Al_2O_3-rGO CE shows in all three cases better electrocatalytic activity with higher I_{cp} and lower R_{ct} and E_{pp}. The performance was better than PEDOT:PPS and pure rGO.

Table 36 *PV performance, EIS and CV results for various CEs. Adapted and reprinted with permission from [135].*

CE	V_{oc} [V]	J_{sc} [mA/cm^2]	FF	η %	I_{cp} [mAcm^2]	E_{pp} [V]	R_{CT} [Ωcm^2]
rGO	0.60	3.23	0.39	2.08	-1.20	0.57	45
PEDOT/Al_2O_3-rGO	0.58	7.40	0.50	2.15	-2.45	0.47	0.6
PEDOT:PSS	0.68	11.0	0.28	2.10	-	-	-

6.117 Zhang et al.: PEDOT CE in DSSC (2019)

Zhang et al synthesized PEDOT polymer and poly(bis-3,4-ethylenedioxythiophene) polymer (P(bis-EDOT)), starting from 5,7-diiodo-2,3-dihydro-thieno[3,4-b][1,4]dioxins and 7,70-diiodo-2,3,20,30-tetrahydro-[5,5']bi[thieno[3,4-b][1,4]dioxinyl] monomers and then use them as conductive polymers as CE in a DSSC [136]. To further increase the photo-electrical conversion efficiency, the polymers were treated with N_2H_4/I_2 through a reduction-reoxidation process. The PV performance of the treated PEDOT was studied and the following efficiencies were not obtained: 7.08 and 6.64% respectively. Instead, the PV performance of the P(bis-EDOT) was lower: 6.35 and 4.25% respectively.

6.118 Di et al.: PEDOT and phosphide compound (2019)

Di et al. studied the performance of two CEs composed of PEDOT and Ni_2P and Co_2P, synthesizing them at low temperature by phosphorization with PEDOT dispersion by electropolymerization [137]. The SEM images confirmed that the phosphide particles were informally dispersed in the PEDOT matrix creating many active sites and good porosity. Different amounts of phosphides were studied, respectively: 20, 40, 60 and 80 mg/ml. The CEs were called PEDOT-Ni_2P-x and PEDOT-Co_2P-x with x=1, 2, 3 and 4 (1=20, 2=40, 3=60 and 4=80 mg/ml respectively). PV performance showed that for both phosphides compounds the concentration that provided better values was 3. PEDOT-Ni_2P-3: : Voc=0.75 [V], Jsc=13.91 [$mAcm^{-2}$], FF=0.68 and η=7.14% and PEDOT-Co_2P-3: : Voc=0.75 [V], Jsc=13.61 [$mAcm^{-2}$], FF=0.68 and η=6.85%. EIS measurements were only conducted on sample 3 and it was observed that PEDOT-Ni_2P-3 showed lower R_{ct} than PEDOT-Co_2P-3 (5.2 Ωcm^2 compared to 6.4 Ωcm^2), CV measurements also showed that the former had higher catalytic activity than the latter, showing the higher cathodic current density.

6.119 Gemeiner et al.: new PEDOT:PSS and halloysite material (2019)

Gemeiner et al. developed a new CE composed of screen-printed PEDOT:PSS and halloysite nanotubes (HNTs), focusing on how the properties of the electrode changed as the HNTs content varied (starting from 0% to 3%) [138]. To monitor the thermal stability of PEDOT:PSS/HNTs, thermogravimetric analyses (TGA) were performed. It was observed that as the temperature and the HNTs content increased, the degradation T increased, therefore with a consequent increase in thermal stability. The root mean square roughness (RMS) also increased as the content increased, starting from 10 nm for 1% and reaching 70 nm for 3%. There was therefore an increase in roughness with a consequent increase in surface area, all factors that benefit from contact with the electrolyte. The resistance of the sheet was measured, and it was obtained that the conformation with the lowest resistance was that with 1% HNTs, dried at 120 °C, the resistance then increased as the HNTs content increased. Conductivity proved to be better again in the case of 1%, with a maximum value of 381 S/cm. The PV performance showed that the CE with 1% HNTs was the best performing: Voc=0.69 [V], Jsc=9.90 [$mAcm^{-2}$], FF=0.65 and η=4.5%.

6.120 Anil et al.: PEDOT:PSS doped with Ag nanoparticles (2019)

Anil et al. studied a CE composed of PEDOT:PSS and how different concentrations of AgNPs could influence its morphology and PV performance [139]. Through the FESEM images it was observed that the PEDOT:PSS was smooth and amorphous. Through the following composition, 250 µl PEDOT:PSS + 75 µl Ag NPs, the morphology changed. Through AgNPs the surface became wrinkled and the contact with the electrolyte improved. As the Ag NPs increased, it was observed that they were no longer evenly distributed. The J-V characteristics showed that by adding Ag NPs the efficiencies increased considerably (by 75%), but after 100 wt% Ag NPs they fell, probably because the concentration of silver blocked the channels useful for the conduction of electrons. The efficiencies that were obtained are the following: 2.02% for PEDOT:PSS pure, 2.73% for PEDOT:PSS/AgNPs at 25 wt%, 3.40% for

PEDOT:PSS/AgNPs at 50wt%, 3.75% for PEDOT:PSS/AgNPs at 75wt% and 3.05 for PEDOT:PSS/AgNPs at 100wt%.

6.121 Xu et al.: PEDOT doped with MoS_2 nanomaterials as CE in DSSC (2020)

Xu et al. combined PEDOT with MoS_2 nanomaterials to form a composite and transparent CE for a DSSC [140]. They investigated how performance varied with the EDOT monomer concentration during polymerization and found that 0.05 M was the best concentration, which achieved the best performance (η: 6.33%). After XRD analysis to verify that the MoS_2 functional group was present in the CE composite, the morphology was studied. The film of MoS_2/PEDOT showed a different morphology from that of pure PEDOT, with very small pores and good uniformity which increased the surface area exposing many active sites. Finally, the most performing thickness was investigated. More layers were distributed (from 1 to 5) and it was found that the conformation with 2 layers obtained the best performance: Voc=0.743 [V], Jsc=13.73 [$mAcm^{-2}$], FF=68.6% and η=7.00%. The EIS measurements showed that PEDOT had very low R_{ct}, but not lower than Pt (5.55 and 3.94 Ωcm^2). The CV measurements showed that MoS_2/PEDOT formed by 2 layers showed better catalytic activity than Pt, with lower peak separation and higher cathodic peak current density (0.318 and 0.331 for ΔE_p and -1.726 and -1.381 $mAcm^{-2}$ for Jcp respectively).

6.122 *Peri et al.: PV performance on PEDOT sintering temperature (2020)*

Peri et al. tested a CE based on PEDOT polymer and tested the dependence of properties and performance on changes in sintering temperature [141]. The nomenclature used will be: Nor for PEDOT not tested with temperature, 50 for sintered PEDOT at 50 °C, 100 for sintered PEDOT at 100 °C and so on. Through AFM it was noticed that there were substantial changes in the morphology of CEs as the temperature increased. The distance between the peaks and valleys became: 122.9, 109, 102, 50.85 and 9.32 nm as the T increased. RMS also varied, decreasing: 39.82, 29.21, 20.73, 16.53 and 4.347nm respectively. CV measurements showed that the highest performing CE was 200, showing higher cathode peak current density and therefore higher electrocatalytic activity. EIS measurements also showed that the 200 had lower internal resistances. In fact, by increasing the sintering T, it decreased R_{ct}, but with a minimum at 200 °C, and then rose again by increasing the T. Table 37 shows the values of the PV performance obtained, it can be noted that the 200 shows better performance, with a considerably higher Jsc and an efficiency of 4.30%.

Table 37 *PV performance of various PEDOT CEs sintered different temperatures. Adapted and reprinted with permission from [141].*

CE	V_{oc} [V]	J_{sc} [$mAcm^{-2}$]	FF	η %
Nor	0.63	6.81	0.54	2.33
50	0.64	9.92	0.49	3.12
100	0.62	10.74	0.52	3.49
150	0.64	12.77	0.46	3.80

200	0.63	14.30	0.48	4.30
300	0.48	0.21	0.15	0.01

6.123 Bella et al.: a new PEDOT derivative polymer (2020)

Bella et al. proposed a derivative of PEDOT containing a cationic ammonium moiety and an iodide counter-anion (cPEDOT), noting how the PSS unit (of PEDOT:PSS) replaced by an ionic moiety can improve the functioning of the CE [142]. The ammonia portion of PEDOT was soluble in aqueous media and therefore improved the repulsion that PSS presented with $I3^-$ ions in the aqueous electrolytic solution. The cPEDOT solution was spin-coated on conductive glass and heat treated in order to make it 100% stable when used with an I^-/I_3^- redox pair. The resulting polymer was characterised by nuclear magnetic resonance (NMR), IR and UV-Vis-NIR. The hygroscopicity of the film was 3300 cm^{-1}, the ammonium moieties absorbed in the UV region and there were no polarons and bipolarons. CV tests were carried out and it was observed that cPEDOT showed high cathodic current density and E_p small, both results suggesting that cPEDOT had good catalytic activity. EIS measurements were made demonstrating once again that the charge transfer resistance, an essential parameter to assess the electrolyte electrode relation, was low (3.29 Ω), lower than that of Pt (5.33 Ω). Tafel's polarization also confirmed these trends. The J-V curves in Figure 39 showed that cPEDOT was significantly better than Pt. The results of the PV performance are summarized in

Table **38**. The comparison with PEDOT:PSS showed that ammonium moiety improved the electrostatic repulsions between PSS and I_3^-. Finally, the stability of cPEDOT with respect to Pt was also demonstrated. It was tested under LED light with an irradiation intensity of 1 sun for 50 days. The cPEDOT CE showed very high stability, maintaining 96% of the initial efficiency, Pt maintained 94%.

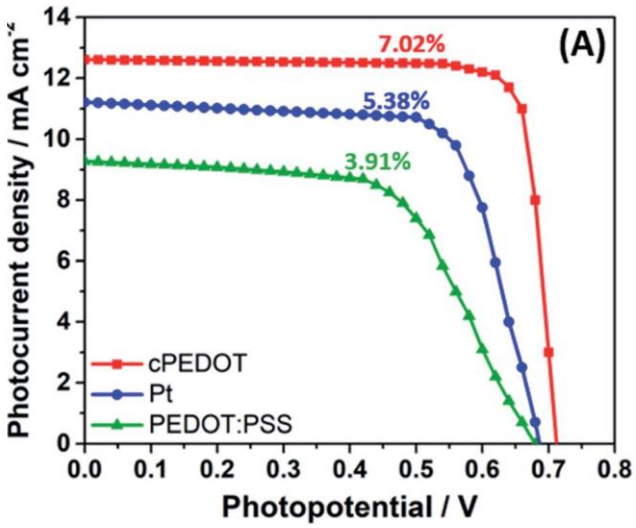

Figure 39 *Photocurrent density vs. photovoltage curves for cPEDOT, Pt and PEDOT:PSS measured under 1 sun irradiation (AM1.5). Reprinted with permission from [142].*

Table 38 *PV performance of various CEs. Adapted and reprinted with permission from [142].*

CE	V_{oc} [V]	J_{sc} [mAcm^{-2}]	FF	η %
Pt	0.66	11.06	0.68	4.95
cPEDOT	0.69	12.41	0.77	6.64
PEDOT:PSS	0.65	8.88	0.61	3.53

6.124 Reddy et al.: PEDOT:PSS single wall carbon nanohorn doped (2020)

In this article, Reddy et al. synthesized a CE composed of PEDOT:PSS and SWCNH (PEDOT:PSS/SWCNH) and tested it in a DSSC [143]. The morphology was studied using AFM and SEM images and it was observed that SWCNH was uniformly dispersed with an average size of 76 nm. CV tests were performed, and it was shown that the CE in question had good catalytic activity, as it had separation between 0.6 V peaks. The EIS and Tafel polarization tests also confirmed this, showing that R_s and R_{ct} had relatively low values of 25.9 Ω and 399 Ω. The PV performance was also investigated with pure PEDOT:PSS and pure SWCNH CEs. Efficiencies of 5.1%, 3.87% and 1.88% were obtained for PEDOT:PSS/SWNCH, PEDOT:PSS and SWCNH respectively, demonstrating how the CE in study in this article reported good performance.

7 PEDOT as Hole Transporting Material (HTM) in Dye-Sensitized Solar Cell

7.1 Saito et al.: first use of PEDOT as HTM in DSSC (2002)

After trying to use photoelectrochemical polymerization of pyrrole as hole transporting phase, Saito et al. reported the construction of DSSCs with chemically polymerized PEDOT as hole transporting material (HTM) [144]. After assembling the TiO_2 electrode, the authors worked on PEDOT preparation: the monomer was added in Fe(III) tris-p-toluenesulfonate-imidazole dissolved in n-butanol, then the dye-loaded TiO_2 film was trickled into the monomer solution and heated. After this step, the polymerization took place and the polymer was treated and dried. The films produced were sandwiched with Pt-sputtered conductive glasses for device assembly. The properties and the performance of the cells was studied by J-V characteristics under dark and under light conditions. From what it can be observed by looking at the data listed in the table below, the FF and V_{oc} showed low values, maybe due to the partially short-circuit of the cells. To overcome this issue, the authors added the ionic liquid 1-ethyl-3-methylimidazolium bis((trifluoromethyl)-slufonyl)amide (EMImTf2N) on the photoanode. This treatment led to better PV performance, as shown in Table 39. After this treatment, to the same electrode was added two different additive and a combination of these: 0.2 M LiTf2N, 0.2 M tBP and 0.2 M LiTf2N + 0.2 M tBP (where tBP: tert-butylpyridine). Furthermore, the authors proved also that these cells were very stable; for example, the cell treated with 0.2 M $LiTf_2N$ + 0.2 M tBP remained stable for 45 days.

Table 39 *Influence of different additives on J-V parameters for DSSC assembled with PEDOT as HTM. Adapted and reprinted with permission from [144].*

additives	V_{OC} [V]	J_{SC} [µA cm^{-2}]	FF	η [x10^{-3},%]
no additives	0.34	48	0.33	5.4
0.2 M $LiTf_2N$	0.30	62	0.36	7.0
0.2 M tBP	0.45	0.54	0.35	8.5
0.2 M $LiTf_2N$ + 0.2 M tBP	0.44	0.68	0.41	12

7.2 Fukuri et al.: Performance improvement of ss-DSCs (2004)

The main problem, which makes the performance still low, was that PEDOT didn't adhere adequately to the dyed TiO_2 films [145]. Direct contact, however, produced short circuit between glass and PEDOT, there was a transfer of back electron that reduce the voltage Jsc, Voc and η. Fukuri et al. proposed two ways in order to improve the performance of the cells. One was inserting in the traditional dye an amphiphilic ruthenium dye with long alkyl chain: Z907 and N719. The second one was a tiny insulating layer such as Nb_2O_5, Al_2O_3 ,MgO, ZrO, Y_2O_3 on the TiO_2 films. The results showed that Z907 improve better than N719 the performance of the cells [Figure 40]. Also, the back electron transfer was suppressed using Z907. The introduction of an insulation layer decreased the charge recombination rate in the electrolyte. The best result was given by γ-Al_2O_3 on the TiO_2.

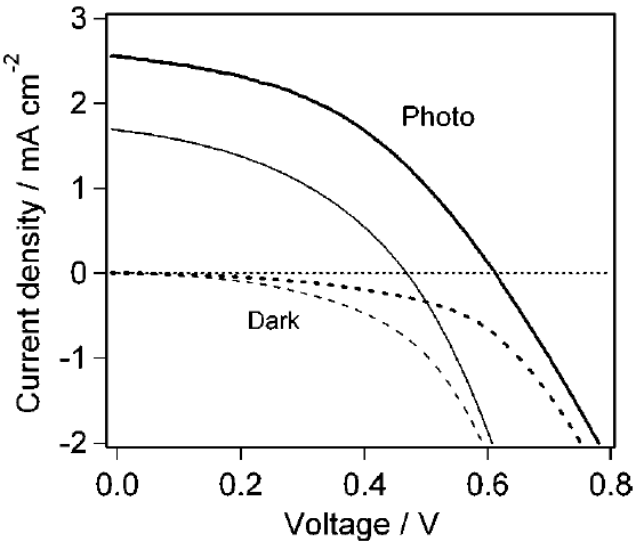

Figure 40 *Photocurrent-voltage characteristics with N719 (-) and Z907 (---) under AM 1.5 irradiation [145].*

7.3 Fukuri et al.: Electron Transport Analysis for PEDOT (2006)

Fukuri et al. analysed the electron transport process in TiO_2 electrodes with PEDOT as HTM and iodide solution as HTM and compared them [146]. The cells were respectively: TiO_2electrode/dye/PEDOT/Au-sputtered as CE and TiO_2-Z907electrode/dye/0.6M1,2-dimethyl-3propylimidazolium iodide (DMPImI) 0.05 MI2, 0.1 M LiI, and 0.5 M tBP in methoxyacetonitrile/Pt-sputtered as CE. The electron transport processes in PEDOT-DSCs was analysed with stepped light induced transient measurements of photocurrent and voltage measurement and EIS. SLIM-PCV demonstrated that photovoltage decay, in PEDOT/DSCs, was faster than in iodide-DSSCs and electron lifetime was 10-30 times shorter than iodide-DSCs. EIS showed that the total impedance of PEDOT-DSCs was higher than iodide-DSCs. Furthermore, the overall measurement suggested the importance of the interfaces in PEDOT/DSCs because the interface molecular organization could be optimized to increase V_{oc}, J_{sc} and FF.

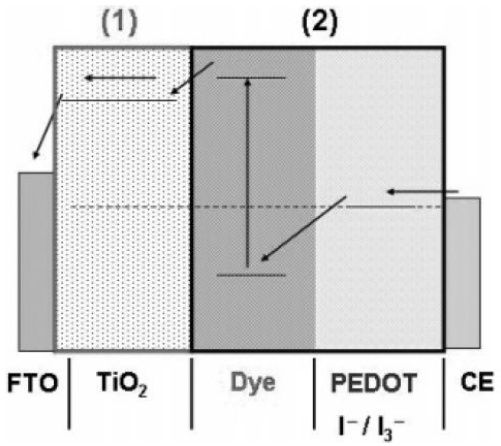

Figure 41 *View of electron transport in DSCs [146].*

7.4 *Kim et al.: TiO_2 ss-DSSC with PEDOT (2008)*

In this article the authors produced solid-state dye sensitized TiO_2 solar cells with Z907 ruthenium dye as sensitizer and PEDOT as HTM [147]. Moreover, in these cells the counter electrode was platinum free and was made by PEDOT. Configuration of the cell: FTO/TiO_2/Dye/PEDOT-PEDOT/FTO. The TiO_2 electrode was filled with the PEDOT through photoelectrochemical polymerization of the bis-EDOT. The authors achieved an open circuit conversion efficiency of 2.26% with high open circuit voltage (0.8 V).

7.5 Xia et al.: Influence of doping anions (2008)

Xia et al. replaced the I^-/I_3 electrolyte in the dye sensitized solar cells with the PEDOT polymer [148]. Subsequently, the authors went to analyse how doping anions (ClO_4^-, $CF_3SO_3^-$, BF_4^- and $TFSI^-$) were going to increase performance of SS-DCSs cells. The best performance occurred when TFSI- anion was used (Figure 42). Electrochemical and impedance tests showed that the anions significantly influenced the I-V curves, conductivity and impedance. The optimal parameters obtained are: Jsc = 5.3 $mAcm^{-2}$, Voc = 750 mV and efficiency 2.85%. All the doping anions increased the performance of the cell (Table 40).

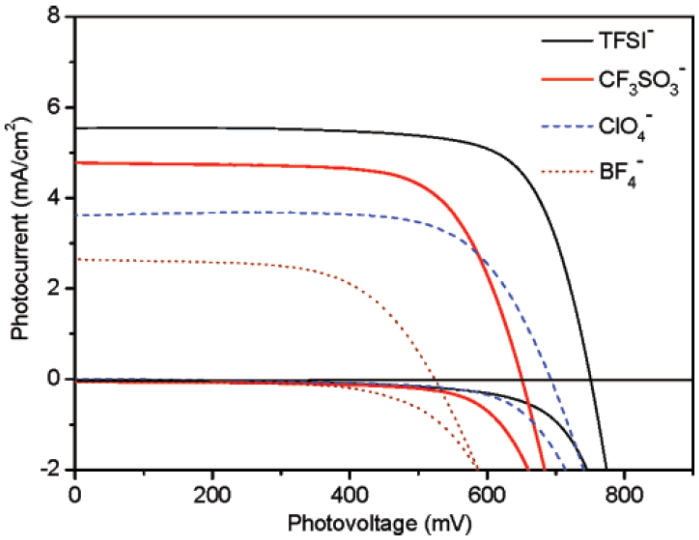

Figure 42 *I-V curves of SS-DSCs using PEDOT as HTM [148].*

Table 40 *PV properties of different doping anions in SS-DSCs. Adapted and reprinted from [148].*

Doping ions	V_{oc} [mV]	J_{sc} [$mAcm^{-2}$]	FF	η [%]
ClO_4^-	690	3.6	0.72	1.8
$TFSI^-$	750	5.3	0.73	2.85
$CF_3SO_3^-$	635	4.8	0.71	2.15
BF_4^-	510	2.8	0.63	0.9

7.6 *Xia et al.: the influence of doping anions (2008)*

The authors investigated the effects of some doped anions applied to PEDOT as HTM in ss-DSSC [149]. The cell in question was formed by a TiO_2 electrode on FTO, PEDOT as HTM,

Ru-dye, Au CE. The anions studied were: perfluorosulfunates $CF_3SO_3^-$, $C_4F_9SO_3^-$, $C_8F_7SO_3^-$; and bis(perfluorosulfunyl)imides $N(CF_3SO_2)_2^-$, $N(C_2F_5SO_2)_2^-$, $N(C_3F_7SO_2)_2^-$, $N(C_4F_9SO_2)_2^-$. Bis(perfluorosulfunyl)imides showed higher performance than other doping anions (Figure 43). The authors also demonstrated that the longer the carbon chain was, the less improved cell performance. In fact, for a carbon chain longer than C8 the performance drops drastically, going to have a negative effect on conductivity and conversion efficiency. The authors also demonstrated that the dark current in bis(perfluorosulfunyl)imides follows this trend: $N(C_4F_9SO_2)_2^- > N(C_3F_7SO_2)_2^- > N(C_2F_5SO_2)_2^- > N(CF_3SO_2)_2^-$. Through CV studies, the authors noted that all doping anions on PEDOT showed the same peak values, ie the oxidative peak at 0.3 V and the reduction peak at -0.5 V. This showed that anions did not change the electrochemical behaviour of PEDOT, as those values are typical of PEDOT used as HTM in ss-DSC.

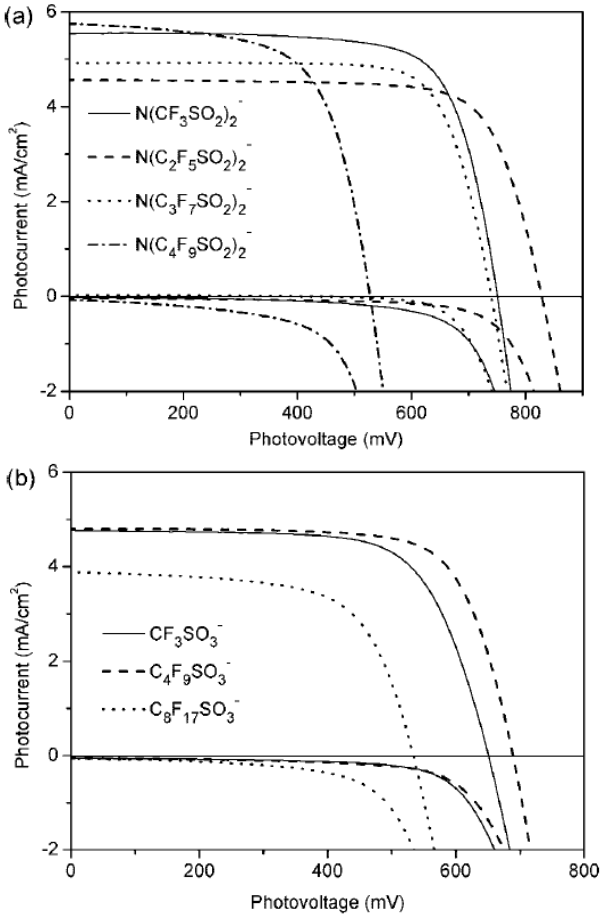

Figure 43 *I-V Curves for ss-DSC using different doping anions on PEDOT as HTM. a) bis(perfluorosulfunyl)imides b) perfluorosulfunates [149].*

7.7 Lee et al.: addition of glycerol to PEDOT (2008)

The authors investigated the influence of glycerol added to PEDOT:PSS as HTM [150]. Later, they also investigated a second addition of an ionic liquid (EMImI) in order to see its effects. The cell in question consisted of: SnO_2/TiO_2/Dye/Electrolyte/Pt where the electrolyte was composed of PEDOT:PSS with addition of glycerol (G-PEDOT:PSS). The addition of glycerol

improved the dark current property of the cells, increased Voc (0.75->0.81) and FF (0.34->0.49). The addition of the ionic liquid further increased the factors (Figure 44).

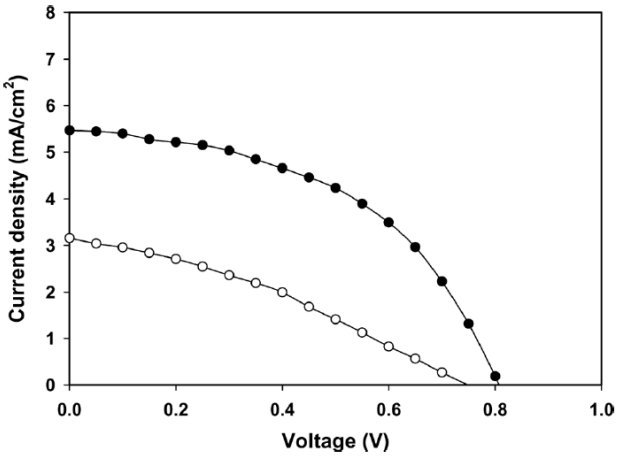

Figure 44 *PV characteristics of SnO_2/TiO_2/Dye/Electrolyte/Pt devices ○) without ionic liquid and •) with ionic liquid [150].*

After that the authors went to investigate how they varied the performance to vary the percentage of glycerol inserted. The best results were obtained with a percentage of 6% glycerol.

7.8 Liu et al.: Organic DSSC with PEDOT (2010)

Liu et al. tested DSSCs using PEDOT as HTM and D149 as dye [151]. The cell was formed by FTO/TiO_2-PEDOT/D149-dye/Au/FTO. In order to compare this cell with the cells normally used, was synthesized another cell with the Z907 dye. D149 dye belong to the section of iodine dyes that were very efficient in DSSCs with organic dye. The SEM images showed the surface morphology of the TiO_2 electrode and showed that a porous layer of PEDOT had formed on the surface of the electrode. Later, the authors investigated cell performance varying the thickness of the TiO_2 layer. The I-V curves showed that the best performances were obtained with a thickness of 5.8 and 4.2 μm. The cell with 5.8 μm thickness showed the best efficiencies: J_{sc}=9.3mAcm^{-2} V_{oc}=0.86V FF=0.75 n=6.1%, the best results on term of efficiency ever obtained.

7.9 Mozer et al.: dye regeneration in a ss-DSSC (2010)

The authors studied dye regeneration kinetics in a ss-DSSC with PEDOT deposited photoelectrochemically as HTM [152]. The regeneration kinetics of the dye in question appeared to be orders of magnitude slower than that with the dye I^-/I_3. The slow regeneration kinetics had the effect of limiting the short-circuit current of the ss-DSSC. The cell consisted of TiO_2/Z907-dye/PEDOT/Pt. The azmount of PEDOT present in the TiO_2 pores varied with the polymerization time. The authors calculated that with 30 min deposition, the ratio Z907-dye/PEDOT was approximately 1.2. With these specifics, the authors achieved η=3%.

7.10 Liu et al.: PEDOT with different light illumination (2012)

The authors studied the best wavelengths of the illumination light were by evaluating the effects on a photoelectrochemical polymerization process in a DSSC [153]. It was shown that using PEDOT as HTM gave good cell performance under continuous spectral light illuminations. The cells were studied under different light illuminations (740, 670, 605 and 540 nm). The authors immediately noticed that the performance increased as the lighting increased, but when it reached 740 nm the performance decreased drastically. The best performances were achieved with 670 nm light illumination with power conversion efficiency (PCE) of 7.1%, J_{sc} of 10.1mAcm^{-2}, V_{oc} of 933 and FF of 0.76. Later, the authors studied that the optimal thickness of the TiO_2 layer was 8μm (with 670 nm light illumination). To understand the limits of other lights illumination the cells were characterized under different monochromatic light illumination, the devices were called $DSSC_{740}$, $DSSC_{670}$, $DSSC_{605}$, $DSSC_{540}$. It was noted that the efficiency decreased as the light illumination decreased and decreased also at 740nm. IPCE spectra were studied, the $DSSC_{740}$ spectrum had lower IPCE value compared to $DSSC_{670}$, both spectra had the same shape. In the case of $DSSC_{605}$, $DSSC_{540}$ the shape of the IPCE spectrum diverged from that of the spectrum transmitter and the IPCE value decreased. To characterize the hole-transport, impedance measurements were conducted. It was noted that under the same intensity of light the resistance increased, with the reduction of the wavelength of light used for polymerization. When the hole-transport resistance increase, the holes will have a greater difficulty of transportation to the CE and the oxidized dye cannot be reduced in time. In this way the performance decreases. The process of charge exchange does not take place in the dark, so if you look the devices in the dark the current that you observe reflects the TiO_2/PEDOT interface resistance. This resistance increases with $DSSC_{605}$, $DSSC_{540}$ and $DSSC_{740}$. Finally, the stability of the $DSSC_{670}$ under LED array (LUXEON, NL98) in a N2 gas filled box was studied. The efficiency decreases slightly lowering the efficiency from 7.03% to 6.92%.

7.11 Park et al.: PEDOT via photoelectrochemical polymer deposition at different light intensities (2013)

Park et al. investigated a DSSC based on PEDOT as HTM [154]. PEDOT was prepared via photoelectrochemical polymer deposition at different light intensities. The authors found that PEDOT prepared with this method was particularly oxidized and contained very significant amounts of polarons ($PEDOT^{+}$), bipolarons ($PEDOT^{++}$) and very little neutral PEDOT. Especially using photoelectrochemical polymer deposition under low light intensity resulted in a very low fraction of neutral PEDOT. The solar cell that was tested with this method of manufacture had very high-PCE thanks to a long lifetime of the electrons, a very fast charge transport and high transparency, due to PEDOT. The DSSC consisted of TiO_2 on FTO as working electrode, stainless steel as CE and PEDOT as HTM.

7.12 Zhang et al.: PEDOT produced via PEP in aqueous solution (2014)

Zhang et al. tested and applied an organic donor-π-acceptor (D-π-A) sensitizers via organic photoelectrochemical polymerisation (PEP) using PEDOT polymerised as HTM in DSSC [155]. By combining D-π-A sensitizers and PEDOT produced via PEP the DSSC showed an

efficiency of 5.6%. After that, the authors tried to produce PEDOT via PEP in aqueous micellar electrolytic medium. This route was explored as it was simpler, less expensive and environmentally friendly. The DSSC with PEDOT synthesized with this last method showed efficiency of 5.2%. The PEDOT produced with the first method showed high conductivity, compact and smooth morphology, while with the second method the morphology was very rough and with high roughness. It was therefore confirmed that the production by aqueous solution is a valid alternative with good efficiencies to produce the PEDOT as HTM.

7.13 PEDOT-carrageenan solid electrolyte for DSSC (2015)

In this article Ng et al. studied PEDOT doped with carrageenan polymer and used it as a solid electrolyte in DSSC [156]. The SEM images showed that pure PEDOT had a smooth and non-porous surface, even pure carrageenan. They studied the electrolyte with different amounts of carrageenan in it: 0.1, 0.2 and 0.5wt%. The surface of PEDOT-carrageenan was wrinkled and with a higher surface area. One could notice the carrageenan aggregates taking the blue colour of PEDOT in the carrageenan matrix. Conductivity was also investigated, and it was observed that as the amount of carrageenan increased, conductivity increased to a maximum of 16.23 S/cm per PEDOT-carrageenan 5wt%. The trend of the glass transition temperature (Tg) was also tested and it was noted that it increased as the amount of carrageenan, Tg increased (Tg=72,748°C for PEDOT-carrageenan 5wt%). The PV performance showed poor results, with efficiency below 1% (Voc=565 [mV], Isc=3.37 [mA], FF=0.221 and η=0.421%).

7.14 Ng et al.: PEDOT:PSS and DNA based HTM (2016)

In this article, Jayme et al. studied an HTM composed of deoxyribonucleic acid (DNA) and PEDOT:PSS [157]. The cell in which this HTM was tested had the following configuration: FTO/TiO_2/dye/DNA-PEDOT:PSS/electrolyte/Pt. The authors measured the conductivity of several samples: pure DNA, DNA with 2%, 5%, 7% and 10% PEDOT:PSS at 25 and 75 °C. It was observed that going from 25 to 75 °C almost all samples increased conductivity by two orders of magnitude, the sample that had the best improvement was pure DNA: $2.5*10^{-5}$ (25°C) and $1.6*10^{-3}$ (75 °C). It was therefore deduced that PEDOT:PSS did not play a leading role in the increase in conductivity. The I-V curves were studied in order to obtain the performance useful to characterize the DSSC In Table 41 it can see how conductivity decreases drastically when using DNA as HTM, and how the situation does not improve when PEDOT:PSS was inserted (5% of PEDOT:PSS in DNA was studied as a reference). The authors hypothesized that the low performance was due to a reduction in light absorption by the DSSC or a change in sample topography after DNA addition. EIS measurements also showed very high resistance compared to an iodine-based cell.

Table 41 *PV performance and EIS results of DNA and DNA-PEDOT:PSS HTMs. Adapted and reprinted with permission from [157].*

HTM	V_{oc} [V]	J_{sc} [mAcm^{-2}]	FF %	η %	R_S [Ω^2]	R_{SH}[Ω^2]
Reference	0.66	5.91	52.33	2.04	35.99	2996.00
DNA	0.49	0.46	30.72	0.07	611.57	617.53
DNA-PEDOT:PSS 5%	0.54	0.56	25.13	0.08	102.94	210.03

7.15 Zhang et al.: high-efficient PEDOT HTM (2016)

Zhang et al. introduced PEDOT as a PPA in an efficient DSSC [158]. The authors also investigated the effect of the particle diameter and surface area of the TiO_2 film when using PEDOT HTM in situ polymerisation. It was observed that the pore size played a major role in the photoelectrochemical polymerisation process (PEP). A smaller pore size favoured the contact with the polymer and dye on the surface of the TiO_2 particles with a greater regeneration efficiency of the dye. However, larger pore sizes allow a more favourable path for precursor diffusion during the PEP process, making it more efficient. Electronic scattering was advantageous in the case of large particle sizes. Using TiO_2 particles with a particle size of 25nm and an organic dye (3-{6-{4-[bis(2',4'-dibutyloxybiphenyl-4-yl)amino-]phenyl}-4,4-dihexyl-cyclopenta- [2,1-b:3,4-b']dithiophene-2-yl} -2-cyanoacrylic acid, LEG4) the efficiency of the DSSC obtained is: 5.2%, higher than commercial (4.5% using TiO_2 Dyesol DSL-30). It was also observed that the dye regeneration yield and photo-induced absorption kinetics were more efficient than those obtained from the Dyesol based cell.

7.16 Li et al.: PEDOT-derivate gel electrolyte (2018)

In this article, PEDOT was used as an electrolyte gel in the following conformations: PEDOT, PEDOT-graphene, PEDOT-graphene/PtCo, all embedded in a 3D poly (acrylic acid)/poly (ethylene glycol) (PAA/PEG) matrix [159]. PPA/PEG had a very high absorption capacity and, by inserting PEDOT and the other substances inside it, it was possible to form a 3D network and to have no losses. Cells composed of N719-TiO_2 electrode and Pt electrode were assembled. CV measurements showed that the catalytic properties were improved by switching from PEDOT to PEDOT-graphene and PEDOT-graphene/PtCo. Especially the reduction peak current intensity, reduction potential and peak separation showed that the conformation with PEDOT-graphene/PtCo is the best. Through EIS measurements the Rs and R_{ct} resistances were investigated. Using Rs it was observed that PEDOT-graphene/PtCo had lower Rs than the others (8.2 Ωcm^2). A low Rs suggests a good incorporation of PEDOT derivative increasing electron conduction in the interface with the CE. As for R_{ct}, it was higher than the others (12.7 Ωcm^2). The PV performance extrapolated from J-V graphs showed that PEDOT-graphene/PtCo possessed high abilities, reaching an efficiency of 8.2% and a very high J_{sc} of 15.82 $mAcm^{-2}$. The authors concluded that using a gel electrolyte the ion diffusion path was significantly reduced thanks to the channels provided by PAA/PEG. This resulted as an advantage by increasing J_{sc} and increasing the concentration of photogenerated electrons.

7.18 Review conclusion

In conclusion, the review work was carried out by investigating the development of DSSC technology using PEDOT as cathode and HTM. Both are more sustainable solutions than the configurations now used and established, and for this reason the research spends time to establish them also at an industrial level.

It is undeniable that DSSCs are the future for silicon-free and smart technologies such as headphones with integrated panels, portable devices or building integration. DSSCs with the advantage of being flexible and also transparent have the leading position in the future for these technologies, despite the evidently much lower efficiencies of a common silicon cell (about 8% efficiency compared to 18-21% for silicon one).

The PEDOT used as a CE has been further studied and from 2002 to the present day has been investigated in all its aspects: morphological, catalytic and photovoltaic. The best performances obtained were produced by Lee et al. in 2011 by testing PEDOT nanofibers: Voc: 0.72 [V], Jsc: 17.5 [$mAcm^{-2}$], FF: 0.72 and η: 9.2 [%] [49].

The PEDOT used instead as HTM has been studied in a less marked way but replacing the classic iodine electrolyte is still an open challenge on the scientific scene. The best performances obtained were produced by Liu et al. in 2012: Voc: 0.933 [V], Jsc: 10.1 [$mAcm^{-2}$], FF: 0.76 and η: 7.1 [%] [153].

8 Experimental experience

Last but not least, here is presented a short laboratory experience were 12 DSSCs devices are fabricated; 8 PEDOT based and 4 Pt based, to investigate the difference between the two different devices. Here is reported all the procedures and all the results obtained. The laboratory experience was carried out at DISAT laboratories of the Politecnico di Torino.

8.1 Preparation of photoanodes

The preparation of photoanodes involves first of all washing the glass used (glass coated on one side with FTO) with water, acetone and ethanol. Once the glass is washed, the area where the precursor paste of TiO_2 will be deposited can be traced. In this case, since we did not have a device to trace the geometries, we used an adhesive tape 55 µm thick. Once the adhesive tape was fixed to the conductive glass, a square area of 0.25 cm^2 was cut out. Subsequently, using the Doctor Blade technique, the precursor paste was applied to the carved sections of the adhesive tape Figure 45 up. In this way the thickness of the paste is 55 µm and its surface 0.25 cm2. Once stretched out the paste is left to dry for 10 min and then heated at 100 °C for 15 min.

Once the paste has been heated and dried (so free of water and more volatile solvents), the adhesive tape can be removed and the anodes are placed in a muffle for a treatment at 450 °C for 30 min Figure 45 down.

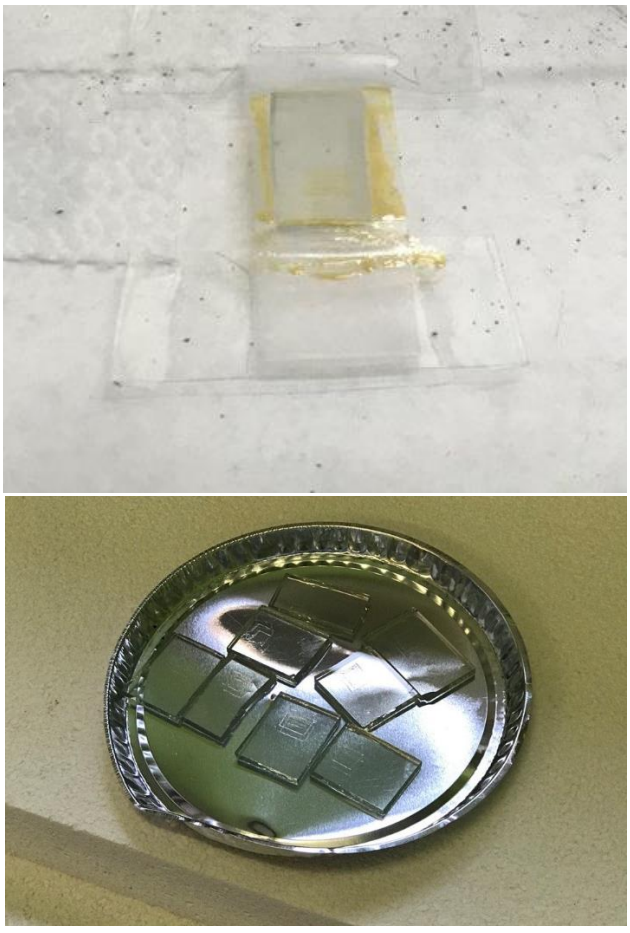

Figure 45 *Up: precursor paste applied with doctor blade technique, down: photoanodes after heat treatment.*

Afterwards the anodes have been treated to increase the available surface area and the absorption of photons.

The treatment that has been carried out is with titanium hexachloride ($TiCl_4$ 2M). A flask of 100 ml volume was used, and the desired solution was 40 mM. $TiCl_4$ was then diluted in ultra-pure water (milli-Q) until the desired concentration was obtained in the 100 ml volume. Specifically, 2 ml of $TiCl_4$ was used. Once the desired solution was obtained, the anodes were inserted by placing the TiO_2 surface downwards and were soaked completely. The anodes are then heated on a plate and the solution is still soaked in the solution. The heating consists of maintaining a temperature of 70 °C for 30 min (Figure 46). Make sure to cover the beaker with a slide in order to avoid solution loss and to have a uniform temperature for all 30 min (under an aspirated hood). After 30 min the anodes were first washed with demineralised water, with milli-Q water and then with ethanol. Subsequently, they were placed with the active phase (conductive glass and TiO_2) upwards and inserted into the muffle at 500 °C for 30 min. This treatment with $TiCl_4$ leads the anode to absorb the photons more efficiently and improves the surface area.

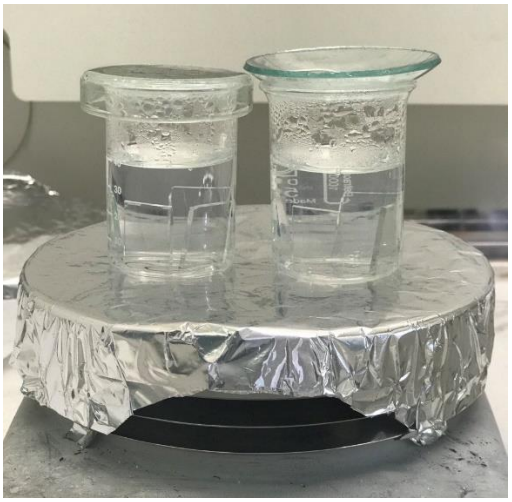

Figure 46 *Photoanodes in $TiCl_4$ solutions.*

Once treated, the anodes are dipped in the dye for 15 h to absorb the dye molecules (Figure 47). It can be seen, after fifteen hours, that the active area of the anode was no longer light yellow but has taken on the violet colour of the dye. The anodes were then washed with ethanol.

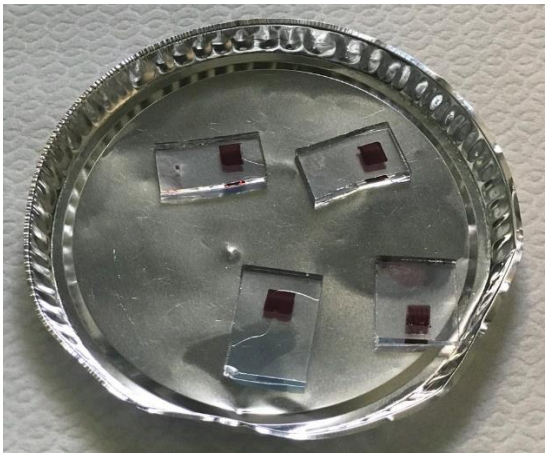

Figure 47 *Photoanodes after ethanol washing.*

8.2 Preparation of the Dye

The dye used is N719 in ethanol. N719 is a colourant based on Ruthenium(II), the main ingredient of the DSSC, which has so far achieved the highest efficiencies (Figure 48).

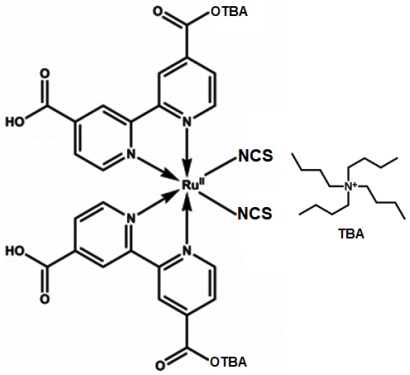

Figure 48 *N719 chemical structure [2].*

The molecular weight of the dye was 1188.55 g/mol. The solution used will be 0.3 mM in ethanol. The flask used had a volume of 10 ml. The following calculations were used to find the weight of the dye to be inserted into the respective volume of the flask:

$n = 0.3*10^{-3}$ [mol/l] * 10^{-3} [l]= $0.3*10^{-6}$ mol

m = 1188.55 [g/mol] * $0.3*10^{-6}$ [mol] = 0.0003566 g

After weighing the correct amount of N719 it was brought to volume with ethanol (Figure 49).

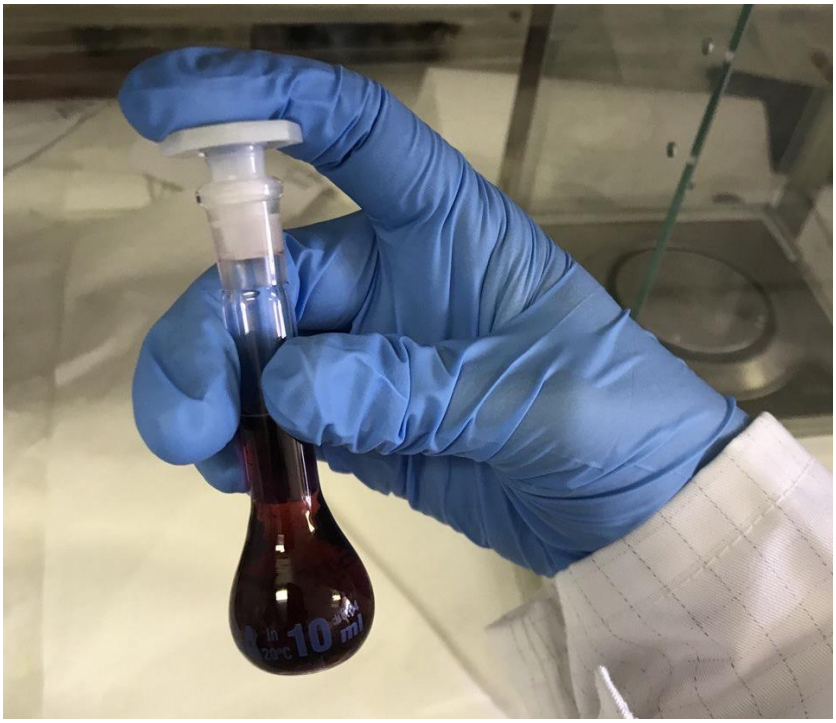

Figure 49 *Dye solution in 10 ml flask.*

8.3 Electrolyte preparation

The electrolyte used is an iodine-based electrolyte, i.e. it exploits the redox shuttle I^-/I_3^-. The solution was composed of iodine in solution with acetonitrile. It was decided to use a gel electrolyte, therefore quasi-solid one. The gelling agent used is polyethylene oxide (PEO, PM 400000 g/mol). PEO was used at 9 % by weight compared to the electrolytic solution. The weights used are as follows: 2.01 g of electrolyte and 0.1809 g of PEO. Once mixed and once the solution was homogenised, it rest overnight in a beaker containing a magnetic stirrer capable of applying the mixture for the entire resting time. The next day the electrolytic solution was well gelled (by turning the beaker upside down there was no overturning Figure 50).

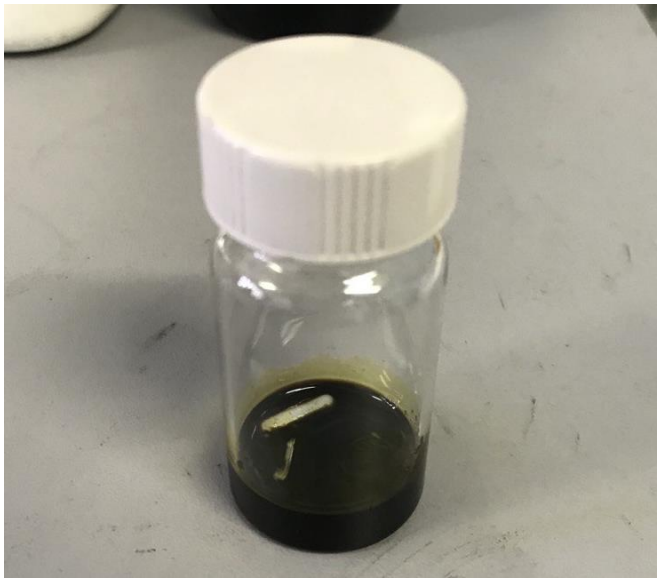

Figure 50 *Gelled electrolyte solution.*

8.4 Cathode preparation

The cathodes were: 8 composed of PEDOT deposited via spin-coating and 4 composed of Pt.

8.4.1 Cathodes in PEDOT

The PEDOT used was the commercial one. Through the spin-coater it was deposited on conductive glass by two different speeds:

- 40 rps: with this speed, the PEDOT deposits uniformly on the slide without taking several steps (4 samples).
- 20 rps: with this speed, however, it was difficult to get a spread on the whole slide of the PEDOT. In fact, half of the samples were deposited with the slide stopped (spin-coater off, 2 samples) and seeing that the dispersion of PEDOT was not optimal the other half was deposited with the spin-coater on (2 samples) at 20 rps thus obtaining a better and more uniform coating on the conductive glass.

Then the cathodes were treated at 70 °C for 30 min in the oven (Figure 51).

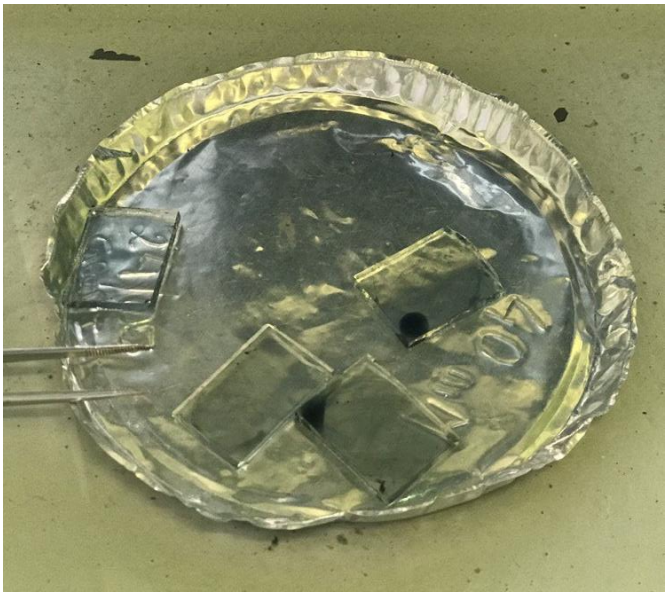

Figure 51 *PEDOT cathodes after heat treatment.*

8.4.2 Cathodes in Pt

A precursor solution of hexachloroplatinic acid (H_2PtCl_6 5 mM) was used to deposit the platinum on conductive glass. The amount deposited on the conductive glass was 20 µl using a micropipette. After depositing the correct amount on each slide, a heat treatment in a muffle at 450 °C was carried out. Subsequently the process was repeated: both the deposition and the heat treatment (Figure 52).

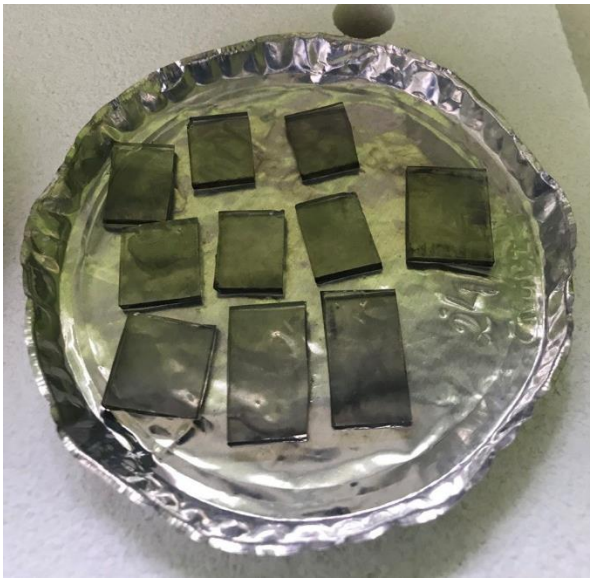

Figure 52 *Pt cathodes after two deposition and two heat treatment.*

8.5 Cell closure

The cells were closed using a heated press (heated only at the top to manipulate the electrodes by placing them on the surface below more easily) at 105 °C. Before closing, 2.1 mg of electrolyte was deposited in the active area of the anodes. Almost all anode manipulation processes have been made dry-room to avoid undesirable effects brought about by air humidity.

In order to guarantee a good seal, Surlyn thermoplastic material, shaped as a "square frame" with internal area 6*6 mm and thickness 2 mm, was used.

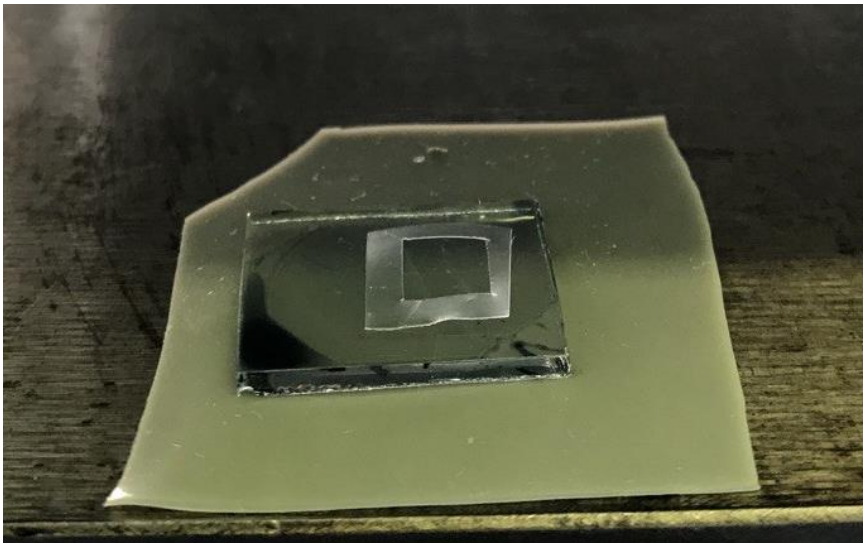

Figure 53 *PEDOT cathode on silicon support and thermoplastic material used for closing the cells.*

The thermoplastic material was inserted on the cathode (the cathode depicted in Figure 53 is PEDOT, recognisable by its blue colour) with the conductive face facing upwards. Then the anode with the electrolyte was placed gently on top so that the square TiO_2 area matches the inner area of the thermoplastic (Figure 54). Once the two electrodes were put in contact, a pressure of 1 bar for about 15-20 s was applied.

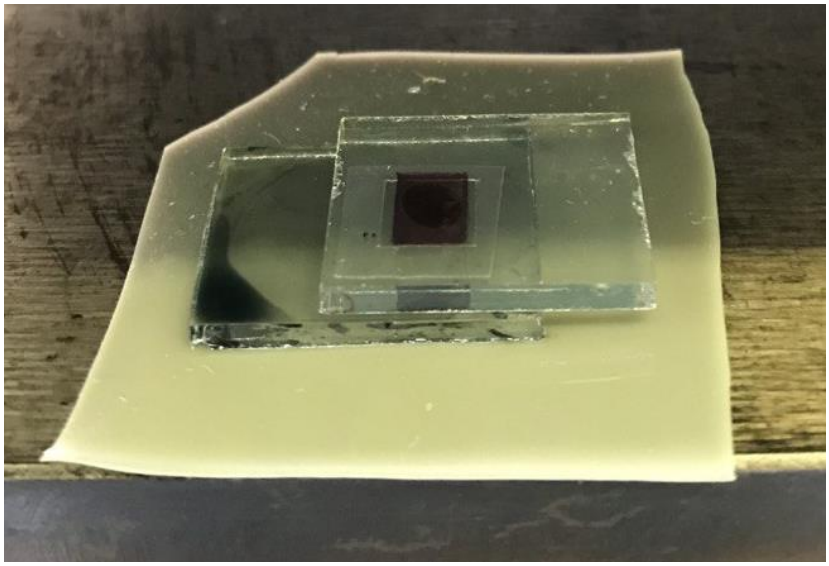

Figure 54 *Cell before the closure.*

Once the press was opened, it was visually checked that the thermoplastic was well melted, and the cell had a good seal. For safety, clamps were applied on both sides.

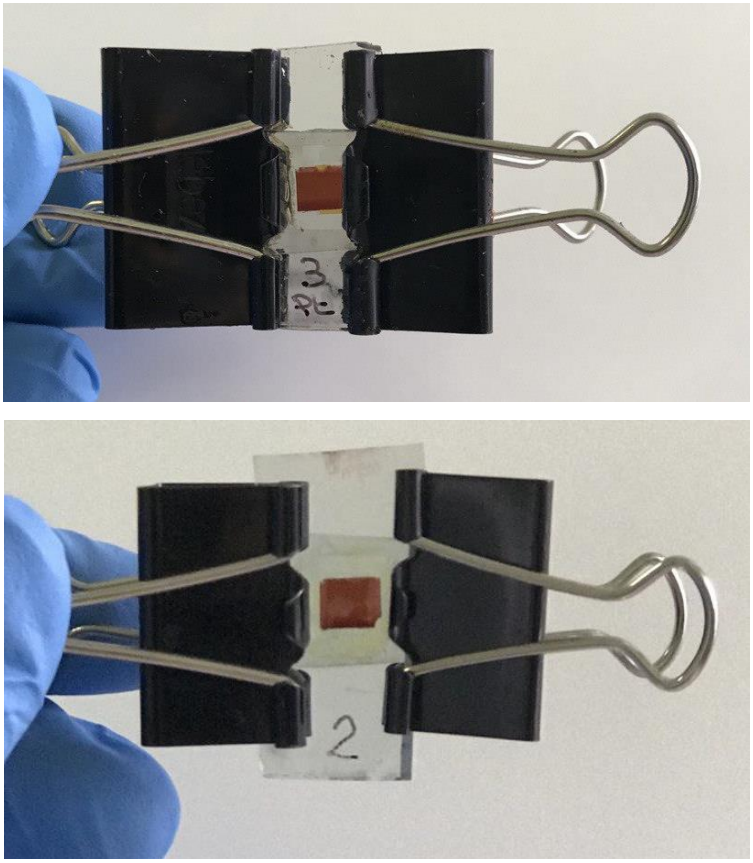

Figure 55 *Up: Pt DSSC based after closure, down: PEDOT DSSC based after closure.*

8.6 Photovoltaic measurements and results

The photovoltaic measurements were carried out using a 6 led solar simulator working at 1 sun and calibrated at 63.50 mW (Figure 58). After connecting the electrodes via terminals to the external circuit, many tests are carried out until the photovoltaic performance stabilizes.

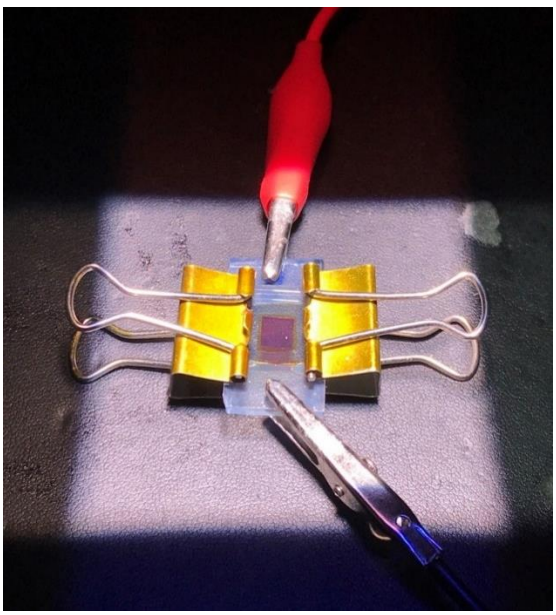

Figure 56 *Dye solution in 10 ml flask.*

The cells using PEDOT have achieved significantly lower photovoltaic performance than those using platinum. Above all, the first 4 cells (PEDOT at 40 rps) achieved efficiency values less than 1 %, while the last 4 cells achieved efficiency values up to 1.45 %. Since the thickness of the PEDOT film is inversely proportional to the speed at which the machine is applied (the thickness of PEDOT applied at 40 rps will be less than the thickness of PEDOT applied at 20 rps), the cells with the thinnest film have shown lower efficiency than those with the thickest film. The thickness of the cathode therefore greatly affects performance.

Table 42 and Table 43 show the average photovoltaic performance values with the corresponding errors. Figure 59 and Figure 60 are I-V curves, one of PEDOT aged 2 days and one of Pt aged 0 day.

Table 42 *Average PV performance of the 8 cells at PEDOT with their respective errors.*

Day	V_{OC} [V]	J_{SC} [mAcm^{-2}]	FF [%]	η [%]
0	0,530 ± 0,06	6,93 ± 0,06	32,67 ± 0,25	1,2 ± 0,26
1	0,519 ± 0,09	5,77 ± 0,53	32,86 ± 0,44	1,0 ± 0,81
2	0,523 ± 0,12	5,61 ± 0,63	34,61 ± 0,43	1,0 ± 0,85
5	0,515 ± 0,09	3,50 ± 0,10	35,66 ± 0,40	0,6 ± 0,72
7	0,530 ± 0,08	3,68 ± 0,10	36,42 ± 0,35	0,6 ± 0,71
8	0,535 ± 0,08	3,39 ± 0,12	41,83 ± 0,42	0,7 ± 0,71
9	0,541 ± 0,06	3,16 ± 0,13	46,15 ± 0,52	0,7 ± 0,72

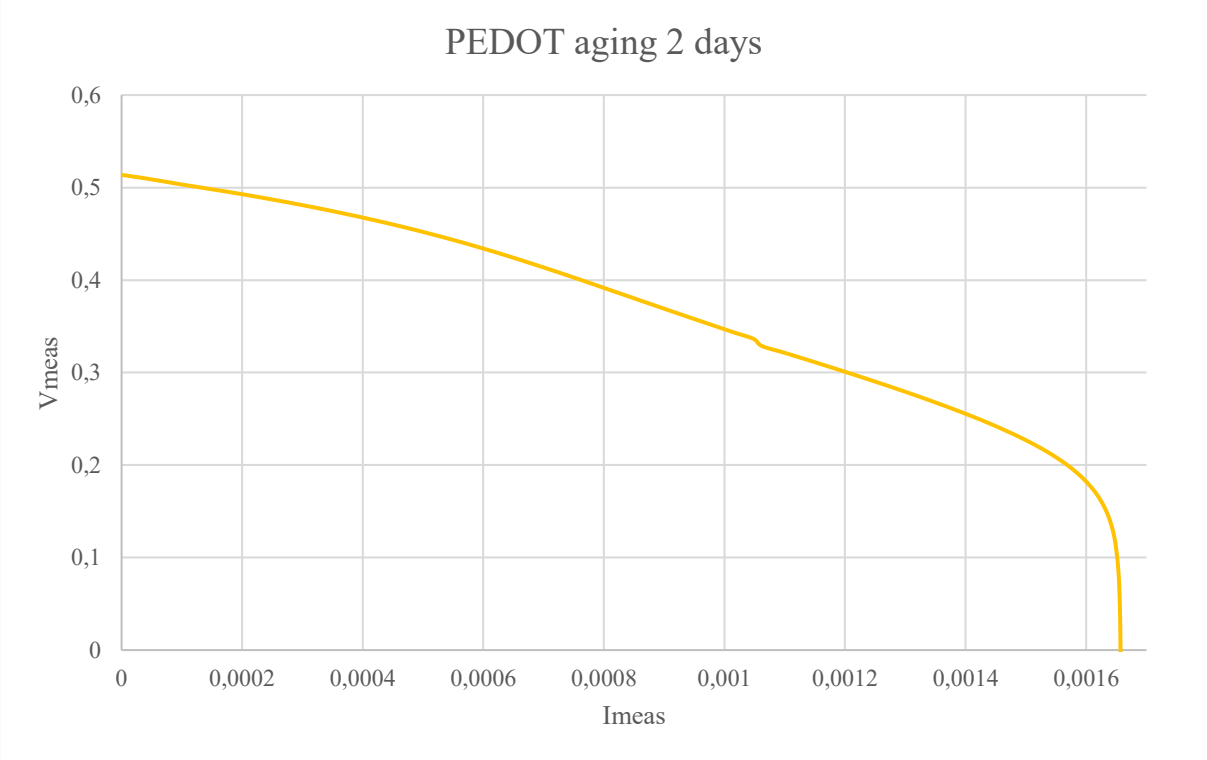

Figure 57 *I-V curve for PEDOT aged 2 days.*

Table 43 *Average PV performance of the 4 cells at Pt with their respective errors.*

Day	V_{OC} [V]	J_{SC} [mAcm^{-2}]	FF [%]	η [%]
0	0,529 ± 0,03	6,86 ± 0,34	66,34 ± 0,04	2,4 ± 0,32
1	0,521 ± 0,05	6,66 ± 0,33	66,21 ± 0,04	2,3 ± 0,41
4	0,526 ± 0,07	6,09 ± 0,26	67,21 ± 0,05	2,2 ± 0,32
5	0,527 ± 0,06	6,00 ± 0,22	67,47 ± 0,04	2,1 ± 0,27
6	0,528 ± 0,07	5,88 ± 0,20	68,38 ± 0,06	2,1 ± 0,28
8	0,528 ± 0,08	5,49 ± 0,20	68,31 ± 0,05	2,0 ± 0,22

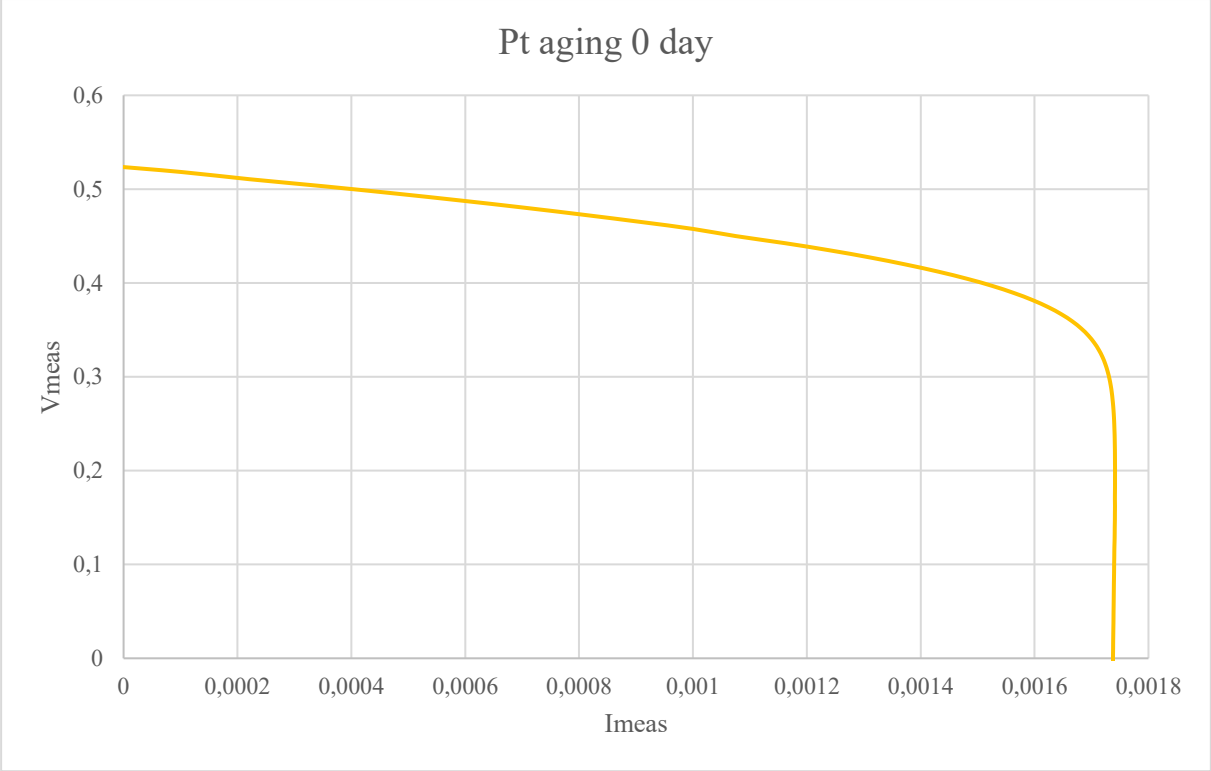

Figure 58 *I-V curve for platinum aged 0 day.*

The photovoltaic properties of all the samples analysed have been collected in graphs (PEDOT from Figure 59 to Figure 62 and Pt form Figure 63 to Figure 66) and studied over time.

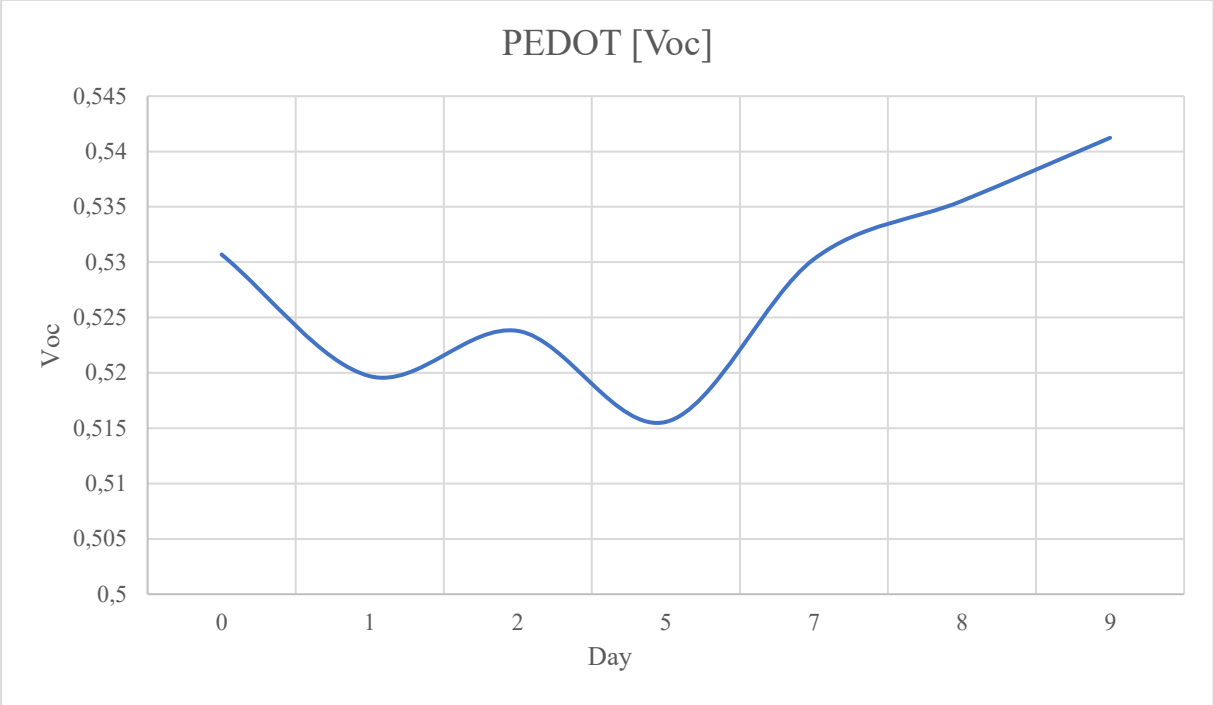

Figure 59 *Voc trend over time for PEDOT.*

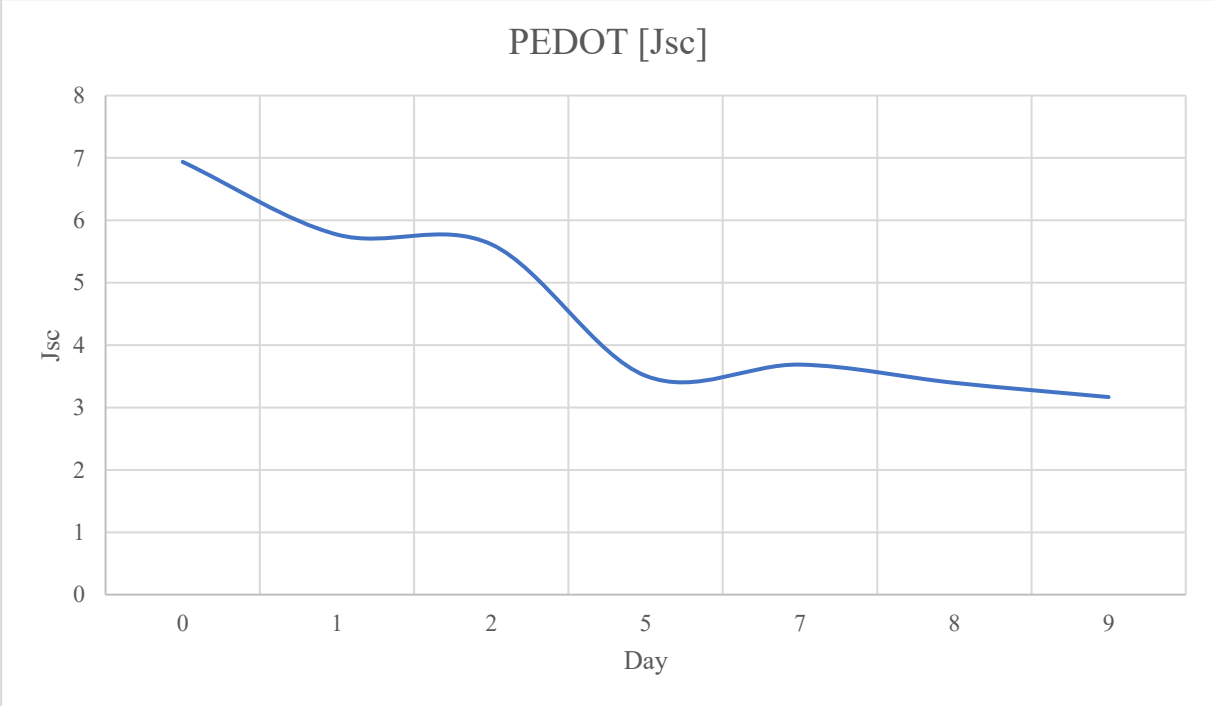

Figure 60 *Jsc trend over time for PEDOT.*

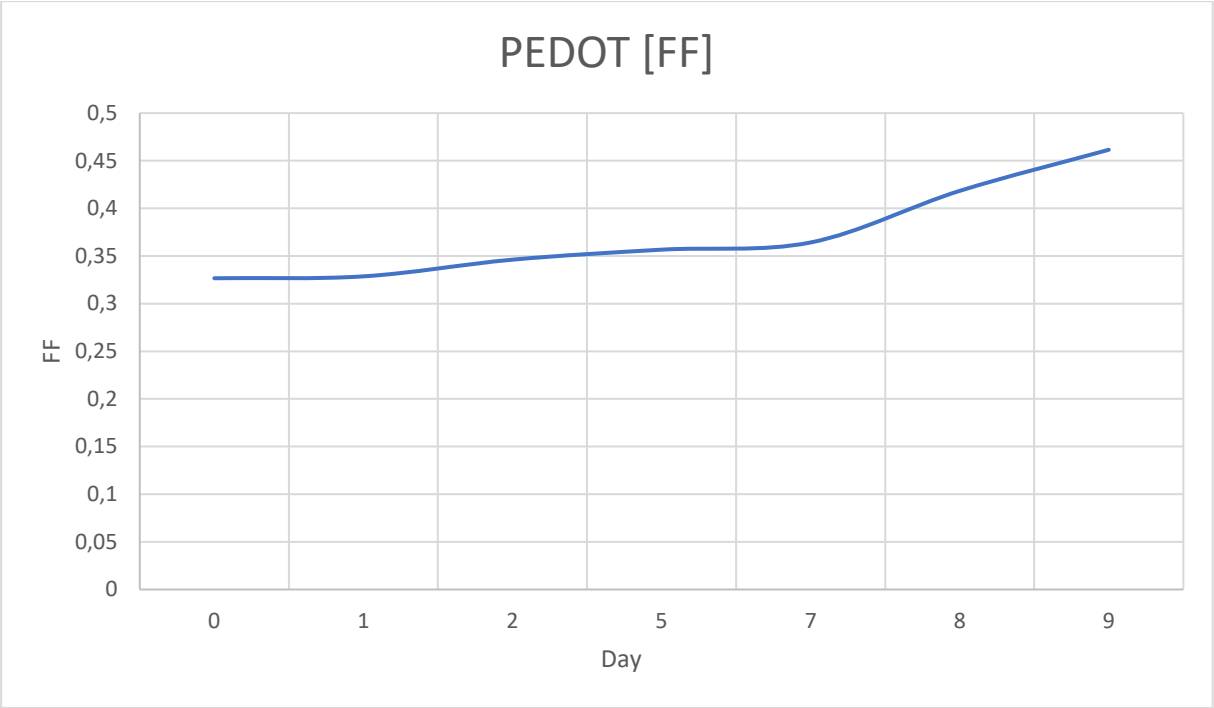

Figure 61 *FF trend over time for PEDOT.*

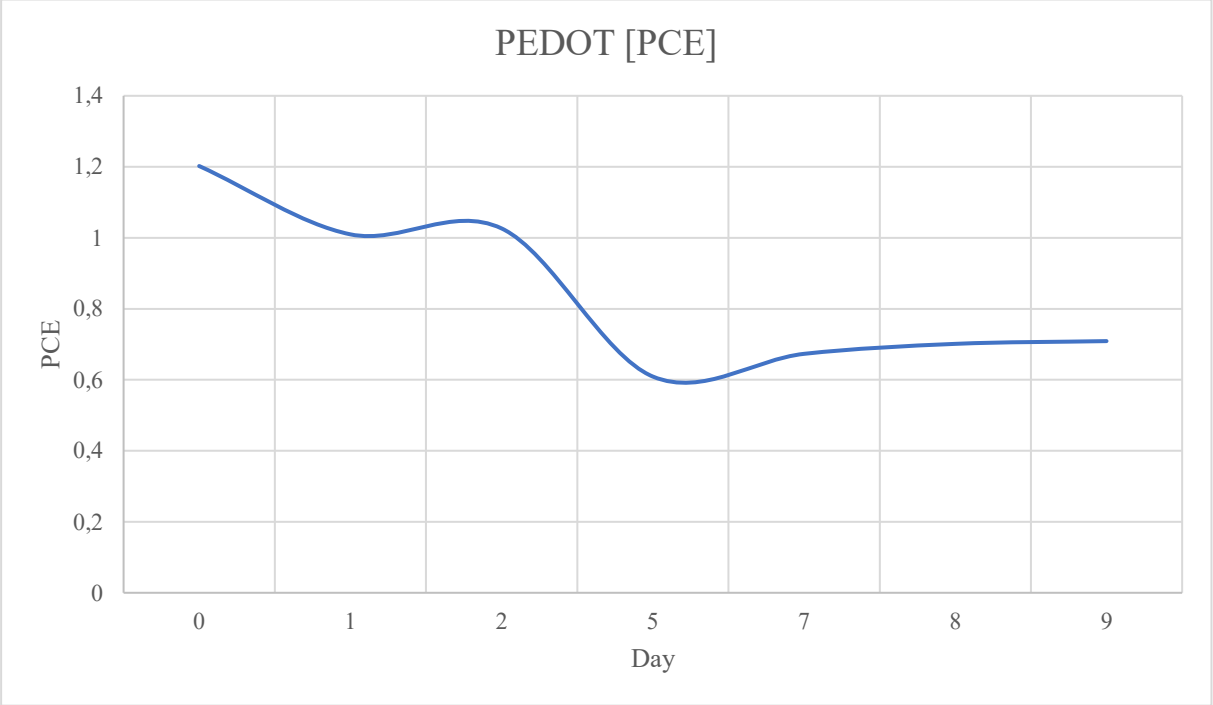

Figure 62 *PCE trend over time for PEDOT.*

As aging proceed, PEDOT has good stability. The Voc grows after an initial oscillation; the FF remains almost stable with a slight increase; Jsc shows a decreasing trend as well as efficiency. Cells composed with PEDOT as cathode have been tested countless times under solar simulator as it was difficult to stabilize them.

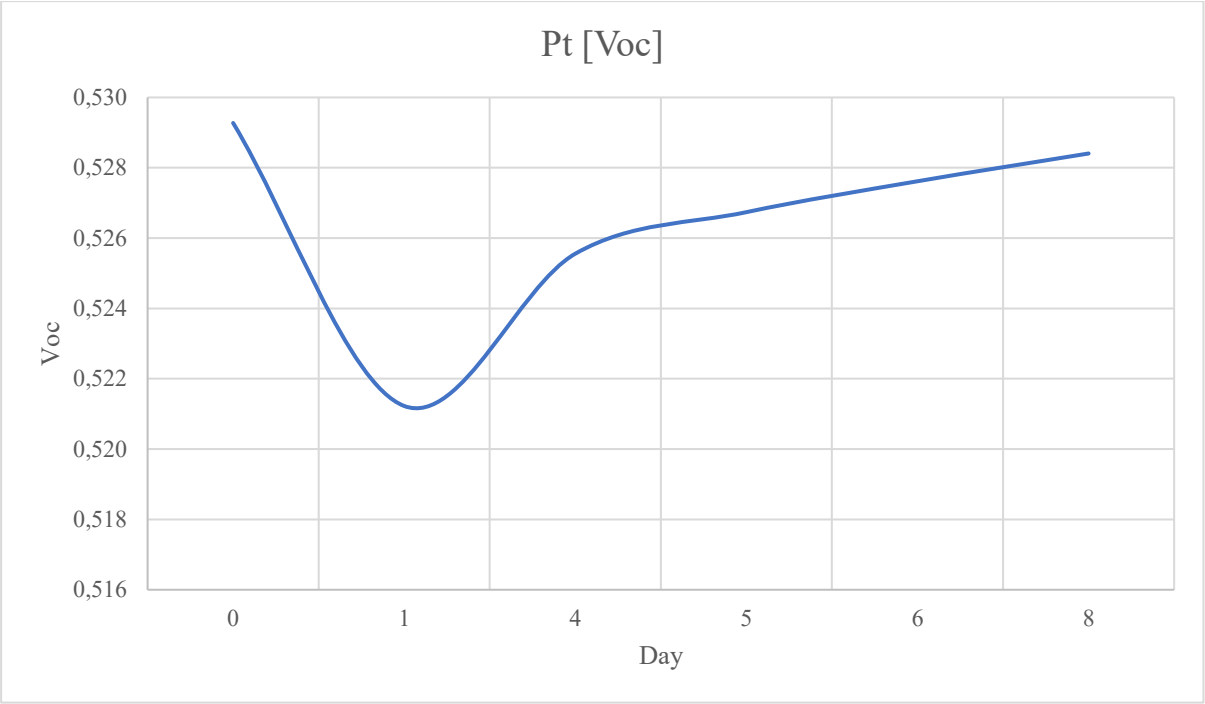

Figure 63 *Voc trend over time for Pt.*

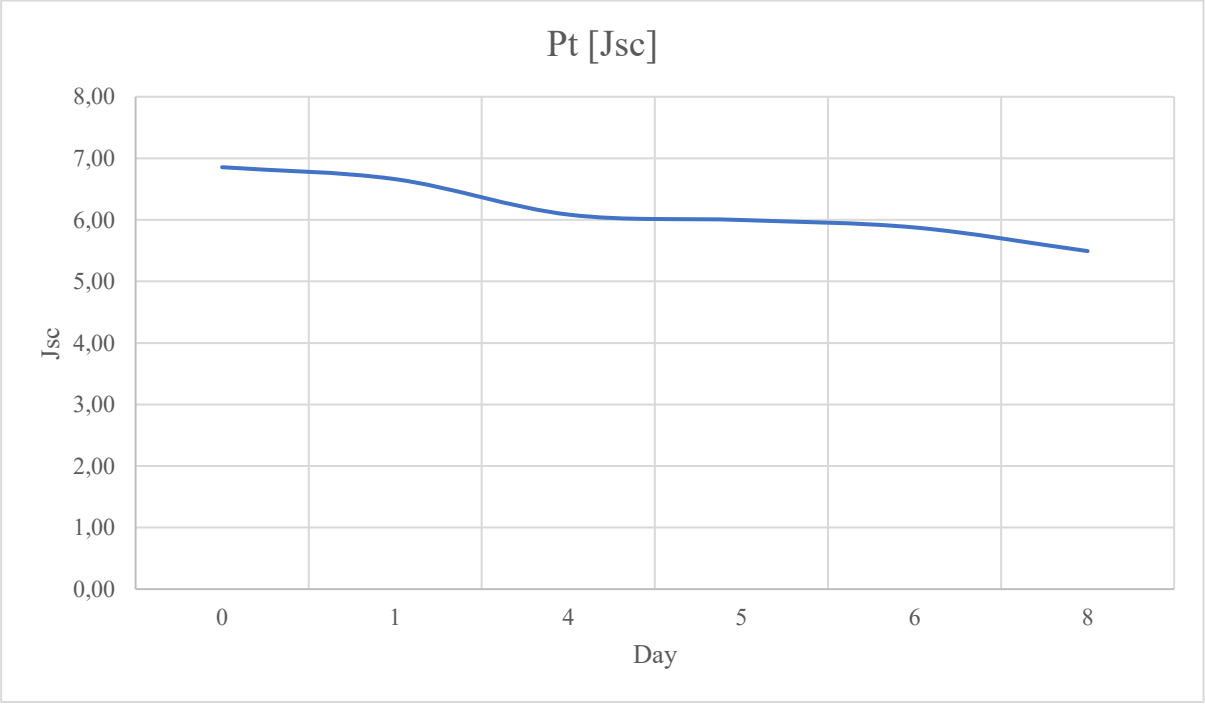

Figure 64 *Jsc trend over time for Pt.*

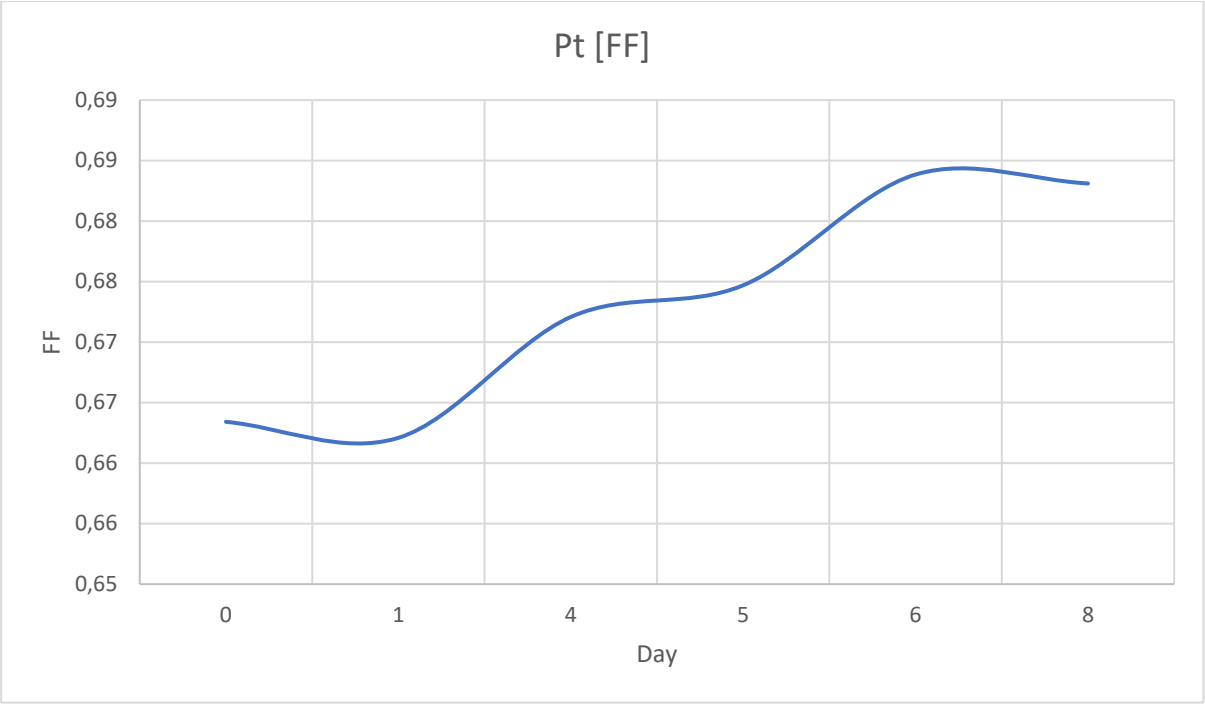

Figure 65 *FF trend over time for Pt.*

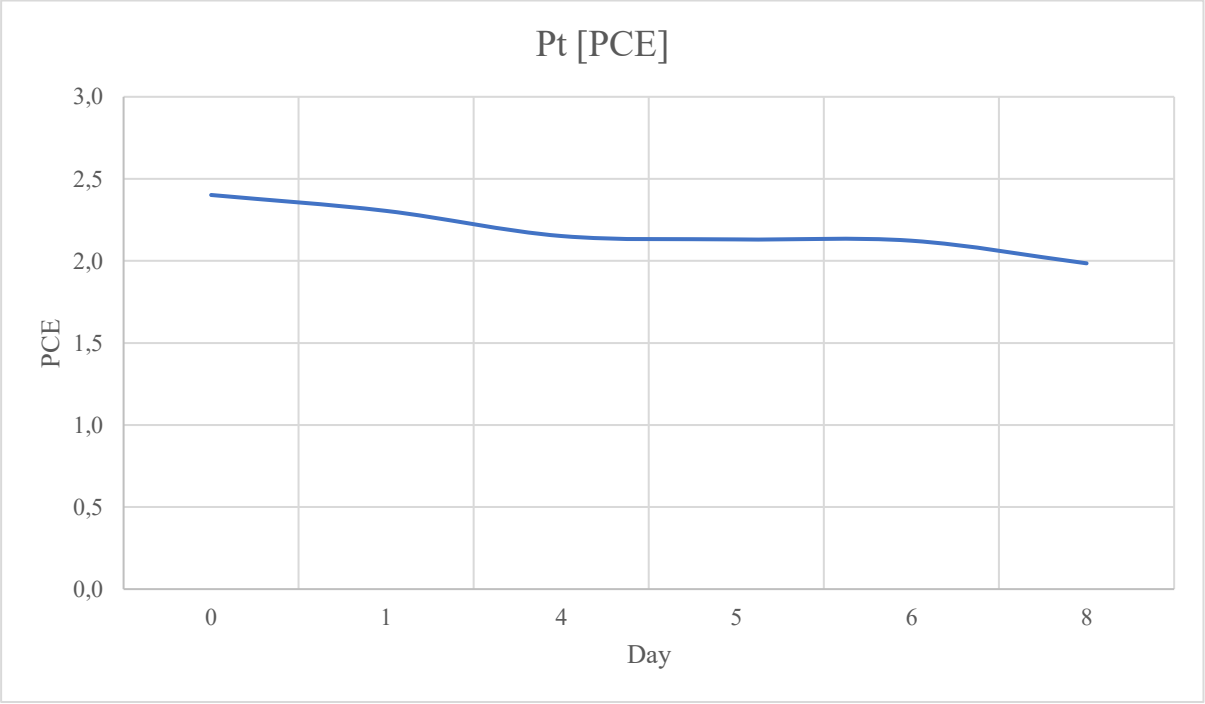

Figure 66 *PCE trend over time for Pt.*

Platinum, on the other hand, shows slightly different trends: Voc after an initial degrowth increases substantially; Jsc, on the other hand, decreases gradually; FF increases steadily over

time, suggesting a consistent internal cell stabilisation and remodification; efficiency remains almost constant.

In general, platinum has more stability over time than PEDOT, but despite this, the serious and costly problems brought about by its use do not preclude PEDOT from being a valid and sustainable alternative.

To get an overview, the following 2 graphs summarize the previous ones (both for PEDOT Figure 67 and for platinum Figure 68)

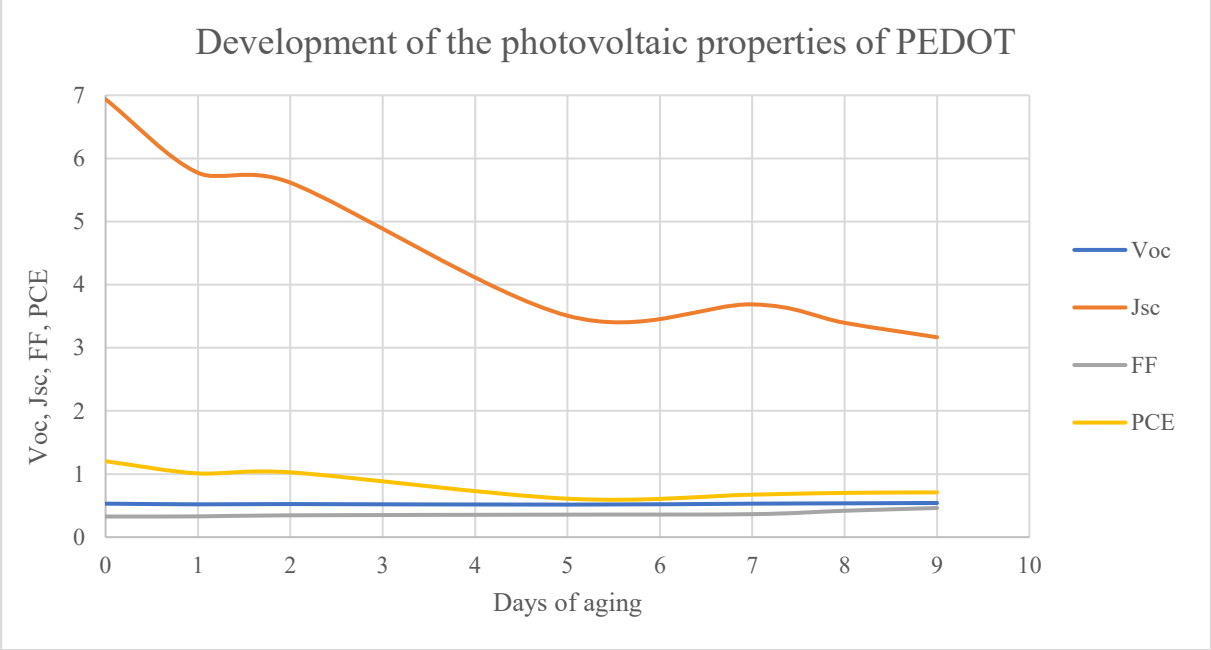

Figure 67 *Development of the PV properties of the cells using PEDOT tested in laboratory.*

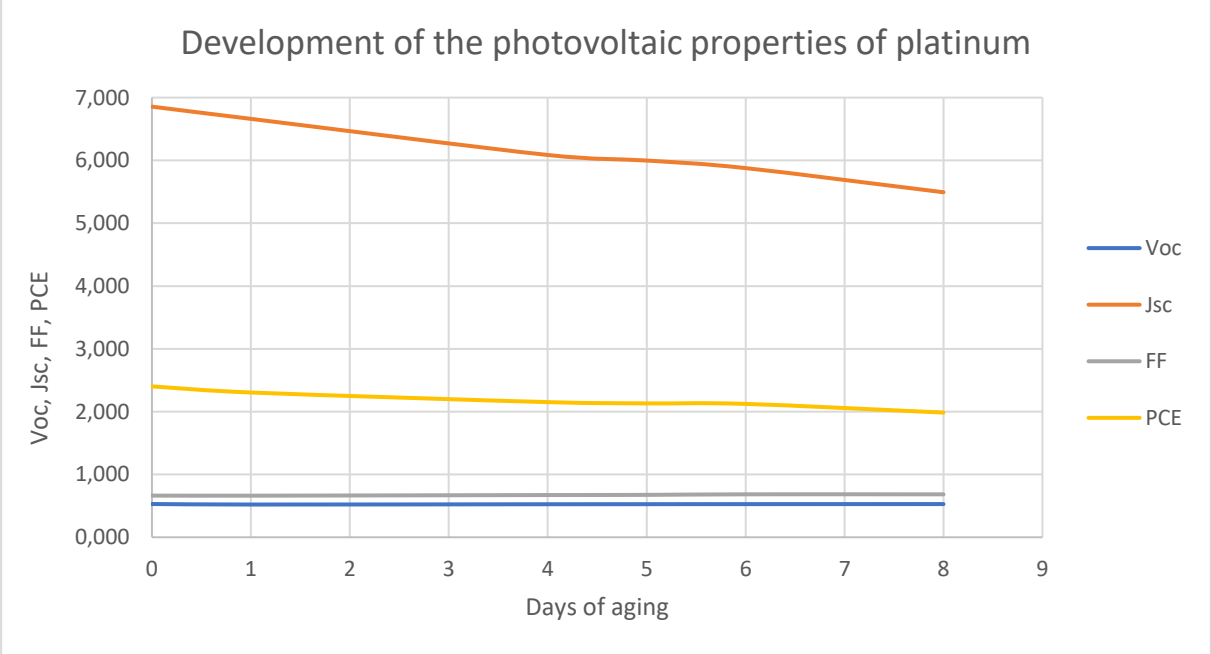

Figure 68 *Development of the PV properties of the cells using Pt tested in laboratory.*

Another phenomenon observed in the cells using PEDOT is a variation in the shape of the I-V curve produced by simulations. In principle, in fact, it can be noted that the "young" cells have a depression in the curve. As the cells age, this depression disappears. This phenomenon has been attributed to the polymer nature of the PEDOT. In fact, the PEDOT interacts more and more intimately with the electrolyte, gradually transforming the interface between the two. Platinum, on the other hand, does not show these variations, the relationship between the metal and the electrolyte remains unchanged as the cell ages. This phenomenon can be seen in Figure 69.

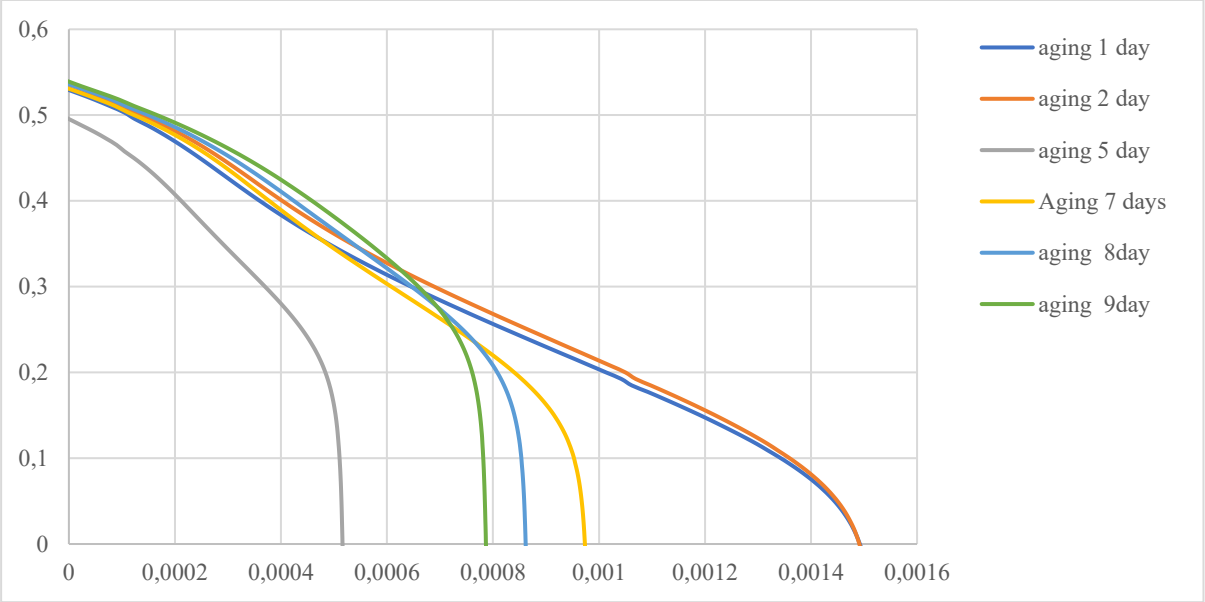

Figure 69 *Evolution of the J-V curves of the cell using the PEDOT.*

In conclusion, PEDOT is a good candidate for the replacement of platinum inside dye-sensitized solar cells. Scientific research has carried out countless tests and trials ranging in all DSSC properties, confirming that PEDOT is versatile and close to large-scale application.

The laboratory experience has led to relatively low efficiencies but, considering that PEDOT had not been treated in any way and that the only treatment carried out was with titan perchlorate on the anodes, the efficiencies are still close to a simple cell using platinum.

[1] bp p.l.c.
Statistical Review of World Energy
(2020) Bp, pp. 1-68.
Link:https://www.bp.com/content/dam/bp/businesssites/en/global/corporate/pdfs/energy-economics/statistical-review/bp-stats-review-2020-full-report.pdf

[2] Reddy, K.G., Deepak, T.G., Anjusree, G.S., Thomas, S., Vadukumpully, S., Subramanian, K.R.V., Nair, S.V., Nair, A.S.
56105373400;55931776800;55794938500;57198912698;33068522700;7202238038;24504029200;54080068900;
On global energy scenario, dye-sensitized solar cells and the promise of nanotechnology
(2014) Physical Chemistry Chemical Physics, 16 (15), pp. 6838-6858. Cited 62 times.
DOI: 10.1039/c3cp55448a

[3] A. E. Becquerel
CR Acad. Sci. Paris
(1839), 9, 14.

[4] Coiante D.,
Fotovoltaico di prima generazione: il punto.
(2013)

[5] Liu, M., Johnston, M.B., Snaith, H.J.
55847412000;7402060419;8833978100;
Efficient planar heterojunction perovskite solar cells by vapour deposition
(2013) Nature, 501 (7467), pp. 395-398. Cited 5276 times.
https://www.scopus.com/inward/record.uri?eid=2-s2.0-
DOI: 10.1038/nature12509

[6] Kalogirou, S.
7005998383;
McEvoy's handbook of photovoltaics: Fundamentals and applications
(2017) McEvoy's Handbook of Photovoltaics: Fundamentals and Applications, pp. 1-1340. Cited 5 times.

[7] Green, M.A., Emery, K., Hishikawa, Y., Warta, W., Dunlop, E.D.
57202528457;7006858697;7103374907;7003828708;7005213734;
Solar cell efficiency tables (Version 45)
(2015) Progress in Photovoltaics: Research and Applications, 23 (1), pp. 1-9. Cited 1312 times.
DOI: 10.1002/pip.2573

[8] Acevedo-Luna, A., Bernal-Correa, R., Montes-Monsalve, J., Morales-Acevedo, A.
57199081591;36004678200;56118605700;7003342955;
Design of thin film solar cells based on a unified simple analytical model
(2017) Journal of Applied Research and Technology, 15 (6), pp. 599-608. Cited 8 times.
DOI: 10.1016/j.jart.2017.08.002

[9] Snaith, H.J.
8833978100;
Perovskites: The emergence of a new era for low-cost, high-efficiency solar cells

(2013) Journal of Physical Chemistry Letters, 4 (21), pp. 3623-3630. Cited 1797 times.
DOI: 10.1021/jz4020162

[10] O'Regan, B., Grätzel, M.
6701529045;35463345800;
A low-cost, high-efficiency solar cell based on dye-sensitized colloidal TiO2 films
(1991) Nature, 353 (6346), pp. 737-740. Cited 23330 times.
DOI: 10.1038/353737a0

[11] Sarker, S., Seo, H.W., Jin, Y.-K., Aziz, M.A., Kim, D.M.
35318826700;55884538200;56567061200;56799888000;35332612900;
Transparent conducting oxides and their performance as substrates for counter electrodes of dye-sensitized solar cells
(2019) Materials Science in Semiconductor Processing, 93, pp. 28-35. Cited 2 times.
DOI: 10.1016/j.mssp.2018.12.023

[12] Narayan, M.R.
50262555600;
Review: Dye sensitized solar cells based on natural photosensitizers
(2012) Renewable and Sustainable Energy Reviews, 16 (1), pp. 208-215. Cited 424 times.
DOI: 10.1016/j.rser.2011.07.148

[13] Ito, S., Murakami, T.N., Comte, P., Liska, P., Grätzel, C., Nazeeruddin, M.K., Grätzel, M.
7404825324;7404261669;7005472021;6602231984;6506481016;35463772200;35463345800;
Fabrication of thin film dye sensitized solar cells with solar to electric power conversion efficiency over 10%
(2008) Thin Solid Films, 516 (14), pp. 4613-4619. Cited 1568 times.
DOI: 10.1016/j.tsf.2007.05.090

[14] Mishra, A., Fischer, M.K.R., Büuerle, P.
55626647800;9334219900;35092104200;
Metal-Free organic dyes for dye-Sensitized solar cells: From structure: Property relationships to design rules
(2009) Angewandte Chemie - International Edition, 48 (14), pp. 2474-2499.
DOI: 10.1002/anie.200804709

[15] Lee, C.-P., Li, C.-T., Ho, K.-C.
55050004100;55507636700;56962715200;
Use of organic materials in dye-sensitized solar cells
(2017) Materials Today, 20 (5), pp. 267-283.
DOI: 10.1016/j.mattod.2017.01.012

[16] Bach, U., Lupo, D., Comte, P., Moser, J.E., Weissörtel, F., Salbeck, J., Spreitzer, H., Grätzel, M.
6604078359;6603722652;7005472021;57202982576;6602531907;56127482800;7003809142;35463345800;
Solid-state dye-sensitized mesoporous TiO2 solar cells with high photon-to-electron conversion efficiencies
(1998) Nature, 395 (6702), pp. 583-585.
DOI: 10.1038/26936

[17] Wu, M., Lin, X., Wang, Y., Wang, L., Guo, W., Qi, D., Peng, X., Hagfeldt, A., Grätzel, M., Ma, T.
55552889400;56441893400;53165103400;57075021800;34769947400;55273366900;35275681500;7005851690;35463345800;7402783978;
Economical Pt-free catalysts for counter electrodes of dye-sensitized solar cells
(2012) Journal of the American Chemical Society, 134 (7), pp. 3419-3428.
DOI: 10.1021/ja209657v

[18] Ramasamy, E., Lee, W.J., Lee, D.Y., Song, J.S.
56814705400;57198750607;15840205100;7404787440;
Spray coated multi-wall carbon nanotube counter electrode for tri-iodide (I3-) reduction in dye-sensitized solar cells
(2008) Electrochemistry Communications, 10 (7), pp. 1087-1089.
DOI: 10.1016/j.elecom.2008.05.013

[19] Hug, H., Bader, M., Mair, P., Glatzel, T.
55941375100;55941185000;57213254610;6603050413;
Biophotovoltaics: Natural pigments in dye-sensitized solar cells
(2014) Applied Energy, 115, pp. 216-225.
DOI: 10.1016/j.apenergy.2013.10.055

[20] Saito, Y., Kitamura, T., Wada, Y., Yanagida, S.
Application of poly(3,4-ethylenedioxythiophene) to counter electrode in dye-sensitized solar cells
(2002) Chemistry Letters, (10), pp. 1060-1061.
DOI: 10.1246/cl.2002.1060

[21] Saito, Y., Kubo, W., Kitamura, T., Wada, Y., Yanagida, S.
7406267398;8094036600;7401578444;35419623900;35420673400;
I-/I3- redox reaction behavior on poly (3,4-ethylenedioxythiophene) counter electrode in dye-sensitized solar cells
(2004) Journal of Photochemistry and Photobiology A: Chemistry, 164 (1-3), pp. 153-157.
DOI: 10.1016/j.jphotochem.2003.11.017

[22] Park, S.-H., Kim, J.-U., Lee, J.-K., Kim, M.-R.
35196738900;22134947700;16052553900;25722572300;
Photovoltaic properties of dye-sensitized solar cells with thermal treated PEDOT:PSS as counter electrodes
(2007) Molecular Crystals and Liquid Crystals, 471 (1), pp. 113-121.
DOI: 10.1080/15421400701545437

[23] Biancardo, M., West, K., Krebs, F.C.
56634744400;7401596747;7006192717;
Quasi-solid-state dye-sensitized solar cells: Pt and PEDOT:PSS counter electrodes applied to gel electrolyte assemblies
(2007) Journal of Photochemistry and Photobiology A: Chemistry, 187 (2-3), pp. 395-401.
DOI: 10.1016/j.jphotochem.2006.11.008

[24] Xia, J., Masaki, N., Jiang, K., Yanagida, S.
7402327380;10739561400;7103330942;35420673400;
The influence of doping ions on poly(3,4-ethylenedioxythiophene) as a counter electrode of a dye-sensitized solar cell
(2007) Journal of Materials Chemistry, 17 (27), pp. 2845-2850.
DOI: 10.1039/b703062b

[25] Hong, W., Xu, Y., Lu, G., Li, C., Shi, G.
54684041600;24170485800;8375614100;56132055300;7402432841;
Transparent graphene/PEDOT-PSS composite films as counter electrodes of dye-sensitized solar cells
(2008) Electrochemistry Communications, 10 (10), pp. 1555-1558.
DOI: 10.1016/j.elecom.2008.08.007

[26] Pringle, J.M., Armel, V., Forsyth, M., MacFarlane, D.R.
7103088434;26655183500;7103154228;7202978608;
PEDOT-coated counter electrodes for dye-sensitized solar cells
(2009) Australian Journal of Chemistry, 62 (4), pp. 348-352.
DOI: 10.1071/CH09006

[27] Balraju, P., Kumar, M., Roy, M.S., Sharma, G.D.
24066297400;7403638034;25938802800;7202756196;
Dye sensitized solar cells (DSSCs) based on modified iron phthalocyanine nanostructured TiO2 electrode and PEDOT:PSS counter electrode
(2009) Synthetic Metals, 159 (13), pp. 1325-1331.
DOI: 10.1016/j.synthmet.2009.03.001

[28] Jiang, H., Sakurai, S., Kobayashi, K.
27171815800;26656026000;55727105900;
Fabrication and enhanced performance of a dye-sensitized solar cell with a ClO4--poly(3,4-ethylenedioxythiophene)/ TiO 2/FTO counter electrode
(2009) Electrochemical and Solid-State Letters, 12 (7), pp. F13-F16.
DOI: 10.1149/1.3122239

[29] Sakurai, S., Jiang, H.-q., Takahashi, M., Kobayashi, K.
26656026000;27171815800;55701031400;55727105900;
Enhanced performance of a dye-sensitized solar cell with a modified poly(3,4-ethylenedioxythiophene)/TiO2/FTO counter electrode
(2009) Electrochimica Acta, 54 (23), pp. 5463-5469.
DOI: 10.1016/j.electacta.2009.04.045

[30] Lee, K.-M., Chiu, W.-H., Wei, H.-Y., Hu, C.-W., Suryanarayanan, V., Hsieh, W.-F., Ho, K.-C.
7501498671;7201503537;57208769801;8392615600;6601983766;55647515700;56962715200;
Effects of mesoscopic poly(3,4-ethylenedioxythiophene) films as counter electrodes for dye-sensitized solar cells
(2010) Thin Solid Films, 518 (6), pp. 1716-1721.
DOI: 10.1016/j.tsf.2009.11.058

[31] Pringle, J.M., Armel, V., MacFarlane, D.R.
7103088434;26655183500;7202978608;
Electrodeposited PEDOT-on-plastic cathodes for dye-sensitized solar cells
(2010) Chemical Communications, 46 (29), pp. 5367-5369.
DOI: 10.1039/c0cc01400a

[32] Mozer, A.J., Panda, D.K., Gambhir, S., Romeo, T.C., Winther-Jensen, B., Wallace, G.G.
8557588100;35491232300;27867754400;36464117700;8718005700;7202483095;
Flexible and compressible goretex-PEDOT membrane electrodes for solid-state dye-sensitized solar cells
(2010) Langmuir, 26 (3), pp. 1452-1455.
DOI: 10.1021/la903507m

[33] Ahmad, S., Yum, J.-H., Xianxi, Z., Grätzel, M., Butt, H.-J., Nazeeruddin, M.K.
57213511606;7004044501;35108508000;35463345800;56036156800;35463772200;
Dye-sensitized solar cells based on poly (3,4-ethylenedioxythiophene) counter electrode derived from ionic liquids
(2010) Journal of Materials Chemistry, 20 (9), pp. 1654-1658.
DOI: 10.1039/b920210b

[34] Sakurai, S., Kawamata, Y., Takahashi, M., Kobayashi, K.
26656026000;54779917600;55701031400;55727105900;
Improved photocurrent of a poly (3,4-ethylenedioxythiophene)-ClO4-/TiO2 thin film-modified counter electrode for dye-sensitized solar cells
(2011) Journal of Oleo Science, 60 (12), pp. 639-646.
DOI: 10.5650/jos.60.639

[35] Zhang, J., Li, X., Guo, W., Hreid, T., Hou, J., Su, H., Yuan, Z.
56808279700;35771117000;34769947400;35490578800;36829511000;7401459139;7401477066;
Electropolymerization of a poly(3,4-ethylenedioxythiophene) and functionalized, multi-walled, carbon nanotubes counter electrode for dye-sensitized solar cells and characterization of its performance
(2011) Electrochimica Acta, 56 (9), pp. 3147-3152.
DOI: 10.1016/j.electacta.2011.01.063

[36] Kitamura, K., Shiratori, S.
37093300800;35592312400;
Layer-by-layer self-assembled mesoporous PEDOT-PSS and carbon black hybrid films for platinum free dye-sensitized-solar-cell counter electrodes
(2011) Nanotechnology, 22 (19), art. no. 195703.
DOI: 10.1088/0957-4484/22/19/195703

[37] Sudhagar, P., Nagarajan, S., Lee, Y.-G., Song, D., Son, T., Cho, W., Heo, M., Lee, K., Won, J., Kang, Y.S.
14020450700;7102013118;37030919400;54685064600;36982414300;45960922000;54083304600;22334025500;7201429776;7402784151;
Synergistic catalytic effect of a composite (CoS/PEDOT:PSS) counter electrode on triiodide reduction in dye-sensitized solar cells
(2011) ACS Applied Materials and Interfaces, 3 (6), pp. 1838-1843.
DOI: 10.1021/am2003735

[38] Shin, H.-J., Jeon, S.S., Im, S.S.
17137430000;8052156000;55599315800;
CNT/PEDOT core/shell nanostructures as a counter electrode for dye-sensitized solar cells
(2011) Synthetic Metals, 161 (13-14), pp. 1284-1288.
DOI: 10.1016/j.synthmet.2011.04.024

[39] Trevisan, R., Döbbelin, M., Boix, P.P., Barea, E.M., Tena-Zaera, R., Mora-Seró, I., Bisquert, J.
55050326000;16306736600;57201846705;15755262400;6506161950;6602706852;7005095919;
PEDOT nanotube arrays as high performing counter electrodes for dye sensitized solar cells. Study of the interactions among electrolytes and counter electrodes
(2011) Advanced Energy Materials, 1 (5), pp. 781-784.
DOI: 10.1002/aenm.201100324

[40] Yue, G., Wu, J., Lin, J., Huang, M., Yao, Y., Fan, L., Xiao, Y.
36005053100;55816456600;8369047300;7404260091;55584444500;13404977200;35621151400;
Application of Poly (3, 4-ethylenedioxythiophene): Polystyrenesulfonate counter electrode in polymer heterojunction dye-sensitized solar cells
(2011) Frontiers of Optoelectronics in China, 4 (4), pp. 369-377.
DOI: 10.1007/s12200-011-0181-6

[41] Thompson, S.J., Pringle, J.M., Zhang, X.L., Cheng, Y.-B.
55310923700;7103088434;47461726300;7404915594;
A novel carbon-PEDOT composite counter electrode for monolithic dye-sensitized solar cells
(2012) Journal of Physics D: Applied Physics, 46 (2), .
DOI: 10.1088/0022-3727/46/2/024007

[42] Xu, H., Zhang, X., Zhang, C., Liu, Z., Zhou, X., Pang, S., Chen, X., Dong, S., Zhang, Z., Zhang, L., Han, P., Wang, X., Cui, G.
55511379100;49362509500;37118342500;36466472500;7410094950;55025799700;57192468166;36466418900;55721899300;55709303000;36466329200;55165003100;12774027000;
Nanostructured titanium nitride/PEDOT:PSS composite films as counter electrodes of dye-sensitized solar cells
(2012) ACS Applied Materials and Interfaces, 4 (2), pp. 1087-1092.
DOI: 10.1021/am201720p

[43] Balis, N., Makris, T., Dracopoulos, V., Stergiopoulos, T., Lianos, P.
36902559200;36984216800;35615323900;6602756609;7006746725;
Quasi-Solid-State Dye-Sensitized Solar Cells made with poly(3,4-ethylenedioxythiophene)-functionalized counter-electrodes
(2012) Journal of Power Sources, 203, pp. 302-307.
DOI: 10.1016/j.jpowsour.2011.12.021

[44] Yue, G., Wu, J., Xiao, Y., Lin, J., Huang, M.
36005053100;55816456600;35621151400;8369047300;7404260091;
Low cost poly(3,4-ethylenedioxythiophene): Polystyrenesulfonate/carbon black counter electrode for dye-sensitized solar cells
(2012) Electrochimica Acta, 67, pp. 113-118.
DOI: 10.1016/j.electacta.2012.02.009

[45] Kim, Y.-K., Park, S.-H., Hwang, W.-P., Seo, M.-H., Park, H.-W., Jang, Y.-W., Kim, M.-R., Lee, J.-K.
57189320816;35196738900;36618944000;12802565900;55713483300;34868121500;25722572300;16052553900;
Impedance spectroscopy on dye-sensitized solar cells with a poly(ethylenedioxythiophene): Poly(styrenesulfonate) counter electrolyte
(2012) Journal of the Korean Physical Society, 60 (12), pp. 2049-2053.
DOI: 10.3938/jkps.60.2049

[46] Yue, G., Wu, J., Xiao, Y., Lin, J., Huang, M., Lan, Z.
36005053100;55816456600;35621151400;8369047300;7404260091;13403665200;
Application of poly(3,4-ethylenedioxythiophene): Polystyrenesulfonate/ polypyrrole counter electrode for dye-sensitized solar cells
(2012) Journal of Physical Chemistry C, 116 (34), pp. 18057-18063.
DOI: 10.1021/jp303958r

[47] Maiaugree, W., Pimanpang, S., Towannang, M., Saekow, S., Jarernboon, W., Amornkitbamrung, V.
31967686300;8601295500;54906145700;35995947100;14030108300;10141558700;
Optimization of TiO 2 nanoparticle mixed PEDOT-PSS counter electrodes for high efficiency dye sensitized solar cell
(2012) Journal of Non-Crystalline Solids, 358 (17), pp. 2489-2495.
DOI: 10.1016/j.jnoncrysol.2011.12.104

[48] Xiao, Y., Lin, J.-Y., Tai, S.-Y., Chou, S.-W., Yue, G., Wu, J.
35621151400;24822648700;55348937900;36902834300;36005053100;55816456600;
Pulse electropolymerization of high performance PEDOT/MWCNT counter electrodes for Pt-free dye-sensitized solar cells
(2012) Journal of Materials Chemistry, 22 (37), pp. 19919-19925.
DOI: 10.1039/c2jm34425d

[49] Lee, T.H., Do, K., Lee, Y.W., Jeon, S.S., Kim, C., Ko, J., Im, S.S.
56122323900;54886281000;57209136278;8052156000;36065487000;7402678484;55599315800;
High-performance dye-sensitized solar cells based on PEDOT nanofibers as an efficient catalytic counter electrode
(2012) Journal of Materials Chemistry, 22 (40), pp. 21624-21629.
DOI: 10.1039/c2jm34807a

[50] Zhang, Z., Zhang, X., Xu, H., Liu, Z., Pang, S., Zhou, X., Dong, S., Chen, X., Cui, G.
55721899300;49362509500;55511379100;36466472500;55025799700;7410094950;36466418900;57192468166;12774027000;
CuInS2 nanocrystals/PEDOT:PSS composite counter electrode for dye-sensitized solar cells
(2012) ACS Applied Materials and Interfaces, 4 (11), pp. 6242-6246.
DOI: 10.1021/am3018338

[51] Xiao, Y.-M., Lin, J.-Y., Wu, J.-H., Tai, S.-Y., Yue, G.-T.
35621151400;24822648700;55816456600;55348937900;36005053100;
Pulse potentiostatic electropolymerization of high performance PEDOT counter electrodes for Pt-free dye-sensitized solar cells
(2012) Electrochimica Acta, 83, pp. 221-226.
DOI: 10.1016/j.electacta.2012.07.113

[52] Xiao, Y., Wu, J., Yue, G., Lin, J., Huang, M., Lan, Z., Fan, L.
35621151400;55816456600;36005053100;8369047300;7404260091;13403665200;13404977200;
Electrodeposition of high performance PEDOT/Ti counter electrodes on Ti meshes for large-area flexible dye-sensitized solar cells
(2012) Electrochimica Acta, 85, pp. 432-437.
DOI: 10.1016/j.electacta.2012.08.077

[53] Jeon, N., Hwang, D.K., Kang, Y.S., Im, S.S., Kim, D.-W.
55751791000;55904888600;7402784151;55599315800;57189201444;
Quasi-solid-state dye-sensitized solar cells assembled with polymeric ionic liquid and poly(3,4-ethylenedioxythiophene) counter electrode
(2013) Electrochemistry Communications, 34, pp. 1-4.
DOI: 10.1016/j.elecom.2013.05.009

[54] Erten-Ela, S., Colak, S.G., Ocakoglu, K.
25624466500;55877289000;36088420200;

The first application of water-soluble ruthenium phenanthroline complex for dye sensitized solar cells from aqueous solution using PEDOT:PSS counter electrode versus platinum counter electrode
(2013) Inorganica Chimica Acta, 405, pp. 252-257.
DOI: 10.1016/j.ica.2013.06.010

[55] Ellis, H., Vlachopoulos, N., Häggman, L., Perruchot, C., Jouini, M., Boschloo, G., Hagfeldt, A.
55785580600;6603277739;14048301300;6603928659;54893775600;6701914421;700585 1690;
PEDOT counter electrodes for dye-sensitized solar cells prepared by aqueous micellar electrodeposition
(2013) Electrochimica Acta, 107, pp. 45-51.
DOI: 10.1016/j.electacta.2013.06.005

[56] Chiang, C.-H., Wu, C.-G.
55681178000;8062718200;
High-efficient dye-sensitized solar cell based on highly conducting and thermally stable PEDOT:PSS/glass counter electrode
(2013) Organic Electronics, 14 (7), pp. 1769-1776.
DOI: 10.1016/j.orgel.2013.03.020

[57] Chou, C.-S., Chou, C.-S., Kuo, Y.-T., Wang, C.-P.
7403593355;55511300900;55510943000;36097107600;
Preparation of a working electrode with a conducting PEDOT:PSS film and its applications in a dye-sensitized solar cell
(2013) Advanced Powder Technology, 24 (1), pp. 336-343.
DOI: 10.1016/j.apt.2012.08.006

[58] Nagarajan, S., Sudhagar, P., Raman, V., Cho, W., Dhathathreyan, K.S., Kang, Y.S.
7102013118;14020450700;7101864749;45960922000;6701399724;7402784151;
A PEDOT-reinforced exfoliated graphite composite as a Pt- and TCO-free flexible counter electrode for polymer electrolyte dye-sensitized solar cells
(2013) Journal of Materials Chemistry A, 1 (4), pp. 1048-1054.
DOI: 10.1039/c2ta00091a

[59] Yun, D.-J., Ra, H., Rhee, S.-W.
22935923900;55348845900;7401852016;
Concentration effect of multiwalled carbon nanotube and poly(3, 4-ethylenedioxythiophene) polymerized with poly(4-styrenesulfonate) conjugated film on the catalytic activity for counter electrode in dye sensitized solar cells
(2013) Renewable Energy, 50, pp. 692-700.
DOI: 10.1016/j.renene.2012.06.056

[60] Yue, G.T., Wu, J.H., Xiao, Y.M., Lin, J.M., Huang, M.L., Fan, L.Q., Yao, Y.
36005053100;55816456600;35621151400;8369047300;7404260091;13404977200;55584 444500;
A dye-sensitized solar cell based on PEDOT: PSS counter electrode
(2013) Chinese Science Bulletin, 58 (4-5), pp. 559-566.
DOI: 10.1007/s11434-012-5352-3

[61] Yuan, C., Guo, S., Wang, S., Liu, L., Chen, W., Wang, E.
57191544115;55272068600;55194567300;56491762900;16244338300;36014864700;

Electropolymerization polyoxometalate (POM)-doped pedot film electrodes with mastoid microstructure and its application in dye-sensitized solar cells (DSSCs)
(2013) Industrial and Engineering Chemistry Research, 52 (20), pp. 6694-6703.
DOI: 10.1021/ie302845z

[62] Yue, G., Wu, J., Xiao, Y., Lin, J., Huang, M., Lan, Z., Fan, L.
36005053100;55816456600;35621151400;8369047300;7404260091;13403665200;13404977200;
Functionalized graphene/poly(3,4-ethylenedioxythiophene): Polystyrenesulfonate as counter electrode catalyst for dye-sensitized solar cells
(2013) Energy, 54, pp. 315-321.
DOI: 10.1016/j.energy.2013.01.037

[63] Song, D., Li, M., Bai, F., Li, Y., Jiang, Y., Jiang, B.
23029092900;8870612500;55311526600;55312227700;55654858400;18133935500;
Silicon nanoparticles/pedot-pss nanocomposite as an efficient counter electrode for dye-sensitized solar cells
(2013) Functional Materials Letters, 6 (4), art. no. 1350048, .
DOI: 10.1142/S1793604713500483

[64] Yin, X., Wu, F., Fu, N., Han, J., Chen, D., Xu, P., He, M., Lin, Y.
55857668000;57198942918;54981298800;57199890685;56582891000;57199852756;74026093 64;25954367800;
Facile synthesis of poly(3,4-ethylenedioxythiophene) film via solid-state polymerization as high-performance Pt-free counter electrodes for plastic dye-sensitized solar cells
(2013) ACS Applied Materials and Interfaces, 5 (17), pp. 8423-8429.
DOI: 10.1021/am401719e

[65] Maiaugree, W., Towannang, M., Thiangkaew, A., Harnchana, V., Jarernboon, W., Pimanpang, S., Amornkitbamrung, V.
31967686300;54906145700;55508756700;26428764900;14030108300;8601295500;10141558700;
Composited NiSO4 and PEDOT:PSS counter electrode for efficient dye-sensitized solar cell based on organic T2/T- electrolyte
(2013) Materials Letters, 111, pp. 197-200.
DOI: 10.1016/j.matlet.2013.08.084

[66] Kung, C.-W., Cheng, Y.-H., Chen, H.-W., Vittal, R., Ho, K.-C.
56496377700;55831283000;7501611025;6602857195;56962715200;
Hollow microflower arrays of PEDOT and their application for the counter electrode of a dye-sensitized solar cell
(2013) Journal of Materials Chemistry A, 1 (36), pp. 10693-10702.
DOI: 10.1039/c3ta10803a

[67] Guan, G., Yang, Z., Qiu, L., Sun, X., Zhang, Z., Ren, J., Peng, H.
54781354500;55716669400;54781654500;55777650200;55549930600;57205396617;88689041 00;
Oriented PEDOT:PSS on aligned carbon nanotubes for efficient dye-sensitized solar cells
(2013) Journal of Materials Chemistry A, 1 (42), pp. 13268-13273.
DOI: 10.1039/c3ta12669b

[68] Li, C.-T., Lee, C.-P., Li, Y.-Y., Yeh, M.-H., Ho, K.-C.

55507636700;55050004100;55931497500;36678491100;56962715200;
A composite film of TiS2/PEDOT:PSS as the electrocatalyst for the counter electrode in dye-sensitized solar cells
(2013) Journal of Materials Chemistry A, 1 (47), pp. 14888-14896.
DOI: 10.1039/c3ta12603j

[69] Yue, G., Zhang, D., Tan, F., Wu, J., Li, F., Chen, C., Lan, Z.
36005053100;57034330300;56383420300;55816456600;55873465100;7501945419;13403665200;
Enhanced performance of dye-sensitized solar cells based on an electrodeposited-poly(3,4-ethylenedioxythiophene)/platinum composite counter electrode
(2014) Synthetic Metals, 197, pp. 204-209.
DOI: 10.1016/j.synthmet.2014.09.018

[70] Li, C.-T., Lee, C.-P., Fan, M.-S., Chen, P.-Y., Vittal, R., Ho, K.-C.
55507636700;55050004100;55179088600;57212666117;6602857195;56962715200;
Ionic liquid-doped poly(3,4-ethylenedioxythiophene) counter electrodes for dye-sensitized solar cells: Cationic and anionic effects on the photovoltaic performance
(2014) Nano Energy, 9, pp. 1-14.
DOI: 10.1016/j.nanoen.2014.06.020

[71] Chen, L., Jin, J., Shu, X., Xia, J.
57192609833;55761104800;57213696822;7402327380;
Solid state synthesis of poly(3,4-ethylenedioxythiophene) as counter electrode for dye-sensitized solar cell
(2014) Journal of Power Sources, 248, pp. 1234-1240.
DOI: 10.1016/j.jpowsour.2013.09.139

[72] Rhee, Y., Ko, M., Jin, H., Jin, J.-H., Min, N.K.
55485721300;7201495119;56121528700;19933834800;7003832641;
Photovoltaic performance of multi-wall carbon nanotube/PEDOT:PSS composite on the counter electrode of a dye-sensitized solar cell
(2014) Japanese Journal of Applied Physics, 53 (8 SPEC. ISSUE 3), art. no. 08NJ02, .
DOI: 10.7567/JJAP.53.08NJ02

[73] Gao, M., Xu, Y., Bai, Y., Jin, S.
55160408900;12804922400;57104153400;55778818100;
Effect of electropolymerization time on the performance of poly(3,4-ethylenedioxythiophene) counter electrode for dye-sensitized solar cells
(2014) Applied Surface Science, 289, pp. 145-149.
DOI: 10.1016/j.apsusc.2013.10.122

[74] Park, B.-W., Pazoki, M., Aitola, K., Jeong, S., Johansson, E.M.J., Hagfeldt, A., Boschloo, G.
35222177400;52364747000;35075662900;57198702485;10046404400;7005851690;6701914421;
Understanding interfacial charge transfer between metallic PEDOT counter electrodes and a cobalt redox shuttle in dye-sensitized solar cells
(2014) ACS Applied Materials and Interfaces, 6 (3), pp. 2074-2079.
DOI: 10.1021/am405108d

[75] Song, D., Li, M., Jiang, Y., Chen, Z., Bai, F., Li, Y., Jiang, B.
23029092900;8870612500;55654858400;55654769100;55311526600;55312227700;18133935500;

Facile fabrication of MoS2/PEDOT-PSS composites as low-cost and efficient counter electrodes for dye-sensitized solar cells
(2014) Journal of Photochemistry and Photobiology A: Chemistry, 279, pp. 47-51.
DOI: 10.1016/j.jphotochem.2014.01.009

[76] Koussi-Daoud, S., Schaming, D., Martin, P., Lacroix, J.-C.
56083098300;24485750400;8602326100;7201505988;
Gold nanoparticles and poly(3,4-ethylenedioxythiophene) (PEDOT) hybrid films as counter-electrodes for enhanced efficiency in dye-sensitized solar cells
(2014) Electrochimica Acta, 125, pp. 601-605.
DOI: 10.1016/j.electacta.2014.01.154

[77] Song, D., Li, M., Li, Y., Zhao, X., Jiang, B., Jiang, Y.
23029092900;8870612500;55312227700;56120852100;18133935500;55654858400;
Highly transparent and efficient counter electrode using SiO 2/PEDOT-PSS composite for bifacial dye-sensitized solar cells
(2014) ACS Applied Materials and Interfaces, 6 (10), pp. 7126-7132.
DOI: 10.1021/am500082x

[78] Tsai, Y.-L., Li, C.-T., Huang, T.-Y., Lee, C.-T., Lin, C.-Y., Chu, C.-W., Vittal, R., Ho, K.-C.
56937627400;55507636700;36171424200;56384553900;56937173200;8397944400;6602857195;56962715200;
Electrocatalytic SiC Nanoparticles/PEDOT: PSS Composite Thin Films as the Counter Electrodes of Dye-Sensitized Solar Cells
(2014) ChemElectroChem, 1 (6), pp. 1031-1039.
DOI: 10.1002/celc.201300242

[79] Liu, W.C., Liu, Y., Jennings, J.R., Huang, H., Wang, Q.
56225657600;36959392300;25225481400;55504185700;7406912318;
Low-cost and flexible poly(3,4-ethylenedioxythiophene) based counter electrodes for efficient energy conversion in dye-sensitized solar cells
(2014) Journal of Materials Chemistry A, 2 (28), pp. 10938-10944.
DOI: 10.1039/c4ta00563e

[80] Park, S.H., Kim, O.-H., Kang, J.S., Lee, K.J., Choi, J.-W., Cho, Y.-H., Sung, Y.-E.
35103125700;56506583500;56149974000;55846114000;56041708300;35172645400;23484028800;
Poly(3,4-ethylenedioxythiophene) inverse opal electrode fabricated from poly(3,4-ethylenedioxythiophene):Poly(styrene sulfonate)-filled polystyrene template for dye-sensitized solar cells
(2014) Electrochimica Acta, 137, pp. 661-667.
DOI: 10.1016/j.electacta.2014.06.025

[81] Song, D., Li, M., Wang, T., Fu, P., Li, Y., Jiang, B., Jiang, Y., Zhao, X.
23029092900;8870612500;56328602200;57194205609;55312227700;18133935500;55654858400;56120852100;
Dye-sensitized solar cells using nanomaterial/PEDOT-PSS composite counter electrodes: Effect of the electronic and structural properties of nanomaterials
(2014) Journal of Photochemistry and Photobiology A: Chemistry, 293, pp. 26-31.
DOI: 10.1016/j.jphotochem.2014.07.014

[82] Chang, L.-Y., Li, Y.-Y., Li, C.-T., Lee, C.-P., Fan, M.-S., Vittal, R., Ho, K.-C., Lin, J.-J.
42260961800;55931497500;55507636700;55050004100;55179088600;6602857195;56962715200;8718905000;
A composite catalytic film of Ni-NPs/PEDOT: PSS for the counter electrodes in dye-sensitized solar cells
(2014) Electrochimica Acta, 146, pp. 697-705.
DOI: 10.1016/j.electacta.2014.08.112

[83] Kim, D.H., Atanasov, S.E., Lemaire, P., Lee, K., Parsons, G.N.
55742870400;55882010200;56462275600;38163133100;7102727818;
Platinum-free cathode for dye-sensitized solar cells using poly(3,4-ethylenedioxythiophene) (PEDOT) formed via oxidative molecular layer deposition
(2015) ACS Applied Materials and Interfaces, 7 (7), pp. 3866-3870.
DOI: 10.1021/am5084418

[84] Ma, X., Yue, G., Wu, J., Lan, Z., Lin, J.-Y.
24338310200;36005053100;55816456600;13403665200;24822648700;
A strategy to enhance overall efficiency for dye-sensitized solar cells with a transparent electrode of nickel sulfide decorated with poly(3,4-ethylenedioxythiophene)
(2015) RSC Advances, 5 (54), pp. 43639-43647.
DOI: 10.1039/c5ra01017a

[85] Xia, X., Wu, W., Ma, J., Liu, T., Fei, D., Liu, X., Gao, C.
56513015500;56470024700;56514299000;56303289100;55220257800;12809723000;74026617408;
Antimony tin oxide porous layers improve the poly(3,4-ethylenedioxythiophene) counter electrode fabricated by vapor deposition for dye-sensitized solar cells
(2015) RSC Advances, 5 (21), pp. 15772-15777.
DOI: 10.1039/c4ra13591a

[86] Yeon, C., Yun, S.J., Kim, J., Lim, J.W.
55803347700;7202777409;57214339671;7403454016;
PEDOT:PSS Films with Greatly Enhanced Conductivity via Nitric Acid Treatment at Room Temperature and Their Application as Pt/TCO-Free Counter Electrodes in Dye-Sensitized Solar Cells
(2015) Advanced Electronic Materials, 1 (10), art. no. 1500121, .
DOI: 10.1002/aelm.201500121

[87] Lin, Y.-F., Li, C.-T., Ho, K.-C.
56984617600;55507636700;56962715200;
A template-free synthesis of the hierarchical hydroxymethyl PEDOT tube-coral array and its application in dye-sensitized solar cells
(2015) Journal of Materials Chemistry A, 4 (2), pp. 384-394.
DOI: 10.1039/c5ta06376k

[88] Wang, H., Hu, Y.
36138418300;25927893100;
Electro-catalytic role of insulator/conductor interface in MgO/PEDOT composite electrodes for dye-sensitized solar cells
(2015) Science China Chemistry, 58 (1), pp. 101-106.
DOI: 10.1007/s11426-014-5210-z

[89] Lan, Z., Gao, S., Wu, J., Lin, J.
13403665200;55937896100;55816456600;8369047300;
High-performing dye-sensitized solar cells based on reduced graphene oxide/PEDOT-PSS counter electrodes with sulfuric acid post-treatment
(2015) Journal of Applied Polymer Science, 132 (41), art. no. 42648, .
DOI: 10.1002/app.42648

[90] Jafari, F., Behjat, A., Khoshroo, A.R., Ghoshani, M.
56439232600;6602139054;35097519700;56527170400;
A dye-sensitized solar cell based on natural photosensitizers and a PEDOT: PSS/TiO2 film as a counter electrode
(2015) EPJ Applied Physics, 69 (2), art. no. 20502, .
DOI: 10.1051/epjap/2015140370

[91] Wan, L., Wang, B., Wang, S., Wang, X., Guo, Z., Dong, B., Zhao, L., Li, J., Zhang, Q., Luo, T.
57202132509;56122397900;57209185916;57211248196;8671116800;23485041400;57094313900;56533645800;56576679400;56747188000;
Well-dispersed PEDOT:PSS/graphene nanocomposites synthesized by in situ polymerization as counter electrodes for dye-sensitized solar cells
(2015) Journal of Materials Science, 50 (5), pp. 2148-2157.
DOI: 10.1007/s10853-014-8777-z

[92] Chen, P.-Y., Li, C.-T., Lee, C.-P., Vittal, R., Ho, K.-C.
57212666117;55507636700;55050004100;6602857195;56962715200;
PEDOT-decorated nitrogen-doped graphene as the transparent composite film for the counter electrode of a dye-sensitized solar cell
(2015) Nano Energy, 12, pp. 374-385.
DOI: 10.1016/j.nanoen.2015.01.010

[93] Lin, J.-Y., Wang, W.-Y., Chou, S.-W.
24822648700;56521105700;36902834300;
Flexible carbon nanotube/polypropylene composite plate decorated with poly(3,4-ethylenedioxythiophene) as efficient counter electrodes for dye-sensitized solar cells
(2015) Journal of Power Sources, 282, pp. 348-357.
DOI: 10.1016/j.jpowsour.2015.01.142

[94] Sekkarapatti Ramasamy, M., Nikolakapoulou, A., Raptis, D., Dracopoulos, V., Paterakis, G., Lianos, P.
56650955100;56651011700;55391174200;35615323900;55479981800;7006746725;
Reduced graphene oxide/polypyrrole/PEDOT composite films as efficient Pt-free counter electrode for dye-sensitized solar cells
(2015) Electrochimica Acta, 173, art. no. 24976, pp. 276-281.
DOI: 10.1016/j.electacta.2015.05.043

[95] Han, R., Lu, S., Wang, Y., Zhang, X., Wu, Q., He, T.
56290293900;55637484100;55989014300;55178104500;57190303622;56410364400;
Influence of monomer concentration during polymerization on performance and catalytic mechanism of resultant poly(3,4-ethylenedioxythiophene) counter electrodes for dye-sensitized solar cells
(2015) Electrochimica Acta, 173, art. no. 25063, pp. 796-803.
DOI: 10.1016/j.electacta.2015.05.130

[96] Kim, T.-Y., Wei, W., Cho, W., Lee, S., Won, J., Kang, Y.S.
56117865700;57204784751;45960922000;56967496600;55791630000;7402784151;

Excellent optical and interfacial performance of a PEDOT-b-PEG block copolymer counter electrode for polymer electrolyte-based solid-state dye-sensitized solar cells
(2015) Chemical Communications, 51 (94), pp. 16782-16785.
DOI: 10.1039/c5cc06546a

[97] Koussi-Daoud, S., Schaming, D., Fillaud, L., Trippé-Allard, G., Lafolet, F., Polanski, E., Nonomura, K., Vlachopoulos, N., Hagfeldt, A., Lacroix, J.-C.
56083098300;24485750400;36552331000;16426483800;6506143640;56638447500;7006791700;6603277739;7005851690;7201505988;
3,4-Ethylenedioxythiophene-based cobalt complex: An efficient co-mediator in dye-sensitized solar cells with poly(3,4-ethylenedioxythiophene) counter-electrode
(2015) Electrochimica Acta, 179, pp. 237-240.
DOI: 10.1016/j.electacta.2015.04.173

[98] Jeong, G.-H., Kim, S.-J., Ko, H.-S., Han, E.-M., Park, K.H.
56921448600;56423813700;55759463600;7101875383;55722189000;
Electrochemical Properties of Graphene/PEDOT:PSS Counter Electrode in Dye-sensitized Solar Cells
(2015) Molecular Crystals and Liquid Crystals, 620 (1), pp. 117-122.
DOI: 10.1080/15421406.2015.1095272

[99] Lee, C.-P., Lin, C.-A., Wei, T.-C., Tsai, M.-L., Meng, Y., Li, C.-T., Ho, K.-C., Wu, C.-I., Lau, S.-P., He, J.-H.
55050004100;35199808900;54884503200;55749550700;56937635600;55507636700;56962715200;35218461900;57193901997;8604364600;
Economical low-light photovoltaics by using the Pt-free dye-sensitized solar cell with graphene dot/PEDOT: PSS counter electrodes
(2015) Nano Energy, 18, pp. 109-117.
DOI: 10.1016/j.nanoen.2015.10.008

[100] Liu, B.-T., Wang, Z.-T.
26643226800;57189443077;
Graphene oxide/poly(3,4-ethylenedioxythiophene):polystyrenesulfonate layers on silver nanowire working electrodes enhance the power conversion efficiencies of dye-sensitized solar cells in a low temperature process
(2016) RSC Advances, 6 (53), pp. 47185-47191.
DOI: 10.1039/c6ra03756a

[101] Xu, S., Luo, Y., Zhong, W., Xiao, Z., Luo, Y., Ou, H.
56170596300;56190013100;53165423500;15833569300;24069237400;56057534300;
Nanoporous TiO2/SnO2/poly(3,4-ethylenedioxythiophene): Polystyrenesulfonate composites as efficient counter electrode for dye-sensitized solar cells
(2016) Journal of Nanoscience and Nanotechnology, 16 (1), pp. 392-399.
DOI: 10.1166/jnn.2016.10819

[102] Kim, H., Veerappan, G., Wang, D.H., Park, J.H.
57214326524;38863187200;35099662400;57194536850;
Large Area Platinum and Fluorine-doped Tin Oxide-free Dye sensitized Solar Cells with Silver-Nanoplate Embedded Poly(3,4-Ethylenedioxythiophene) Counter Electrode
(2016) Electrochimica Acta, 187, pp. 218-223.
DOI: 10.1016/j.electacta.2015.11.051

[103] Zheng, M., Huo, J., Tu, Y., Jia, J., Wu, J., Lan, Z.

56496101500;55819675900;55886856400;56583243200;55816456600;13403665200;
An in situ polymerized PEDOT/Fe3O4 composite as a Pt-free counter electrode for highly efficient dye sensitized solar cells
(2016) RSC Advances, 6 (2), pp. 1637-1643.
DOI: 10.1039/c5ra21878k

[104] Anothumakkool, B., Agrawal, I., Bhange, S.N., Soni, R., Game, O., Ogale, S.B., Kurungot, S.
55786367700;56191982400;55786525000;56583752100;36160172900;55157007700;6507304522;
Pt- and TCO-Free Flexible Cathode for DSSC from Highly Conducting and Flexible PEDOT Paper Prepared via in Situ Interfacial Polymerization
(2016) ACS Applied Materials and Interfaces, 8 (1), pp. 553-562.
DOI: 10.1021/acsami.5b09579

[105] Seo, H., Son, M.-K., Itagaki, N., Koga, K., Shiratani, M.
24829484000;24829525500;35605327000;55204680500;7004068078;
Polymer counter electrode of poly(3,4-ethylenedioxythiophene):Poly(4-styrenesulfonate) containing TiO2 nano-particles for dye-sensitized solar cells
(2016) Journal of Power Sources, 307, pp. 25-30.
DOI: 10.1016/j.jpowsour.2015.12.112

[106] Belekoukia, M., Ramasamy, M.S., Yang, S., Feng, X., Paterakis, G., Dracopoulos, V., Galiotis, C., Lianos, P.
57190132184;55980785900;56612466600;13406555300;55479981800;35615323900;7006740945;7006746725;
Electrochemically exfoliated graphene/PEDOT composite films as efficient Pt-free counter electrode for dye-sensitized solar cells
(2016) Electrochimica Acta, 194, pp. 110-115.
DOI: 10.1016/j.electacta.2016.02.073

[107] Susmitha, K., Mamatha Kumari, M., Naresh Kumar, M., Giribabu, L., Theerthagiri, J., Madhavan, J., Raghavender, M.
48662978100;55861942200;57189057833;6602917953;55510359000;8955335700;57185574100;
Carbon nanohorns functionalized PEDOT:PSS nanocomposites for dye sensitized solar cell applications
(2016) Journal of Materials Science: Materials in Electronics, 27 (4), pp. 4050-4056.
DOI: 10.1007/s10854-015-4261-z

[108] Huang, Y.-J., Fan, M.-S., Li, C.-T., Lee, C.-P., Chen, T.-Y., Vittal, R., Ho, K.-C.
57034502600;55179088600;55507636700;55050004100;57190047477;6602857195;56962715200;
MoSe2 nanosheet/poly(3,4-ethylenedioxythiophene): poly(styrenesulfonate) composite film as a Pt-free counter electrode for dye-sensitized solar cells
(2016) Electrochimica Acta, 211, pp. 794-803.
DOI: 10.1016/j.electacta.2016.06.086

[109] Mustafa, M.N., Shafie, S., Zainal, Z., Sulaiman, Y.
56998209500;23991445600;7004044551;13806413500;
A Novel Poly(3,4-ethylenedioxythiophene)-graphene Oxide/Titanium Dioxide Composites Counter Electrode for Dye-Sensitized Solar Cell
(2017) Journal of Nanomaterials, 2017, art. no. 4045672, .

DOI: 10.1155/2017/4045672

[110] Li, H., Xiao, Y., Han, G., Hou, W.
57192818360;35621151400;7202923222;57016052200;
Honeycomb-like poly(3,4-ethylenedioxythiophene) as an effective and transparent counter electrode in bifacial dye-sensitized solar cells
(2017) Journal of Power Sources, 342, pp. 709-716.
DOI: 10.1016/j.jpowsour.2017.01.007

[111] Li, Y.-C., Jia, S.-R., Liu, Z.-Y., Liu, X.-Q., Wang, Y., Cao, Y., Hu, X.-Q., Peng, C.-L., Li, Z.
55922450500;57194344482;57194782529;7409287232;56796182600;57188768591;57194782037;57194782709;57189006479;
Fabrication of PEDOT films: Via a facile method and their application in Pt-free dye-sensitized solar cells
(2017) Journal of Materials Chemistry A, 5 (17), pp. 7862-7868.
DOI: 10.1039/c7ta00990a

[112] Moolsarn, K., Tangtrakarn, A., Pimsawat, A., Duangsa, K., Mongkolkachit, C., Maiaugree, W., Amornkitbamrung, V.
57194689324;55355063800;36169953400;57194690384;26534720500;31967686300;10141558700;
A Dye-Sensitized Solar Cell Using a Composite of PEDOT: PSS and Carbon Derived from Human Hair for a Counter Electrode
(2017) International Journal of Photoenergy, 2017, art. no. 1064868, .
DOI: 10.1155/2017/1064868

[113] Edalati, S., Houshangi Far, A., Torabi, N., Baneshi, Z., Behjat, A.
55636991400;57193167853;56439673500;57193169262;6602139054;
Heuristic method of fabricating counter electrodes in dye-sensitized solar cells based on a PEDOT:PSS layer as a catalytic material
(2017) Journal of Physics D: Applied Physics, 50 (6), art. no. 065501, .
DOI: 10.1088/1361-6463/aa52a6

[114] Wu, K., Ma, J., Cui, W., Ruan, B., Wu, M.
7404512248;57199107618;56212220300;36466979700;55552889400;
The Impact of Metal Ion Doping on the Performance of Flexible Poly(3,4-ethylenedioxythiophene) (PEDOT) Cathode in Dye-Sensitized Solar Cells
(2017) Journal of Photochemistry and Photobiology A: Chemistry, 340, pp. 29-34.
DOI: 10.1016/j.jphotochem.2017.02.023

[115] Maiaugree, W., Pimparue, P., Jarernboon, W., Pimanpang, S., Amornkitbamrung, V., Swatsitang, E.
31967686300;57193644146;14030108300;8601295500;10141558700;16239879400;
NiS(NPs)-PEDOT-PSS composite counter electrode for a high efficiency dye sensitized solar cell
(2017) Materials Science and Engineering B: Solid-State Materials for Advanced Technology, 220, pp. 66-72.
DOI: 10.1016/j.mseb.2017.03.006

[116] Li, Z., Xu, J., Chen, L., Zhang, R., Yang, X., Xia, J.
55761560700;57194198653;57192609833;57189871235;55992268700;7402327380;
Influence of Sheet Resistance Effect on Poly(3,4-ethylenedioxythiophene) Counter Electrode for Dye-Sensitized Solar Cell
(2017) Electrochimica Acta, 242, pp. 219-226.
DOI: 10.1016/j.electacta.2017.04.172

[117] Gemeiner, P., Peřinka, N., Švorc, Ľ., Hatala, M., Gál, L., Belovičová, M., Syrový, T., Mikula, M.
37088586600;55945204900;16205696600;56988922800;25621503200;57193926396;57208239405;6603786768;
Pt-free counter electrodes based on modified screen-printed PEDOT:PSS catalytic layers for dye-sensitized solar cells
(2017) Materials Science in Semiconductor Processing, 66, pp. 162-169.
DOI: 10.1016/j.mssp.2017.04.021

[118] Thuy, C.T.T., Kim, D.W., Thogiti, S., Jo, H.-J., Kim, J.H., Cheruku, R.
57188972485;57191865555;57195921688;55193116100;55894848300;36909817200;
Improved performance of dye-sensitized solar cells based on solution treated PEDOT as efficient counter electrode
(2017) Molecular Crystals and Liquid Crystals, 653 (1), pp. 91-98.
DOI: 10.1080/15421406.2017.1350030

[119] Li, H., Xiao, Y., Han, G., Zhang, Y.
57192818360;35621151400;7202923222;39661408400;
A transparent honeycomb-like poly(3,4-ethylenedioxythiophene)/multi-wall carbon nanotube counter electrode for bifacial dye-sensitized solar cells
(2017) Organic Electronics, 50, pp. 161-169.
DOI: 10.1016/j.orgel.2017.07.048

[120] Mustafa, M.N., Shafie, S., Zainal, Z., Sulaiman, Y.
56998209500;23991445600;7004044551;13806413500;
Poly(3,4-ethylenedioxythiophene) doped with various carbon-based materials as counter electrodes for dye sensitized solar cells
(2017) Materials and Design, 136, pp. 249-257.
DOI: 10.1016/j.matdes.2017.09.053

[121] Ahmed, A.S.A., Xiang, W., Saana Amiinu, I., Zhao, X.
57202904827;55532027200;57189355022;7407542254;
Zeolitic-imidazolate-framework (ZIF-8)/PEDOT:PSS composite counter electrode for low cost and efficient dye-sensitized solar cells
(2018) New Journal of Chemistry, 42 (21), pp. 17303-17310.
DOI: 10.1039/C8NJ03192D

[122] Kim, J.C., Rahman, M.M., Ju, M.J., Lee, J.-J.
55757759800;55339273100;49961620500;56585542900;
Highly conductive and stable graphene/PEDOT:PSS composite as a metal free cathode for organic dye-sensitized solar cells
(2018) RSC Advances, 8 (34), pp. 19058-19066.
DOI: 10.1039/c8ra02668h

[123] Yun, D.-J., Jeong, Y.J., Ra, H., Kim, J.-M., An, T.K., Rhee, S.-W., Jang, J.
22935923900;56033346800;55348845900;36903727100;35190164200;7401852016;55730015300;
Systematic optimization of MWCNT-PEDOT:PSS composite electrodes for organic transistors and dye-sensitized solar cells: Effects of MWCNT diameter and purity
(2018) Organic Electronics, 52, pp. 7-16.
DOI: 10.1016/j.orgel.2017.10.007

[124] Kim, T.-Y., Wei, W., Lee, T.K., Kim, B.S., Park, S.C., Lee, S., Suh, E.H., Jang, J., Bisquert, J., Kang, Y.S.

56117865700;57204784751;56105909900;57199939882;57196438369;56967496600;571
69824500;55730015300;7005095919;7402784151;
Imidazolium Iodide-Doped PEDOT Nanofibers as Conductive Catalysts for
Highly Efficient Solid-State Dye-Sensitized Solar Cells Employing Polymer
Electrolyte
(2018) ACS Applied Materials and Interfaces, 10 (3), pp. 2537-2545.
DOI: 10.1021/acsami.7b16017

[125] Ma, J., Qingfeng, S., Fengbao, Z., Mingxing, W.
57199107618;57200085332;7801693146;57200088395;
Improvement on the catalytic activity of the flexible PEDOT counter
electrode in dye-sensitized solar cells
(2018) Materials Research Bulletin, 100, pp. 213-219.
https://www.scopus.com/inward/record.uri?eid=2-s2.0-
DOI: 10.1016/j.materresbull.2017.12.031

[126] Ma, J., Yuan, S., Yang, S., Lu, H., Li, Y.
24833343000;57200501472;55277423400;57213294068;7502085144;
Poly(3,4-ethylenedioxythiophene)/reduced graphene oxide composites as
counter electrodes for high efficiency dye-sensitized solar cells
(2018) Applied Surface Science, 440, pp. 8-15.
DOI: 10.1016/j.apsusc.2018.01.100

[127] Vasanth, A., Sreekala, C.O., Sreelatha, K.S., Jinchu, I.
57202988874;51564922900;6602796270;55165377600;
Micro contact printed PEDOT: PSS as cathode in dye sensitized solar cells
(2018) Proceedings of 2017 IEEE International Conference on Technological
Advancements in Power and Energy: Exploring Energy Solutions for an
Intelligent Power Grid, TAP Energy 2017, pp. 1-5.
DOI: 10.1109/TAPENERGY.2017.8397325

[128] Di, Y., Xiao, Z., Liu, Z., Chen, B., Feng, J.
57192195987;56384810900;16031851700;56384618000;7403884688;
Hybrid films of PEDOT containing transition metal phosphates as high
effective Pt-free counter electrodes for dye sensitized solar cells
(2018) Organic Electronics, 57, pp. 171-177.
DOI: 10.1016/j.orgel.2018.03.012

[129] Maiaugree, W., Karaphun, A., Pimsawad, A., Amornkitbamrung, V.,
Swatsitang, E.
31967686300;56185335500;57202216166;10141558700;16239879400;
Influence of SrTi1-xCoxO3 NPs on electrocatalytic activity of SrTi1-xCoxO3
NPs/PEDOT-PSS counter electrodes for high efficiency dye sensitized solar
cells
(2018) Energy, 154, pp. 182-189.
DOI: 10.1016/j.energy.2018.04.122

[130] Yun, D.-J., Jung, C., Byun, S., Ra, H., Kim, J.-M., Lee, S., Hwang, J.,
Park, S.-H.
22935923900;55747781500;55857100000;55348845900;36903727100;23100535200;568
98317100;57188642959;
Nanotube and poly(3,4-ethylenedioxythiophene): Polystyrene sulfonate
(PEDOT:PSS) composite film for the electrode applications in organic thin-
film transistor and dye-sensitized solar cells
(2018) Nanotechnology, 29 (39), art. no. 395704, .
DOI: 10.1088/1361-6528/aad15a

[131] Ahmed, A.S.A., Xiang, W., Hu, X., Qi, C., Amiinu, I.S., Zhao, X.
57202904827;55532027200;57202901190;57203624042;55951426700;7407542254;
Si3N4/MoS2-PEDOT: PSS composite counter electrode for bifacial dye-sensitized solar cells
(2018) Solar Energy, 173, pp. 1135-1143.
DOI: 10.1016/j.solener.2018.08.062

[132] Wang, C., Li, X., Wu, Y., Tan, S.
57191870348;57211670411;57195246875;55659428600;
An efficient and thermally stable dye-sensitized solar cell based on a lamellar nanostructured thiolate/disulfide liquid crystal electrolyte and carbon/PEDOT composite nanoparticle electrode
(2019) RSC Advances, 9 (61), pp. 35924-35930.
DOI: 10.1039/c9ra07043e

[133] Wang, C., Li, X., Wu, Y., Tan, S.
57191870348;57211670411;57195246875;55659428600;
An efficient and thermally stable dye-sensitized solar cell based on a lamellar nanostructured thiolate/disulfide liquid crystal electrolyte and carbon/PEDOT composite nanoparticle electrode
(2019) RSC Advances, 9 (61), pp. 35924-35930.
DOI: 10.1039/c9ra07043e

[134] Shenouda, S.S., Yahia, I.S., Hafez, H.S., Yakuphanoglu, F.
56330870700;14421963500;26534218300;56247755900;
Facile and low-cost synthesis of PEDOT:PSS/FTO polymeric counter electrode for DSSC photosensor with negative capacitance phenomenon
(2019) Materials Research Express, 6 (6), art. no. 065004, .
DOI: 10.1088/2053-1591/ab0861

[135] Wan Khalit, W.N.A., Mustafa, M.N., Sulaiman, Y.
57208926286;56998209500;13806413500;
Synergistic effect of poly(3,4-ethylenedioxythiophene), reduced graphene oxide and aluminium oxide) as counter electrode in dye-sensitized solar cell
(2019) Results in Physics, 13, art. no. 102355, .
DOI: 10.1016/j.rinp.2019.102355

[136] Zhang, R., Xu, J., Qian, J., Xia, J.
57189871235;57194198653;57190669506;7402327380;
Facile synthesis of poly(3,4-ethylenedioxythiophene) and poly(bis-3,4-ethylenedioxythiophene) via UV-irradiation polymerization and their reduction/iodine oxidation post-treatment for the application as counter electrodes for dye-sensitized solar cells
(2019) Electrochimica Acta, 313, pp. 505-512.
DOI: 10.1016/j.electacta.2019.05.043

[137] Di, Y., Jia, S., Li, N., Hao, C., Zhang, H., Hu, S., Liu, H.
57192195987;14029943500;56434883800;57209856534;57209858960;23099991100;23397007900;
Electrocatalytic films of PEDOT incorporating transition metal phosphides as efficient counter electrodes for dye sensitized solar cells
(2019) Solar Energy, 189, pp. 8-14.
DOI: 10.1016/j.solener.2019.07.039

[138] Gemeiner, P., Kuliček, J., Syrový, T., Ház, A., Khunová, V., Hatala, M., Mikula, M., Hvojnik, M., Gál, L., Jablonský, M., Omastová, M.

37088586600;56365949400;57208239405;25621319500;6701710469;56988922800;6603786768;57202199352;25621503200;57204542238;7004071813;
Screen-printed PEDOT:PSS/halloysite counter electrodes for dye-sensitized solar cells
(2019) Synthetic Metals, 256, art. no. 116148, .
DOI: 10.1016/j.synthmet.2019.116148

[139] Anil, A., Sambhudevan, S., Sreekala, C.O., Shankar, B.
57211665203;54895135800;51564922900;37036165800;
Effect of silver nanoparticle in the PEDOT: PSS counter electrode of dye sensitized solar cell
(2019) AIP Conference Proceedings, 2162, art. no. 020123, .
DOI: 10.1063/1.5130333

[140] Xu, T., Kong, D., Tang, H., Qin, X., Li, X., Gurung, A., Kou, K., Chen, L., Qiao, Q., Huang, W.
56471115400;57216154145;57204454392;17435767700;56534342000;57189343061;57216343235;57191500938;57216156690;57216354891;
Transparent MoS2/PEDOT Composite Counter Electrodes for Bifacial Dye-Sensitized Solar Cells
(2020) ACS Omega, .
DOI: 10.1021/acsomega.0c00175

[141] Peri, R., Mathan Kumar, P., Muthuraaman, B.
57214330937;57200560667;8955335800;
Improved performance of dye-sensitized solar cells upon sintering of a PEDOT cathode at various temperatures
(2020) RSC Advances, 10 (8), pp. 4521-4528.
DOI: 10.1039/c9ra09715e

[142] Bella, F., Porcarelli, L., Mantione, D., Gerbaldi, C., Barolo, C., Grätzel, M., Mecerreyes, D.
55600535900;55650463700;42861949400;57206405317;6602578023;35463345800;7003711085;
A water-based and metal-free dye solar cell exceeding 7% efficiency using a cationic poly(3,4-ethylenedioxythiophene) derivative
(2020) Chemical Science, 11 (6), pp. 1485-1493.
DOI: 10.1039/c9sc05596g

[143] Reddy, A.C.K., Gurulakshmi, M., Susmitha, K., Raghavender, M., Thota, N., Subbaiah, Y.P.V.
57215022812;57215960666;48662978100;57185574100;56210914000;8620489100;
A novel PEDOT:PSS/SWCNH bilayer thin film counter electrode for efficient dye-sensitized solar cells
(2020) Journal of Materials Science: Materials in Electronics, 31 (6), pp. 4752-4760.
DOI: 10.1007/s10854-020-03032-3

[144] Saito, Y., Kitamura, T., Wada, Y., Yanagida, S.
7406267398;7401578444;35419623900;35420673400;
Poly(3,4-ethylenedioxythiophene) as a hole conductor in solid state dye sensitized solar cells
(2002) Synthetic Metals, 131 (1-3), pp. 185-187.
DOI: 10.1016/S0379-6779(02)00198-4

[145] Fukuri, N., Saito, Y., Kubo, W., Rohan Senadeera, G.K., Kitamura, T., Wada, Y., Yanagida, S.

6507626767;7406267398;8094036600;6507098723;7401578444;35419623900;35420673400;
Performance improvement of solid-state dye-sensitized solar cells fabricated using poly(3,4-ethylenedioxythiophene) and amphiphilic sensitizing dye
(2004) Journal of the Electrochemical Society, 151 (10), pp. A1745-A1748.
DOI: 10.1149/1.1793711

[146] Fukuri, N., Masaki, N., Kitamura, T., Wada, Y., Yanagida, S.
6507626767;10739561400;7401578444;35419623900;35420673400;
Electron transport analysis for improvement of solid-state dye-sensitized solar cells using poly(3,4-ethylenedioxythiophene) as hole conductors
(2006) Journal of Physical Chemistry B, 110 (50), pp. 25251-25258.
DOI: 10.1021/jp064439a

[147] Kim, Y., Sung, Y.-E., Xia, J.-B., Lira-Cantu, M., Masaki, N., Yanagida, S.
56066689000;23484028800;7402327380;6602286691;10739561400;35420673400;
Solid-state dye-sensitized TiO2 solar cells using poly(3,4-ethylenedioxythiophene) as substitutes of iodine/iodide electrolytes and noble metal catalysts on FTO counter electrodes
(2008) Journal of Photochemistry and Photobiology A: Chemistry, 193 (2-3), pp. 77-80.
DOI: 10.1016/j.jphotochem.2007.06.009

[148] Xia, J., Masaki, N., Lira-Cantu, M., Kim, Y., Jiang, K., Yanagida, S.
7402327380;10739561400;6602286691;56066689000;7103330942;35420673400;
Influence of doped anions on poly(3,4-ethylenedioxythiophene) as hole conductors for iodine-free solid-state dye-sensitized solar cells
(2008) Journal of the American Chemical Society, 130 (4), pp. 1258-1263.
DOI: 10.1021/ja075704o

[149] Xia, J., Masaki, N., Lira-Cantu, M., Kim, Y., Jiang, K., Yanagida, S.
7402327380;10739561400;6602286691;56066689000;7103330942;35420673400;
Effect of doping anions' structures on poly(3,4-ethylenedioxythiophene) as hole conductors in solid-state dye-sensitized solar cells
(2008) Journal of Physical Chemistry C, 112 (30), pp. 11569-11574.
DOI: 10.1021/jp801878a

[150] Lee, J.-K., Jang, S.-I., Jung, B.-H., Choi, H.-J., Lee, S.-B., Park, S.-H., Kim, M.-R.
16052553900;55566336600;37087227200;57212853172;57192518809;35196738900;25722572300;
Photovoltaic properties of Dye-Sensitized Solar Cells using glycerol-modified PEDOT:PSS
(2009) Molecular Crystals and Liquid Crystals, 505 (1), pp. 175/[413]-183/[421].
DOI: 10.1080/15421400902946194

[151] Liu, X., Zhang, W., Uchida, S., Cai, L., Liu, B., Ramakrishna, S.
12809723000;55175089400;57194136450;34767952600;57209810523;57205523298;
An efficient organic-dye-sensitized solar cell with in situ polymerized poly(3,4-ethylenedioxythiophene) as a hole-transporting material
(2010) Advanced Materials, 22 (20), pp. E150-E155.
DOI: 10.1002/adma.200904168

[152] Mozer, A.J., Panda, D.K., Gambhir, S., Winther-Jensen, B., Wallace, G.G.
8557588100;35491232300;27867754400;8718005700;7202483095;

Microsecond dye regeneration kinetics in efficient solid state dye-sensitized solar cells using a photoelectrochemically deposited PEDOT hole conductor
(2010) Journal of the American Chemical Society, 132 (28), pp. 9543-9545.
DOI: 10.1021/ja1026453

[153] Liu, X., Cheng, Y., Wang, L., Cai, L., Liu, B.
12809723000;55487652100;53864492200;34767952600;57209810523;
Light controlled assembling of iodine-free dye-sensitized solar cells with poly(3,4-ethylenedioxythiophene) as a hole conductor reaching 7.1% efficiency
(2012) Physical Chemistry Chemical Physics, 14 (19), pp. 7098-7103.
https://www.scopus.com/inward/record.uri?eid=2-s2.0-84860385751&doi=10.1039%2fc2cp40882a&partnerID=40&md5=6624 0d4ea3e23fd42637486371761643

[154] Park, B.-W., Yang, L., Johansson, E.M.J., Vlachopoulos, N., Chams, A., Perruchot, C., Jouini, M., Boschloo, G., Hagfeldt, A.
35222177400;57155179400;10046404400;6603277739;49561019300;6603928659;54893775600;6701914421;7005851690;
Neutral, polaron, and bipolaron states in pedot prepared by photoelectrochemical polymerization and the effect on charge generation mechanism in the solid-state dye-sensitized solar cell
(2013) Journal of Physical Chemistry C, 117 (44), pp. 22484-22491.
DOI: 10.1021/jp406493v

[155] Zhang, J., Yang, L., Shen, Y., Park, B.-W., Hao, Y., Johansson, E.M.J., Boschloo, G., Kloo, L., Gabrielsson, E., Sun, L., Jarboui, A., Perruchot, C., Jouini, M., Vlachopoulos, N., Hagfeldt, A.
55966766100;57155179400;55965806700;35222177400;36918409900;10046404400;67019144 21;7003886256;57193542938;55701772900;57211032192;6603928659;54893775600;6603277739;7005851690;
Poly(3,4-ethylenedioxythiophene) hole-transporting material generated by photoelectrochemical polymerization in aqueous and organic medium for all-solid-state dye-sensitized solar cells
(2014) Journal of Physical Chemistry C, 118 (30), pp. 16591-16601.
DOI: 10.1021/jp412504s

[156] Ng, C.A., Camacho, D.H.
56797300400;7003773991;
Polymer electrolyte system based on carrageenan-poly(3,4-ethylenedioxythiophene) (PEDOT) composite for dye sensitized solar cell
(2015) IOP Conference Series: Materials Science and Engineering, 79 (1), art. no. 012020, .
DOI: 10.1088/1757-899X/79/1/012020

[157] Jayme, C.C., Kanicki, J., Kajzar, F., Nogueira, A.F., Pawlicka, A.
55601764500;7006407567;7006216850;7102266163;7003923415;
Influence of DNA and DNA-PEDOT: PSS on dye sensitized solar cell performance
(2016) Molecular Crystals and Liquid Crystals, 627 (1), pp. 38-48.
DOI: 10.1080/15421406.2015.1137680

[158] Zhang, J., Pazoki, M., Simiyu, J., Johansson, M.B., Cheung, O., Häggman, L., Johansson, E.M.J., Vlachopoulos, N., Hagfeldt, A., Boschloo, G.
55966766100;52364747000;23967232500;57016114200;55124548100;14048301300;10046404400;6603277739;7005851690;6701914421;

The effect of mesoporous TiO2 pore size on the performance of solid-state dye sensitized solar cells based on photoelectrochemically polymerized Poly(3,4-ethylenedioxythiophene) hole conductor
(2016) Electrochimica Acta, 210, pp. 23-31.
DOI: 10.1016/j.electacta.2016.05.083

[159] Li, Q., Li, H., Jin, X., Chen, Z.
56157911800;57191365305;57208453092;57191852675;
PEDOT and derivatives tailored conducting gel electrolytes for high-efficiency quasi-solid-state dye-sensitized solar cells
(2018) Electrochimica Acta, 260, pp. 413-419.
DOI: 10.1016/j.electacta.2017.12.113

Ringraziamenti

Ringrazio il *Professor Federico Bella* per avermi seguito con molta pazienza e per avermi supportato in una situazione universitaria molto delicata. Ringrazio anche *Lucia* di avermi seguito con molta pazienza nella pratica di laboratorio.

Grazie a mia mamma, **Daniela**, per avermi fatto da sostegno, ancora e appiglio in tutto il mio percorso. La ringrazio per non aver mai smesso di credere in me nemmeno quando non riuscivo a farlo io e per aver sempre avuto una carezza e una dolcezza in serbo qualsiasi cosa accadesse. Grazie per avermi insegnato che qualsiasi cosa ci si pari davanti, in due è tutto più facile e che niente è impossibile, niente, perché siamo insieme. Sei tutte le cose belle del mondo, te l'ho sempre detto.

Grazie a mio papà, **Francesco**, che con una figura solida e sempre presente non ha mai smesso di fare il tifo e mai smetterà. In silenzio dietro alle quinte ha sempre permesso alla mia vita di proseguire con facilità, ha reso anche le cose più pesanti leggere come una piuma.

Grazie ai miei due fratellini, **Giacomo** e **Diego**, che fratellini non sono più molto. Siete cresciuti provando sempre entusiasmo per quello che faccio e non mi immagino persone più pure di voi nella mia vita.

Un grazie anche a **Silvia**, che con la sua grinta di sconfiggere qualsiasi cosa le si pari davanti mi ha insegnato molto. Grazie a **Giulia** e **Federico**, che sono sempre stati presenti nel mio percorso con tutte le risate e i momenti felici di sempre.

E poi grazie a lei, a **Martina**. La persona che è stata una ventata di aria fresca nella mia vita, la persona che vede in me quello che io non vedrò mai ma che lo vede con tanta intensità che ogni tanto mi pare di scorgerlo. Martina è stata un punto di rifermento per tutto il mio percorso, è stata la persona che sapeva senza parlare cosa fare in ogni occasione e che non mi ha mai lasciato un momento nelle mie paure. Grazie anche ad **Enrico**, che con la sua dolcezza mi fa sentire una persona speciale ogni volta. Sei stato un amico, sempre. Dai momenti di pazzia e di sconforto ai momenti al pianoforte ai momenti di silenzio, rendendo questo silenzio più leggero perché insieme.

Grazie a **Marcella**, che ha condiviso con me moltissime risate, pianti, emozioni ed episodi unici. Mi ha insegnato che se la vita ti schiaccia tu ti devi spostare e farle vedere che non sta funzionando.

Un grazie anche a **Tommaso**, che nonostante ormai siamo lontani è sempre una figura imprescindibile e solida dei primi anni pazzi di Politecnico.

Ultimo, ma non per importanza, grazie a **Matteo**. È con la sua calma e con tutto l'amore che mi ha dimostrato che so di poter affrontare tutto, insieme a lui. Mi ha messo sempre prima di ogni cosa, non avendo occhi per altro. Mi ha sempre tenuto a galla anche quando magari non stava a galla nemmeno da solo. E non solo mi teneva a galla, mi porterà a solcare gli oceani e a fare la vita che tanto sogniamo. Grazie!